SPECIAL PAPER 14

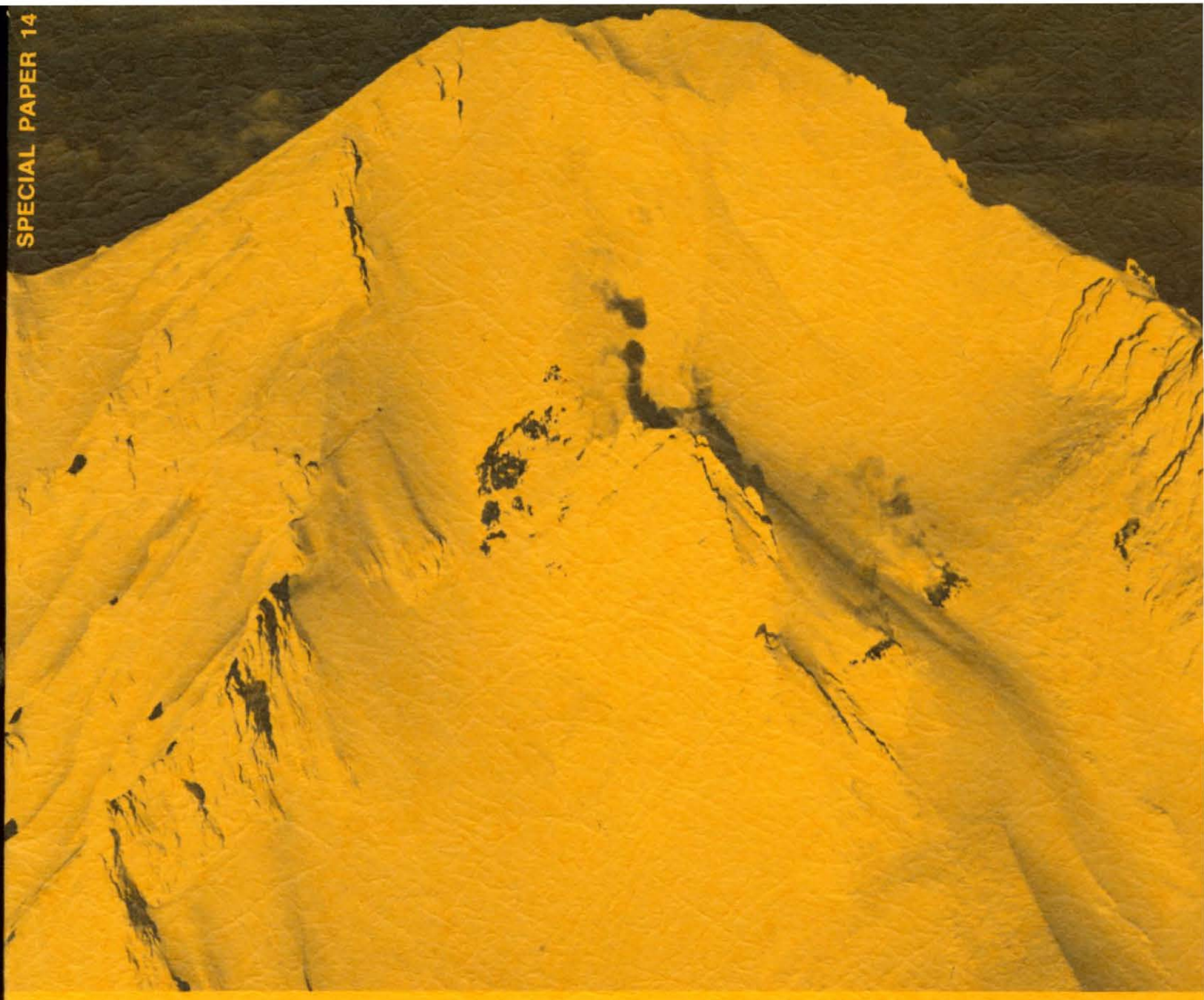

GEOLOGY AND GEOTHERMAL RESOURCES OF THE MOUNT HOOD AREA, OREGON

1982

STATE OF OREGON
DEPARTMENT OF GEOLOGY AND MINERAL INDUSTRIES
DONALD A. HULL, STATE GEOLOGIST

STATE OF OREGON
DEPARTMENT OF GEOLOGY AND MINERAL INDUSTRIES
1005 State Office Building, Portland, Oregon 97201

Special Paper 14

GEOLOGY AND GEOTHERMAL RESOURCES OF THE MOUNT HOOD AREA, OREGON

Edited by

George R. Priest and Beverly F. Vogt
Oregon Department of Geology and Mineral Industries

1982

Conducted in conformance with ORS 516.030

Funded by U.S. Department of Energy Contract DE FC 07-79-ID-12044
to the Oregon Department of Geology and Mineral Industries

NOTICE

The Oregon Department of Geology and Mineral Industries is publishing this paper because the subject matter is consistent with the mission of the Department. To facilitate timely distribution of information, some parts of this publication are included as camera-ready copy submitted by the authors and have not been edited by the staff of the Oregon Department of Geology and Mineral Industries. Matters of consistency between individual articles by various authors are not addressed in agency editing.

Conversion factors for SI metric and U.S. customary units of measurements

To convert from	To	Factor	Factor for opposite conversion
centimeter (cm)	inch (in)	0.3937	2.54
meter (m)	foot (ft)	3.281	0.3048
kilometer (km)	mile (mi)	0.6214	1.609
centimeter^3 (cm^3)	inch^3 (in^3)	0.06102	16.39
meter^3 (m^3)	foot^3 (ft^3)	35.31	0.02832

Temperature °F = 1.8 temp. °C + 32. Temperature °C = (temp. °F −32)/1.8.

CONTENTS

COVER PHOTO. Fumaroles at Crater Rock and Devils Kitchen, south side of Mount Hood, Oregon. Photo courtesy Herbert G. Schlicker.

GEOLOGY AND GEOTHERMAL RESOURCES OF THE MOUNT HOOD AREA, OREGON

INTRODUCTION

by George R. Priest, Geothermal Specialist,
Oregon Department of Geology and Mineral Industries

On July 1, 1977, the Oregon Department of Geology and Mineral Industries (DOGAMI) began research on two geothermal-resource projects funded by the U.S. Energy Research and Development Administration (ERDA; now the U.S. Department of Energy [USDOE]) under Contract No. EG-77-C-06-1040. These projects were (1) a geothermal resource assessment of Mount Hood volcano in the Cascade Range and (2) a statewide inventory of low-temperature geothermal resources. An application for an extension and additional funding of these projects was submitted to ERDA (USDOE) on September 14, 1977, funded on December 28, 1977, and later extended to December 31, 1978. A no-cost extension to the contract was issued by USDOE on January 1, 1979, with the original completion date as specified in Article II of the contract changed to June 15, 1979, and the contract number changed from EG-77-C-06-1040 to AC06-77-ET-28369. Results of this Phase I investigation at Mount Hood were published as DOGAMI Open-File Report O-79-8 in July 1979 (Hull and Riccio, 1979).

The Phase I study involved drilling, geologic analysis, and geophysical surveys of the Mount Hood area. In 1978, twelve shallow temperature-gradient wells were completed by DOGAMI to depths of 76-152 m (see Hook, this volume), and temperature gradients were measured in 50 existing wells in the northern Cascades area. Also, a 1,220-m test at Old Maid Flat (OMF-1, Figure 1) was completed by DOGAMI in the summer of 1978. A northern Cascades gravity survey conducted by the Oregon State University Geophysics Group in 1977 and 1978 and interpreted in DOGAMI Open-File Report O-79-8 has been incorporated into DOGAMI Special Paper 11 (in preparation), which presents an analysis of gravity measurements of the entire Oregon Cascades. Open-File Report O-79-8 also contains a preliminary interpretation of the geologic data from the Old Maid Flat area by Marvin H. Beeson and Michael R. Moran, Portland State University Earth Sciences Department, and an analysis of similar data for the Mount Hood volcano by Craig M. White, University of Oregon Department of Geology. White's data are more fully presented in DOGAMI Special Paper 8 (White, 1980). Heat-flow modeling of the temperature-gradient data in the Phase I study was completed by David D. Blackwell and John L. Steele, Southern Methodist University, and included in Open-File Report O-79-8.

The Phase I study paved the way for additional drilling programs in 1978, 1979, and 1980. These projects were conducted by Northwest Geothermal Corporation (NWGC), the U.S. Geological Survey (USGS), and USDOE. NWGC completed holes to depths of 151-610 m, while the USGS drilled wells to depths of 295-1,220 m. The Nevada Operations Office of USDOE supervised drilling of an 1,837-m test well at Old Maid Flat (OMF-7A, Figure 1) and supported deepening of the OMF-1 well from 610 m to 1,220 m.

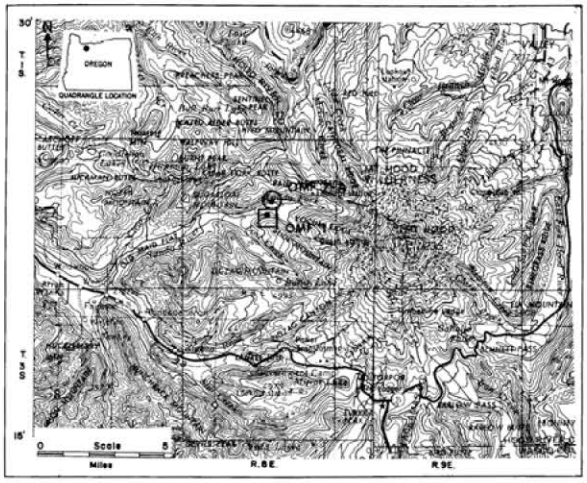

Figure 1. Mount Hood study area, with locations of deep drill holes OMF-1 (square), depth 1,220 m (4,002 ft), and OMF-7A (circle), depth 1,837 m (6,027 ft).

Scientific data acquisition and analysis for the OMF-7A well was conducted by DOGAMI under Task 8 of USDOE Cooperative Agreement No. DE-FC07-79ID2044, Amendment No. A001 (effective January 1, 1980, through December 31, 1980, and extended by Modification No. M002 to January 31, 1981). All of the nonproprietary data from these drilling programs, as well as the Phase I data, exclusive of the gravity survey and the details of White's report (see DOGAMI Special Papers 8 and 11), are summarized in this paper. Geophysical and lithologic logs of OMF-7A have been released in DOGAMI Open-File Reports O-80-11 (MacLeod and Hill, 1980), O-81-2A, and O-81-2B (Oregon Department of Geology and Mineral Industries, 1981). Logs of OMF-1 are in DOGAMI Open-File Report O-78-6 (Oregon Department of Geology and Mineral Industries, 1978). Temperature-gradient data for most of the 1978, 1979, and 1980 drilling are available in DOGAMI Open-File Reports O-81-3A, O-81-3B, and O-81-3C, respectively (Blackwell and others, 1981).

The Mount Hood geothermal assessment project is the result of cooperative efforts of a large number of people from both government and industry. John W. Hook, Richard G. Bowen, and Northwest Natural Gas Company first generated interest in the area by obtaining geothermal leases and conducting exploration. David L. Williams, USGS, spearheaded efforts to organize a comprehensive geothermal assessment of the area by government agencies. His interpretations of geology and geophysics of the area were included with the contributions of other workers in the April

10, 1982, issue of the *Journal of Geophysical Research* (v. 87, no. B4, p. 2767-2828). The excellent data sets summarized in both the present paper and the *Journal of Geophysical Research* are a tribute to the pioneering efforts of these individuals and organizations.

REFERENCES CITED

Blackwell, D.D., Black, G.L., and Priest, G.R., 1981, Geothermal-gradient data: Oregon Department of Geology and Mineral Industries Open-File Report O-81-3A (for 1978), 63 p.; O-81-3B (for 1979), 98 p.; O-81-3C (for 1980), 374 p.

Hull, D.A., investigator, and Riccio, J.F., eds., 1979, Geothermal resource assessment of Mount Hood: Oregon Department of Geology and Mineral Industries Open-File Report O-79-8, 273 p.

MacLeod, T., and Hill, J., logging geologists, R.F. Smith Corporation, 1980, Engineering and air and mud drilling data of DOGAMI geothermal exploratory well Old Maid Flat 7A: Oregon Department of Geology and Mineral Industries Open-File Report O-80-11, 1 sheet folded into 16 p.

Oregon Department of Geology and Mineral Industries, 1978, Geophysical logs, Old Maid Flat No. 1, Clackamas County, Oregon: Oregon Department of Geology and Mineral Industries Open-File Report O-78-6, 6 logs.

— — — 1981, Geophysical logs, Old Maid Flat No. 7A, Clackamas County, Oregon: Oregon Department of Geology and Mineral Industries Open-File Report O-81-2, 2 parts: O-81-2A (shallow, 96-1,190 ft), 4 logs; O-81-2B (deep, 96-5,952 ft), 12 logs.

White, C.M., 1980, Geology and geochemistry of Mount Hood volcano: Oregon Department of Geology and Mineral Industries Special Paper 8, 26 p.

Williams, D.L., Hull, D.A., Ackerman, H.D., and Beeson, M.H., 1982, The Mt. Hood region: volcanic history, structure, and geothermal energy potential: Journal of Geophysical Research, v. 87, no. B4, p. 2767-2781.

HISTORY OF GEOTHERMAL EXPLORATION IN THE MOUNT HOOD AREA, OREGON

By John W. Hook, Consulting Geologist, Portland, Oregon

The fumaroles at Crater Rock near the summit of Mount Hood and Swim Hot Springs on its southern flank are manifestations of geothermal energy which have been known for many years. The Swim Hot Springs are near Summit Meadow, a stop on the old Barlow Trail. They were used as a spa around the turn of the century, but the old hotel burned, and the area has now returned to its natural state.

The potential for geothermal energy development at Mount Hood was recognized by the U.S. Geological Survey (USGS) in the early 1970's, when the area around Crater Rock was declared a Known Geothermal Resource Area (KGRA). When the U.S. Bureau of Land Management (BLM) first started accepting geothermal lease applications under the Geothermal Steam Act, the City of Burbank, California, filed lease applications adjacent to the KGRA in

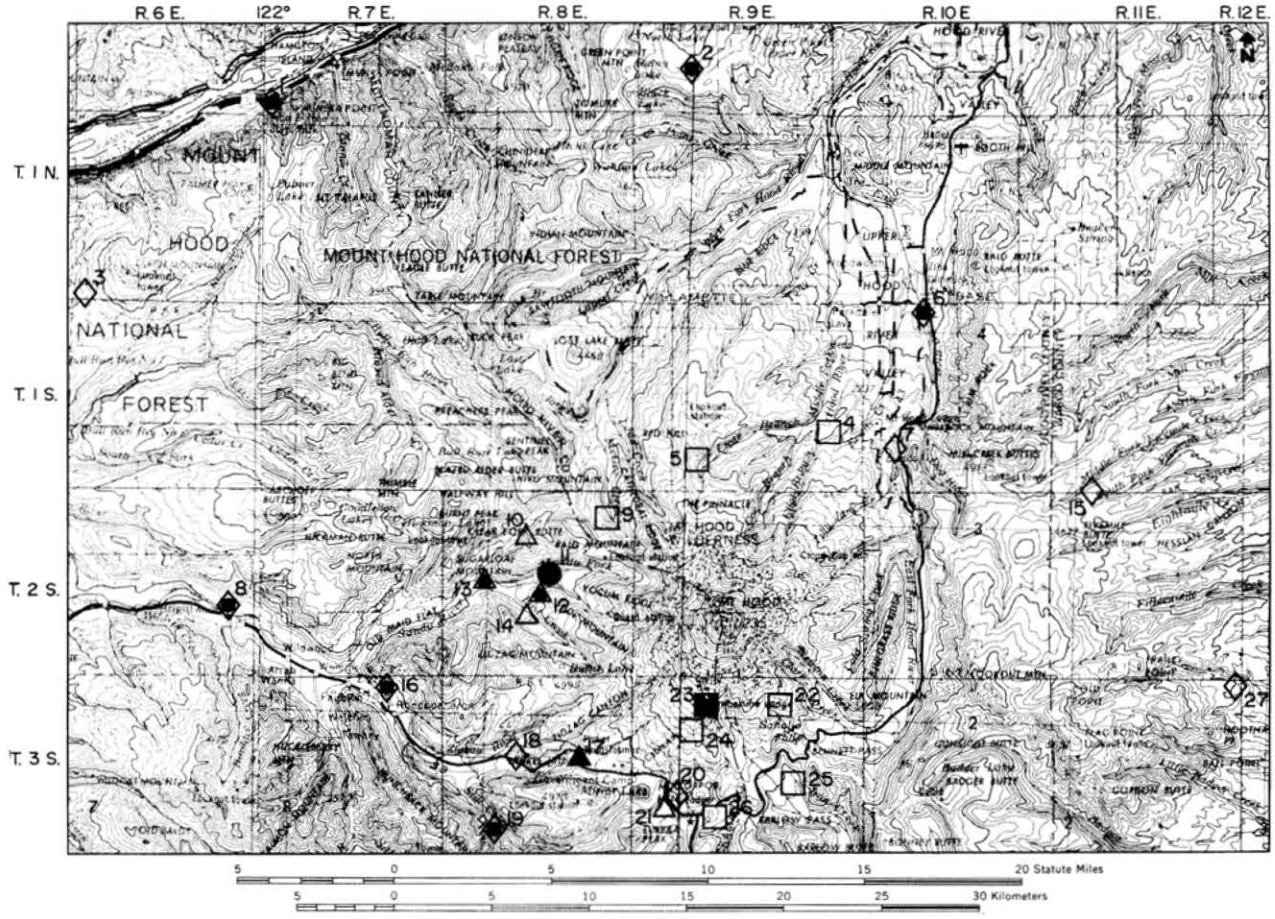

Figure 1. Geothermal drilling in the Mount Hood area. Solid dot = funded by U.S. Department of Energy (USDOE), managed by USDOE and Oregon Department of Geology and Mineral Industries (DOGAMI); dot in diamond = funded by USDOE and State of Oregon, managed by DOGAMI; dot in triangle = funded by USDOE and Northwest Natural Gas Company (NWNG), managed by NWNG and DOGAMI; open diamond = funded by State of Oregon, managed by DOGAMI; open triangle = funded and managed by NWNG; open square = funded by USDOE, managed by the U.S. Geological Survey (USGS); solid triangle = funded by USDOE and NWNG and managed by NWNG; solid square = funded by USDOE and managed by DOGAMI, NWNG, and USGS. Numbers refer to Table 1. Additional data for each hole appear also in Table 1.

Table 1. *Geothermal drilling accomplished in the Mount Hood area through September 1981. Chief organizations involved are the U.S. Department of Energy (USDOE), the State of Oregon (OR), the U.S. Geological Survey (USGS), the Oregon Department of Geology and Mineral Industries (DOGAMI), and Northwest Natural Gas Company (NWNG) through their affiliate Northwest Geothermal Corporation.*

No. on Figure 1	Hole name	Location	Depth (m)	Managed by	Funded by
1.	McCord Creek	2N/7E-31BD	152	DOGAMI	USDOE, OR
2.	Mt. Defiance	2N/9E-29AD	97	DOGAMI	USDOE, OR
3.	Larch Mtn.	1N/6E-31CD	152	DOGAMI	OR
4.	Eliot Branch	1S/9E-26ABA	250	USGS	USDOE
5.	Clear Branch	1S/9E-31AB	310	USGS	USDOE
6.	Parkdale	1S/10E-9BC	152	DOGAMI	USDOE, OR
7.	Routson Park	1S/10E-29CA	150	DOGAMI	OR
8.	Brightwood Quarry	2S/6E-24CA	152	DOGAMI	USDOE, OR
9.	McGee Creek	2S/8E-1CD	608	USGS	USDOE
10.	Last Chance Mtn.	2S/8E-9AC	151	NWNG	NWNG
11.	OMF-7A	2S/8E-15AC	1,836	USDOE-DOGAMI	USDOE
12.	OMF-1	2S/8E-15CD	1,220	NWNG-DOGAMI	USDOE, NWNG
13.	OMF-3	2S/8E-17CC	398	NWNG-DOGAMI	USDOE, NWNG
14.	OMF-10	2S/8E-28AA	131.5	NWNG	NWNG
15.	Fivemile Butte	2S/11E-6AA	152	DOGAMI	OR
16.	Road 19	3S/7E-3AA	65	DOGAMI	USDOE, OR
17.	Kiwanis Camp Rd.	3S/8E-14BC	285	NWNG	USDOE, NWNG
18.	Laurel Hill	3S/8E-16CD	125	DOGAMI	OR
19.	Still Creek	3S/8E-29DDC	~153	DOGAMI	USDOE, OR
20.	Snow Bunny	3S/8.5E-25AA	82	DOGAMI	OR
21.	Trillium Lake	3S/8.5E-25DB	339	NWNG	NWNG
22.	Mt. Hood Meadows	3S/9E-3CCA	350	USGS	USDOE
23.	Timberline Lodge	3S/9E-6DD	21 152 396	DOGAMI-NWNG- USGS	USDOE
24.	Pucci Chairlift	3S/9E-7DBB	1,220	USGS	USDOE
25.	White River	3S/9E-16DB	300	USGS	USDOE
26.	Junction of Highways 26 and 35	3S/9E-30ADB	296	USGS	USDOE
27.	Owl Hollow	3S/11E-1AA	127	DOGAMI	OR

January 1974. Their interest was in finding a resource to generate electrical power.

The next application was filed in February 1975 by this author for an area at Old Maid Flat on the west side of Mount Hood. The objective was to find a source of hot water to be piped to the Portland area for direct use in industry and residential heating in a manner analogous to that at Reykjavic, Iceland, where 98 percent of the homes are heated with hot water from wells as far as 19 km (12 mi) away. A 72-km (45-mi)-long pipeline seemed practical to the engineers of Northwest Natural Gas Company (NWNG), who were operating over 16,000 km (10,000 mi) of pipelines in Oregon and Washington. Their economic feasibility study indicated that the energy could be delivered to major industrial users at less than the cost of equivalent heat from oil or gas. NWNG wanted to start exploratory drilling immediately but was restrained by federal regulatory requirements.

The first hole on Mount Hood was drilled by the Oregon Department of Geology and Mineral Industries (DOGAMI) at Timberline Lodge in August 1976 to a depth of 152 m (500 ft). Caving and loss of tools, however, reduced the effective thermal-gradient measurements to 55 m (180 ft) (Table 1, Figure 1). The drill was scheduled to move to Old Maid Flat next, but the area was closed by a court order affecting the entire Bull Run Reserve, and drilling was delayed a full year in Old Maid Flat. In 1976 DOGAMI drilled two additional holes outside of the closed area at Laurel Hill and Snow Bunny (Table 1, Figure 1).

The Mount Hood Assessment Project was begun in 1977 with geologic mapping, geochemical and geophysical studies, and an attempted deep test at Timberline Lodge. The geophysical findings were encouraging: a 4-volt SP anomaly near the top of the Magic Mile chair lift (Don Hoover, USGS) and extremely high conductivity at Cloud Cap found by magnetotelluric survey (Norm Goldstein, Lawrence Berkeley Laboratory). The attempted deep test at Timberline failed to set surface casing and was abandoned at 21 m (70 ft).

The "Mini Bull Run Act" opened Old Maid Flat to recreation and geothermal exploration in the fall of 1977. NWGC drilled the Old Maid Flat OMF-1 well to 564 m (1,850 ft), finding a thermal gradient of 67° C/km. In 1978, this well was deepened to 1,220 m (4,002 ft) by U.S. Department of Energy (USDOE) as part of the Mount Hood Assessment Project and completed for thermal-gradient observations. The bottom-hole temperature was 82° C, but subsequent flow testing in 1980 did not find any significant flow of thermal water.

In all, 27 sites have been drilled for thermal-gradient tests in the Mount Hood area by DOGAMI, USDOE, USGS, and NWNG (Table 1). Of special interest among these are the Pucci well, with a temperature of 85° C at 1,220 m (4,000 ft), and the McGee Creek well, with a gradient of 88° C/km and a temperature of 60° C at 608 m (1,994 ft).

During the summer of 1980, a production test (OMF-7A) was drilled by USDOE to 1,836 m (6,027 ft) at Old Maid Flat. The well was drilled near a major fault zone, but the rock at depth was nearly impermeable. Microquartz diorite intrusions which were encountered near the fault zone may represent sills and possibly dikes that helped to reduce the fracture permeability. The temperature at the bottom was 119° C, and the overall thermal gradient was about 63° C/km. The well had an artesian flow from fractures at about 480 m (1,600 ft), but with a packer set at 1,200 m (4,000 ft), a swabbing test yielded less than 1 gal/min from the lower part of the well.

The failure of OMF-7A to find water had a dampening effect on exploration efforts in 1981, and the only work done during that year was by the USGS at Pucci, McGee Creek, and Mount Hood Meadows. The Pucci well confirmed the existence of an aquifer capable of yielding 110 gal/min of hot water near Timberline Lodge. Potential temperatures in this well should approach the bottom-hole temperature of 80° C (USGS press release, 1981). It is hoped that the success at Pucci will stimulate renewed interest in exploration at Mount Hood.

OVERVIEW OF THE GEOLOGY AND GEOTHERMAL RESOURCES OF THE MOUNT HOOD AREA, OREGON

By George R. Priest, Geothermal Specialist
Oregon Department of Geology and Mineral Industries

ABSTRACT

The Mount Hood area has been the site of intermediate to silicic subduction-related volcanism and associated hydrothermal activity since at least 16 m.y. ago. Small-scale basaltic volcanism, possibly related to increased east-west extension, began to occur in the Pliocene or latest Miocene. The post-Pleistocene Parkdale flow on the northeast flank of Mount Hood is the latest product of this volcanism. Northwest-trending right-lateral strike-slip faulting and northeast-trending folding and thrust faulting began at least 16 m.y. ago during eruption of the Grande Ronde Basalt, but the northeast-trending structures are now clearly truncated by the northwest-trending structures. North-south-trending normal faults and fracture zones began to be active concurrently with basaltic volcanism (e.g., the Boring Lava) in the latest Miocene or Pliocene, with much of the deformation focused on the Mount Hood area where a large subsidence block was formed.

Geothermal exploration should be concentrated in the High Cascade heat-flow anomaly and the somewhat higher Mount Hood heat-flow anomaly where permeable rocks are present in thermal zones. Permeable rocks and hydrothermal circulation systems are most probable where Columbia River basalt or phaneritic plutonic rocks occur and where fracture permeability has been enhanced by faulting. North-south-trending normal faults and "pressure shadows" in northwest-trending faults with strike-slip motion are probably the most favorable structures for fracture permeability. Intersection of these structures with the Laurel Hill and Still Creek plutons and areas near youthful volcanic vents on the north and east sides of Mount Hood are very favorable exploration targets, especially where the Columbia River Basalt Group is present at depth.

INTRODUCTION

This summary of the geology and geothermal resources of the Mount Hood area draws heavily on previous work by Wise (1961, 1968, 1969), Beeson and Moran (1979), Blackwell and others (1978), Crandell (1980), and White (1980a). It is also based on new detailed mapping and sampling in the Old Maid Flat area (Figure 1), where lithologic data from two deep drill holes and several shallow geothermal wells are available (e.g., Blackwell and others, Holdaway and Bussey, and Priest and others, all this volume). New heat-flow analyses of the Mount Hood volcano by Blackwell and Steele (1979) and Steele and others (this volume) are also briefly summarized.

New K-Ar and chemical data of Priest and others (this volume) and information on hydrothermal alteration in the Old Maid Flat area (Holdaway and Bussy, this volume) have altered previously accepted stratigraphic and volcanotectonic interpretations of the pre-Mount Hood volcanic rocks. Major subduction-related calc-alkaline volcanism began between 16 and 14 m.y. ago, as deduced from interfingering of andesitic debris flows between the Priest Rapids and Frenchman Springs Members of the Wanapum Basalt (Priest and others, this volume), and some andesitic interbeds in the upper part of the low-MgO chemical type of the Grande Ronde Basalt (Anderson, 1978). Also, sills of hornblende-biotite microquartz diorite have been identified in both deep drill holes at Old Maid Flat and appear to correlate with emplacement of the Laurel Hill-Still Creek magmas and a widespread zeolite-facies metamorphic event between about 11 and 8 m.y. ago (Priest and others, Holdaway and Bussey, both this volume). This event was roughly coincident with eruption, west of Mount Hood, of megacrystic two-pyroxene andesite lavas of distinctly more mafic character than underlying Rhododendron rocks (the Last Chance andesite of Priest and others, this volume). Eruption of these megacrystic lavas was the beginning of a general trend toward increasingly mafic volcanism throughout the Neogene and may have been related to the increasing influence of extensional tectonic forces in the Mount Hood area. Priest and others and Holdaway and Bussey (both this volume) present chemical and mineralogic methods which serve to delineate these igneous and metamorphic units in the Old Maid Flat area. This paper utilizes the geology, heat flow, and tectonics of the region to characterize the geothermal resources in the Mount Hood area. Recommendations for specific exploration techniques and targets are also given.

For detailed discussions of the geophysics of the area, the reader is referred to Couch and Gemperle (1979) for gravity; Friedman and Frank (1977) and Friedman and others (1982) for infrared photography; Kohler and others (1978, 1982), Westhusing (1973), and Weaver and others (1982) for seismic studies; Flanagan and Williams (1982) for magnetic surveys; and Goldstein and others (1982) for electrical surveys.

ERUPTIVE HISTORY

Volcanic rocks of Eocene(?) to Holocene age occur in the Mount Hood area (Table 1). The oldest volcanic rocks encountered so far are highly altered Eocene(?) tholeiitic andesite to dacite lavas and flow breccias (greenstones) intercepted at a depth of 1,707-1,837 m (5,600-6,027 ft) in the Old Maid Flat 7A (OMF-7A) drill hole.

After an unknown period of uplift and erosion, Oligocene volcaniclastic sediments and mudflows of andesitic lavas of the Eagle Creek Formation came into the

Scale 1:500,000

Explanation

Qral	Recent alluvium and landslide deposits
Qpgl	Glacial deposits
Qpln	River terrace deposits
Qa	Pleistocene andesite to dacite
Qb	Pleistocene basalt
Qi	Pleistocene mafic intrusive rocks
QTba	Pliocene-Pleistocene basalt, andesite, and pyroclastic rocks
QTw	Pliocene-Pleistocene volcaniclastic deposits
QTim	Pliocene-Pleistocene mafic intrusive rocks
Tpb	Pliocene basalt
Tpi	Pliocene mafic intrusive rocks
Tpw	Dalles Formation (Miocene-Pliocene)
QTif	Upper Miocene hornblende diorite intrusives
Tmua	Upper Miocene Rhododendron Formation
Tmmb	Middle Miocene Columbia River Basalt Group
Tmop	Eagle Creek Formation (Oligocene)
	Anticline (dotted where covered)
	Syncline (dotted where covered)
	Normal fault—bar and ball on downdropped side (dotted where covered)
	Wrench fault—arrows indicate relative motion (dotted where covered)
	Thrust fault—teeth indicate upper plate (dotted where covered)

Figure 1. Generalized geologic map of the Mount Hood area. Geology taken from Wells and Peck (1961); additional structures taken from Anderson (1980), Hammond and others (1980), Beeson and others (this volume), and Beeson and others (in preparation). Geologic symbols are modified from Wells and Peck (1961), but descriptions listed here are specific to local geology.

SUBGROUP	FORMATION	MEMBER
YAKIMA BASALT	SADDLE MTNS BASALT	POMONA*
	WANAPUM BASALT	PRIEST RAPIDS*
		FRENCHMAN SPRINGS
	GRANDE RONDE BASALT	
*indicates intracanyon flow		

Figure 2. Columbia River Basalt Group stratigraphy in western Oregon. Figure from Anderson (1980). Pomona dated at 12 m.y., Grande Ronde Basalt at between 14 and 16.5 m.y. (Swanson and others, 1979).

area from eruptive centers north of the Columbia River and south of the Clackamas River (Beeson and Moran, 1979). During the middle Miocene, a northeast-trending topographic low developed in the present-day Mount Hood area, and through it tholeiitic basalts of the Columbia River Basalt Group flowed into the area from the east (Figures 2 and 3). Major calc-alkalic volcanism began near the Mount Hood area between times of eruption of the Frenchman Springs and the Priest Rapids Members of the Wanapum Basalt, Columbia River Basalt Group (Priest and others, this volume), although some andesitic rocks also occur in upper Grande Ronde interbeds in the Clackamas River area to the south (Anderson, 1978). Hornblende-bearing dacite and two-pyroxene andesite debris flows and lavas of the Rhododendron and Chenoweth Formations (formerly the Dalles Formation) then erupted mainly from volcanic centers in the western and central parts of the Mount Hood area between about 16 and 10.7 m.y. ago (Anderson, 1978; Priest and others, this volume). This volcanic pile was intruded by hornblende diorite magmas of the Still Creek and Laurel Hill intrusions toward the end of eruption of the Rhododendron lavas (Figure 1). Similar, but more silicic, microquartz diorites intruded the Old Maid Flat area at about this same time (Priest and others, this volume). Then, about 10.7 m.y. ago, megacrystic two-pyroxene andesite flows of somewhat more mafic composition than the Rhododendron lavas were erupted onto a dissected surface of Rhododendron rocks (Wise, 1969; Priest and others, this volume). These andesites probably came from vents in the western part of the Mount Hood area, near Old Maid Flat.

Figure 3. Regional distribution of Columbia River Basalt Group (dot pattern) shown relative to the Cascade Range (line pattern). Distribution of basalt from Waters (1961). Figure from Anderson (1980).

Geothermal systems that were active during and after eruption of the Rhododendron lavas caused widespread zeolite-facies (laumontide-grade) alteration in the Rhododendron Formation (Holdaway and Bussey, this volume). The zeolite-facies event reset most K-Ar ages of Rhododendron and older rocks to between 12.2±1.7 and 5.9±1.1 m.y. at Old Maid Flat (White, 1979; Priest and others, this volume). Because the range of K-Ar ages of the hornblende quartz diorite and diorite intrusives (11.5-8.0 m.y., according to Bickerman, 1970; White, 1980a; Priest and others, this volume) fall into the same time interval, it is probable that the intrusions helped supply heat which drove the zeolite-facies hydrothermal systems.

After the zeolite-facies metamorphism and late Miocene volcanism, eruptive activity around Mount Hood during the Pliocene began to produce increasing but subordinate quantities of mafic lavas (Figure 4). These mafic lavas are locally iron-rich compared to typical calc-alkaline basalts according to Miyashiro's tholeiitic-calc-alkaline boundary (1974) (Figure 4). Many can be characterized as high-alumina olivine tholeiites (Figures 4 and 5), and some samples plot in Kuno's (1966) alkali basalt field (Figure 5b), revealing their slightly alkaline character. Similar basalts with alkaline affinities occur in the late Miocene to Pliocene central and southern Cascades (Naslund, 1977; White, 1980b; Avramenko, 1981; Flaherty, 1981). Pliocene lavas capping the horst block east of the Hood River fault at Lookout Mountain and basalts occurring near Bull Run Lake are good examples of these anomalously iron-rich, high-alumina basalts. Some of the lavas from Sandy Glacier volcano (west margin of Mount Hood) and Badger Butte (Figure 1) also appear to be somewhat tholeiitic in character, while others are typical calc-alkalic andesites (Figure 4). If these basaltic lavas are roughly contemporaneous with the Lookout Mountain lavas (K-Ar age of 3.0 m.y., according to Wise, 1969), then most of them were probably erupted in the Pliocene just prior to formation of the Hood River fault, which cuts Lookout Mountain lavas occurring at the top of the fault scarp. Eruption of contemporaneous Boring basaltic lavas in Pliocene-Pleistocene time west of the Mount Hood area (Allen, 1975) is evidence that mafic volcanism covered a much wider area than andesitic volcanism. Eruption of the Holocene Parkdale flow on the northeast flank of Mount Hood is evidence of continuing mafic volcanism. It is important to emphasize that throughout the Neogene silicic to intermediate calc-alkaline lavas continued to be volumetrically predominant in eruptions in the vicinity of Mount Hood.

Quaternary volcanism has been dominated by eruptions of intermediate to silicic lavas from Mount Hood volcano. The composite cone at Mount Hood began activity within the last 700,000 years (Wise, 1969) and has experienced repeated eruptions of calc-alkaline basaltic andesite to hornblende dacite lava and pyroclastic rocks into historic time (Crandell, 1980).

The volcanic history of the Mount Hood volcano may be broadly divided into six major episodes of volcanism, based on mappable lithologic units:

1. The Main Stage lavas are basaltic andesite, pyroxene

andesite, hornblende dacite flows, and pyroclastic debris flows (White, 1980a) which were erupted between 700,000 yr B.P. (all are normally polarized, according to Wise, 1969) and 29,000 yr B.P. (all are affected by the Fraser Glaciation, according to Crandell, 1980). These lavas comprise about 90 percent of the volume of Mount Hood (White, 1980a).

2. The Pollalie eruptive period occurred between 15,000 and 12,000 yr B.P. (late Fraser time) and resulted in eruption of hot pyroclastic debris flows and associated lithic ash clouds from explosion of a hornblende-bearing hypersthene dacite plug dome (Crandell, 1980).
3. The Timberline eruptive period occurred between 1,800 and 1,500 yr B.P. and consisted of hot debris flows, related lithic ash falls, and cooler mudflows from the explosion of hornblende-hypersthene dacite plug domes emplaced at approximately the location of Crater Rock (Crandell, 1980).
4. The Old Maid eruptive period occured sometime between 250 yr B.P. (^{14}C dating on trees within the Old Maid Flat mudflow) and 176 yr B.P. (growth-ring data on trees in Old Maid Flat) and consisted of emplacement of hypersthene-hornblende dacite mudflows from plug-dome explosions (Crandell, 1980). About 140 million m^3 of debris was erupted into the Sandy River and White River drainages during this period (Crandell, 1980).
5. The Crater Rock dome formed during the Old Maid eruptions and consists of hypersthene-hornblende andesite (62.6 percent SiO_2, recalculated volatile-free to 100 percent from Crandell's 1980 analysis). Twenty fumarole vents on the east and northeast sides of Crater Rock range in temperature from 50° to 90° C, providing compelling evidence that the plug dome is still cooling (Ayres and Creswell, 1951; Wise, 1968).
6. A historic pumice eruption probably occurred during either of two eruptions witnessed in 1859 and 1865 A.D. or in some other unobserved eruption occurring at about the same time (Crandell, 1980). This eruption produced a small quantity of gray hypersthene-hornblende dacite (63.5 percent SiO_2, recalculated volatile-free to 100 percent) pumice lapilli on the south, east, and northeast flanks of Mount Hood (Crandell, 1980).

Table 1. *Stratigraphy of the Mount Hood area, Oregon*

Age	Mount Hood area (Wise, 1969)	Old Maid Flat (Priest and others this volume)	Lithology
200 yr B.P.	Old Maid mudflow	Old Maid mudflow	Andesitic lahar.
Less than 700,000 yr B.P.	Mount Hood volcanic rocks		Chiefly andesites with minor basalt at Parkdale.
About 5 to 2 m.y. B.P.	Upper Pliocene basalts and andesites	Late Pliocene lavas	Chiefly andesites with some Fe-rich, slightly alkaline basalt.
		Miocene-Pliocene lavas	Chiefly andesite with lesser dacite.
About 12(?) to 5 m.y. B.P.	Lower Pliocene basalts and andesites; Laurel Hill and Still Creek plutons	Last Chance andesite and microquartz diorite	Megacrystic andesitic and dioritic rocks.
16(?) to 12 m.y. B.P.	Dalles and Rhododendron Formations	Rhododendron Formation	Generally altered (laumontite-grade zeolitic alteration) dacite and high-silica andesite lahars and minor lavas.
16.7 to 14 m.y. B.P.	Yakima Basalt	Wanapum Basalt	Tholeiitic basalt interbedded with the Rhododendron Formation.
		Grande Ronde Basalt	
Oligocene to early Miocene	Eagle Creek Formation	Volcaniclastic rocks (unfossiliferous)	Volcaniclastic rocks and some intermediate to mafic lavas; minor tuff.
Eocene(?)		Greenstone	Fe-rich dacitic to andesitic flows.

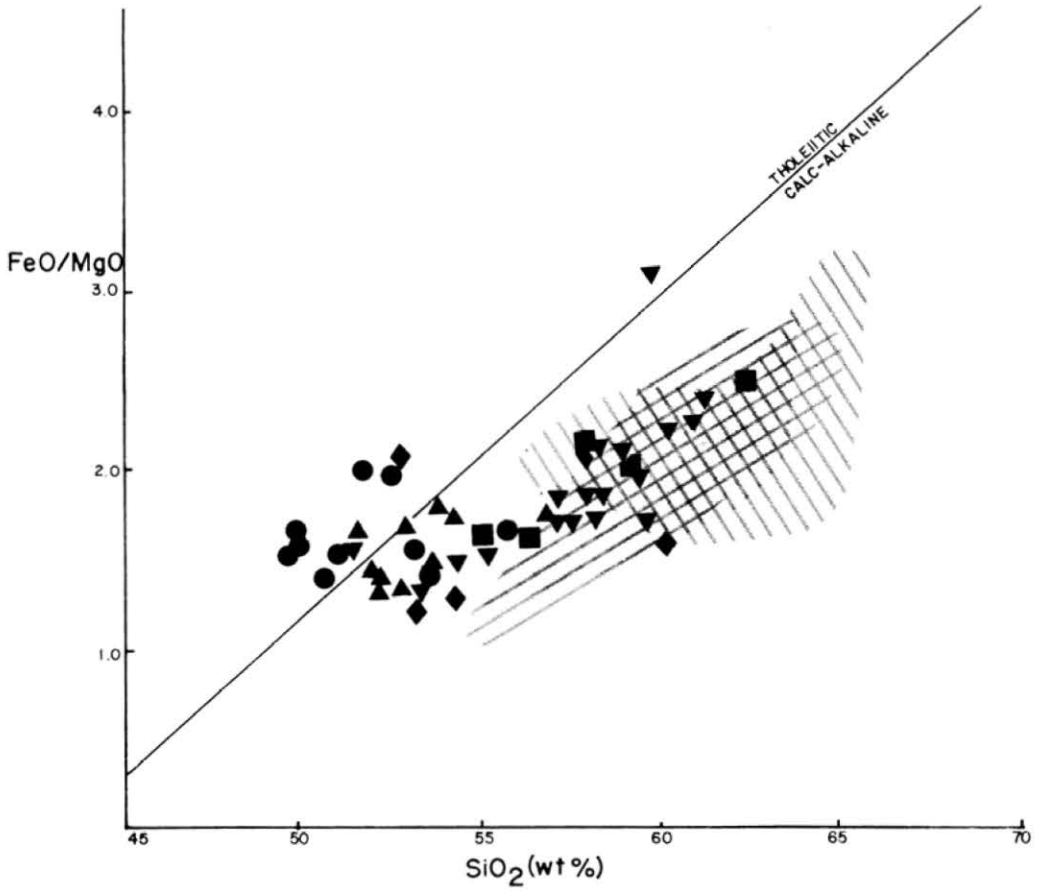

Figure 4. Comparison of volcanic suites of the upper Pliocene rocks (solid triangles = Bull Run and Lost Lakes; solid circles = Lookout Mountain; solid squares = Gunsight Butte; inverted triangle = Badger Butte; solid diamond = Sandy Glacier volcano) and lower Pliocene rocks (gray-shaded area) of Wise (1969). Note the more mafic and tholeiitic character of younger Pliocene lavas compared to the typical calc-alkalic rocks of Mount Hood (right-slanted lines; data from Wise, 1969) and the Rhododendron Formation (left-slanted lines; data from Priest and others, this volume). The tholeiitic-calc-alkaline boundary is from the equation of Miyashiro (1974).

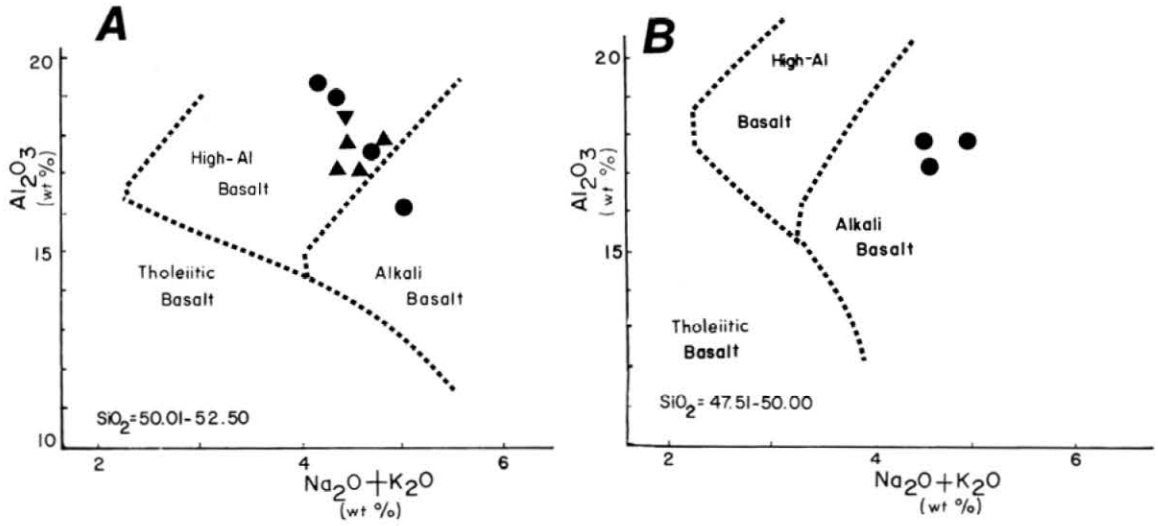

Figure 5. Chemical character of upper Pliocene basalts of Wise (1969). Same symbols as Figure 4. Composition boundaries of basalt types taken from Kuno (1966).

On the basis of his investigation of the petrology of Mount Hood volcano, White (1980a) concludes that eruptions occurred from many discrete magma batches rather than a single long-lived magma chamber. He also estimates that the post-Fraser dacitic magmas were at a temperature of about 935° C and were located at least 8 km (5 mi) beneath Mount Hood immediately prior to eruption. He concludes that post-Fraser magma chambers at 8-10 km (5-6 mi) would probably "have little influence on near-surface geothermal systems." It may be, however, that the Main Stage magmas, which account for 90 percent of the volume of the volcano, and which were intruded 8-10 km (5-6 mi) from the surface, could affect the present regional geothermal gradient (White, 1980a). Steele and others (this volume) show that there is, in fact, a heat-flow anomaly associated with the Mount Hood volcano. Deeply penetrating ground water in this area of high heat flow should generate economically attractive geothermal water, if permeable rocks are present.

STRUCTURAL GEOLOGY

Introduction

A considerable body of structural data is available for rocks younger than Oligocene in the Mount Hood area (e.g., Beeson and others, this volume, and in preparation), but very little is available for older rocks. This is primarily due to lack of sufficient exposure of Paleogene rocks in the area. This discussion will be confined to Neogene tectonism, which is probably most germane to the geothermal resources.

Major structural features

Miocene to Recent structures and tectonic patterns are apparent from lineation analyses (Venkatakrishnan and others, 1980) and detailed studies of Columbia River Basalt Group stratigraphy (Wise, 1969; Beeson and Moran, 1979; Priest and others, this volume; Beeson and others, in preparation), as well as the younger volcanic stratigraphy. Gravity anomalies at Mount Hood also show patterns which can be interpreted as structural offsets (Couch and Gemperle, 1979).

Major mapped folds and faults are summarized in Figure 1. Most of these structures are taken from Beeson and others (in preparation). It is apparent that the Mount Hood area is dominated by northwest- and north- to north-northwest-trending faults and a series of extensive northeast-trending folds, some of which have thrust-faulted limbs. Many of the northwest-trending faults have evidence of right-lateral strike-slip movement (Beeson and Moran, 1979; Beeson and others, in preparation). A major right-lateral wrench fault zone occurs along the Clackamas River, where numerous en echelon right-lateral and normal faults oriented about N. 30° W. make up a wrench zone striking N. 45° W. (Beeson and Moran, 1979). N. 10°-20° W.-trending faults and fractures commonly have little vertical offset but do frequently have Boring-type (Pliocene-Pleistocene) basaltic dikes and other cavity fillings (Beeson and Moran, 1979). Gravity anomaly patterns show intersecting north-south and N. 75° W. trends (Couch and Gemperle, 1979).

The Hood River fault zone is the major north-south-trending fault in the area. It appears to be the eastern boundary fault of a large downdropped crustal block which encloses Mount Hood (Allen, 1966; Beeson and Moran, 1979; Beeson and others, in preparation; unpublished mapping of N.M. Woller and J.L. Anderson). The western boundary of this crustal block appears to be a diffuse zone of faults and fractures (Williams and others, 1982). A fault striking N. 45° W. across Old Maid Flat in the western boundary zone of the Mount Hood block may have as much as 400 m (1,300 ft) of normal offset down to the east (Priest and others, this volume). Gravity data interpreted by Couch and Gemperle (1979) and seismic-refraction data of Weaver and others (1982) also support the existence of a major grabenlike structure under Mount Hood.

Timing of deformation

Movement on northeast-trending folds and thrust faults probably began during extrusion of the Grande Ronde Basalt (Beeson and Moran, 1979; Beeson and others, in preparation). Northwest-trending wrench faults were active after the northeast-trending structures ceased activity, with some movement in post-Sardine Formation time (Beeson and Moran, 1979; Beeson and others, in preparation). It is not known if the wrench faults are currently active.

North-south- to N. 20° W.-trending faults and fractures appear to be the result of east-west extension during the time of extrusion of the Boring Lava (Beeson and Moran, 1979). The timing of Boring volcanism is very imperfectly known, but it may have begun as early as latest Miocene 8(?) m.y. B.P., if extrusion of these diktytaxitic lavas was concurrent with similar volcanism in the Central Cascades (e.g., Taylor, 1968, 1981; Priest and others, 1981). Beeson and Moran (1979) speculate that the Boring-type lavas which have, in part, reversed polarity were erupted about 3 m.y. B.P. They also point out that Boring-type lavas are tilted 10° to the east toward the Hood River fault. Because lavas K-Ar dated at 3.0 m.y. B.P. occur at Lookout Mountain at the crest of the upthrown block of the Hood River fault (Wise, 1969), it seems probable that the tilted Boring-type lavas in the Hood River Valley are also older than the post-3 m.y. B.P. fault.

East-west extension, which localized small faults and fractures filled by the Boring-age dikes, probably continued to produce deformation in the period after 3 m.y. B.P. The north-south-trending Hood River fault is probably younger than 3.0 m.y., as discussed above. It follows that subsidence of the Mount Hood block is also, at least in part, younger than 3 m.y., since the Hood River fault is the eastern boundary of the block. No deformation of Holocene deposits by north-south-trending faults in the Mount Hood area is known to the writer. North-south alignment of youthful cinder cones and dikes north of Mount Hood (J.W. Hook, 1980, personal communication; Beeson and others, in preparation), however, suggests that east-west extension is probably continuing.

Structural interpretation

On the basis of overall structural patterns in the northern Cascades of Oregon, Venkatakrishnan and others (1980) postulate that the Neogene stress regime is principally horizontal compression, with the major compressive stress oriented north-northwest. In this model, the intermediate stress axis is vertical, and the minimum stress axis is oriented approximately east-west. This could account for the northwest-trending, right-lateral wrench faults and north- to north-northwest-trending normal faults as well as the northeast-trending folds and faults. Withdrawal of magma and thermal weakening associated with Mount Hood volcanism may have concentrated extensional faulting and resultant graben formation in the vicinity of Mount Hood. Loading of the crust by the volcanic edifice at Mount Hood and earlier

volcanoes could also account for much of the subsidence of the Mount Hood block (Williams and others, 1982).

Most favorable structures for geothermal resources

It is well known that many geothermal systems are controlled by some form of fracture permeability (e.g., Basin and Range hydrothermal systems such as at Beowawe, Nevada). Steeply dipping zones of sheared or fractured brittle rocks can allow meteoric water to circulate into thermal zones. In areas within the High Cascade heat-flow anomaly around Mount Hood, gradients of about 60°-70° C/km can be expected (Blackwell and others, 1978; Blackwell and Steele, 1979; Blackwell and others, this volume). Meteoric water would have to circulate to a depth of at least 2.71 km (8,900 ft) to reach 200° C.

Faults with high-angle dips and fractured zones unsealed by secondary minerals or high confining pressure occurring within the High Cascades heat-flow anomaly of Steele and others (this volume) would be good targets. The north- to N. 20° W.-trending faults which show evidence of movement in latest Pliocene time or later are probably the best targets. These faults are subparallel to the principal regional compressive stress and are generally of youthful age. One of the most outstanding examples of these faults is the Hood River fault on the east side of Mount Hood (Figure 1). This fault occurs on the edge of the High Cascade heat-flow anomaly (Blackwell and others, 1978; Steele and others, this volume), and its movement is probably younger than 3 m.y. (see previous section). A north-trending alignment of youthful cinder cones and lineaments on the north side of Mount Hood through Red Hill may be another promising fracture or fault zone (J.W. Hook, 1980, personal communication).

Northwest-trending faults may also be good targets where there is evidence of youthful movement and if there are factors present which tend to mitigate their position at an angle to the major compressive stress. The regional north-northwest compressive stress would tend to close up these faults, but the following factors might tend to increase their vertical permeability:

1. Intersection by other faults, particularly the north-south-trending faults.
2. Occurrence in unusually brittle and unreactive rocks, such as silicic plutonic rocks (e.g., the Laurel Hill and Still Creek plutons) or the Columbia River Basalt Group.
3. In fault zones with strike-slip components of movement such as the Salmon River or Clackamas River zones (Figure 1), large deviations in strike can produce "pressure shadows" behind locked segments of the faults (Figure 6). Such pressure shadows in en echelon strike-slip faults of the Mother Lode Gold District of the western Sierra Nevada in California have localized deep-seated (hypothermal) hydrothermal ore deposits (Lindgren, 1933).

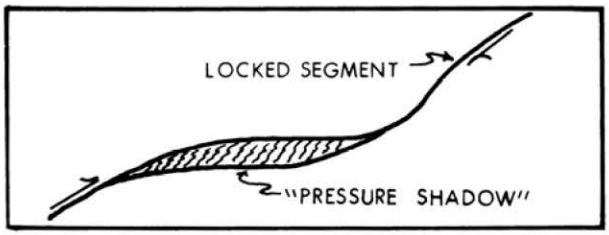

Figure 6. Illustration of the way in which a right-lateral strike-slip fault can have areas of low tectonic stress ("pressure shadows") behind locked segments. Pressure shadows may occur in oblique-slip faults as well.

The northeast-trending structures are chiefly folds and low-angle thrust faults which probably lack large zones of vertical permeability. Any fracture permeability caused by these structures may be sealed up, since they are thought to be older than north- and northwest-trending structures in the area (Beeson and Moran, 1979; Beeson and others, in preparation).

GEOTHERMAL RESERVOIR CHARACTERISTICS OF THE COLUMBIA RIVER BASALT GROUP

If permeable, the Columbia River Basalt Group could serve as a major stratiform geothermal reservoir rock in the Mount Hood area. Although no significant quantities of thermal water were recovered from 485 m (1,590 ft) of Columbia River Basalt Group intercepted in thermal zones of OMF-7A and OMF-1, diamond core from OMF-7A indicated that there may be very significant fracture permeability in these rocks at depths of 1 km (0.6 mi) or more (Priest and others, this volume). Meteoric water probably failed to reach the basalts at Old Maid Flat because of impermeability in highly altered overlying andesitic rocks of the Rhododendron Formation (Priest and others, this volume). Where they intercept the basalts in thermal zones, steeply dipping plutonic contacts and fault or fracture zones may provide conduits for deeply circulating meteoric water which could be stored in the basalts (Priest and others, this volume). Areas which may provide these characteristics are the contact zones of the Still Creek or Laurel Hill plutons, if the basalts are deep enough at these contacts to be at high temperature. Unfortunately, Couch and Gemperle (1979) have estimated from gravity data that the elevation of the Columbia River Basalt Group near these plutons is not greatly different from that of the topographic surface (i.e., within about 609 m [2,000 ft] of the surface). This estimate, however, is based on regional gravity reductions with many uncertain assumptions about rock density. For instance, at Old Maid Flat, where the gravity-predicted elevation of the top of the basalt is at about 800 m (2,625 ft) above sea level, the actual top of the basalt is at about 308 m (1,010 ft) below sea level. Also, the northwest-trending fault at Old Maid Flat may persist southeast to the Still Creek pluton (J. W. Hook, 1980, personal communication). If this is the case, then the basalt may be offset downward on this fault by as much as 400 m (1,300 ft) in the vicinity of the Still Creek plutonic contact (Priest and others, this volume). The combination of tectonic fractures and cooling and unloading fractures in the plutonic rocks could provide ideal pathways for meteoric waters to reach the basalt at depth. A detailed mapping and drilling program adjacent to the Still Creek and Laurel Hill plutonic contacts is necessary to test this hypothesis.

GEOTHERMAL RESOURCES OF THE MOUNT HOOD VOLCANO

The geothermal resource potential of the Mount Hood volcano is discussed in detail by Steele and others (this volume). Their results are based on temperature and hydro-

logic data from 25 wells around the flanks of Mount Hood. Important conclusions from their paper include the following:

1. No large, shallow magma chamber exists beneath Mount Hood (no chamber greater than 4-6 km [2.4-3.6 mi] in diameter or less than 3 km [1.8 mi] in depth).
2. A small, deeply buried "hot zone," 2-3 km (1.2-1.8 mi) in diameter, may exist beneath the volcano.
3. A small necklike magma conduit has probably existed in the central axis of Mount Hood throughout much of its existence.
4. Factors 2 and 3 above may account for increase of heat flow from the regional value of 80 mW/m^2 at 12 km (7.5 mi) from the volcano to 130 to 150 mW/m^2 at 5-8 km (3-4.8 mi) from the apex.
5. There is little evidence of significant vertical permeability in rocks encountered below about 200 m (660 ft) in the Pucci Chairlift hole, but significant lateral permeability does exist in some stratigraphic units. For example, significant quantities of fluid were encountered in various parts of the Pucci Chairlift hole between 1,100 and 1,200 m (3,600 and 4,000 ft) including thermal water adequate for direct use. The static water level in the well, however, tended to fall as the well was drilled, indicating significant underpressure in deeper aquifers and, therefore, little vertical permeability. These data may not apply to other areas on the volcano, where holes have encountered high vertical permeability to depths of at least 300 m (990 ft).
6. The largely undrilled north and east flanks may be favorable areas for hydrothermal circulation systems. Additional drilling at the McGee Creek hole on the north-northwest side of the mountain and near the vent for the Parkdale flow on the north-northeast side of Mount Hood is recommended.
7. Deepening of the McGee Creek hole could encounter electrical-grade fluid in excess of 200° C at 3 km (1.8 mi), if observed gradients project to depth and permeable rocks are present.

RELATION OF VOLCANISM TO TECTONICS

Blackwell and others (1978) have shown that the combination of high heat flow in the High Cascades and sharply lower heat flow in the Western Cascades of Oregon is best explained by a subduction-zone model. Subduction of cool oceanic lithosphere can depress heat flow west of the High Cascades, while mantle melting from subduction may produce high heat and volcanism along the High Cascade axis. Tectonic models of Atwater (1970) and Atwater and Molnar (1973) also agree with this model, although the Oregon High Cascades are probably in the dying phases of active subduction. Petrologic interpretations by White and McBirney (1978), however, suggest that subduction may not have produced the High Cascade volcanoes. Nevertheless, the location of composite cones such as Mount Hood and the rest of the High Cascade volcanoes in a north-south-trending line and presence of a classic subduction zone heat-flow pattern are compelling evidence that the High Cascades are at least partly the result of subduction processes. Similar volcanism during Rhododendron (middle Miocene) and late Miocene time suggests earlier subduction, although the focus of volcanism was somewhat west of the High Cascade axis.

One complication to this simple model is the apparent shift of volcanism toward more mafic compositions in latest Miocene and later times (e.g., the Boring Lava and mafic lavas in Wise's [1969] "late Pliocene" unit). Priest and others (1981, and in preparation) argue that this shift to more mafic volcanism in the Oregon High Cascades may correlate with increasing influence of extensional deformation similar to Basin and Range tectonism in latest Miocene (10-8 m.y. B.P.) and later times. This change in volcanism may correlate with postulated changes in the plate tectonic environment 10-8 m.y. ago (e.g., Atwater, 1970; Atwater and Molnar, 1973; Zoback and Thompson, 1978; Hammond, 1979; Davis, 1981).

Another complication is the decrease in amplitude of the High Cascade heat-flow anomaly in the vicinity of the Clackamas River. Steele and others (this volume) show that regional heat flow in the High Cascade anomaly around Mount Hood is about 80 mW/m^2, similar to the anomaly in Washington, while the anomaly south of the Clackamas River is about 100 mW/m^2. White and McBirney (1978) point out that the volume of Quaternary volcanic rocks in central Washington is less than in the central Oregon Cascades, primarily because of a sharp decrease in the volume of basaltic volcanism. The same is true of the predominantly andesite Neogene volcanic rocks of the Mount Hood area north of the Clackamas River when compared to the voluminous mafic Neogene volcanic pile of the central Cascades south of the river. It may be that these changes in both basaltic volcanism and heat flow near the Clackamas River are related. More basaltic volcanism and higher heat flow in the central High Cascades south of the Clackamas River may be the result of increased partial melting from extensional tectonic processes similar to Basin and Range spreading processes. The fact that the Clackamas River area is a major right-lateral wrench-fault zone (Beeson and Moran, 1979; Beeson and others, in preparation) suggests that this area may be a boundary between more extended crust in the central Cascades and less extended crust in the Mount Hood area.

RECOMMENDATIONS AND CONCLUSIONS

The Mount Hood area has been the site of volcanism and hydrothermal activity since at least 16 m.y. ago. The Mount Hood volcano has been active for about the last 700,000 years and will probably continue to be active in the future. The volcano has active fumaroles at the apex and probably has a small conduit of molten to partially molten magma throughout its central axis. There is, however, no evidence of a large shallow magma chamber beneath Mount Hood, although small high-level heat sources may exist in unexplored parts of the volcano. Important areas in need of exploration are the north and east flanks, particularly near the vent of the Parkdale flow and in the Red Hill area. Deepening of the McGee Creek hole, where an anomalously high gradient was encountered, would be a very cost-effective exploration step which might reveal electrical-quality geothermal fluids, if permeable rocks and similar temperature gradients occur to depths of 3 km (1.8 mi). If innovative drilling techniques which mitigate severe caving problems in Quaternary volcanic rocks of the volcano can be developed, angle or directional drilling toward the axis of Mount Hood from flank areas might reach moderate- to high-temperature fluids.

In areas removed from the Mount Hood volcano, drilling should be concentrated where heat flow and rock permeability are at a maximum. Exploration should be focused

on the High Cascade heat-flow anomaly where the presence of one or more of the following factors may increase permeability:

1. Columbia River basalt or phaneritic plutonic rocks in the thermal zone.
2. North-northwest- and north-south-trending faults (e.g., the Hood River fault) or intersections of these faults with other faults, particularly northwest-trending faults.
3. "Pressure shadows" (Figure 6) of low tectonic pressure behind locked portions of faults with some strike-slip movement (e.g., the Clackamas River fault zone).

Further drilling and geologic mapping in key areas such as the north and east flanks of Mount Hood and at intersections of major faults with plutonic contacts (e.g., the southeast continuation of the mapped fault at Old Maid Flat) may reveal not only additional direct-use resources, as at the Pucci well, but also high-temperature fluids capable of electrical generation. Exploration holes in the young Mount Hood volcanic rocks should be deeper than 300 m (990 ft) to escape the effects of active shallow ground-water systems.

Detailed geophysical surveys should also be conducted to outline possible hydrothermal fluids and high-level magma bodies. Seismic, gravity, electrical, and most importantly, heat-flow measurements should help to constrain possible drilling targets.

ACKNOWLEDGMENTS

This paper is largely a summary of the other excellent papers in this volume. David L. Williams of the U.S. Geological Survey and Marvin H. Beeson and Paul E. Hammond of Portland State University provided good critical reviews of the paper. The U.S. Department of Energy provided most of the financial support for the project.

REFERENCES CITED

Allen, J.E., 1966, The Cascade Range volcano-tectonic depression of Oregon, *in* Lunar Geological Field Conference, Bend, Oreg., August 1965, transactions: Oregon Department of Geology and Mineral Industries, in cooperation with Oregon Division of Planning and Development, p. 21-23.

— — — 1975, Volcanoes of the Portland area, Oregon: Oregon Department of Geology and Mineral Industries, Ore Bin, v. 37, no. 9, p. 145-157.

Anderson, J.L., 1978, The stratigraphy and structure of the Columbia River Basalt in the Clackamas River drainage: Portland, Oreg., Portland State University master's thesis, 136 p.

— — — 1980, Pomona Member of the Columbia River Basalt Group: an intracanyon flow in the Columbia River Gorge, Oregon: Oregon Department of Geology and Mineral Industries, Oregon Geology, v. 42, no. 12, p. 195-199.

Armentrout, J.M., 1981, Correlation and ages of Cenozoic chronostratigraphic units in Oregon and Washington, *in* Armentrout, J.M., ed., Pacific Northwest Cenozoic biostratigraphy: Boulder, Colo., Geological Society of America Special Paper 184, p. 137-148.

Atwater, T., 1970, Implications of plate tectonics for the Cenozoic tectonic evolution of western North America: Geological Society of America Bulletin, v. 81, no. 12, p. 3513-3535.

Atwater, T., and Molnar, P., 1973, Relative motion of the Pacific and North American Plates deduced from sea-floor spreading in the Atlantic, Indian, and South Pacific Oceans, *in* Kovach, R.L., and Nur, A., eds., Tectonic problems of the San Andreas fault system, Conference Proceedings: Stanford, Calif., Stanford University Publications in Geological Science, v. 13, p. 136-148.

Avramenko, W., 1981, Volcanism and structure in the vicinity of Echo Mountain, central Oregon Cascade Range: Eugene, Ore., University of Oregon master's thesis, 156 p.

Ayres, F.D., and Creswell, A.E., 1951, The Mount Hood fumaroles: Mazama, v. 33, no. 13, p. 33-40.

Beeson, M.H., and Moran, M.R., 1979, Stratigraphy and structure of the Columbia River Basalt Group in the Cascade Range, Oregon, *in* Hull, D.A., investigator, and Riccio, J.F., ed., Geothermal resource assessment of Mount Hood: Oregon Department of Geology and Mineral Industries Open-File Report O-79-8, p. 5-77

Beeson, M.H., Moran, M.R., Anderson, J.L., and Vogt, B.F., in preparation, Stratigraphy and structure of the Columbia River Basalt Group in the Cascade Range, Oregon.

Bikerman, M., 1970, K-Ar ages of Laurel Hill pluton and dike, Oregon: Oregon Department of Geology and Mineral Industries, Ore Bin, v. 32, no. 11, p. 211-215.

Blackwell, D.D., Hull, D.A., Bowen, R.G., and Steele, J.L., 1978, Heat flow of Oregon: Oregon Department of Geology and Mineral Industries Special Paper 4, 42 p.

Blackwell, D.D., and Steele, J.L., 1979, Heat flow modeling of the Mount Hood Volcano, Oregon, *in* Hull, D.A., investigator, and Riccio, J.F., ed., Geothermal resource assessment of Mount Hood: Oregon Department of Geology and Mineral Industries Open-File Report O-79-8, p. 190-264.

Couch, R., and Gemperle, M., 1979, Gravity measurements in the area of Mount Hood, Oregon, *in* Hull, D.A., investigator, and Riccio, J.F., ed., Geothermal resource assessment of Mount Hood, Oregon: Oregon Department of Geology and Mineral Industries Open-File Report O-79-8, p. 137-188.

Crandell, D.R., 1980, Recent eruptive history of Mount Hood, Oregon, and potential hazards from future eruptions: U.S. Geological Survey Bulletin 1492, 81 p.

Davis, G.A., 1981, Late Cenozoic tectonics of the Pacific Northwest with special reference to the Columbia Plateau: Washington Public Power Supply System Final Safety Analysis Report, Appendix 2.5 N, draft, preliminary, revised March 30, 1981, 44 p.

Flaherty, G.M., 1981, The Western Cascade-High Cascade transition in the McKenzie Bridge area, central Oregon Cascade Range: Eugene, Oreg., University of Oregon master's thesis, 178 p.

Flanagan, G., and Williams, D.L., 1982, A magnetic investigation of Mount Hood, Oregon: Journal of Geophysical Research, v. 87, no. B4, p. 2804-2814.

Friedman, J.D., and Frank, D., 1977, Structural and heat-flow implications of infrared anomalies at Mount Hood, Oregon: U.S. Geological Survey Open-File Report 77-599, 29 p.

Friedman, J.D., Williams, D.L., and Frank, D., 1982, Structural and heat flow implication of infrared anomalies at Mount Hood, Oregon, 1972-1977: Journal of Geophysical Research, v. 87, no. B4, p. 2793-2803.

Goldstein, N.E., Mozley, E., and Wilt, M., 1982, Interpretation of shallow electrical features from electromagnetic and magnetotelluric surveys at Mount Hood, Oregon: Journal of Geophysical Research, v. 87, no. B4, p. 2815-2828.

Hammond, P.E., 1979, A tectonic model for evolution of the Cascade Range, *in* Armentrout, J.M., Cole, M.R., and Terbest, H., Jr., eds., Cenozoic palcogcography of the western United States: Pacific Section, Society of Economic Paleontologists and Mineralogists, p. 219-237.

Hammond, P.E., Anderson, J.L., and Manning, K.J., 1980, Guide to the geology of the upper Clackamas and North Santiam Rivers area, northern Oregon Cascade Range, *in* Oles, K.F., Johnson, J.G., Niem, A.R., and Niem, W.A., eds., Geologic field trips in western Oregon and southwestern Washington: Oregon Department of Geology and Mineral Industries Bulletin 101, p. 133-167.

Kohler, W.M., Healy, J.H., and Wegener, S.S., in preparation, Upper crustal structure of the Mount Hood, Oregon, region as revealed by time-term analysis.

Kuno, H., 1966, Lateral variation of basalt magma type across

continental margins and island arcs: Bulletin Volcanologique, v. 29, p. 195-222.

Lindgren, W., 1933, Mineral deposits: New York, McGraw-Hill, p. 849-850.

Miyashiro, A., 1974, Volcanic rock series in island arcs and active continental margins: American Journal of Science, v. 274, p. 321-355.

Naslund, H.R., 1977, The geology of the Hyatt Reservoir and Surveyor Mountain quadrangles, Oregon: Eugene, Oreg., University of Oregon master's thesis, 127 p.

Priest, G.R., Woller, N.M., and Evans, S., 1981, Late Cenozoic modification of calc-alkalic volcanism, central Oregon Cascades [abs.]: American Academy for the Advancement of Science Abstracts with Programs, 1981 Pacific Division meeting, p. 32.

— — — in preparation, Overview of the geology and geothermal resources of the Central Oregon Cascades, *in* Priest, G.R., and Vogt, B.F., eds., Geology and geothermal resources of the central Cascades, Oregon: Department of Geology and Mineral Industries Special Paper 15.

Swanson, D.A., Anderson, J.L., Camp, V.E., Hooper, P.R., Taubeneck, W.H., and Wright, T.L., 1981, Reconnaissance geologic map of the Columbia River Basalt Group, northern Oregon and western Idaho: U.S. Geological Survey Open-File Report 81-797, 32 p., scale 1:250,000, 5 sheets.

Swanson, D.A., Wright, T.L., Hooper, P.R., and Bentley, R.D., 1979, Revisions in stratigraphic nomenclature of the Columbia River Basalt Group: U.S. Geological Survey Bulletin 1457-G, 56 p.

Taylor, E.M., 1968, Roadside geology, Santiam and McKenzie Pass Highways, Oregon, *in* Dole, H.M., ed., Andesite Conference guidebook: Oregon Department of Geology and Mineral Industries Bulletin 62, p. 3-33.

— — — 1981, Central High Cascade roadside geology, Bend, Sisters, McKenzie Pass, and Santiam Pass, Oregon, *in* Johnston, D.A., and Donnelly-Nolan, J., eds., Guides to some volcanic terranes in Washington, Idaho, Oregon, and northern California: U.S. Geological Survey Circular 838, p. 55-58.

Trimble, D.E., 1963, Geology of Portland, Oregon, and adjacent areas: U.S. Geological Survey Bulletin 1119, 119 p.

Venkatakrishnan, R., Bond, J.G., and Kauffman, J.D., 1980, Geological linears of the northern part of the Cascade Range, Oregon: Oregon Department of Geology and Mineral Industries Special Paper 12, 25 p.

Weaver, C.S., Green, S.M., and Iyer, H.M., 1982, Seismicity of Mount Hood and structure as determined from teleseismic *P* wave delay studies: Journal of Geophysical Research, v. 87, no. B4, p. 2782-2792.

Wells, F.G., and Peck, D.L., 1961, Geologic map of Oregon west of the 121st meridian: U.S. Geological Survey Miscellaneous Investigations Map I-325, scale 1:500,000.

Westhusing, J.K., 1973, Reconnaissance surveys of near-event seismic activity in the volcanoes of the Cascade Range, Oregon: Bulletin Volcanologique, v. 37, p. 258-286.

White, D.M., 1979, Geology and geochemistry of Mt. Hood volcano, *in* Hull, D.A., investigator, and Riccio, J.F., ed., Geothermal resource assessment of Mount Hood: Oregon Department of Geology and Mineral Industries Open-File Report O-79-8, p. 78-136.

White, C.M., 1980a, Geology and geochemistry of Mt. Hood volcano: Oregon Department of Geology and Mineral Industries Special Paper 8, 26 p.

— — — 1980b, Geology of the Breitenbush Hot Springs quadrangle, Oregon: Oregon Department of Geology and Mineral Industries Special Paper 9, 26 p.

White, C.M., and McBirney, A.R., 1978, Some quantitative aspects of orogenic volcanism in the Oregon Cascades, *in* Smith, R.B., and Eaton, G.P., eds., Cenozoic tectonics and regional geophysics of the western Cordillera: Boulder, Colo., Geological Society of America Memoir 152, p. 51-92.

Williams, D.L., Hull, D.A., Ackerman, H.D., and Beeson, M.H., 1982, The Mt. Hood region: volcanic history, structure, and geothermal energy potential: Journal of Geophysical Research, v. 87, no. B4, p. 2767-2781.

Wise, W.S., 1961, The geology and mineralogy of the Wind River area, Washington: Baltimore, Md., Johns Hopkins University doctoral dissertation, 258 p.

— — — 1968, Geology of the Mount Hood volcano: International Upper Mantle Project Science Report 16-5; and *in* Dole, H.M., ed., Andesite Conference guidebook: Oregon Department of Geology and Mineral Industries Bulletin 62, p. 81-98.

— — — 1969, Geology and petrology of the Mt. Hood area: a study of High Cascades volcanism: Geological Society of America Bulletin, v. 80, no. 6, p. 969-1006.

Zoback, M.L., and Thompson, G.A., 1978, Basin and Range rifting in northern Nevada: Clues from a mid-Miocene rift and its subsequent offsets: Geology, v. 6, no. 2, p. 111-116.

GEOLOGY, GEOCHEMISTRY, AND GEOTHERMAL RESOURCES OF THE OLD MAID FLAT AREA, OREGON

By George R. Priest, Oregon Department of Geology and Mineral Industries, and Marvin H. Beeson, Marshall W. Gannett, and Dulcy A. Berri, Department of Earth Sciences, Portland State University, Portland, Oregon 97207

ABSTRACT

Two deep drill holes, OMF-1 (1,220 m [4,002 ft]) and OMF-7A (1,837 m [6,027 ft]) were drilled into open-fractured basalt of the Columbia River Basalt Group near a late Pliocene fault with a probable dip-slip offset of at least 400 m (1,300 ft). Although temperatures near or in excess of 100° C were encountered in both holes, no significant quantities of thermal water were found. These results suggest that further drilling at Old Maid Flat may have low probability of success.

Detailed chemical and mineralogical analysis of well cuttings and surface outcrops allowed correlation of stratigraphic units. Analysis of samples of the Rhododendron Formation gave the first comprehensive chemical and mineralogical characterization of this unit. At least 183 m (600 ft) of a distinctive megacrystic two-pyroxene andesite unit (the Last Chance andesite), K-Ar dated at 10.7±0.5 m.y. B.P., overlies the Rhododendron Formation; the lower part of the Rhododendron Formation interfingers with Wanapum Basalt of the Columbia River Basalt Group. The Last Chance andesite is distinctly more mafic than most of the Rhododendron rocks and appears to be the first indication of a gradual shift to increasingly mafic volcanism which occurred in the latest Miocene. Eruption of small volumes of olivine basalt in the late Pliocene was the culmination of this overall trend toward more mafic volcanism.

Intrusion of numerous biotite-bearing hornblende microquartz diorite sills (K-Ar age of 9.3±0.87 m.y.) into the Rhododendron Formation and older units occurred at roughly the same time as widespread laumontite-grade metamorphism and intrusion of large hornblende diorite plutons of the Laurel Hill (K-Ar ages of 11.6-8.0 m.y.) and Still Creek intrusions. Chemical coherence of the intrusives with the Rhododendron rocks suggests that they may be part of a genetically related magmatic series.

INTRODUCTION

Exploration at Old Maid Flat was begun in 1978 by the Oregon Department of Geology and Mineral Industries (DOGAMI) and Northwest Geothermal Corporation (NWGC), an affiliate of Northwest Natural Gas Corporation, with support from the U.S. Energy Research and Development Administration (ERDA, now the U.S. Department of Energy [USDOE]). A deep drill hole (OMF-1) was drilled to 1,220 m (4,002 ft), and four shallower wells were drilled the same season in 1978 (Figure 1) (see Covert and Meyer, 1979). Flow testing of the OMF-1 well revealed essentially no significant water from the thermal zone of the well, although the bottom-hole temperature was 83° C and the gradient was approximately 67° C/km (Blackwell and Steele, 1979). Interception of highly fractured basalt of the Columbia River Basalt Group near the thermal zone, however, suggested that if water were to reach the basalt through some high-angle fault, sufficient hot water for space-heating applications might be obtained.

John W. Hook (consulting geologist) and Jack Meyer (geologist, NWGC) located a lineation which appeared to be controlled by a high-angle shear zone trending northwest through the upper Sandy River drainage parallel to Yocum Ridge at Old Maid Flat (Figure 1). Outcrops of the shear zone on both the north and south sides of Last Chance Mountain, as well as termination of lithologic units across the zone, provided good evidence for its existence. A second deep well (OMF-7A) was then sited on the northeast side of the projection of this shear zone into the valley of the Muddy Fork of the Sandy River (Figure 1).

The OMF-7A well was completed to 1,837 m (6,027 ft) in the fall of 1980 by USDOE (see USDOE, 1980 and 1981). Geological management and analyses of cores, cuttings, and nearby surface outcrops were conducted by DOGAMI. Analysis of alteration mineralogy in OMF-7A was subcontracted by DOGAMI to Michael J. Holdaway of Southern Methodist University, Dallas, Texas (see Holdaway and Bussey, this volume), while geophysical analysis of the well was subcontracted to David D. Blackwell (see Blackwell and others, this volume). Marvin H. Beeson and Marshall W. Gannett of Portland State University picked cutting samples and chemically analyzed most units from both wells (see data tables of Appendices A and B). George R. Priest of DOGAMI supervised preliminary work on the drill hole and completed analysis of surface geology in the area. All K-Ar dates in OMF-7A and adjacent outcrops were determined by Stanley Evans of the University of Utah Research Institute, Salt Lake City, Utah. The complete K-Ar data set will be published in an upcoming issue of *Isochron/West,* although data are given here in Table 1.

Flow testing of the OMF-7A well shortly after completion revealed less than 3.8 L/min (1.0 gal/min) flow of water from the thermal zone, although a good overall gradient (63° C/km) and adequate temperatures (100°-119° C) were encountered. Analyses of water samples from the well are given in Appendix C, along with geothermometric temperatures. No discussion of the water chemistry is warranted, since drilling water overwhelmed the formation water because of low flow rates.

No obvious vertical offset of Columbia River Basalt Group units could be demonstrated between the OMF-1 and OMF-7A holes below 244 m (800 ft), although numerous slickensided surfaces in cores and cuttings indicate that some faulting occurred through parts of both wells. It appears unlikely that OMF-7A intersected the main fault zone within the Columbia River basalt or within any part of the

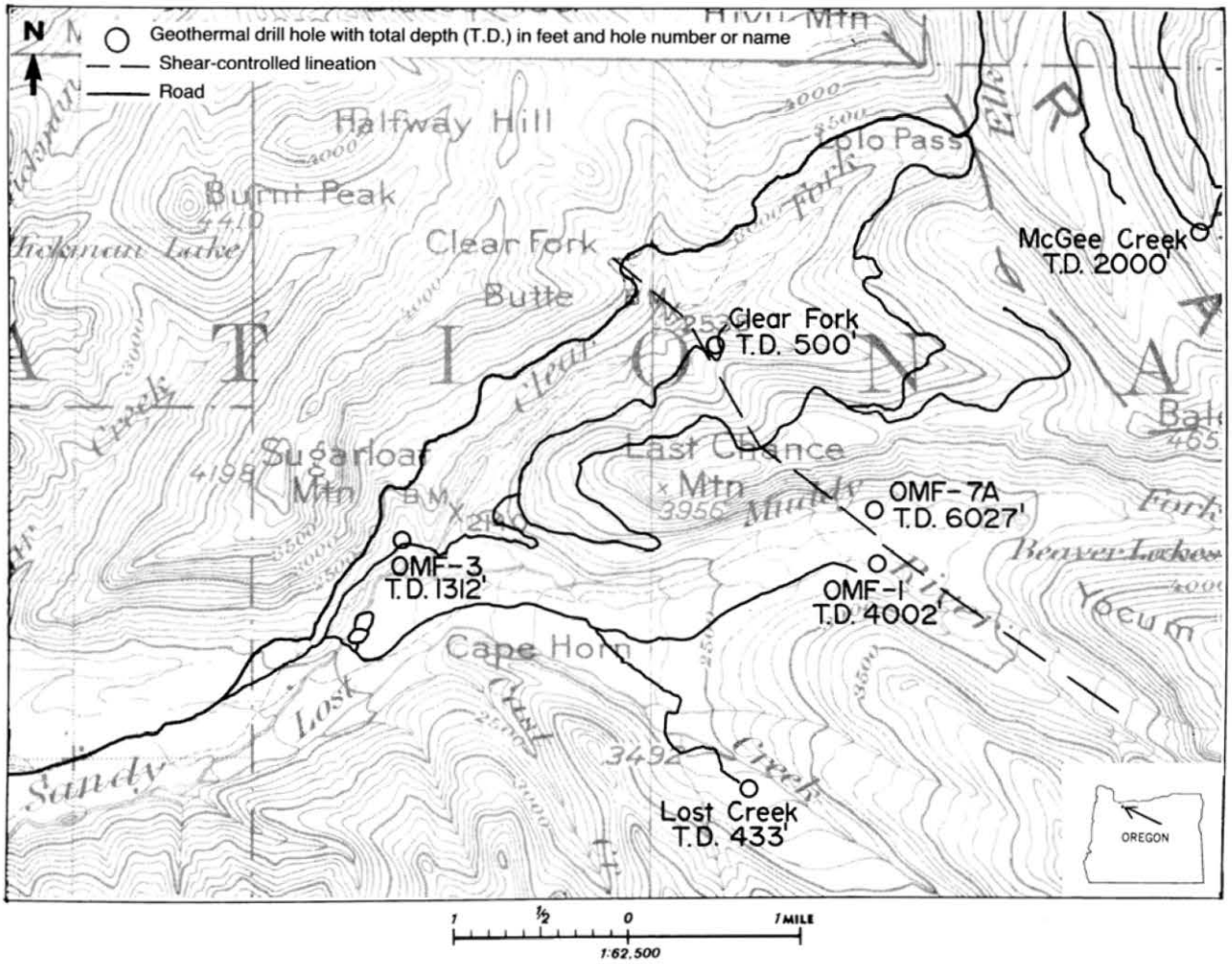

Figure 1. Geothermal drill holes in the Old Maid Flat area with location of a major lineation which was the target of OMF-7A.

Table 1. *K-Ar ages of rocks in the Old Maid Flat area, Oregon*[1]

Sample no.[5]	Location	Unit	Age (m.y.)	Material dated
OMF-7A-3750[2]	3,750-ft depth in OMF-7A	Hornblende microquartz diorite	9.3±0.9	Fresh hornblende
MH-10[2]	T. 2 S., R. 8 E., 15BDCC	Upper Rhododendron	10.6±0.5	Lightly altered whole rock
MH-19[2]	T. 2 S., R. 8 E., 16DBBA	Upper Rhododendron	9.5±2.4	Altered whole rock
MH-20[2]	T. 2 S., R. 8 E., 16DBBA	Upper Rhododendron	12.1±1.7	Altered whole rock
LCM[2]	T. 2 S., R. 8 E., 16BDBA	Last Chance andesite	10.7±0.5	Whole rock
LCM[2]	T. 2 S., R. 8 E., 16BDBA	Last Chance andesite	10.5±0.5	Whole rock
OMF-2953[3]	2,953-ft depth in OMF-1	CRBG[4]	12.2±2.0	Whole rock
OMF-3530[3]	3,530-ft depth in OMF-1	CRBG[4]	5.9±1.1	Whole rock
OMF-3970[3]	3,970-ft depth in OMF-1	Andesite	7.9±0.8	Whole rock

[1]All rocks are from the south side of Last Chance Mountain and the OMF-1 and OMF-7A drill holes.
[2]Unpublished K-Ar data of Stanley Evans, University of Utah Research Institute, Salt Lake City, Utah.
[3]Data from White (1979).
[4]CRBG = Columbia River Basalt Group.
[5]Sample localities shown in Figure 5, p. 23.

thermal zone. Lack of any evidence of lateral flow of geothermal waters from the fault zone into the highly fractured Columbia River basalt of either OMF-1 or OMF-7A suggests that there may be little chance of encountering thermal water by further drilling around this fault zone in the Old Maid Flat area.

The balance of this report summarizes the geology of the Old Maid Flat area based on detailed study of cores and cuttings of the OMF-1 and OMF-7A drill holes and on surface geologic mapping. Stratigraphic information from this study should aid future exploration in the Mount Hood area by providing quantitative chemical and mineralogical parameters to characterize igneous and metamorphic units.

ANALYTICAL METHODS

Samples were analyzed by standard instrumental neutron activation analysis (INAA) and X-ray fluorescence (XRF) methods (Tables 1-6, Appendix B). All drill cuttings were carefully picked under a binocular microscope and were at least 95 percent free of contaminants. All samples for trace-element analysis were cleaned with an ultrasonic cleaning device using distilled water.

INAA values in Tables 3, 4, 5, and 6 (Appendix B) are listed with estimated analytical errors at 1σ in parentheses next to each value. Average analytical errors at 1σ for XRF, as a percentage of the listed value, are as follows: SiO_2, 1 percent; Al_2O_3, 2 percent; FeO, 2 percent; MgO, 3-7 percent; CaO, 2 percent; Na_2O, 25-50 percent; K_2O, 2 percent; MnO, 5-20 percent; TiO_2, 3-5 percent; and P_2O_5, 3-6 percent.

The mode of phenocrystic minerals in each specimen is estimated where whole-rock or core samples were available (Tables 1 and 2, Appendix B). No volume percent is listed for most samples of cuttings.

VOLCANIC STRATIGRAPHY

A generalized stratigraphic column of the Old Maid Flat area is shown in Figure 2. Formation names used in the present study are listed together with corresponding general informal rock and time-stratigraphic units of Wise (1969). Time units used here are those of Armentrout (1981).

The oldest unit in the area is an Eocene(?) greenstone encountered in the OMF-7A well from about 1,707 m (5,600 ft) to the bottom at 1,837 m (6,027 ft) (see Figures 3 and 4; Table 3, Appendix A). Units roughly equivalent to the Eagle Creek Formation are represented by clastic rocks encountered between a major unconformity at the top of the greenstone (Figure 3) at 1,707 m (5,600 ft) and the Columbia River Basalt Group at 1,408 m (4,620 ft). This unconformity is defined by a sharp change in metamorphic grade from greenschist facies to zeolite facies (Holdaway and Bussey, this volume).

The Columbia River basalt represented in the study area is part of the Yakima Basalt Subgroup. Flows of the Prineville chemical type and of the low- and high-MgO basalt of Grande Ronde Basalt of the Columbia River Basalt Group are represented in a thick section of basalt at 783-1,259 m (2,570-4,130 ft) in OMF-7A and at 817-1,173 m (2,680-3,880 ft) in OMF-1. Had OMF-1 been drilled beyond 1,220 m (4,002 ft), it probably would have encountered additional Columbia River basalt flows beyond the interbed zone at the bottom of the well, as did OMF-7A (Figure 3). Calc-alkalic dacitic to andesitic lavas and debris flows occur in increasing

<table>
<tr><th colspan="4">Units of this study at Old Maid Flat</th><th>Wise (1969)</th></tr>
<tr><td colspan="4">Old Maid mudflow (200 yr B.P.)</td><td>Holocene mudflow</td></tr>
<tr><td colspan="4">Upper Pliocene(?) two-pyroxene andesite and hornblende dacite</td><td>Upper Pliocene volcanic rocks</td></tr>
<tr><td colspan="4">Lower Pliocene(?) megacrystic hornblende-bearing two-pyroxene andesite</td><td rowspan="3">Lower Pliocene volcanic rocks</td></tr>
<tr><td colspan="4">Miocene-Pliocene(?) two-pyroxene andesites</td></tr>
<tr><td colspan="4">Last Chance andesite (10.7±0.5 m.y.)</td></tr>
<tr><td colspan="4">Hornblende microquartz diorite</td><td>Still Creek and Laurel Hill stocks</td></tr>
<tr><td colspan="4">Rhododendron Formation</td><td>Rhododendron Formation</td></tr>
<tr><td rowspan="4">CRBG</td><td rowspan="2">Wanapum Basalt</td><td colspan="2">Priest Rapids Member(?)</td><td rowspan="4">Columbia River Basalt Group</td></tr>
<tr><td colspan="2">Frenchman Springs Member</td></tr>
<tr><td rowspan="2">Grande Ronde Basalt</td><td>High MgO</td><td></td></tr>
<tr><td>Low MgO</td><td>Prineville chemical type</td></tr>
<tr><td colspan="4">Oligocene(?) volcaniclastic rocks (Eagle Creek Formation?)</td><td rowspan="2"></td></tr>
<tr><td colspan="4">Eocene(?) greenstones</td></tr>
</table>

Figure 2. Volcanic units in the Old Maid Flat area. Columbia River Basalt Group is divided into formal formations; members; and informal high-Mg, low-Mg, and Prineville chemical types. The lower part of the Rhododendron Formation interfingers with Wanapum Basalt.

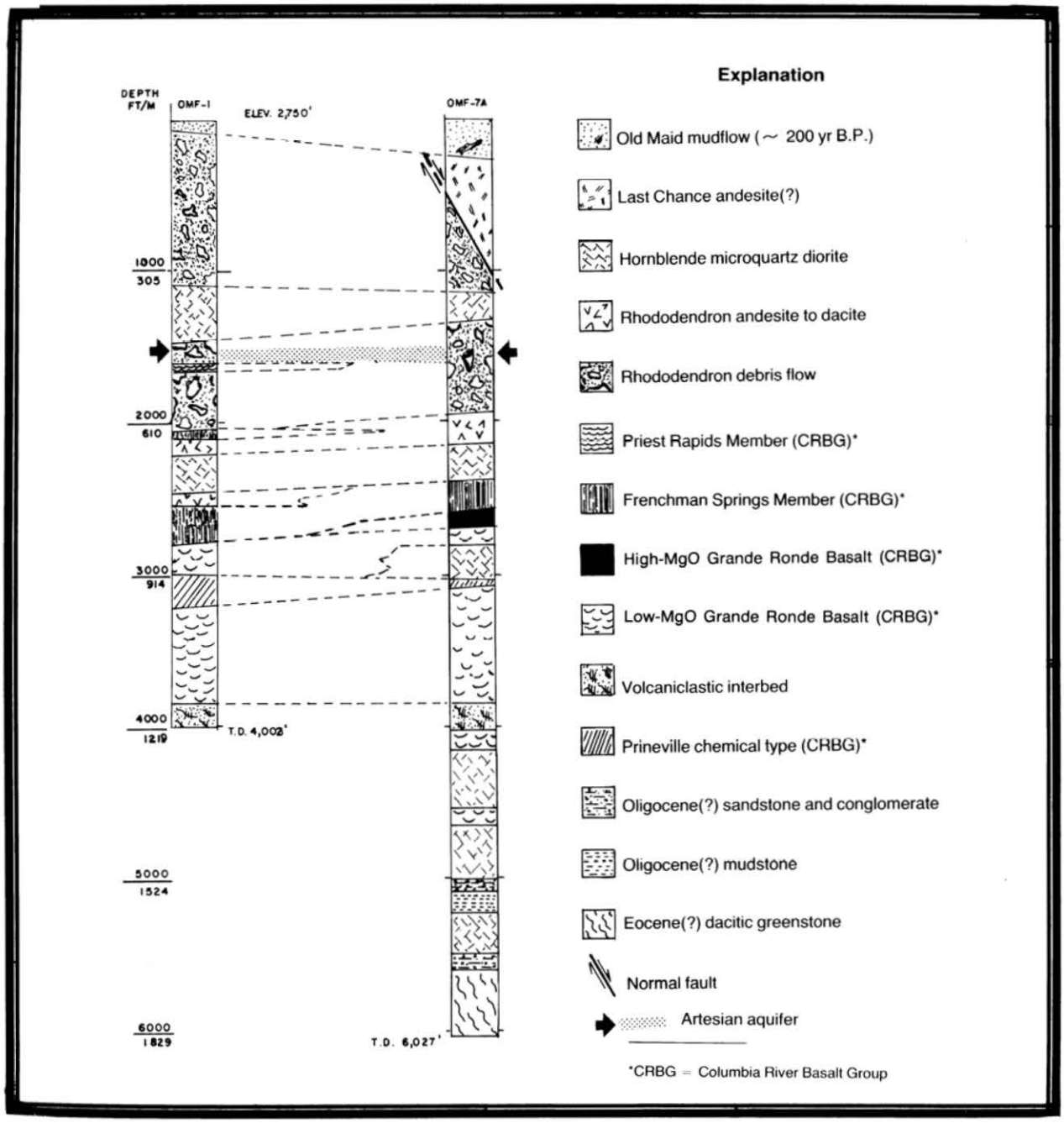

Figure 3. Generalized cross section between drill holes OMF-1 and OMF-7A. Taken from detailed logs in Appendix A.

quantities as interbeds within the overlying Wanapum Basalt; for example, between 491 and 30 m (1,610 and 100 ft) in OMF-1 and between 753 and 244 m (2,470 and 800 ft) in OMF-7A, calc-alkalic volcanic rocks of the Rhododendron Formation are the only rocks present (Figures 3 and 4; Appendix A).

Changes in hydrothermal alteration, rock chemistry, and phenocryst mineralogy help to distinguish mappable units above the Columbia River Basalt Group. An older sequence of rather silicic andesitic and hornblende-bearing dacitic lavas and debris flows occurs in the upper part of both OMF-1 and OMF-7A, as well as in other wells and outcrops in the area (Figures 3, 4, 5; Tables 2 and 3, Appendix A). These rocks are characterized by prevalence of moderate to heavy zeolitic (stilbite±laumontite) and partial to complete smectite-chlorite alteration of mafic silicate phenocrysts, abundant epiclastic volcanic material, and somewhat more silicic chemical composition compared to overlying units.

The rocks of this sequence are here grouped with the Rhododendron Formation, but it may be possible to separate them into two mappable units on the basis of alteration. No

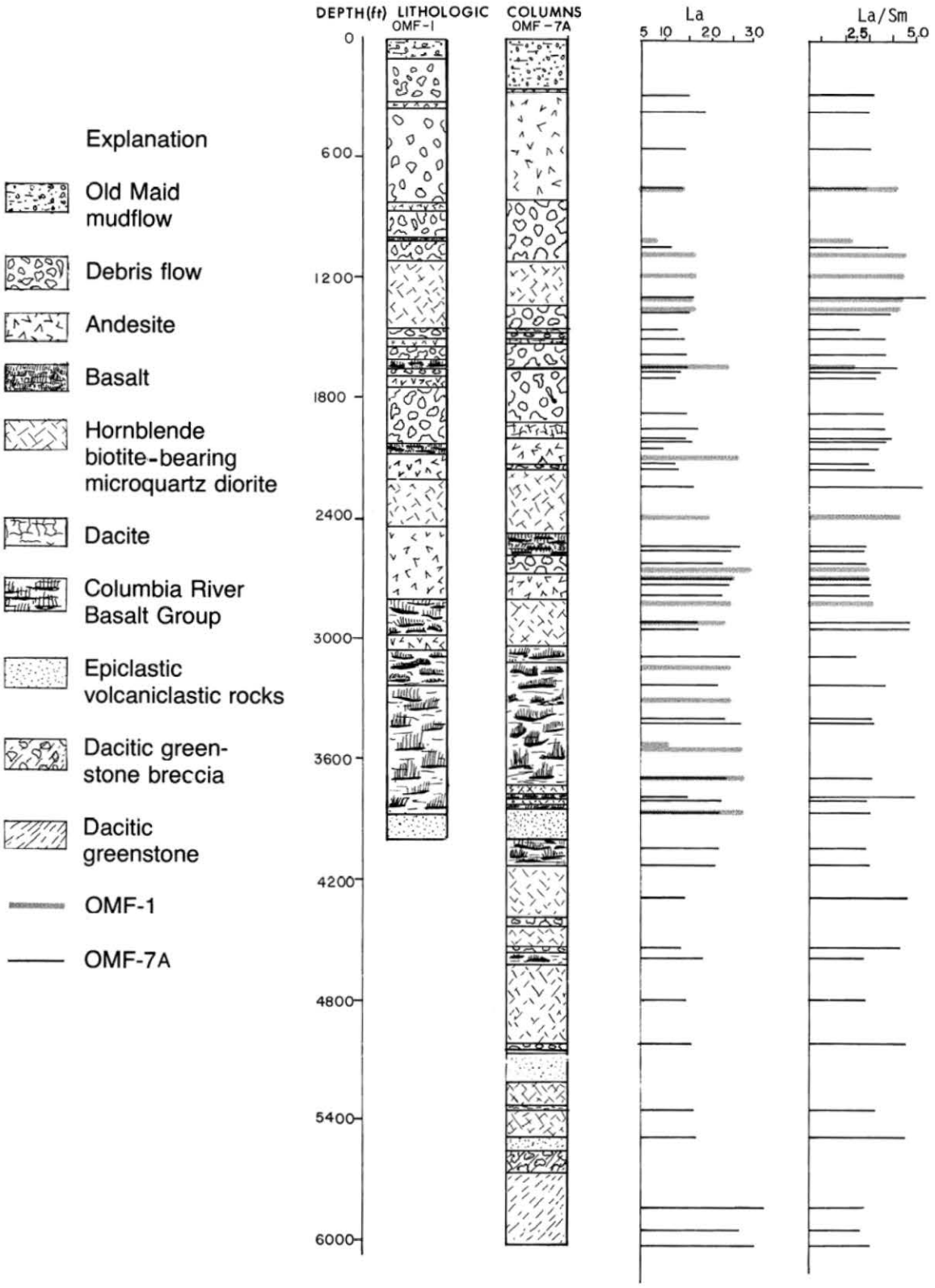

Figure 4. Geochemical correlation chart for OMF-1 and OMF-7A (both pages). Elements are in ppm, except for Fe, which is in percent.

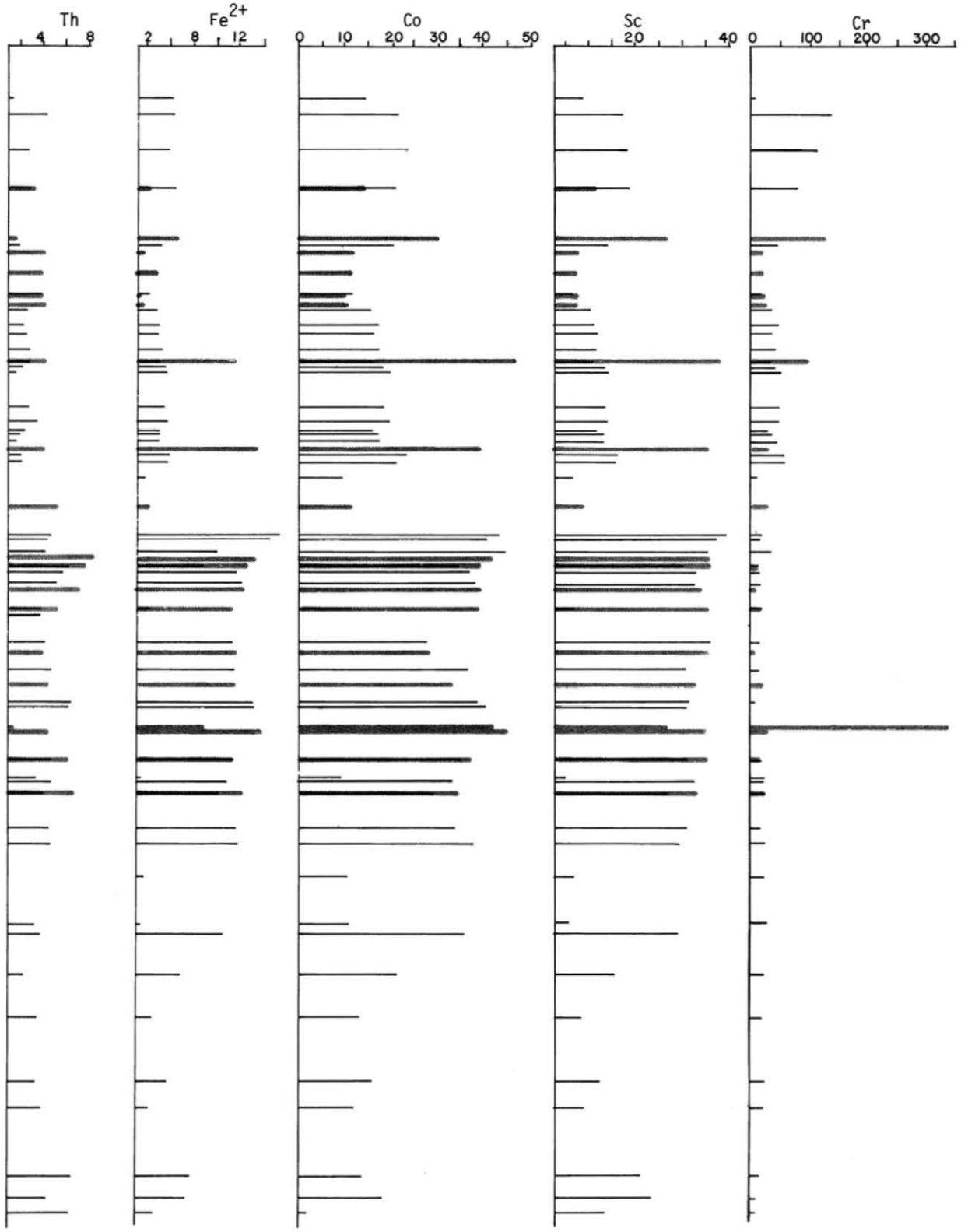
Th
4
8
Fe2+
2
8
12
Co
0
10
20
30
40
50
Sc
20
40
Cr
0
100
200
300

pyroxene survives alteration to smectite-chlorite minerals in andesite units below depths of 244 m (800 ft) in OMF-7A (Holdaway and Bussey, this volume) or below about 85 m (280 ft) in OMF-1 (Appendix A). In addition, heavy laumontite alteration affects only those rocks below about 457 m (1,500 ft) in OMF-7A (Holdaway and Bussey, this volume) and below about 244 m (800 ft) in OMF-1 (Appendix A). If these breaks in alteration occur at widespread unconformities, then presence or absence of these alteration minerals may allow mapping separate units within the Rhododendron.

A preliminary effort to do this in outcrops surrounding Old Maid Flat, however, has revealed problems with this method. First of all, many Miocene-Pliocene andesitic rocks exhibit partial alteration of orthopyroxene to smectite-chlorite. It is also common for lavas with very little alteration to be interbedded with very heavily altered debris flows and breccias of high permeability. Presence of laumontite can be determined only by X-ray diffraction, which requires substantial quantities of zeolite for detection. Samples with only small amounts of laumontite are thus impossible to identify. In spite of these problems, however, it was found in this study that if an entire sequence of andesitic volcanic rocks is free of unaltered pyroxene and full of detectable laumontite, it is certain that the rocks are part of the lower portion of the Rhododendron Formation.

The lower part of the Rhododendron may be interbedded with less altered rocks of the Priest Rapids or Frenchman Springs Members of the Wanapum Basalt (Figure 3; Tables 2 and 3, Appendix A). Apparently, the tholeiitic rocks of the Columbia River Basalt Group are not as reactive to metamorphic fluids as are the calc-alkalic rocks.

Biotite-bearing hornblende microquartz diorite sills and possibly dikes cut the lower Rhododendron Formation in both the OMF-1 and OMF-7A drill holes. Occurrence of some of the intrusives at essentially the same elevation in both wells suggests that they are sills, at least in part (Figure 3; Tables 2 and 3, Appendix A). Hornblende is relatively fresh in microquartz diorites from the lower part of OMF-7A but becomes totally altered to saponite-chlorite in the upper part of OMF-7A (Holdaway and Bussey, this volume). Either rocks from deeper parts of the hole were close enough to the hornblende stability field during metamorphism so that little reaction occurred, or lack of significant fluids prevented reactions at deeper levels. Perhaps both of these factors operated. Holdaway and Bussey (this volume) point out that the deeper hornblende may have changed composition during metamorphism or deeper sills may be from a younger intrusive than higher level sills or dikes.

A K-Ar age of 9.3±0.9 m.y. (Table 1) was obtained on fresh hornblende from a microdiorite at 1,143 m (3,750 ft) in the OMF-7A drill hole. K-Ar ages of 8.4±0.6 m.y., 8.0±0.6 m.y. (hornblende separates of Bikerman, 1970), and 11.6±1.2 m.y. (whole rock of Wise, 1969) on the Laurel Hill intrusion suggest that it is roughly contemporaneous with the microquartz diorite at Old Maid Flat. Wise (1969) suggests that the Still Creek pluton is correlative with the Laurel Hill pluton, so the ages probably apply to both. All of these K-Ar ages probably reflect low-grade hydrothermal alteration which is known to affect the intrusives at Old Maid Flat (Holdaway and Bussey, this volume).

On the basis of X-ray and petrographic analysis of cuttings from OMF-7A, Holdaway and Bussey (this volume) infer that the microquartz diorites and older units were affected by laumontite-grade metamorphism. Laumontite was not, however, identified in diamond core samples of the intrusive (Holdaway and Bussey, this volume). If laumontite identified in cuttings of the microquartz diorite is contamination by vein material of the older rocks, then it is possible that the plutonic event postdates laumontite-grade metamorphism. Holdaway and Bussey (this volume), however, conclude that the microquartz diorite and Laurel Hill-Still Creek plutons are probably broadly synchronous with the laumontite-grade alteration. The K-Ar ages might be best viewed as reflecting widespread hydrothermal alteration from geothermal circulation systems operating shortly after the plutonic event. Relatively unaltered megacrystic two-pyroxene andesite lavas that cap Last Chance Mountain were probably roughly contemporaneous with the microquartz diorites (Figure 5). The andesite has yielded K-Ar ages of 10.7±0.5 and 10.5±0.5 m.y. (Table 1) and is here informally called the Last Chance andesite.

The Last Chance andesite also occurs along the upper part of the Lolo Pass road north of the study area, where it crops out at a lower elevation than on Last Chance Mountain. It also crops out at a lower elevation (975 m [3,200 ft]) on the north side of Last Chance Mountain than on the south side (1,036 m [3,400 ft]). This suggests that either the sequence dips gently toward the north or that there was a paleocanyon at Lolo Pass when the andesites were erupted. Because the attitude of a tuffaceous mudstone interbed at Last Chance Mountain is N. 62° E. 23° SE., it is probably more likely that there was a paleocanyon at Lolo Pass.

The Last Chance andesite correlates with similar rocks described by Wise (1969) on Zigzag Mountain and andesites intercepted between 84 and 244 m (275 and 800 ft) in OMF-7A (Figure 3). Wise (1969) included samples from Last Chance Mountain in his lower Pliocene unit.

Unaltered to very slightly altered andesites east of Last Chance Mountain can be tentatively grouped into three mappable units (Figures 2 and 5). From oldest to youngest these are:

1. Miocene-Pliocene(?) two-pyroxene andesites, which are distinguished by small plagioclase phenocrysts and slight alteration of mafic minerals to saponite (e.g., Sample 7, Figure 5) or saponite-chlorite (e.g., Sample 12, Figure 5).
2. Lower Pliocene(?) megacrystic hornblende-bearing two-pyroxene andesite, which crops out in the northeast part of the map area (Figure 5).
3. Upper Pliocene(?) two-pyroxene andesite and hornblende dacite, which cap the sequence. These rocks are distinguished by a light color, very fresh appearance, and presence of two generations of plagioclase phenocrysts. The phenocrysts are not as large as those of the megacrystic units. Olivine basalts of approximately the same age as these units crop out about 1.0 km (0.6 mi) northeast of the map area of Figure 5. Thickening of the late Pliocene(?) units toward the east indicates that a nearby source may lie in that direction. A K-Ar age of 3.0 m.y. (Wise, 1969) was obtained from a sample at the top of a similar sequence of rocks at Lookout Mountain on the Hood River fault scarp.

All of the above age assignments are tentative because no K-Ar data are, as yet, available from these rocks. The Miocene-Pliocene(?) lavas are difficult or impossible to distinguish from least altered pyroxene andesites of the upper part of the Rhododendron Formation, unless stratigraphic relationships with the Last Chance andesite are apparent. If correlation of andesites in the upper 244 m (800 ft) of OMF-7A with the Last Chance andesite is in error (Figure 3), then the Miocene-Pliocene(?) lavas may be equivalents of the

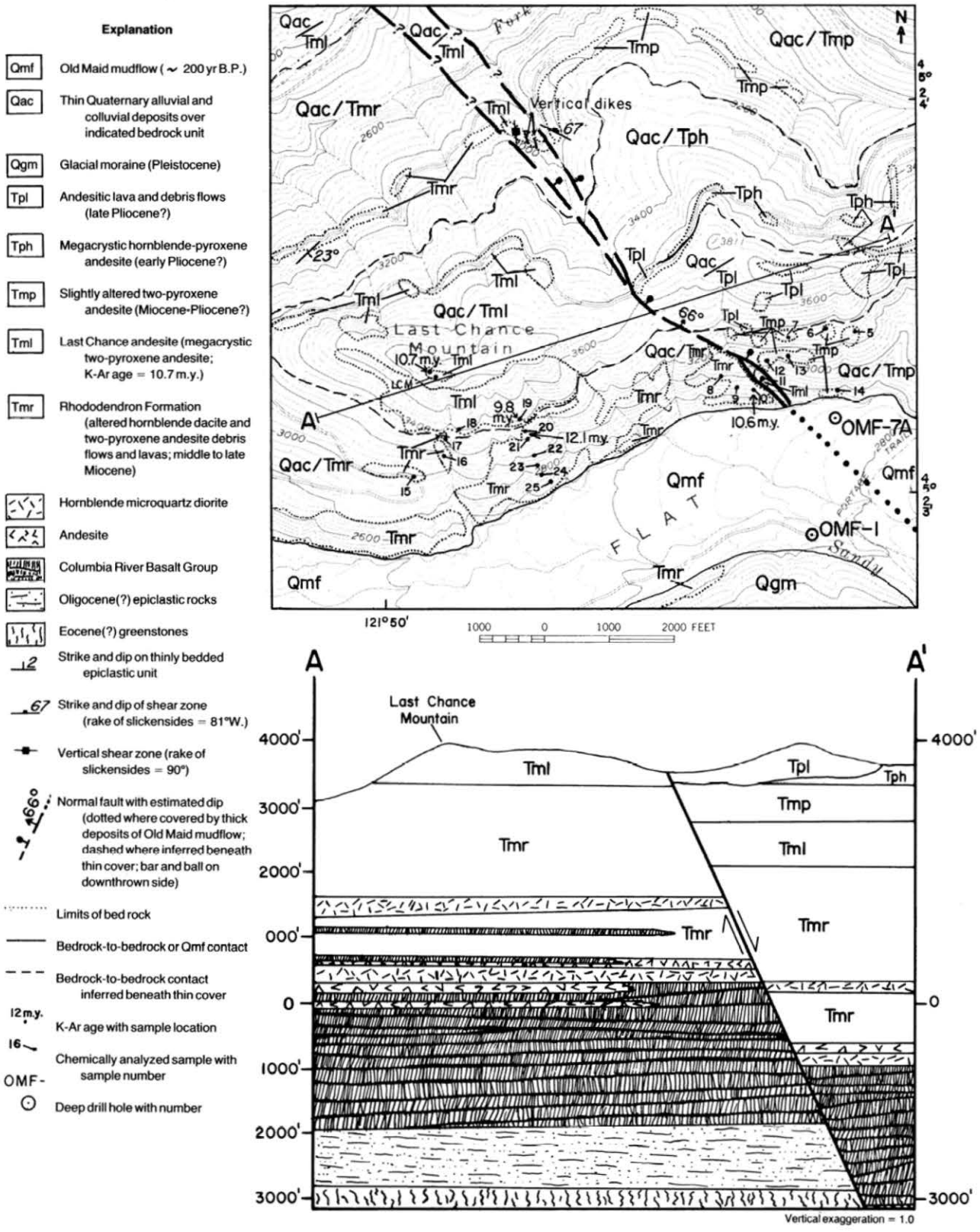

Figure 5. Outcrop map and cross section of the Last Chance Mountain-Old Maid Flat area. Sample numbers appear in Tables 2 and 4, Appendix B, and are prefixed by letters "MH."

upper Rhododendron Formation, and the vertical displacement on the fault shown in Figure 5 may be incorrect. Because the nature of the fault is of such fundamental importance to interpretation of the stratigraphy, it is appropriate to review, in detail, evidence for the attitude and displacement on this fault. This will be addressed in the sections on structural geology and geochemistry.

The youngest volcanic unit is the Old Maid mudflow which covered the floor of the Sandy River valley about 200 yr B.P. (Crandell, 1980). The mudflow was deposited when dacitic domes at Crater Rock repeatedly grew and collapsed into the surrounding drainages (Crandell, 1980). Charring of wood fragments and resetting of the remanent magnetic field in some clasts suggests that at least some of the mudflow was quite hot when emplaced (Crandell, 1980).

STRUCTURAL GEOLOGY

The only major structure identified in this study is a northwest-trending fault which offsets units east of Last Chance Mountain (Figure 5). Several lines of evidence support the existence of a fault with considerable normal dip-slip movement:

1. Lithologic units in surface outcrops appear to terminate at the fault.
2. A small allochthonous block of the lowest flow of the Last Chance andesite is displaced about 150 m (500 ft) downward within the fault zone on the south side of Last Chance Mountain, and a large sliver of the Last Chance andesite is similarly displaced on the north side of the mountain (Figure 5). It is, however, possible to interpret both of these blocks as dikes within the fault zone.
3. Units apparently correlative with the Last Chance andesite appear between 84 and 244 m (275 and 800 ft) in the OMF-7A drill hole. Units below 244 m (800 ft) in OMF-7A, however, appear to be directly correlative with rock at corresponding depths in OMF-1 on the west block of the fault (Figures 3 and 4). The fault was therefore placed at about 244 m (800 ft) in OMF-7A. The 244-m (800-ft) intercept in OMF-7A and the surface expression of the fault yield a best-fit strike and dip of N. 45° W. 66° NE. Normal dip slip across the whole zone is at least 400 m (1,300 ft), if the Last Chance andesite is at least 180 m (600 ft) thick. These estimates are based on intersection of OMF-7A with the contact between the Miocene-Pliocene sequence and the top of the Last Chance andesite at 84 m (275 ft) (Appendix A) and a minimum exposed thickness of 180 m (600 ft) of Last Chance andesite on Last Chance Mountain (Figure 5).
4. There was a sharp change in drilling penetration rate and various gas emissions (CO_2 and hydrocarbons) between 244 and 253 m (800 and 830 ft). Hydrocarbon emissions particularly show an increase at 244 m (800 ft) and are generally much higher above 244 m (800 ft) than below (MacLeod and Hill, 1980).
5. Sharp breaks in the Schlumberger fracture identification and variable density logs at 244 m (800 ft) also suggest a fault zone (see Oregon Department of Geology and Mineral Industries, 1981).

The above data provide good evidence that a major normal fault displaces Pliocene and older units down toward the east at Old Maid Flat. It is also possible that lateral movement has occurred, although no low-angle rakes were observed in major shear zones on the north side of Last Chance Mountain. This fault may be part of the diffuse zone of shear and fracture postulated by Williams and others (1982) which bounds the west side of the Mount Hood graben. The east side is bounded by the Hood River fault. This graben may have formed in the late Pliocene in response to tectonic forces and withdrawal of magmatic material (Priest, this volume; Williams and others, 1982).

GEOCHEMISTRY

Introduction

Chemical variations of igneous rocks can lend insight into stratigraphic correlations and petrologic problems. This is particularly true of trace elements, which tend to vary logarithmically in igneous processes (e.g., Leeman and Lindstrom, 1978). Trace elements which are strongly retained in either bulk crystal cumulates or liquids during crystallization and melting (e.g., Co, Sc, Cr, Zn, Th, Hf, Rb, Cs, Ba, and Sr) will tend to show wide variation (Arth, 1976). Trace-element ratios which are not strongly changed by melting and crystallization processes (e.g., Th/U and rare-earth element [REE] ratios) may reveal clues about the nature of parental magmas and source materials (Arth, 1976; Allegre and others, 1977).

In this paper, data are plotted on binary variation diagrams, and rock names have been assigned on the basis of the K_2O and SiO_2 contents (Figure 6). Major elements are

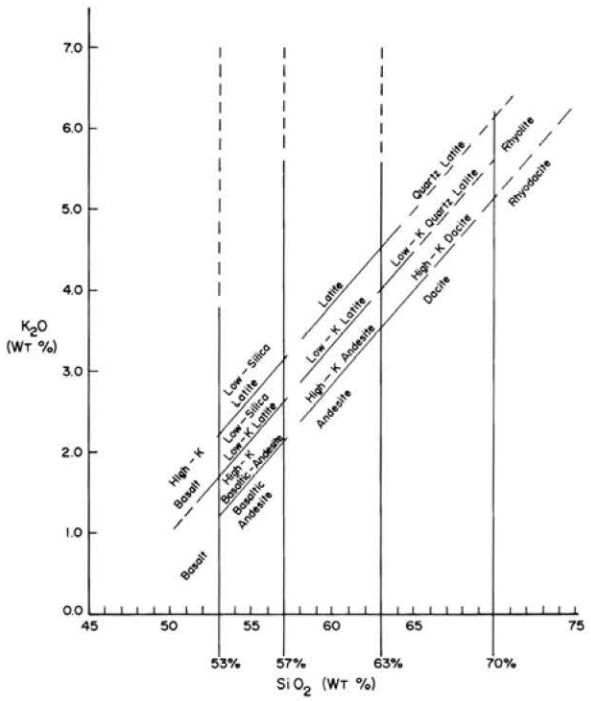

Figure 6. Nomenclature used in this paper for volcanic rocks (modified from informal classifications used by E.M. Taylor, Oregon State University, and Priest, 1979). The prefix "tholeiitic" is attached to the rock name when samples plot well into the tholeiitic field on the FeO/MgO versus SiO_2 diagram of Miyashiro (1974).

plotted against SiO_2 (Figures 7 and 8), and most trace elements are plotted against MgO (Figures 9 and 11-14). Both SiO_2 and MgO are indices of differentiation. SiO_2 generally increases in calc-alkaline magmas as differentiation occurs (e.g., Osborn, 1959; Ringwood, 1975) but may remain constant or even decrease slightly in tholeiitic differentiation series (e.g., Wager and Brown, 1967). MgO tends to decrease in both calc-alkaline and tholeiitic differentiation series, owing to early crystallization of Mg-rich phases, such as olivine and pyroxene, in both series (e.g., Yoder and Tilley, 1962; O'Hara, 1965; Ringwood, 1975). SiO_2 was chosen as the abscissa in major-element plots because of historic usage and the fact that the SiO_2 content is over 50 percent in most rock analyses.

MgO was chosen over SiO_2 as the abscissa for trace-element plots because it is more sensitive to small differences in degree of differentiation in both tholeiitic and calc-alkalic differentiation series. Because trace elements may vary by orders of magnitude as crystallization and melting processes proceed, a reliable indicator of differentiation was needed to show changes from probable high-level differentiation processes so that fundamental differences in parental magmas could be more easily observed.

Chemical correlations

All mappable volcanic and plutonic units in the area also have distinctive geochemical signatures. Major units such as the greenstones, Columbia River Basalt Group, Rhododendron Formation, Last Chance andesite, and the hornblende microquartz diorite all have distinctive chemical compositions on the major- and trace-element diagrams (Figures 7-14). Trace-element correlations by one of the authors (Beeson) allowed assignment of member and formation names to units within the Columbia River Basalt Group, even in highly altered rocks.

A number of compositional overlaps are apparent on the diagrams. Data from outcrops of the upper part of the Rhododendron Formation overlap completely with compositional fields of the lower part of the Rhododendron from the drill holes, and the hornblende microquartz diorite shows very close chemical coherence with the Rhododendron. Outcrop samples of the Last Chance andesite plot within compositional limits of OMF-7A drill hole samples from 84-244 m (277-805 ft) on all of the diagrams. The Last Chance andesite correlation is particularly impressive on the Cr, Co, Sc, Hf, Th, and REE MgO variation diagrams (Figures 9, 11, 14) as well as the Co-Sc diagram (Figure 10). The most unfortunate overlap is that of the sparse data for the Miocene-Pliocene unit with the Rhododendron Formation. These two units overlap on all diagrams except on the Th diagram (Figure 11), which shows somewhat lower Th for most Miocene-Pliocene samples.

Chemical changes through time

Volcanism in the Mount Hood area appears to have shifted from intermediate and silicic calc-alkalic lavas to increasingly mafic lavas in the late Miocene to Pliocene (Priest, this volume). This is dramatically illustrated in Figure 8, which shows a progressive shift of composition from typical silicic calc-alkalic rocks of the middle to upper Miocene Rhododendron Formation to increasingly mafic lavas of more tholeiitic character in the Pliocene.

This shift to more mafic magmas also occurred in the Old Maid Flat area. The Last Chance andesite (10.7 m.y.) is somewhat more mafic in character than much of the Rhododendron Formation (Figures 8, 9, and 10), and olivine basalts of late Pliocene(?) age occur just 1 km (0.6 mi) northeast of the map area of Figure 5.

It is equally apparent that silicic to intermediate lavas of calc-alkalic character continued to erupt throughout the Neogene. Rocks of andesitic to dacitic composition are found throughout the geologic section, the most recent example being the edifice of Mount Hood. Sources and processes able to evolve intermediate to silicic calc-alkalic magmas apparently operated throughout the overall shift to more mafic magmas and account for the vast majority of total volcanism in the area.

Priest (this volume) suggests that increasing influence of extensional tectonics in the latest Miocene to Quaternary favored eruption of more mafic magmas. He concludes, however, that subduction-related processes continued to evolve the dominant calc-alkalic magmas throughout the Neogene in the Mount Hood region.

Chemical nature of the Eocene(?) greenstones

Although the greenstones intercepted in the bottom of the OMF-7A drill hole are of silicic composition, they display a marked chemical affinity to the tholeiitic rocks of the Columbia River Basalt Group. The greenstones are much higher in FeO and FeO/MgO than calc-alkalic rocks of the Rhododendron and younger lavas (Figures 7 and 8), and trace-element differences (Figures 9-14) between the greenstones and the calc-alkaline rocks are the same differences displayed by the Columbia River Basalt Group (e.g., higher in large-ion lithophile elements, higher in Mn, Co, Sc, Zn, and Ti, and lower in CaO, Sr, and La/Sm).

Possible reasons for the marked tholeiitic character of the greenstones are the following:

1. The greenstones and Columbia River basalt were evolved by similar melting and crystallization processes from similar sources.
2. The source rock and conditions which evolved the greenstone magmas differed significantly from the source and conditions which generated the calc-alkalic magmas.
3. The greenstones may be tholeiitic basalts which have undergone significant metasomatism so that their silica contents have been raised to those of andesite and dacite.
4. Metasomatic processes affecting the greenstones have fortuitously caused changes from calc-alkalic to tholeiitic character.

Factors 1 and 2 are probably the most likely reasons for the marked similarity of the greenstones to the Columbia River basalt. Factor 3 is unlikely, because the Co and Sc variations (Figures 9 and 10) indicate that the greenstones fall along well-defined differentiation paths with vectors pointing to lower ferromagnesian trace elements at lower MgO. The variation of Co to Sc (Figure 10) for the greenstones is also sharply linear and parallel to variations of much less altered lavas. Such parallelism would be unlikely if the greenstone Co and Sc values were significantly changed by metamorphic processes. Factor 4 is similarly unlikely, since it is highly improbable that metamorphic processes fortuitously operated in just the correct manner to effect changes from calc-alkalic to more tholeiitic character while preserving coherent Co and Sc variations.

If the greenstones share a common genesis with other tholeiitic-series lavas, then it is likely that they were erupted

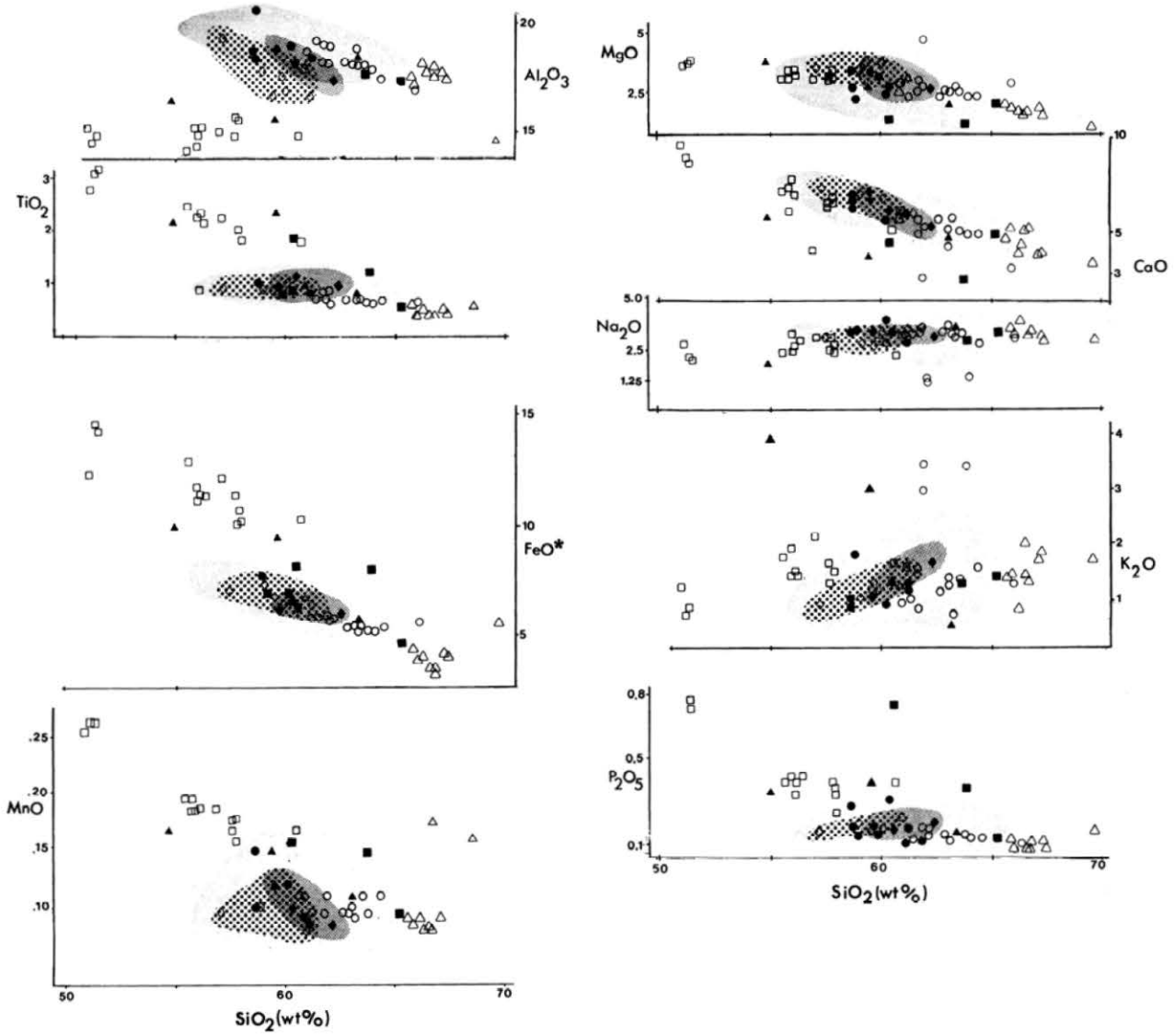

Figure 7. Harker diagrams for all major oxides. All values are in weight percent for Miocene-Pliocene lavas (dots), microquarz diorite (open triangles), Last Chance andesite in the upper 244 m (800 ft) of OMF-7A (solid diamonds) and in outcrop (open diamonds), Columbia River Basalt Group (open squares), interbeds in the Grande Ronde Basalt in OMF-7A (solid triangles), and Eocene(?) greenstones (solid squares). Light-gray area is the compositional field of outcrops of the upper part of the Rhododendron Formation which compares closely with compositions of the lower Rhododendron Formation (circles) encountered in OMF-7A. See Appendix B for data tables. Coarse stipples accent the field of Last Chance andesite outcrops relative to the samples from the upper 244 m (800 ft) of OMF-7A (medium stipples). FeO = FeO + 0.9 Fe_2O_3.*

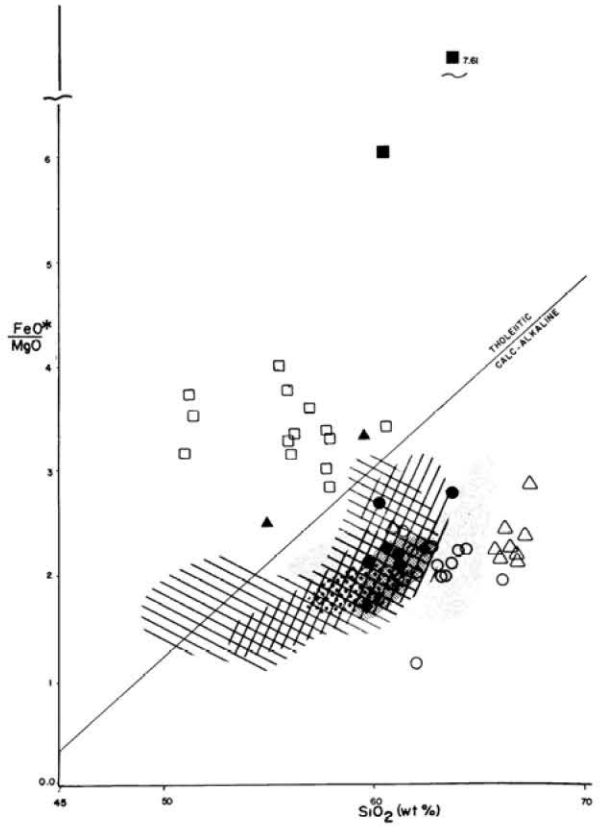

Figure 8. FeO/MgO versus SiO_2. Symbols and patterns as in Figure 7. Left diagonal pattern is Wise's (1969) late Pliocene assemblage; right diagonal pattern indicates his early Pliocene rocks.

from an extensional volcano-tectonic regime or from an oceanic basin environment similar to that which produced the Hawaiian Island or French Polynesian volcanoes. If they have an origin within an oceanic plate, then the greenstones may be Eocene(?) oceanic crust that was tectonically attached to the North American Plate in the Paleogene. Location of the greenstones below a major unconformity under probable Oligocene sedimentary rocks of the Eagle Creek Formation suggests that they may be Eocene or older. Tectonic attachment to North America could thus have taken place any time in the Paleogene.

RESERVOIR CHARACTERISTICS OF ROCK UNITS FROM DIAMOND CORE DATA

Open fractures were demonstrated in diamond core of only the Columbia River basalt in the OMF-7A drill hole. The low-MgO Grande Ronde basalt appeared to have numerous intersecting fractures at all angles on a spacing of 10 cm (4 in) or less throughout the cored interval of 1,030-1,036 m (3,381-3,399 ft). Because this interval seems in no way unique relative to other parts of the Columbia River Basalt Group, it is probable that the entire group is a good reservoir rock where not anomalously altered. No significant fluid

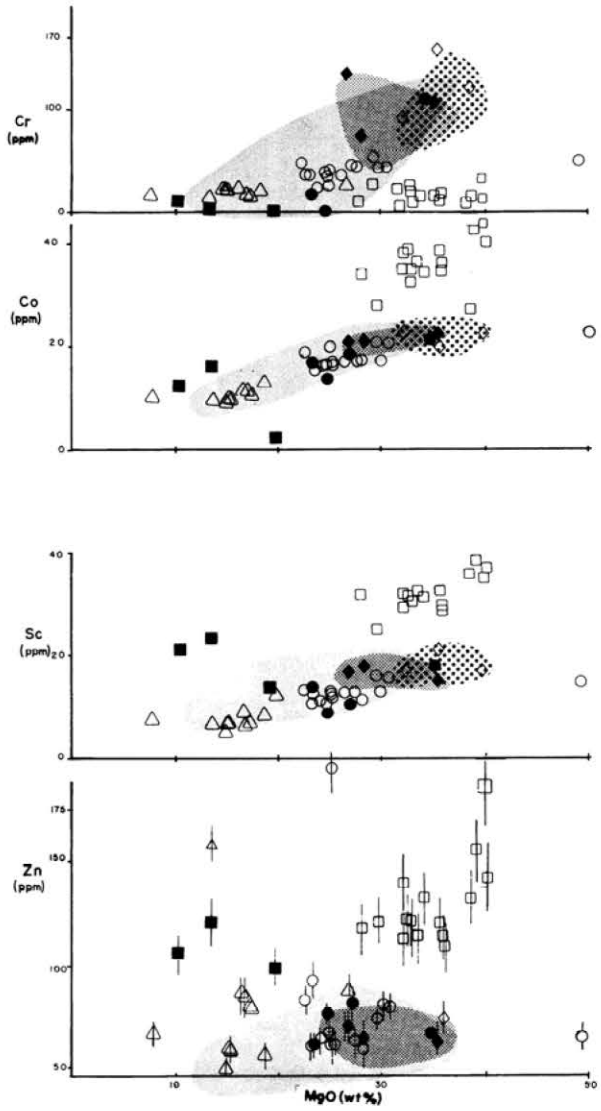

Figure 9. Ferromagnesian elements versus MgO. Symbols as in Figure 7. Vertical lines = error at 1 σ. Some elements below detection limits.

was, however, recovered from the Columbia River Basalt Group.

The greenstone at the bottom of OMF-7A appears to be extremely tight and free of any fracture permeability. No open fractures and very few mineral veins occur in the excellent core from 1,832-1,837 m (6,011-6,027 ft). A pronounced, highly contorted, low-grade schistosity that occurs throughout the greenstone at 55°-70° from the horizontal is superimposed on a totally rehealed autobrecciated texture.

The epiclastic volcaniclastic rocks between the Columbia River basalt and the greenstones were not successfully cored, but the small pieces of core recovered at 1,561-1,570 m (5,122-5,152 ft) and at 1,339-1,346 m (4,394-4,417 ft) indicate that the rocks are very highly indurated, poorly sorted, and highly sheared and fractured in the deeper core. Dominant shears were at 80° and 35°-55° from the horizontal, with 80° rakes on slickensides. The highly indurated and

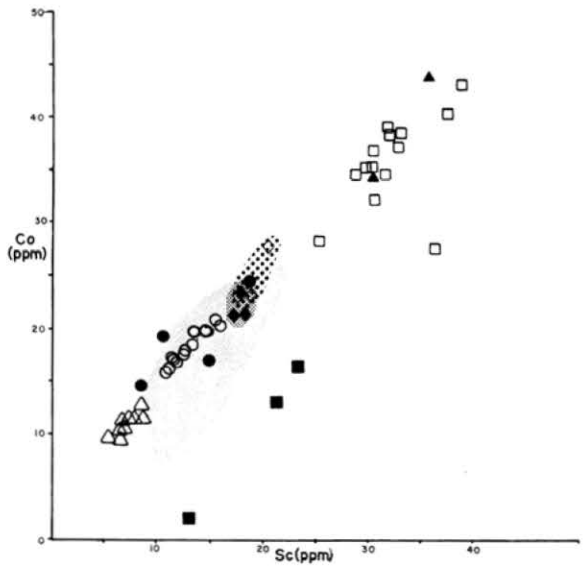

Figure 10. Co versus Sc. Symbols as in Figure 7.

clay-rich nature of these rocks probably means that they have low permeability. A dip of 15°-25° from the horizontal was obtained on a contact at 1,339 m (4,394 ft).

A core of the microquartz diorite at 888 m (2,914 ft) was too short (1.65 m [5.41 ft]) to reveal the extent of widely spaced fractures. One fracture at 80° from the horizontal was coated with quartz and minor calcite but was so poorly cemented that the core fell apart along the fracture while being pulled out of the drill hole. The fracture had been sheared, as evidenced by lineations raking 43° on smoothed surfaces of the quartz. If this fracture is open or so weakly sealed that it will respond to hydrofracturing and acidification, the microquartz diorite may have good reservoir characteristics.

The Rhododendron Formation was cored in a typical debris flow at 486-495 m (1,595-1,625 ft). Most fractures and minor shears were rehealed with calcite or calcite-quartz mixtures. A few were sealed with quartz and phyllosilicates. A large number of fractures appeared to have been induced at 25°-30° and at 50°-60° from the horizontal during drilling and handling. These induced fractures appear to be controlled by a pervasive tectonic fabric of microfractures. Prominent shear directions were at 30° and between 55°-60° from the horizontal. None of the fractures or shears appeared to have significant permeability.

The relative lack of pervasive alteration in both the Columbia River basalt and the hornblende microquartz diorite is evidence that both rock types may be less reactive, and therefore less easily sealed by metamorphic fluids, than the Rhododendron Formation. Possible widely spaced open or partly sealed fractures in the microquartz diorite and many open fractures in the Columbia River basalt are additional evidence that these rocks are the best reservoir rocks in the area.

DISCUSSION AND RECOMMENDATIONS

The drilling program at Old Maid Flat has not revealed any new geothermal resources but has contributed greatly to the knowledge of the volcanic stratigraphy of the Mount Hood area. Distinctive geochemical and mineralogic differ-

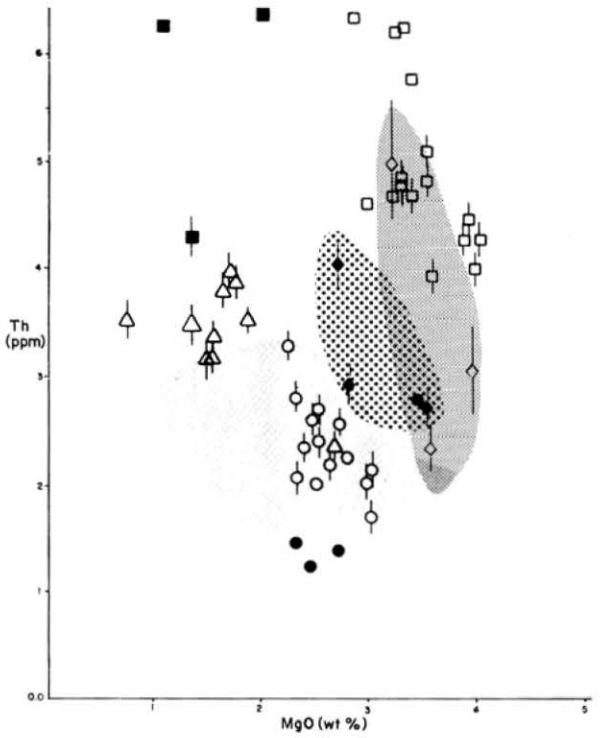

Figure 11. Th versus MgO. Symbols as in Figure 7, except coarse and medium stipple patterns are reversed on this diagram. Vertical lines = error at 1 σ.

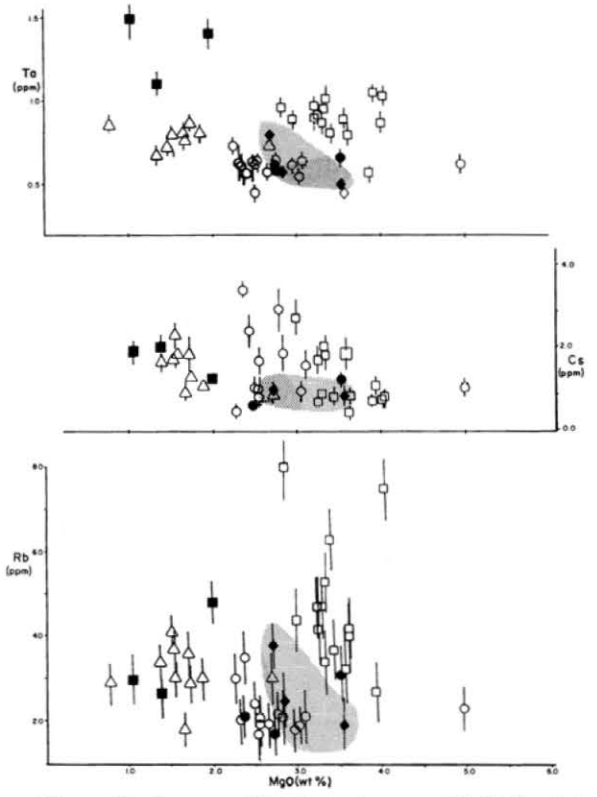

Figure 12. Incompatible elements versus MgO. Symbols as in Figure 7. Vertical lines = error at 1 σ.

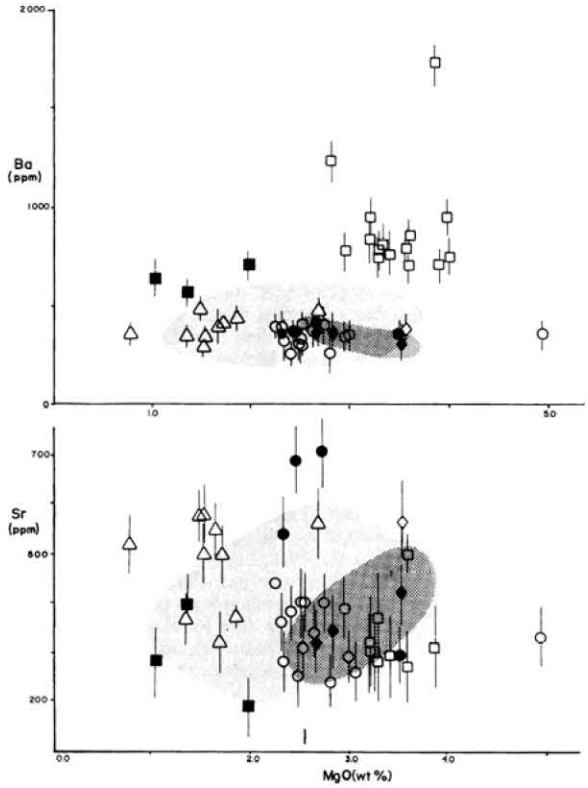

Figure 13. Alkaline earths versus MgO. Symbols as in Figure 7. Vertical lines = error at 1 σ.

ences exist between calc-alkaline units of the Neogene as well as between tholeiitic units within the Columbia River Basalt Group. Laumontite-grade alteration and silicic calc-alkalic (low FeO and FeO/MgO and high CaO) chemistry characterize the Rhododendron Formation. The Last Chance andesite is a two-pyroxene andesite with megacrystic texture and is distinctly more mafic than the silicic Rhododendron and microquartz diorite magma types. This shift to more mafic magmas about 10.7 m.y. ago culminated in the late Pliocene in eruption of olivine basalt lavas near Old Maid Flat. On the northeast side of Mount Hood near Parkdale, basaltic lavas have continued to erupt into the Holocene (Wise, 1969).

Chemical and mineralogic correlations across a northwest-trending shear zone through the Old Maid Flat area put important constraints on the nature of the offset. The overall dip of the zone appears to be 66° to the northeast, and normal dip-slip movement in the amount of at least 400 m (1,300 ft) has occurred. The fault is probably at least as young as late Pliocene, since it appears to cut units of that age. It does not appear to cut Pleistocene deposits.

The OMF-7A drill hole probably intercepted the main part of the fault zone at about 244 m (800 ft), well above the thermal zone. Lack of any significant aquifer at the probable fault-zone intercept or within open-fractured Columbia River basalt in the thermal zone indicates that it is unlikely that deeply convecting hydrothermal fluids are present at Old Maid Flat. This may be a function of the pervasive alteration which seals all fractures within lower Rhododendron Formation andesites. Movement on the shear zone is apparently not sufficiently youthful (late Pliocene) to create enough permeability within the Rhododendron Formation to allow meteoric water egress to deep levels in the crust. Similar lack of vertical permeability was noted in andesitic units at the Pucci Chairlift hole on Mount Hood (Blackwell and others, this volume).

More attractive geothermal targets in the area should be free of geological deficiencies noted at Old Maid Flat. Fault-zone targets should be Quaternary in age, if located in areas capped by lower Rhododendron Formation or with Rhododendron in the thermal zone. Older faults may have significant geothermal resources, if they cut brittle nonreactive rocks such as Columbia River basalt or silicic intrusives at both shallow and deep levels. Conditions of this kind might exist where extensions at the Old Maid Flat fault or other faults intersect Columbia River Basalt Group contacts with the Laurel Hill or Still Creek plutons.

In any case, targets for deep drilling should be selected only after careful shallow- (150-200 m [450-600 ft]) and intermediate- (300-700 m [900-2,100 ft]) level drilling has demonstrated anomalously high heat flow indicative of upward convecting geothermal fluids. Detailed geologic mapping should precede all drilling efforts.

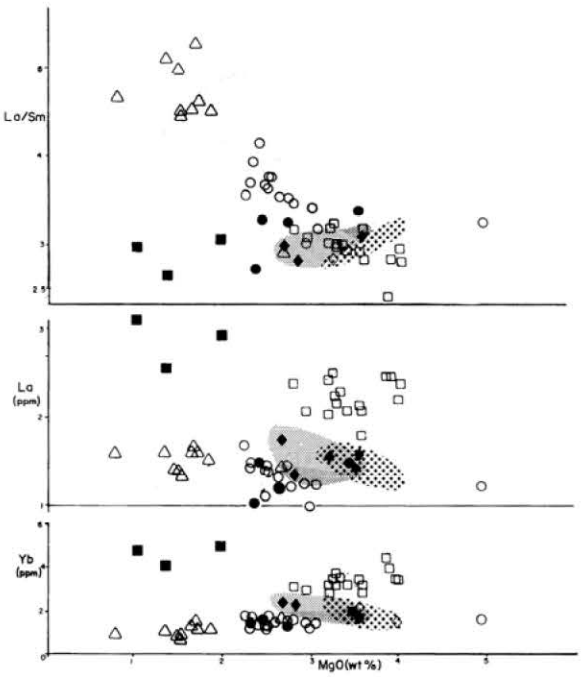

Figure 14. La/Sm (a measure of light rare-earth enrichment relative to heavy rare earths), La (light rare earth), and Yb (heavy rare earth) versus MgO. Symbols as in Figure 7.

ACKNOWLEDGMENTS

The authors gratefully acknowledge the support by USDOE for M.H. Beeson's, D.A. Berri's, and G.R. Priest's portions of this study. M.W. Gannett's work was made possible by grants from Northwest Natural Gas Corporation, Mazamas, and Sigma Xi. Peter Hooper of Washington State University provided X-ray fluorescence analyses at reduced cost.

REFERENCES CITED

Allegre, C.J., Treuil, M., Minster, J.F., Minster, B., and Albarade, F., 1977, Systematic use of trace element in igneous process, Part I: Fractional crystallization processes in volcanic suites: Contributions to Mineralogy and Petrology, v. 60, p. 57-75.

Armentrout, J.M., 1981, Correlation and ages of Cenozoic chronostratigraphic units in Oregon and Washington, *in* Armentrout, J.M., ed., Pacific Northwest Cenozoic biostratigraphy: Boulder, Colo., Geological Society of America Special Paper 184, p. 137-148.

Arth, J.G., 1976, Behavior of trace elements during magmatic processes — a summary of theoretical models and their applications: U.S. Geological Survey Journal of Research, v. 4, no. 1, p. 41-47.

Bikerman, M., 1970, K-Ar ages of Laurel Hill pluton and dike, Oregon: Oregon Department of Geology and Mineral Industries, Ore Bin, v. 32, no. 11, p. 211-215.

Blackwell, D.D., and Steele, J.L., 1979, Heat flow modeling of the Mount Hood volcano, Oregon, *in* Hull, D.A., investigator, and Riccio, J.F., ed., Geothermal resource assessment of Mount Hood: Oregon Department of Geology and Mineral Industries Open-File Report O-79-8, p. 190-264.

Covert, W.F., and Meyer, H.J., 1979, Geothermal observation wells Mt. Hood, Oregon. Final report for Oct. 4, 1977-July 9, 1979: Portland, Oreg., Northwest Geothermal Corporation (for USDOE), DOE/ET/28417-1, 28 p.

Crandell, D.R., 1980, Recent eruptive history of Mount Hood, Oregon, and potential hazards from future eruptions: U.S. Geological Survey Bulletin 1492, 81 p.

Leeman, W.P., and Lindstrom, D.J., 1978, Partitioning of Ni^{+2} between basaltic and synthetic melts and olivines — an experimental approach: Geochimica et Cosmochimica Acta, v. 42, p. 801-816.

MacLeod, T., and Hill, J., logging geologists, R.F. Smith Corporation, 1980, Engineering and air and mud drilling data, DOGAMI well Old Maid Flat 7A: Oregon Department of Geology and Mineral Industries Open-File Report O-80-11, 16 p.

Miyashiro, A., 1974, Volcanic rock series in island arcs and active continental margins: American Journal of Science, v. 274, no. 4, p. 321-355.

O'Hara, M.J., 1965, Primary magmas and the origin of basalts: Scottish Journal of Geology, v. 1, p. 19-40.

Oregon Department of Geology and Mineral Industries, 1981, Geophysical logs, Old Maid Flat No. 7A, Clackamas County, Oregon. Interval from 96-1,190 ft: Oregon Department of Geology and Mineral Industries Open-File Report O-81-2A, 4 logs.

Osborn, E.F., 1959, Role of oxygen pressure in the crystallization and differentiation of basaltic magma: American Journal of Science, v. 257, no. 9, p. 609-647; erratum, no. 10, p. 778.

Priest, G.R., 1979, Geology and geochemistry of the Little Walker volcanic center, Mono County, California: Corvallis, Oreg., Oregon State University doctoral dissertation, 253 p.

Ringwood, A.E., 1975, Composition and petrology of the earth's mantle: San Francisco, Calif., McGraw-Hill, 618 p.

U.S. Department of Energy, 1980, Mt. Hood geothermal exploratory drilling and testing plan, Old Maid Flat holes no. 1 and no. 7A: U.S. Department of Energy, Nevada Operations Office, NVO-218, var. pag.

— — — 1981, Old Maid Flat geothermal exploratory hole no. 7A, drilling and completion report (Mt. Hood Geothermal Resource Assessment): U.S. Department of Energy, Nevada Operations Office, NVO-230, var. pag.

Wager, L.R., and Brown, G.M., 1967, Layered igneous rocks: San Francisco, Calif., W.H. Freeman and Company, 588 p.

White, C.M., 1979, Geology and geochemistry of Mt. Hood volcano, *in* Hull, D.A., investigator, and Riccio, J.F., ed., Geothermal resource assessment of Mount Hood: Oregon Department of Geology and Mineral Industries Open-File Report O-79-8, p. 78-136.

Williams, D.L., Hull, D.A., Ackerman, H.D., and Beeson, M.H., 1982, The Mt. Hood region: volcanic history, structure, and geothermal energy potential: Journal of Geophysical Research, v. 87, no. B4, p. 2767-2781.

Wise, W.S., 1969, Geology and petrology of the Mt. Hood area: a study of High Cascade volcanism: Geological Society of America Bulletin, v. 80, p. 969-1006.

Yoder, H.S., and Tilley, C.E., 1962, Origin of basalt magmas: an experimental study of natural and synthetic rock systems: Journal of Petrology, v. 3, p. 342-532.

HEAT FLOW IN THE VICINITY OF THE MOUNT HOOD VOLCANO, OREGON

By John L. Steele and David D. Blackwell, Department of Geological Sciences, Southern Methodist University, Dallas, Texas 75275; and James H. Robison, U.S. Geological Survey, Water Resources Division, 345 Middlefield Road, Menlo Park, California 94025.

ABSTRACT

Geothermal data from 25 wells within a 20-km radius of the Mount Hood stratovolcano in north-central Oregon are described. The wells range in depth from 65 m to 1.8 km. There are two holes 1.2 km in depth, eight holes in the depth range of 250-600 m, and the rest in the depth range of 100-250 m. Thermal conditions are a complicated function of position around the volcano. As a general rule, there is an increasing resistance to fluid flow with increasing age of the rocks, so that (1) generally conductive heat-flow measurements are observed in Miocene and older units, and (2) increasingly convection-dominated measurements are seen in younger units. An exception to this generalization occurs in the southwest corner of the mountain, where two quartz diorite plutons have a high fracture permeability, and temperatures are affected by a forced ground-water system in this fractured granitic rock. Heat-flow values range from 65-150 mW/m^2. As the volcano is approached, there is a general increase in heat flow from regional values of approximately 80 mW/m^2 at a distance of 12 km or greater from the volcano, to heat-flow values on the order of 130-150 mW/m^2 at a distance of 5-8 km from the apex of the mountain. No holes were drilled closer than 5 km to the apex. The results have not unequivocally outlined a magma chamber which might be associated with the volcano; however, the presence of a hot, near-magmatic temperature zone along the axis of the volcano is likely, and the heat-flow data are not close enough to the apex of the volcano to detect such a magma chamber. The gradual rise in gradients toward the mountain can be explained by a more deeply buried hot zone with a diameter of 2-3 km. No geothermal systems of electrical grade have been outlined by the present studies; however, the heat-flow values are high enough that temperatures suitable for space heating exist at reasonable depths, and in at least one place, the holes may be used for such an application. Large areas of the mountain are as yet untested, and some attractive regions remain to be explored.

INTRODUCTION

During the past few years, the Mount Hood stratovolcano in north-central Oregon has been the site of extensive geological and geophysical studies. The objective of these studies has been to permit characterization of all aspects of the geological and geophysical setting of the volcano. Results of some of these studies are presented elsewhere (Williams and others, 1982, and associated papers). Thermal measurements on a regional basis around Mount Hood and in the Oregon Cascade Range are discussed by Blackwell and others (1978), Blackwell and Steele (1979), and Steele and others (in preparation). The focus of this report will be on those data within a radius of approximately 20 km from the apex of the volcano. Because of the detailed discussion of the geological and other geophysical data elsewhere, those results will not be summarized here except as pertinent to this study.

Mount Hood is a typical stratovolcano of the Cascade Range. It is composed of Pleistocene/Holocene andesitic and dacitic flows, lahars, and ash deposits sitting on a Pliocene andesite-basalt platform typical of the High Cascade Range (Wise, 1969). The Pliocene rocks in turn overlie a hydrothermally altered section of rocks of Miocene and older age. Locally these rocks are the Rhododendron Formation, the underlying Columbia River basalt, and older volcanic and volcaniclastic units. Mount Hood itself is believed to be composed of volcanic rocks younger in age than 700,000 years, because all the rocks associated with the volcano are normally magnetized. The activity postdating the glacial period has occurred in three main episodes, each episode producing rocks that are dacitic in composition, with ages of about 12,000-15,000, 1,500-1,800, and 200-300 years. Minor activity may have occurred in the mid-1800's (Crandell, 1980). A large area of fumaroles still exists at the top of the mountain; there, an area covering several hundred square meters has temperatures of 85° C or higher at very shallow depths (Wollenberg and others, 1979). Flows of olivine andesite have been erupted from satellite vents on the north flank of the volcano in post-glacial times (Parkdale flow).

The general thermal setting of the Oregon Cascade Range has been discussed by Blackwell and others (1978, in press). The mean geothermal gradient in the High Cascade Range, corrected for topography and observed in Miocene rocks underlying the younger Pliocene and Pleistocene volcanic rocks, is 65°±3° C/km, and the related heat flow is 100±5 mW/m^2. There is a transition to the west from the high heat flow of the Cascade Range to low heat flow characteristic of the Western Cascade Range and Willamette Valley provinces. The transition takes place over a distance of approximately 20 km. Mean heat-flow values and gradients for the Western Cascade Range are approximately 45±2 mW/m^2 and 29°±2° C/km, respectively. This thermal pattern remains unchanged from the South Fork of the McKenzie River to as far north as the Clackamas River (south of Mount Hood). There is, however, a major change in this pattern north of the Clackamas River. The heat-flow pattern along the axis of the Cascade Range in southern Washington is characterized by a lower background gradient (45°±5° C/km) and heat flow (80±10 mW/m^2), with localized areas of higher heat flow which are directly related to recent intrusions or geothermal systems. The Mount Hood region may be more characteristic of the pattern observed in the Washington part of the Cascade Range rather than in the

central and southern part of the Cascade Range.

A total of 25 drill holes is available within a radius of 20 km of Mount Hood. The history of the drilling and geothermal resource assessment can be found in Hull and Riccio (1979). The holes which have yielded significant gradient information range in depth from 65 m to 1.8 km. One hole is 1.8 km in depth, two are 1.2 km in depth, eight range from 250 to 600 m in depth, and the rest range from 100-250 m in depth. The gradient data are summarized in Table 1. Included are township/range-section location, province name, latitude, longitude, collar elevation, depth interval of calculation of gradient, mean harmonic thermal conductivity, uncorrected and terrain-corrected geothermal gradient, and heat flow. The collection and measurement of the thermal data and thermal conductivity (both cutting and core) follow the techniques of Roy and others (1968) and Sass and others (1971). A detailed description of the technique for terrain correction to the thermal gradient is found in Blackwell and others (1980).

The heat flow of the deepest of the holes (OMF-7A) is discussed in an accompanying paper (Blackwell and others, this volume); that of the second deepest hole (OMF-2) is discussed by Blackwell and Steele (1979), who also list preliminary values for several of the shallower holes shown in Table 1. Heat-flow values in the remainder of the holes as presented in Table 1 have not been discussed elsewhere.

The nature of heat transfer associated with the andesite volcano is complicated and locally variable, and it is not possible to make generalizations on the scale of the whole volcano. Rather, the thermal structure of the volcano has to be discussed with reference to specific geographic areas. Thus a simple table of data as shown in Table 1 is relatively uninformative, and the objective of the remainder of this paper is to discuss the heat flow in different areas around the mountain.

The locations of all the holes, as well as the topographic settings, are shown in Figure 1. The holes closest to the top of the mountain are at a distance of approximately 5 km, near Timberline Lodge, a ski resort on the south side of the mountain. Three holes, with a maximum depth of 1.2 km, are located there. A fourth hole, 3CCA, 354 m in depth, is located approximately 3.5 km to the east of Timberline Lodge at about 5 km radial distance from the top of the mountain, near the Mount Hood Meadows ski resort. Most of the remainder of the informative holes are distributed about 8-12 km from the apex of the volcano on all sides of

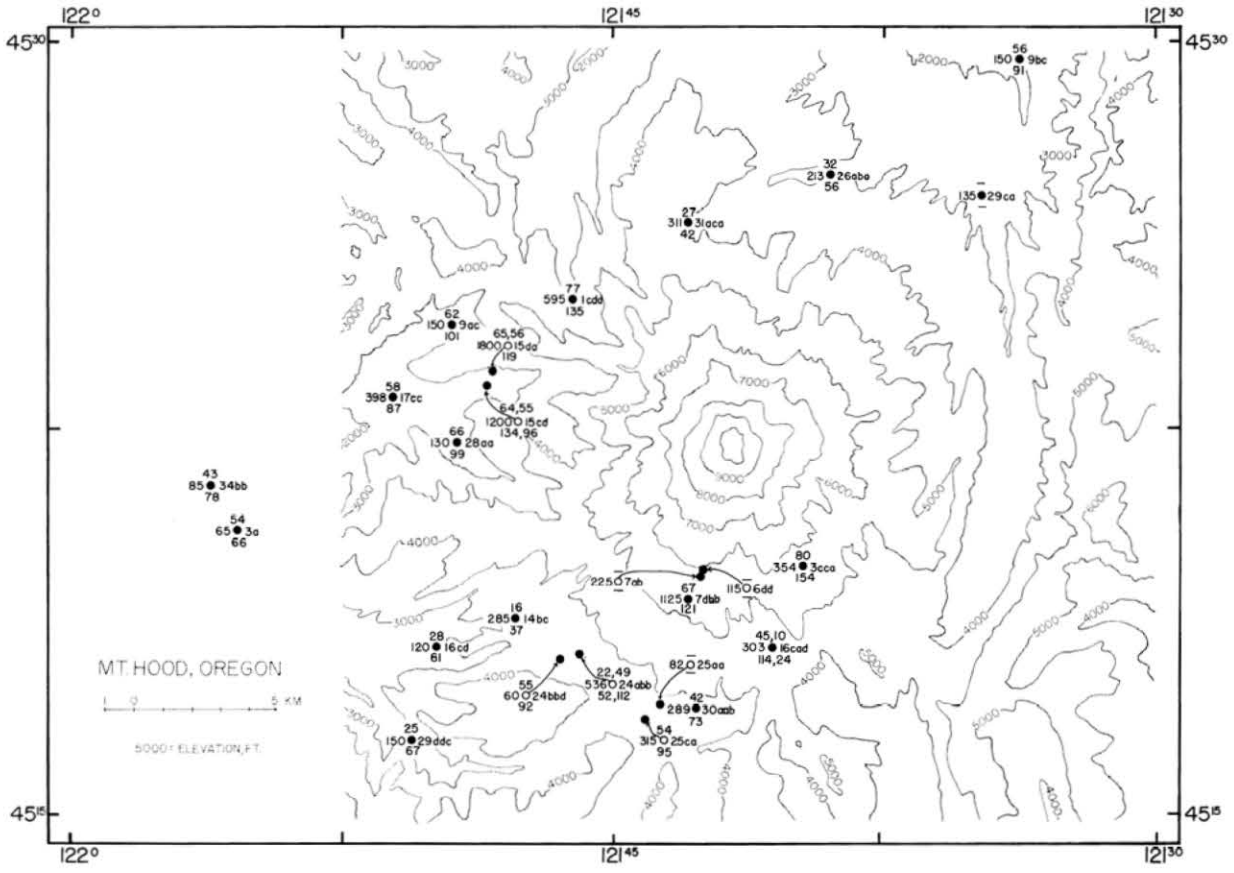

Figure 1. Topography and well-site location map for Mount Hood. Topographic contours at 1,000-ft (304.8-m) intervals are shown. Also shown are the sites for which geothermal data have been obtained. Shown clockwise around each hole location, beginning on the left side, are the hole depth, geothermal gradient, section and subsection location, and heat flow. Where gradient and heat flow are ambiguous or undeterminable, only bars are shown. If the gradient and/or heat flow change with depth, more than one value may be shown, with the shallowest value being the one shown on the left-hand side. The depths of the holes are in meters, the heat-flow values are in mW/m², and the gradients are in °C/km.

the volcano except the east side. The U.S. Forest Service declined permission for all holes planned on the east side, and therefore that side of the mountain remains undrilled. The various areas of the mountain will be discussed separately because of their contrasting thermal character. The discussion will proceed counterclockwise around Mount Hood, beginning on the northwest side.

NORTHWEST AND WEST SIDES

Eight holes are available on the northwest and west sides of Mount Hood. The temperature-depth curves for these holes are shown in Figure 2, and their locations are shown in Figure 1. The nature of heat transfer in these holes is conductive, at least to the maximum depth reached in each of the holes. Six of the holes are approximately 10-12 km from the apex of the volcano, and most are in, or close to, valley bottoms along the major drainages leading away from the mountain. The heat-flow values of the closest holes range from 87-133 mW/m^2. The hole in this group most distant from the mountain, 17CC, has a heat flow of 87 mW/m^2 and a mean terrain-corrected gradient of 58° C/km. Terrain-corrected gradients of 64°± 2° C/km are typical of the holes closer to the mountain. The McGee Creek hole, 1CD, has the highest gradient observed in any of the holes around the volcano. The gradient averages 81° C/km after topographic corrections, and the heat flow is 133 mW/m^2. The thermal-conductivity values in holes OMF-7A (15DA) and OMF-2 (15CD) are higher than in 17CC, so the same heat-flow value is obtained in those two holes even though the gradients are lower.

Below shallow disturbances generally less than 70 m in depth, all of these holes show linear temperature-depth curves, with minor variations caused by intraborehole water flow, particularly in the OMF-2 (15CD) drill hole. Thus, the heat flow is conductive in this set of drill holes. Most of these holes were collared in rocks of the Miocene Rhododendron Formation, which consists of andesite debris flows. The overall permeability in this unit is quite low, and, as demonstrated by the OMF-7A drill hole, gradient and heat-flow values observed in 150-m holes are characteristic of those observed to a depth of almost 2 km, if allowances are made for changes in rock type (thermal conductivity) with depth.

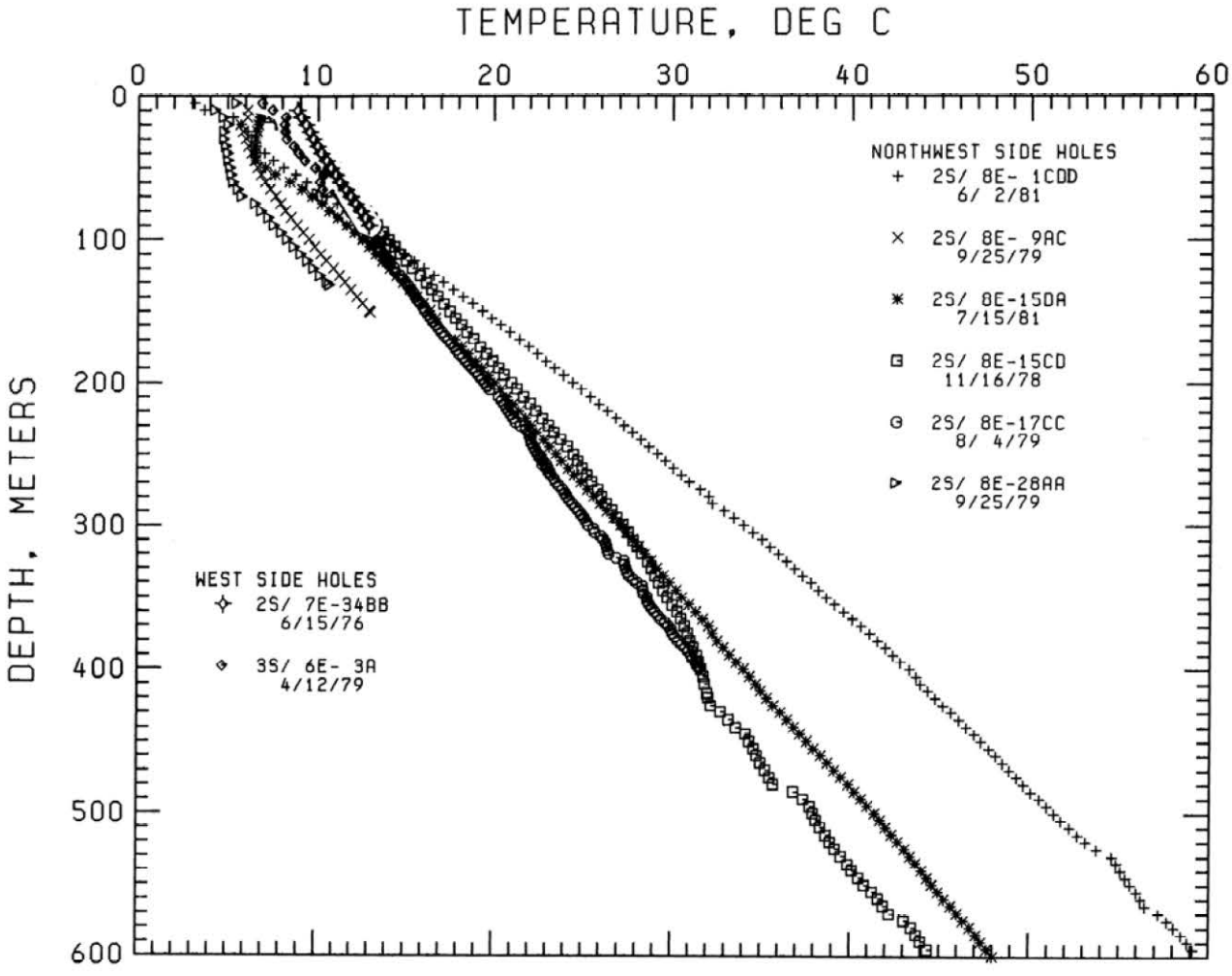

Figure 2. Temperature-depth plots for holes on the northwest and west sides of the mountain. The scale used in this figure is used for all subsequent temperature-depth plots, so that the curves can be directly compared.

Table 1. *Heat-flow data from 25 wells within a 20-km radius of Mount Hood stratovolcano, Oregon*

T., R. sec.[1]	Province name[2]	N. lat. deg. min.	W. long. deg. min.	Hole and date (m)	Collar elev. (m)	Depth interval (m)	Avg. thermal conductivity[3,4] ($Wm^{-1}K^{-1}$)	No. of thermal conductivity measurements[3]	Uncorrected gradient[4,5] (°C/km)	Corrected gradient (°C/km)	Uncorrected heat flow[5] (mWm^{-2})	Corrected heat flow[5] (mWm^{-2})	Quality of heat flow[6]
1 S., 9 E. 26ABA	HC	45-27.55	121-38.98	Eliot Br 8/30/80	884	101.0 160.0	1.76	2	24.3 0.8	21.9	43	39	C
						101.0 213.0	1.77 0.04	4	35.1 2.6	31.6	62	56	C
1 S., 9 E. 31ACA	HC	45-26.62	121-42.92	Clear Bk 8/21/81	1,265	100.0 250.0	1.55 0.08	4	27.3 0.5	30.0	42	46	B
						100.0 311.0	1.55 0.08	5	24.5 0.8	27.0	38	42	B
1 S., 10 E. 9BC	DU	45-29.79	121-33.75	RDH-RP 4/12/79	560	10.0 20.0	(1.46)	—	273.0 3.0	—	(400)	—	—
						10.0 150.0	1.63 0.10	5	<61.0	<56.0	<100	<91	C
1 S., 10 E. 29CA	DU	45-27.14	121-34.79	RDH-PD 4/11/79	725	.0 135.0	1.83 0.08	5	—	—	—	—	X
2 S., 7 E. 34BB	HC	45-21.51	121-56.10	CCPA-WW 6/15/76	442	10.0 35.0	—	—	45.4 0.6	39.0	—	—	B
						35.0 85.0	(1.80)	—	55.5 1.0	43.3	100	78	B
2 S., 8 E. 1CDD	HC	45-25.13	121-46.10	USGS-MCG 5/30/80	902	50.0 300.0	(1.26)	—	102.2 2.3	84.3	(128)	(106)	C
						50.0 595.0	1.64 0.10	7	92.7 2.9	81.4	152	134	B
						300.0 595.0	1.74 0.07	6	84.7 1.1	77.3	148	135	B
2 S., 8 E. 9AC	HC	45-24.64	121-49.47	NNG-LCM1 9/25/79	893	80.0 150.0	1.63 0.13	6	67.5 0.5	62.1	110	101	B
2 S., 8 E. 15CD	HC	45-23.46	121-48.47	NNG-OMF2 11/16/78	777	100.00 250.0	(2.09)	—	69.4 0.3	64.0	(145)	(134)	C
						490.0 600.0	(1.55)	—	67.8 2.2	65.0	(105)	(101)	B
						600.0 850.0	1.87 0.08	9	51.4 5.0	51.4	97	97	B
						1,000.0 1,200.0	1.75 0.06	21	55.0	55.0	96	96	B
2 S., 8 E. 15DA	HC	45-23.74	121-48.33	DOEOMF7A 7/15/81	841	90.0 1,250.0	1.82	—	65.2 0.2	62.6	119	114	B
						1,250.0 1,790.0	2.27	—	57.0 0.3	56.8	129	129	B
						Best Value						119 10	B
2 S., 8 E. 17CC	HC	45-23.25	121-51.07	NNG-OMF3 12/21/78	658	100.0 398.0	1.51 0.13	5	63.7 2.4	57.9	96	87	B
2 S., 8 E. 28AA	HC	45-22.36	121-49.30	NNGOMF10 9/25/79	810	75.0 130.0	1.49 0.08	4	73.7 0.4	66.3	110	99	B
3 S., 7 E. 3A	HC	45-20.64	121-55.37	RDH-RD19 4/12/79	148	30.0 65.0	(1.21)	3	57.7	54.0	70	66	D
3 S., 8 E. 14BC	HC	45-18.94	121-47.70	NNG-KC-1 9/25/79	953	100.0 285.0	2.24 0.08	18	18.1 0.7	16.4	41	37	B

Table 1. *Heat-flow data from 25 wells within a 20-km radius of Mount Hood stratovolcano, Oregon*—Continued

T., R. sec.[1]	Province name[2]	N. lat. deg. min.	W. long. deg. min.	Hole and date (m)	Collar elev. (m)	Depth interval (m)	Avg. thermal conductivity[3,4] ($Wm^{-1}K^{-1}$)	No. of thermal conductivity measure-ments[3]	Uncorrected gradient[4,5] (°C/km)	Corrected gradient (°C/km)	Uncorrected heat flow[5] (mWm^{-2})	Corrected heat flow[5] (mWm^{-2})	Quality of heat flow[6]
3 S., 8 E. 16CD	HC	45-18.38	121-49.85	CR-LH 2/7/77	762	50.0 120.0	2.18 0.06	9	26.3 0.3	28.0	57	61	B
3 S., 8 E. 24ABB	HC	45-18.24	121-45.91	THNDRHDL 8/19/80	1,127	50.0 536.0	(2.30)	—	22.3 2.2	22.3	(52)	(52)	D
						500.0 536.0	(2.30)	—	48.7 0.7	48.7	(112)	(112)	D
3 S., 8 E. 24BBD	HC	45-18.13	121-46.45	SKI-BOWL 5/25/77	1,106	0.0 60.0	(1.67)	—	(60.0)	(55.0)	(100)	(92)	D
3 S., 8 E. 29DDC	HC	45-16.57	121-50.55	RDH-SC 1/5/79	722	100.0 150.0	2.64 0.18	5	34.1 1.7	25.2	90	67	C
3 S., 8½ E. 25AA	HC	45-17.25	121-43.68	CR-SB 2/7/77	1,167	0.0 82.5	1.67 0.11	6	—	—	—	—	X
3 S., 8½ E. 25CA	HC	45-16.96	121-44.10	NNG-TRLK 10/23/79	1,109	180.0 315.0	(1.76)	—	53.9 0.4	53.9	(95)	(95)	B
3 S., 9 E. 3CCA	HC	45-19.95	121-39.73	MEADOWS 8/21/81	1,634	275.0 310.0	(2.01)	—	45.6 0.2	51.2	(92)	(92)	D
						310.0 354.0	(1.92)	—	71.0 0.3	79.8	(137)	(154)	C
						275.0 354.0	2.02 0.08	4	61.0 0.9	68.5	123	139	C
3 S., 9 E. 6DD	HC	45-19.88	121-42.50	CR-HH 9/14/76	1,798	10.0 115.0	1.85 0.07	4	—	—	—	—	X
3 S., 9 E. 7AB	HC	45-19.75	121-42.58	RDH-TBLG 12/13/78	1,761	0.0 195.0	—	—	—	—	—	—	X
						195.0 225.0	(1.84)	—	201.7 7.0	201.7	(371)	(371)	D
3 S., 9 E. 7DBB	HC	45-19.30	121-42.93	USGS-PUC 8/15/81	1,631	220.0 330.0	—	—	137.4 4.7	—	—	—	D
						330.0 580.0	(1.55)	—	71.8 1.8	71.8	(111)	(111)	B
						560.0 1,125.0	1.79 0.03	20	67.2 1.5	67.2	121	121	B
3 S., 9 E. 16CAD	HC	45-18.37	121-40.57	WHT RIVR 7/2/81	1,330	100.0 303.0	2.51 0.13	4	39.0 1.5	—	98	—	D
						100.0 250.0	2.51 0.13	4	45.4 0.4	45.4	114	114	D
						250.0 303.0	2.37	2	10.2 0.4	10.2	24	24	D
3 S., 9 E. 30ADB	HC	45-17.17	121-42.69	USGS-HWY 10/22/79	1,108	80.0 289.0	(1.76)	—	41.5 0.5	41.5	(73)	(73)	B

[1]Location of holes within a section is given by the convention that A, B, C, and D represent NE, NW, SW, and SE subdivisions, respectively, and the sequence is from ¼ to ¼¼ to ¼¼¼ section. Thus hole 2ABB is in the NW ¼ of the NW ¼ of the NE ¼ of sec. 2.

[2]DU = Deschutes-Umatilla Plateau, HC = High Cascades.

[3]Values in parentheses were assumed, based on measurements of typical lithologies of the area or from one or two samples from cuttings from the hole.

[4]Standard error is shown below average value.

[5]Values in parentheses are based on assumed thermal conductivities or on conductivities based on one or two samples from cuttings from the hole.

[6]A = 100+-m linear gradient, core thermal conductivity, estimated error ± 5 percent; B = linear gradient, estimated error ± 10 percent; C = disturbed gradient or uncertain thermal conductivity, estimated error ± 25 percent; D = estimated value; X = value disturbed by ground-water flow.

SOUTHWEST SIDE

There are five holes at the southwest corner of the Mount Hood volcano. All of these holes penetrate the 9-m.y.-old quartz diorite Still Creek and Laurel Hill plutons. These plutons must be somewhat larger than their exposed surfaces indicate since holes 14BC and 24ABB encountered quartz diorite below a surface cover of the andesite flows and lahars. Hole 29DDC is in the Still Creek pluton, which is probably connected in the subsurface with the Laurel Hill pluton. The microquartz diorite intervals observed in OMF-7A (15DA) may represent apophyses at the edges of this pluton. None of the heat-flow values in this set of holes is regional, and there appear to be two types of effects present. When holes 14BC, 16CD, and 29DDC are taken together, it would appear that there is a local forced convection system driven by the topographic differences between the holes in which heat is being transferred from the higher elevations to the lower elevations in a medium-scale ground-water system. A thermal model of this type of convection system has been used by Morgan and others (1981) in explaining regional heat-flow variations in the Rio Grande Rift. Their model is based on the approximate solution to ground-water flow discussed by Domenico and Palciauskas (1973). Typical overall permeability values of 50-100 millidarcies are required for such a system to exist.

The redistribution of heat is illustrated by the temperature-depth curves in Figure 3. The two holes at higher elevation have subnormal gradients and heat-flow values, while the hole at the lowest elevation, in the bottom of the Still Creek valley, has very high heat flow at shallow depth and a decreasing heat flow (to very low values) at greater depths. The hole probably has a regional gradient just below the depth to which the hole was drilled. The temperature-depth curve for hole 2S/8E 17CC (Figure 2) shows a background gradient. Hole 24ABB, farther to the east, is somewhat different. Overall, the temperature-depth curve indicates downflow to a depth of at least 350 m; however, there may be lateral flow of slightly warm water indicated by the shape of the upper part of the temperature-depth curve. The heat flow in the bottom of the hole may represent the regional value.

TIMBERLINE LODGE

Three holes were drilled in the vicinity of Timberline Lodge. These holes were drilled sequentially, with each succeeding hole to greater depth. The deepest hole is 7DBB,

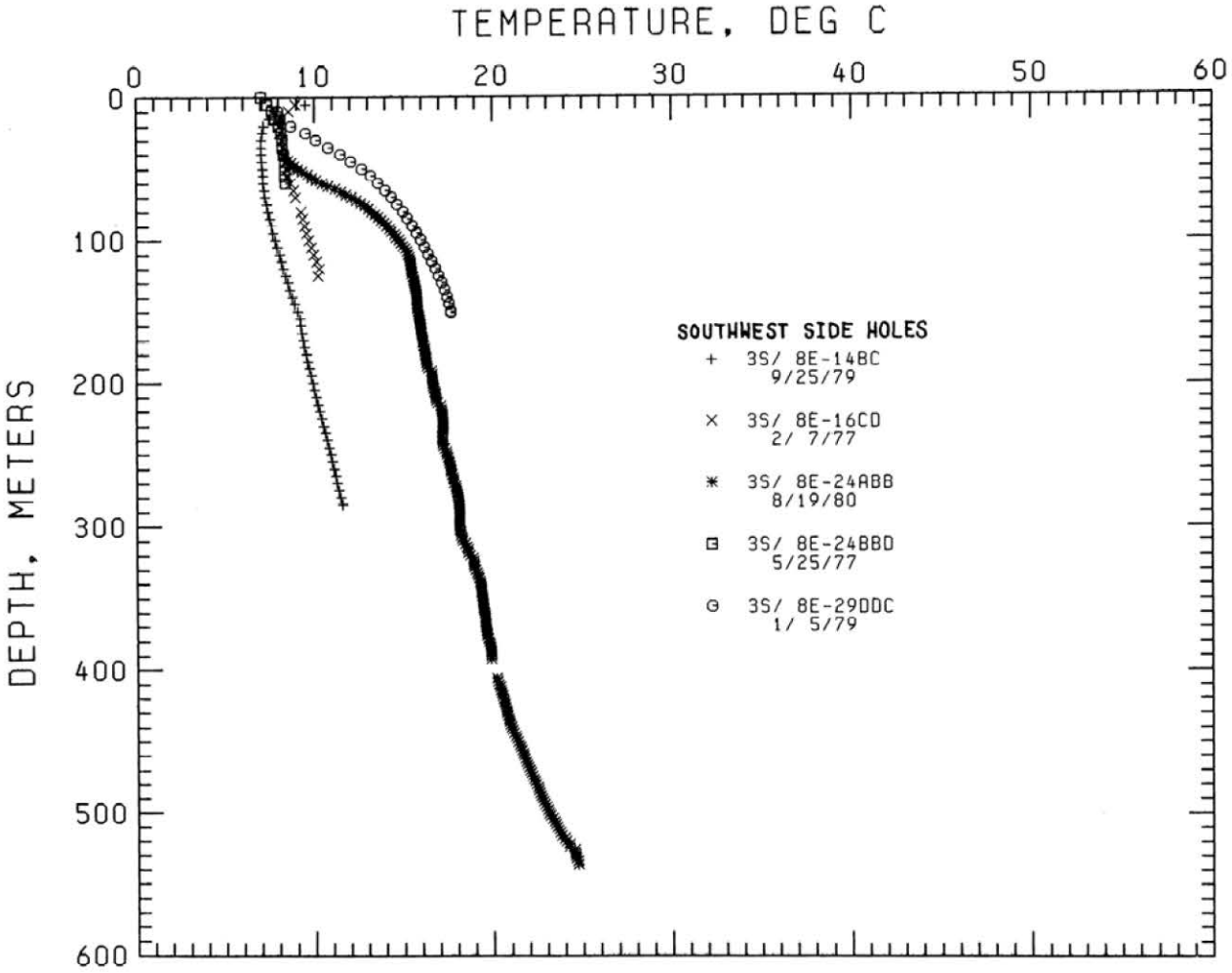

Figure 3. Temperature-depth plots for holes on the southwest side of the mountain in the Laurel Hill and Still Creek quartz diorite plutons.

at the base of the Pucci Chairlift. This hole has a characteristic water disturbance in the upper part. There is essentially no gradient to a depth of about 200 m, at which point there is a very steep gradient of over 200° C/km, which then decreases to a mean gradient (terrain-corrected) of 72° ± 2° C/km, which is almost constant to a depth of 1.2 km (see Figure 4). The heat flow calculated for this hole is 121 mW/m^2, based on thermal-conductivity measurements of cuttings with in situ conductivities calculated using porosity values estimated from commercial geophysical logs which were run in the hole.

The combination of low gradients in an aquifer in the outermost layers of the volcano, coupled with very high gradients immediately below the aquifer, indicates a groundwater system that is extracting part of its thermal energy from the underlying rocks. The temperature-depth data indicate that the apparent conductive surface is at a depth of 150 m rather than at the topographic surface and that removal of 150 m of material from the mountain would cause no disturbance to the temperature-depth curve. This phenomenon is characteristic of the types of temperature-depth curves seen in other places in the High Cascade Range and indicates that, in general, the very permeable upper parts of the young volcanic section are transparent to heat flow. Thus, a large thickness of these rocks can be deposited and eroded without modifying the temperatures at greater depths to any significant extent. This phenomenon, in turn, implies that estimates of depth of erosion and the effect of erosion on heat flow, based on volumes of sediment eroded into associated geosynclines, may not be valid and that, in fact, erosion effects may be much less than have been assumed in many past reconstructions.

Data from this hole indicate conductive heat transfer between depths of 200 m and 1.2 km. Measurements of the elevation of the water level in the well are very interesting. The water level varied, ranging from 80 m when the hole was 100 m deep, to 200 m when the hole was 600 m deep, to 570 m when the hole was 1.2 km in depth. This decrease of water level with increasing depth implies that the lower parts of the hole are underpressured with respect to the upper parts of the hole. Therefore, it would appear that the vertical permeability is very small; otherwise, the higher pressure shallower water would invade the lower pressure deeper zones. Flow tests indicate, however, that the portion of the hole between 1,100 and 1,200 m is capable of producing significant quantities of fluid, and therefore there is at least some horizontal permeability present. This difference between horizontal and vertical permeability is very character-

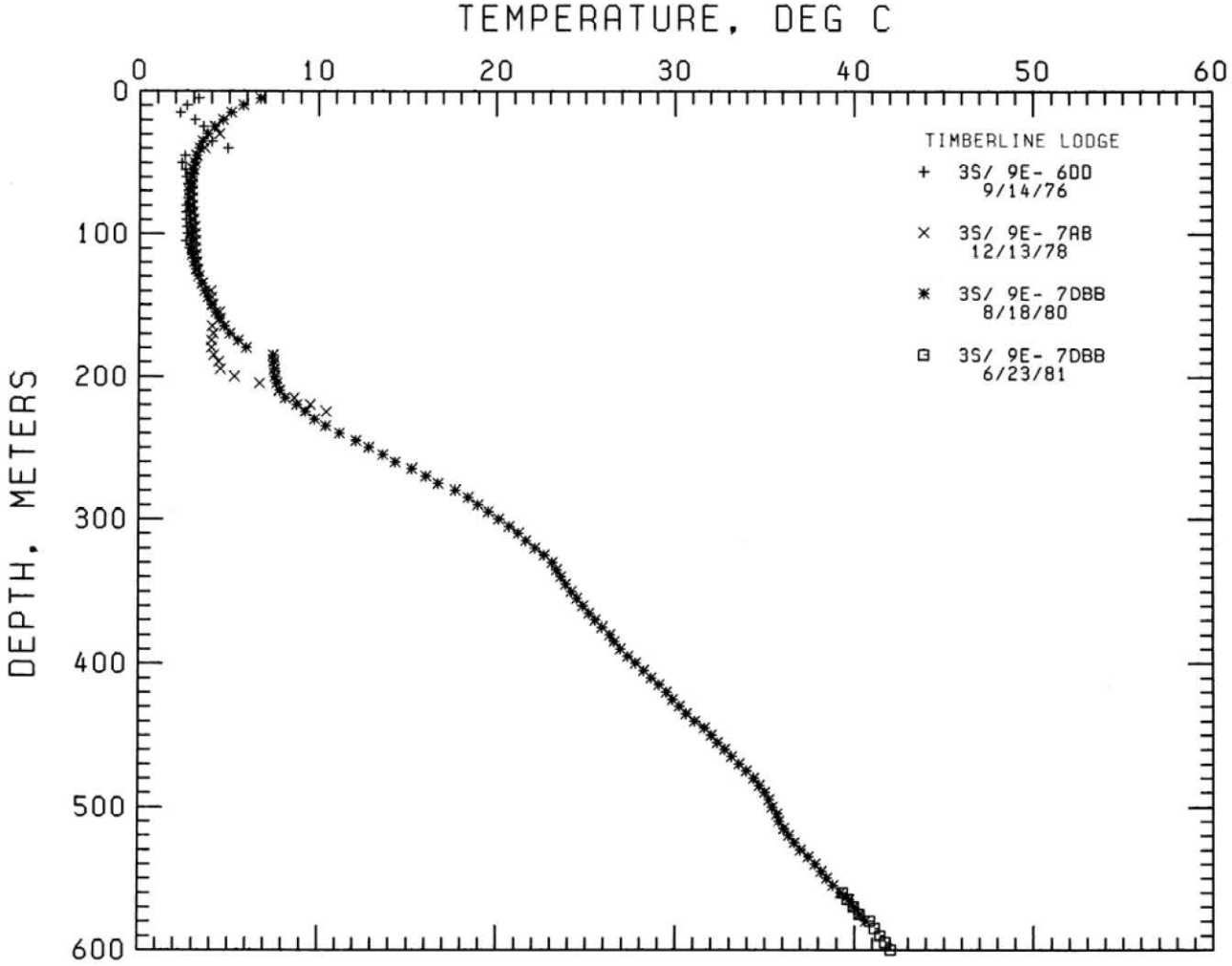

Figure 4. Temperature-depth plots for the holes near Timberline Lodge. Hole 3S/9E-7DBB was actually drilled to a depth of 1.2 km, but the temperature-depth plot is linear below 600 m, with a bottom-hole temperature of 76°C at 1,125 m.

istic of volcanic rock aquifers and seems to indicate that, at least at the place where this hole was drilled, the vertical permeability is not great enough to allow rapid downflow and heating of ground water and thus the generation of very high temperatures at relatively shallow depth. However, the lateral permeability is high, and water levels in various layers are controlled by the elevation of outcrop of the various zones.

SOUTH SIDE

Three holes were available directly south of the volcano. One of the holes, 25AA, is relatively shallow and is completely disturbed by shallow ground-water flow. The two deeper holes also show low gradients (Figure 5). The shape of one of these, 25CA, is similar to the temperature-depth curve observed at Timberline Lodge, with very low gradients, then very high gradients, and then what appears to be the regional gradient extending in this case from 80-300 m with no significant variation. In hole 30AB, the shallow aquifer is somewhat warmer and thus apparently less active, and there is no high gradient at the base of the shallow aquifer. For hole 25CA, the apparent surface of the earth is the same as the topographic surface, even though the upper part of the hole is disturbed. The gradients in these two holes are somewhat lower than those observed in the northwest side of the mountain. As no thermal-conductivity samples were available from either of these drill holes, the values shown in Table 1 are estimates. The rocks are Pliocene lava flows with a low porosity. The heat-flow values, 95 and 73 mW/m^2, are less than those observed on the northeast side.

SOUTHEAST SIDE

Two holes are available on the southeast side of the mountain (Figure 6). These holes are quite close to the Timberline Lodge holes and are among the closest to the apex of the volcano. The nature of the heat transfer indicated by both of these holes is quite different, however, in that the holes do not appear to show conductive heat flow. Hole 3CCA is the second highest in elevation on the mountain. This hole, which is located at Mount Hood Meadows ski lodge, indicates a uniform downward component of water flow in an aquifer. This downward component of water flow can be calculated using the equation of Sorey (1971), which has become very popular recently and has been used by a number of authors, notably Mansure and Reiter (1979), Lachenbruch and Sass (1977), and others. It

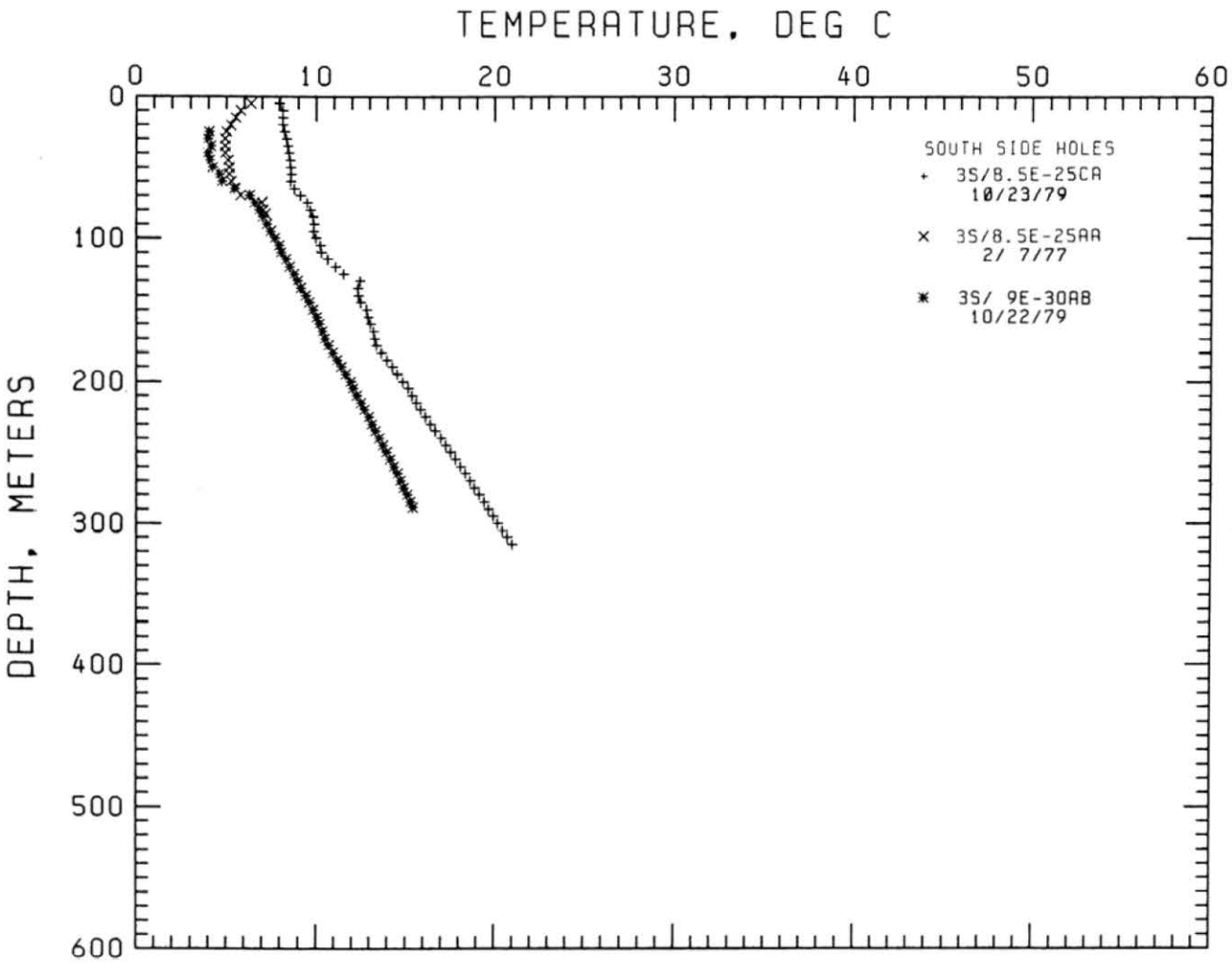

Figure 5. Temperature-depth plots for holes on the south side of the mountain.

should be pointed out, however, that in many of the situations to which this equation is applied, the total component of water flow is not downflow, and the component of flow only in the vertical direction is actually obtained by the equation. An alternative way of viewing this curve is as the recharge end of a forced convective system such as that observed in the Still Creek and Laurel Hill plutons (see above).

Located at a somewhat lower elevation, hole 16CAD also has an enigmatic temperature-depth curve. If this hole had been drilled another 100 m, we would probably be able to clearly understand the characteristics of heat transfer in the hole. The temperature-depth curve could be caused by borehole upflow or lateral flow of warm water in a generally colder regime, so that the curve might be very similar to that observed in the upper parts of holes 24ABB and 9BC. Without deeper information, however, it is not possible to say much about either of these holes; the gradient in the bottom of the holes may or may not indicate the regional gradient. The heat-flow values calculated for the bottom part of hole 3CCA and the upper part of hole 16CAD are probably not regional values, but they are similar to those observed elsewhere at about the same distance from the apex. Without deeper information, we cannot unequivocally evaluate the heat flow on the southeast side of the mountain.

NORTH AND NORTHEAST SIDES

Since no holes were available for the east side of the mountain, the final set of data to be discussed is from the north and northeast. All these holes are relatively shallow; the deepest hole is 311 m. Temperature-depth curves are shown in Figure 6. Hole 29CA is isothermal to its total depth of 150 m, indicating that the hole did not penetrate below the shallow aquifer. Hole 9BC has a very interesting temperature-depth curve. This hole was drilled in Columbia River basalt, near the Hood River fault. The curve is interpreted to indicate lateral flow of warm water in a very shallow aquifer at a depth of about 40 m. The mean background gradient is less than 60° C/km. Regional data in this part of the mountain indicate that the regional gradients are probably about 45° C/km, and regional heat-flow values are about 60-70 mW/m^2, although there is some evidence for slightly higher values directly north and farther away from the mountain (Black-

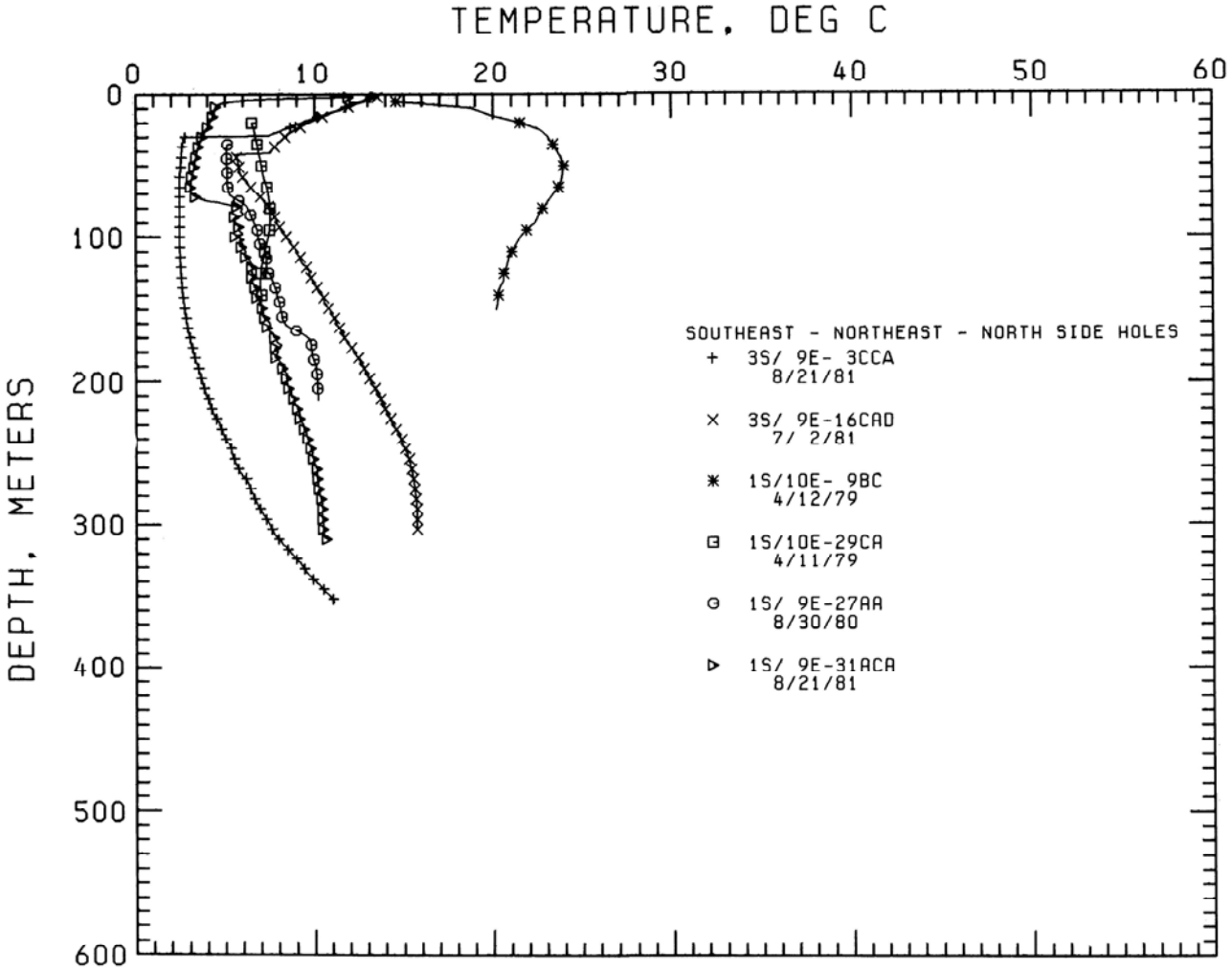

Figure 6. Temperature-depth plots for the southeast, northeast, and north sides of the mountain. The holes on the southeast are 3S/9E-3CCA (Mount Hood Meadows) and 3S/9E-16CAD. The holes on the northeast side of the mountain are 1S/10E-9BC and 1S/10E-29CA. The two holes on the north side of the mountain are 1S/9E-27AA and 1S/9E-31ACA.

well and Steele, 1979; Steele and others, in preparation). The interpretation of this type of temperature-depth curve has been discussed by Ziagos and Blackwell (1981).

Holes 27AA and 31ACA both have very low gradients, much lower than those characteristic of conductive heat flow elsewhere around the mountain. These holes, which were drilled in Pliocene lava flows, have not penetrated below the shallow ground-water aquifer, and only a small component of the total heat flow is being measured. Thus the heat-flow values calculated for these holes, 40-60 mW/m^2, are not considered characteristic of the conductive heat flow on the north side of the mountain.

DISCUSSION OF GEOTHERMAL POTENTIAL

The results of the measurements in the vicinity of Mount Hood represent a unique study of the geothermal character of a stratovolcano and allow us to make some generalizations about its thermal structure which may or may not be applicable to other stratovolcanoes. Only similar studies in other areas will allow us to extrapolate the model obtained for Mount Hood. Data from the holes at Timberline Lodge and on the northwest side of the mountain seem to give relatively reliable conductive information on the nature of the deep thermal conditions. Similar reliable information may or may not be obtained for those holes directly south of the volcano. Temperatures in holes southwest, north, and northeast of the volcano are dominated by forced ground-water convection and do not give reliable estimates of the conductive heat flow from depth. In Pliocene or younger lava flows, permeability is so great that conductive heat transfer is not oberved in most cases, and holes must be drilled to a depth on the order of 300 m to get below the effects of convective heat transfer. The maximum depth of circulation in these areas is not yet known. In a general way, as the rocks get older or more deeply buried, the permeability decreases. The diorite intrusives along the southwest side of the mountain are an exception to this generalization, however, demonstrating that in the older rocks secondary permeability (fracture zones, fault zones), such as is the case in the Still Creek and Laurel Hill plutons, is necessary if much fluid flow is to take place.

A summary of the heat-flow data around the mountain is shown in Figure 7. The heat-flow data are plotted as a function of distance from the apex of the mountain. There is quite a wide variation in possible heat-flow values associated

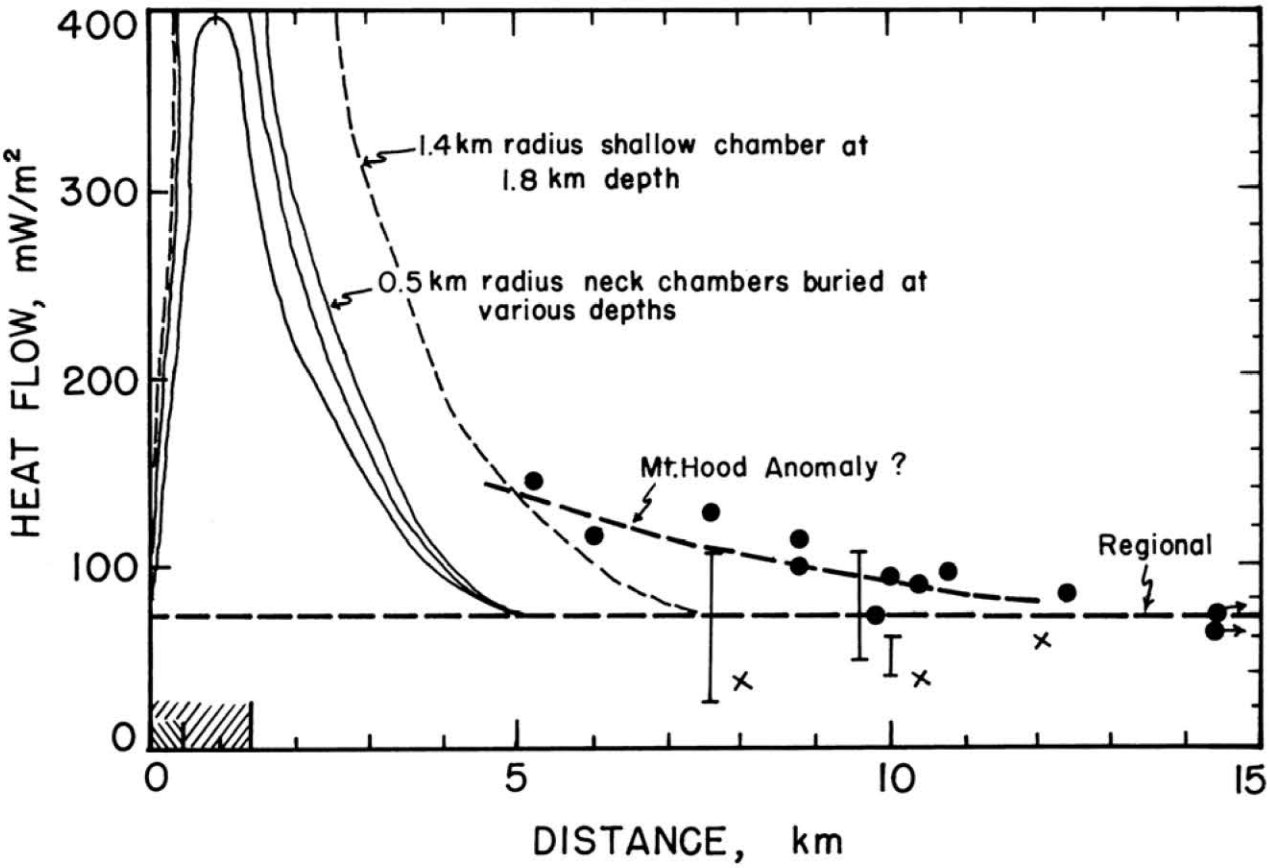

Figure 7. Heat flow as a function of distance from the apex of Mount Hood. Ranges of heat-flow values are shown for holes which have various kinds of disturbances. The probable regional background heat-flow value (80 mW/m^2) is shown as a horizontal dashed line. Speculative fits to the data as a function of distance away from the mountain are shown. Data which are assumed to be subregional and lowered by shallow ground-water flow are indicated by x's. Conductive heat-flow anomalies from neck-type magma chambers beneath the axis of the mountain are shown as solid lines. These models were calculated with a finite difference program assuming steady state and a volcano topography. The depth at the top of the magma chamber is as indicated. The models are discussed in more detail by Steele and others (in preparation).

with several of the holes, and the total range of variation is shown by the bars in Figure 7. The regional background heat flow in this area ranges from somewhere between the 100 mW/m^2 value to the south (Blackwell and others, in press) and the 80 mW/m^2 value characteristic of the Washington Cascades (Schuster and others, 1978). Consideration of the regional heat-flow data away from the mountain suggests that the best regional background heat-flow value for the area around Mount Hood is probably 80 mW/m^2 (Steele and others, in press). A horizontal line at 80 mW/m^2 has been shown in Figure 7. An argument can be made for a gradual increase in heat flow beginning approximately 12 km from the volcano toward the apex of the volcano, with a slope of about 20 mW/m^2. It is possible that there is a slightly different rate of variation for holes on the northwest side of the volcano and for holes to the south.

Also plotted on Figure 7 are theoretical heat-flow values from a neck-type magma chamber 1 km in diameter at depths of 0.5, 1.4, and 2.1 km below the surface. These models were calculated for the actual topography of the volcano and have been discussed in more detail by Steele and others (in press). It is clear that we do not yet have data sufficiently close to the apex of the mountain to detect the presence of a neck-type magma chamber. It is quite clear that such a magma chamber must exist, however, because of the presence of active fumaroles at the top of the mountain and the fact that the recurrence rate of volcanism in the mountain is sufficient to keep the axis at near-magmatic temperatures (Hardee, in preparation). The data do indicate the presence of increasing temperature at depth toward the center of the mountain. Because we have data only from the extreme tails of the anomaly, an analysis of the shape of, and depth to, the possible heat source is not possible. Since the holes at Timberline Lodge are as close to the top of the mountain as existing roads will allow, it is unlikely that we will obtain additional data closer to the apex of the anomaly. We therefore will not be able to obtain a good resolution of possible shapes of magma chambers which might be associated with Mount Hood. Such a chamber, if present in addition to the neck-type chamber, must be rather deeply buried and/or old.

This information from the holes which give conductive gradients suggests that there is no large, shallow subvolcanic magma chamber (i.e., a chamber with a top of 3 km or less and a radius greater than 2-3 km), as has been proposed for many stratovolcanoes. Other heat-flow data from the vicinity of Mount Jefferson and Mount St. Helens suggest that the same conclusion can be applied to these volcanoes. The repetitive activity of the volcanoes and the presence of active summit fumaroles indicates, however, that there is some volume of hot rock beneath the volcano. The calculations of the thermal history of neck-type magma chambers which were discussed by Steele and others (in preparation) suggest that recurrence rates of less than 1,000 years will keep the conduit of the volcano at near-magma temperatures. This condition is required for a repetitive intrusion of relatively small magma bodies of high viscosity at the same location, as is typical of many andesite and dacite volcanoes. Hardee (in preparation) found that a neck-type magma chamber would be a permanent feature of the volcano if the volume rate of volcanic products exceeded about 10^{-3} km/yr, regardless of the time spacing of the volcanic events.

The model for geothermal anomalies associated with many stratovolcanoes is a downward percolation near the axis of the summit, then lateral flow of the hot water to the flanks of the volcano (see Wollenberg and others, 1979). The results at the Pucci site indicate that the vertical permeability in at least part of the mountain is quite low in the rocks below 200 m. In other areas, the results suggest that the vertical permeability is quite high to depths of at least 300 m. The lack of major hot springs around the flanks of the volcano may be evidence that there is not a lot of recharge to great depth in the carapace of the volcano. However, if the background gradients are similar to those observed at Old Maid Flat or in the Pucci hole, then several of the holes indicate subregional temperatures. So some heat is being transferred convectively downslope in the shallow part of the volcano. Whether the circulation systems have developed sufficient depth for generation of geothermally interesting temperatures, however, is problematical.

In terms of the possible location of circulation systems, large portions of the volcano which appear most favorable for circulation, i.e., the east and north parts, are as yet undrilled. The youngest lava flow is the Parkdale flow on the north side of the mountain. Certainly, there is little present heat from the flow itself, and holes in the vicinity have low gradients. However, as there may be hotter water at depth beneath this region, this area is certainly one of the prime targets for deeper drilling. Lateral warm-water flow has been discovered in hole 9BC. According to the silica geothermometer, the water in this shallow aquifer may have a reservoir temperature of about 100° C (J.F. Riccio, 1980, personal communication). The highest gradient observed is in the McGee Creek hole on the north-northwest side of the volcano. This gradient is significantly higher than the remainder of the gradients, but the heat flow is not. Only deeper drilling will tell whether a lateral flow of some sort is present or not. If the observed gradients continue to a depth of 3 km, and if permeable rocks are present at that depth, then electrical-grade temperatures (>200°C) and production of fluid might be obtained.

In summary, the heat-flow data indicate a very complicated pattern of heat transfer associated with the volcano. The heat-flow data also indicate that no magma chamber with a radius of several kilometers is present at shallow depths beneath the volcano. The data elucidate the nature of shallow ground-water circulation associated with the stratovolcano and indicate that it is variable from place to place. Thus geothermal exploration in this area is complicated by the variable surface conditions. Even with the extensive drilling at Mount Hood, there are still significant areas with possibilities for geothermal temperatures. In about half of the area of the volcano, drill holes less than 400 m in depth are not sufficient to obtain a true picture of the existing thermal structure.

ACKNOWLEDGMENTS

This study was supported by U.S. Department of Energy (DOE) contract No. DE-AS07-79ID12037 and by subcontracts with the Oregon Department of Geology and Mineral Industries from its DOE contracts No. DE-FC07-79ET27220 and No. AC06-77ET28369.

Field data were collected by the authors and by Gerald Black, Jim Williams, and Steve Worsham. Laboratory measurements and data reduction were carried out by Karen Smith and Cynthia Gwinn. Temperature and thermal-conductivity equipment was manufactured and maintained by Robert Spafford.

REFERENCES CITED

Blackwell, D.D., Bowen, R.G., Hull, D.A., Riccio, J.F., and Steele, J.L., in press, Heat flow, arc volcanism, and subduction in northern Oregon: Journal of Geophysical Research.

Blackwell, D.D., Hull, D.A., Bowen, R.G., and Steele, J.L., 1978, Heat flow of Oregon: Oregon Department of Geology and Mineral Industries Special Paper 4, 42 p.

Blackwell, D.D., and Steele, J.L., 1979, Heat-flow modeling of the Mount Hood volcano, Oregon, *in* Hull, D.A., investigator, and Riccio, J.F., ed., Geothermal resource assessment of Mount Hood: Oregon Department of Geology and Mineral Industries Open-File Report O-79-8, p. 190-264.

Blackwell, D.D., Steele, J.L., and Brott, C.A., 1980, The terrain effect on terrestrial heat flow: Journal of Geophysical Research, v. 85, p. 4757-4772.

Crandell, D.R., 1980, Recent eruptive history of Mount Hood, Oregon, and potential hazards from future eruptions: U.S. Geological Survey Bulletin 1492, 81 p.

Domenico, P.A., and Palciauskas, V.V., 1973, Theoretical analysis of forced convective heat transfer in regional ground-water flow: Geological Society of America Bulletin, v. 84, no. 12, p. 3803-3813.

Hardee, H.C., in preparation, Incipient magma chamber formation as a result of repetitive intrusions.

Hull, D.A., investigator, and Riccio, J.F., ed., 1979, Geothermal resource assessment of Mount Hood: Oregon Department of Geology and Mineral Industries Open-File Report O-79-8, 273 p.

Lachenbruch, A.H., and Sass, J.H., 1977, Heat flow in the United States and the thermal regime of the crust, *in* Heacock, J.G., ed., The nature and physical properties of the earth's crust: American Geophysical Union Geophysical Monograph 20, p. 625-675.

Mansure, A.J., and Reiter, M., 1979, A vertical ground-water movement correction for heat flow: Journal of Geophysical Research, v. 84, p. 3490-3496.

Morgan, P., Harder, V., Swanberg, C.A., and Daggett, P.H., 1981, A ground-water convection model for Rio Grande Rift geothermal resources, *in* Ruscetta, C.A., and Foley, D., eds., Geothermal Direct Heat Program, Glenwood Springs Technical Conference Proceedings, v. 1: Salt Lake City, Utah, Earth Science Laboratory, University of Utah Research Institute (for U.S. Department of Energy), DOE/ID/12079-39, p. 228-231.

Roy, R.F., Decker, E.R., Blackwell, D.D., and Birch, F., 1968, Heat flow in the United States: Journal of Geophysical Research, v. 73, p. 5207-5221.

Sass, J.H., Lachenbruch, A.H., and Monroe, R.J., 1971, Thermal conductivity of rocks from measurements on fragments and its application to heat-flow determinations: Journal of Geophysical Research, v. 76, p. 3391-3401.

Schuster, J.E., Blackwell, D.D., Hammond, P.E., and Huntting, M.T., 1978, Heat-flow studies in the Steamboat Mountain-Lemei Rock area, Skamania County, Washington: Washington Division of Geology and Earth Resources Information Circular 62, 56 p.

Sorey, M.L., 1971, Measurement of vertical ground-water velocity from temperature profiles in wells: Water Resources Research, v. 7, p. 963-970.

Steele, J.L., Blackwell, D.D., Riccio, J.F., and Black, G.L., in preparation, Regional heat flow of Mount Hood and vicinity, northern Oregon Cascade Range.

Williams, D.L., Hull, D.A., Ackermann, H.D., and Beeson, M.H., 1982, The Mt. Hood region: volcanic history, structure, and geothermal energy potential: Journal of Geophysical Research, v. 87, no. B4, p. 2767-2781.

Williams, J.W., 1981, In situ thermal conductivity measurement from geophysical well logs in the eastern Snake River Plain: Dallas, Tex., Southern Methodist University master's thesis, 79 p.

Wise, W.S., 1969, Geology and petrology of the Mount Hood area: A study of High Cascade volcanism: Geological Society of America Bulletin, v. 80, no. 6, p. 969-1006.

Wollenberg, H.A., Bowen, R.G., Bowman, H.R., and Strisower, B., 1979, Geochemical studies of rocks, water, and gases at Mount Hood, Oregon: Berkeley, Calif., Lawrence Berkeley Laboratory (for U.S. Department of Energy), LBL-7092, 57 p.

Ziagos, J.P., and Blackwell, D.D., 1981, A model for the effect of horizontal fluid flow in a thin aquifer on temperature-depth profiles: Geothermal Resources Council Transactions, v. 5, p. 221-224.

THE RELATIONSHIP OF THE COLUMBIA RIVER BASALT GROUP TO THE GEOTHERMAL POTENTIAL OF THE MOUNT HOOD AREA, OREGON

By Marvin H. Beeson and Michael R. Moran[1], Earth Sciences Department, Portland State University, Portland, Oregon 97207; James L. Anderson, Department of Geological Sciences, University of Southern California, Los Angeles, California 90007; and Beverly F. Vogt, Oregon Department of Geology and Mineral Industries

INTRODUCTION

The Columbia River basalt occurs as a layer about 600 m thick underlying the northern Oregon Cascades (Beeson and others, in preparation). An understanding of its stratigraphy and structure in this region is therefore of value in evaluating the geothermal potential of the Mount Hood area. Beeson and others (in preparation) have interpreted the stratigraphy and structure of the Columbia River Basalt Group in the Cascade Range of Oregon on the basis of geologic mapping of exposures within the range (Figure 1) and study of cuttings from the Old Maid Flat drill holes, located just west of Mount Hood. Their structural model, summarized below, is the basis for the following discussion of geothermal potential of the Mount Hood area as related to the Columbia River basalt.

BASALT STRUCTURE MODEL

The structural model of Beeson and others (in preparation) consists of the following elements:

1. A pre-Columbia River basalt trough which extended through the site of the present Cascade Range.
2. Several northeast-trending folds passing through the Cascade Range and merging with folds of the Columbia Plateau, with faulting and thrusting of at least one of the major anticlines.
3. North- to northwest-striking fractures and faults, some with right-lateral movement and some of the more northerly oriented being the locus of dike injection.
4. Cascade upwarp and cauldron-type faulting around Mount Hood.

Because of the limited exposures of Columbia River basalt in this area, considerable extrapolation was required to extend known structures beneath the younger Cascade rocks. Strong evidence, however, suggests that Columbia River basalt underlies the entire northern Oregon Cascade Range. Deep drill holes anywhere in the area should encounter it, thereby providing stratigraphic control and additional structural detail, whether or not the basalt flows themselves are a target for geothermal exploration. There are two types of information that may be derived from this study of Columbia River basalt: (1) location of heat sources, and (2) factors governing the hydrology of potential geothermal water.

[1]Present address: Kennecott Minerals Co., P.O. Box 11248, Salt Lake City, Utah 84147.

IMPLICATIONS FOR GEOTHERMAL POTENTIAL

Heat sources

The Cascade Range of Oregon possesses a higher than normal geothermal gradient (Hull and others, 1977), and further definition of more local heat sources is desirable. Although a very young intrusion of silicic to intermediate composition is generally considered to be an ideal potential heat source, no such body has yet been located near Mount Hood. Two small plutons, the Still Creek and Laurel Hill intrusions, are exposed in this area, but they have been dated respectively as 11.6 m.y. B.P. (Wise, 1969) and 8 m.y. B.P. (Bikerman, 1970), much too old to possess adequate heat. These intrusives are located along a projected northeast-trending syncline within the Columbia River basalt. It should be noted, however, that evidence for the location of this syncline is very sparse, since the only Columbia River basalt known to occur along this line and near the intrusions is a brecciated basalt that crops out on the west side of a major northwest-trending fracture zone in the South Fork of the Salmon River. If structures in the Columbia River basalt controlled the emplacement of these intrusions (and perhaps of Mount Hood itself), the most likely location for a younger pluton would be along this northeast trend, possibly under Mount Hood, as the ages of the plutons appear to decrease in that direction. Whether the bulk of these intrusions ponded above the Columbia River basalt or rose to their present positions as the heavier basalt settled through them is not known.

The dominant regional stress pattern has produced fractures and dikes, most of which trend north to northwest; those features having different trends may be an indication of an unexposed intrusion. An andesite dike in the upper Salmon River near the Still Creek intrusion has a northeast trend, and other eruptive centers in the Cascades also have dikes which vary from the regional pattern, such as in the Fish Creek area south of the Clackamas River area. No Columbia River basalt area mapped for this study contains a significant number of fractures which have orientations other than north-northwest.

Factors relating to hydrology

Whether the heat source is a near-surface, still-hot intrusion or the more regional abnormally high heat flow of the Cascade Range, paths for water movement must be present for this heat to be easily extracted. The structure and stratigraphy of the Columbia River basalt are important as either aquifers or barriers to water movement and therefore critical to an evaluation and exploration of geothermal re-

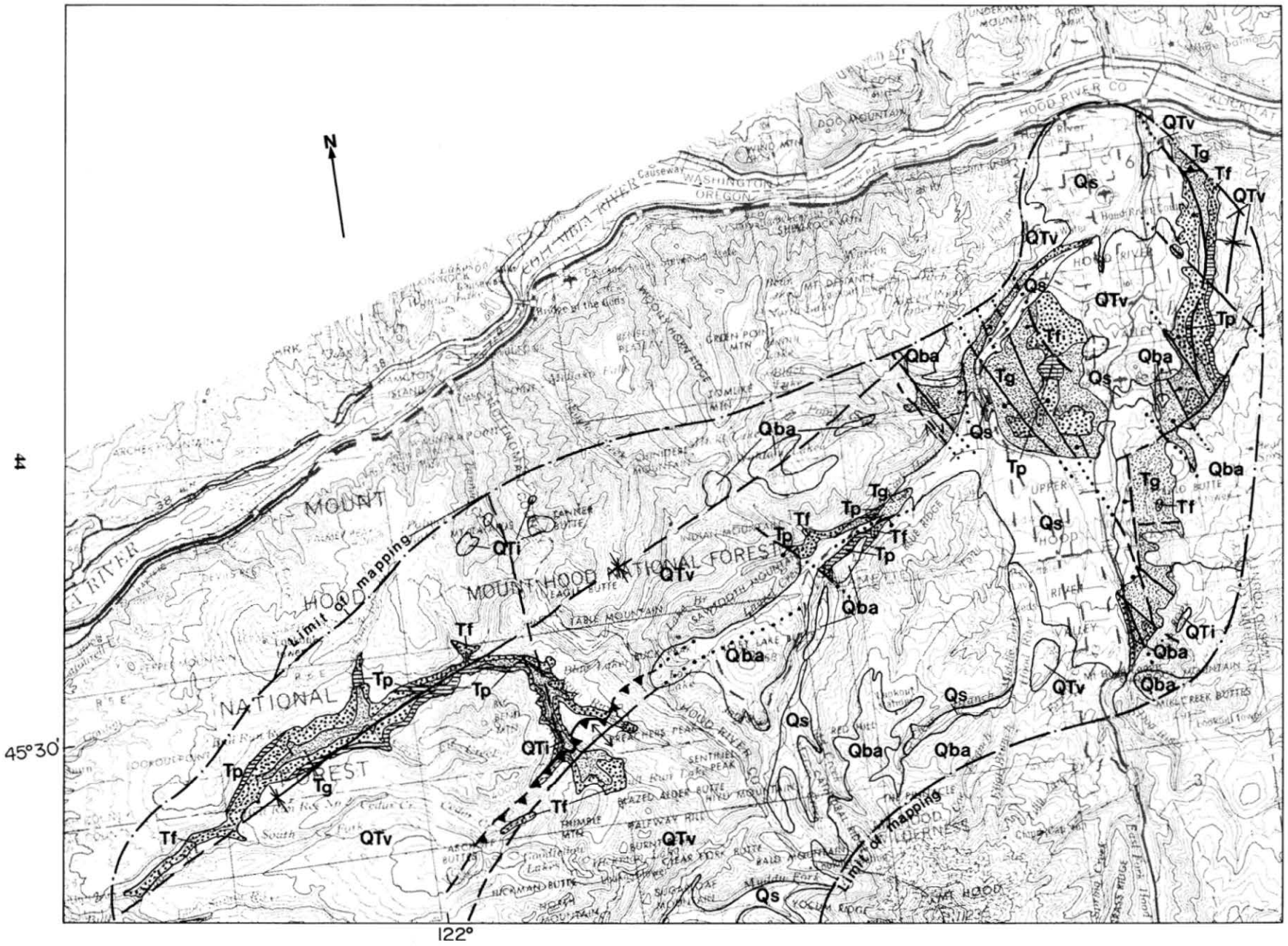
N
Limit of mapping
Limit of mapping
MOUNT HOOD NATIONAL FOREST
QTv
Tg
Tf
Qs
Tp
Qba
QTi
45°30'
122°

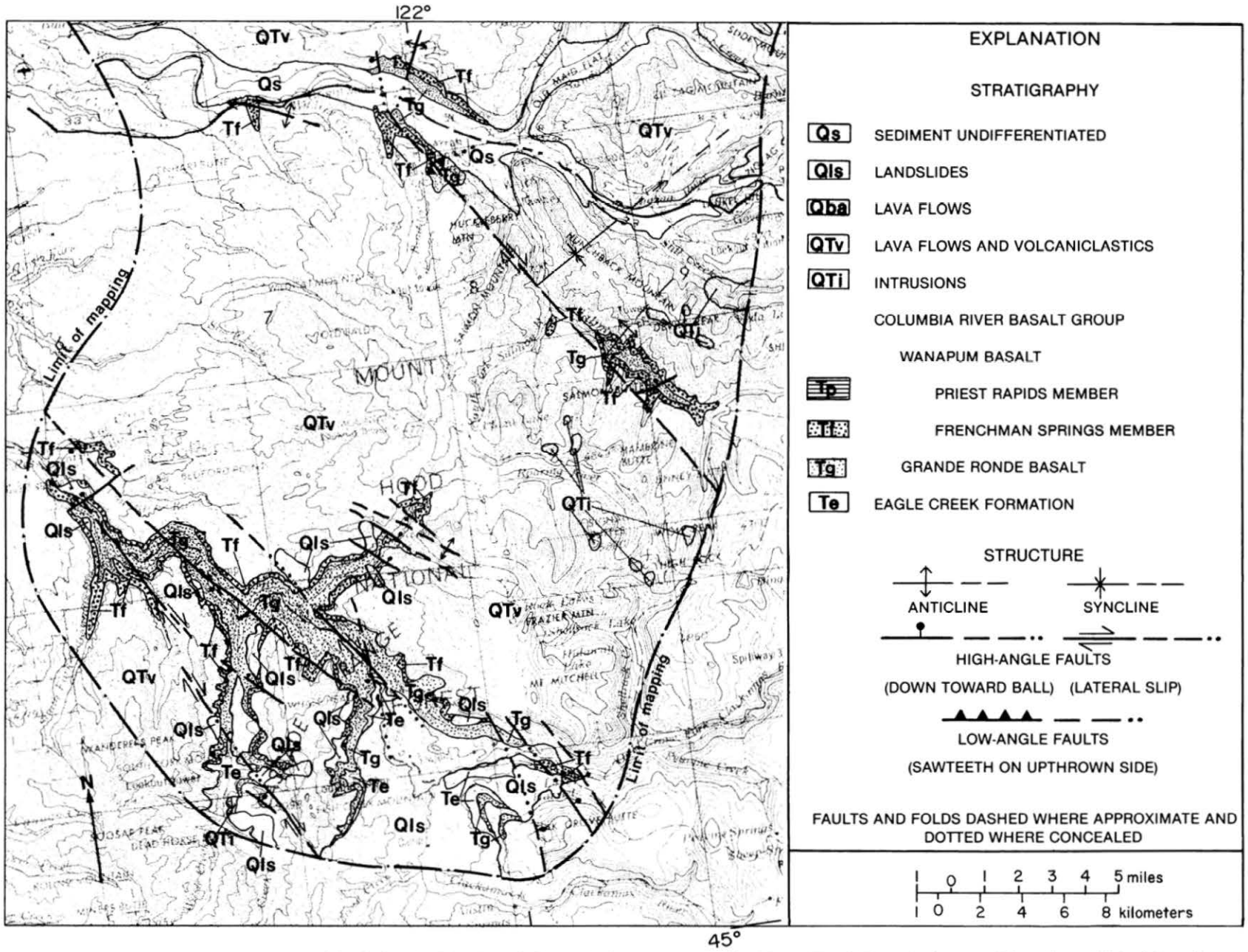

Figure 1. Stratigraphy and structure of the Columbia River Basalt Group in the area surrounding Mount Hood. From Anderson, 1978, and unpublished data; Beeson and Moran, 1979; Timm, 1979; Vogt, 1979, 1981; and Beeson and others, in preparation.

sources. Important features to consider in this regard are as follows:

Interflow areas: Subareal basalt flow sequences often have vesicular, rubbly interflow zones that stand out as natural lateral aquifers. However, hydrologic studies in the Pasco Basin (Gephart and others, 1978) show that some vesicular flow tops have very low hydraulic conductivities (10^{-6}-10^{-13} cm/s). The interflow zones in the Columbia River basalt in the Cascade Range show considerable lateral variation perpendicular to the strike of the major folds and thrusts. Relative consistency seems more the rule along the structures, probably due to the presence of incipient northeast-trending structures during the outflowing of the basalt flows into the area. Low, synclinal areas tended to contain standing water where thin sedimentary layers were formed, and pillow palagonite complexes resulted with the next influx of lava. These zones seem to be linear and extensive, as, for example, in the syncline along the Bull Run River and its possible extension along the West Fork of the Hood River. Present structural highs, both anticlines and thrusts, tend not to contain these interflow features. The low synclinal zones, marked by sedimentary interbeds and pillow basalts, are candidates for good, laterally continuous aquifiers. It should be noted, however, that both northwest- and north-trending structures which could limit lateral continuity occur.

Thrust faults and anticlines: A study in the Pasco Basin indicates that anticlines in the Columbia River basalt may act as barriers to ground-water movement (Gephart and others, 1978). This may be partly due to the lack of interbeds and pillow palagonite complexes as described above, but it may also be that anticlines in the Columbia River basalt tend to be faulted parallel to strike. The best exposed anticline mapped for this study, the Bull Run anticline, is associated with a large thrust fault. The thrust zone contains more than a hundred meters of massive, nonporous tectonic breccia which appears to be quite impermeable. On the basis of field observation only, this breccia zone is judged to be a very poor aquifer and likely a barrier to lateral water movement. In addition, these thrust faults are probably quite shallow features confined largely to the basalt flows. Therefore, a thrust zone is not a preferred target as a geothermal aquifer.

Northwest-trending faults: Northwest-trending faults found in the Columbia River basalt of the study area generally have fairly narrow breccia zones. They are often mineralized and/or contain dikes, which indicates great vertical continuity. These fractures have been the locus of geothermal water at one time, but mineralization has tended to make them impermeable, at least near the surface. These northwest-trending fractures and dikes are probably very good vertical conduits, if recently active and not mineralized at depth, and may bring hot water nearer the surface and perhaps into the lateral aquifers between lava flows. Heat-flow measurements near these fractures may provide a test of this hypothesis.

Caldera or subsidence faults: Some of the arcuate-shaped lineations around Mount Hood are probably the results of subsidence-induced faulting. The depressed elevation of the Columbia River basalt below Old Maid Flat suggests subsidence. Extensive breccia zones are not expected to exist along these faults; however, they should be the most directly connected faults to the subsurface magmatic activity. The Parkdale lava flow, for example, appears to originate from along one of these trends. Therefore, these faults, if young and permeable, may have potential as geothermal conduits.

Non-Columbia River basalt aquifers: The intermediate eruptive episode present in the Old Maid Flat drill holes indicates another possible aquifer, a buried eruptive center. This zone is quite mineralized and impermeable at this location, but perhaps, near the eruptive center, greater permeability may allow greater circulation and less precipitation. Too few data are yet available to speculate on the location of the vent for these eruptions.

Alluvial deposits from a major stream (ancestral Columbia River) flowing through this area prior to the incursion of the Columbia River basalt may form another potential aquifer. Unfortunately, there are almost no data to indicate the position of this former channel. Pre-Columbia River basalt alluvial gravels are not exposed in the Columbia River Gorge, the Clackamas River drainage, or in the drill hole at Old Maid Flat. Perhaps a former stream course would have been structurally controlled by the same tectonic system that produced folds in the Columbia River basalt. If so, it may have been located in the Bull Run syncline or in The Dalles syncline which projects under Mount Hood.

ACKNOWLEDGMENTS

This study was partially funded by the U.S. Department of Energy, administered by the Oregon Department of Geology and Mineral Industries, and subcontracted to Portland State University (PSU Grant No. 90-262-8126).

REFERENCES CITED

Anderson, J.L., 1978, The structure and stratigraphy of the Columbia River basalt in the Clackamas River drainage: Portland, Oreg., Portland State University master's thesis, 136 p.

Beeson, M.H., and Moran, M.R., 1979, Stratigraphy and structure of the Columbia River Basalt Group in the Cascade Range, Oregon, *in* Hull, D.A., investigator, and Riccio, J.F., ed., Geothermal resource assessment of Mount Hood: Oregon Department of Geology and Mineral Industries Open-File Report O-79-8, p. 5-77.

Beeson, M.H., Moran, M.R., Anderson, J.L., and Vogt, B.F., in preparation, Stratigraphy and structure of the Columbia River Basalt Group in the Cascade Range, Oregon.

Bikerman, M., 1970, K-Ar ages of Laurel Hill pluton and dike, Oregon; Oregon Department of Geology and Mineral Industries, Ore Bin, v. 32, no. 11, p. 211-215.

Gephart, R.E., Arnett, R.C., and Leonhart, L.S., 1978, Status of the Pasco Basin hydrology studies, *in* Basalt Waste Isolation Program Annual Report—Fiscal Year 1978: Richland, Wash., Rockwell Hanford Operations RHO-BWI-78-100, p. 114-121.

Hull, D.A., Bowen, R.G., Blackwell, D.D., and Peterson, N.V., 1977, Preliminary heat-flow map and evaluation of Oregon's geothermal energy potential: Oregon Department of Geology and Mineral Industries, Ore Bin, v. 39, no. 7, p. 109-123.

Timm, S., 1979, The structure and stratigraphy of Columbia River Basalt in the Hood River Valley, Oregon: Portland, Oreg., Portland State University master's thesis, 56 p.

Vogt, B.F., 1979, Columbia River Basalt group stratigraphy and structure in the Bull Run Watershed, Western Cascades, northern Oregon [abs.]: Proceedings of the Oregon Academy of Science, v. 15, p. 51-52.

——— 1981, The stratigraphy and structure of the Columbia River Basalt Group in the Bull Run Watershed, Multnomah and Clackamas Counties, Oregon: Portland, Oreg., Portland State University master's thesis, 151 p.

Wise, W.S., 1969, Geology and petrology of the Mount Hood area—a study of High Cascade volcanism: Geological Society of America Bulletin, v. 80, no. 6, p. 969-1006.

HEAT FLOW AND GEOPHYSICAL LOG ANALYSIS FOR OMF-7A GEOTHERMAL TEST WELL, MOUNT HOOD, OREGON

By David D. Blackwell, Charles F. Murphey, and John L. Steele, Department of Geological Sciences, Southern Methodist University, Dallas, Texas 75257

ABSTRACT

Geothermal test well OMF-7A is located in NE¼ SE¼ sec. 15, T. 2 S., R. 8 E., in northwestern Oregon. This hole was the first deep geothermal test hole drilled in the High Cascades of Oregon, and extensive logging, cutting analyses, and core measurements have been carried out in order to evaluate as completely as possible the physical and chemical properties of the rocks encountered in the drill hole. The various rock units encountered in the hole range from basalts to dacites. Discussed in this paper are the geophysical well logs including the velocity, density, gamma-ray, natural gamma-ray, and neutron porosity logs. Crossplots of a range of parameters show that velocity and density are characteristic parameters and allow the separation of the basalts from the remainder of the units. The andesites and dacites tend to behave in very similar fashion in most of the physical property analyses. Measurements of heat production suggest that the mean heat generation for the rocks encountered in the hole is about 1μW/m^3. Detailed laboratory measurements of thermal conductivity and velocity from core samples obtained during the drilling are also presented, and equations relating thermal conductivity to velocity are calculated. A comparison between the laboratory measurements of physical properties and the log measurements shows quite a good correlation, typical errors being less than 5 percent between the properties measured on core samples in the lab and those measured in the equivalent depth in the hole by the geophysical logs. There appear to be at least three groups of lithologies in the hole, based on their velocity-thermal conductivity relationship. Andesites and basalts appear to behave similarly, whereas the dacites have a higher thermal conductivity for a given velocity and the metamorphosed greenstones in the bottom of the hole have a thermal conductivity-velocity relationship which appears to be similar to that of rhyolitic rocks. In the last part of the paper, the velocity-thermal conductivity and temperature-gradient data are combined to calculate thermal conductivity and heat-flow logs for the hole. The overall geothermal gradient in the hole decreases with depth from a surface value of over 70°C/km to a value at the bottom of the hole of approximately 50°C/km. On the other hand, thermal conductivity rises with depth at least proportionally to the decrease in gradient. The terrain effect also contributes to the higher gradients observed at the shallow depths. The mean heat flow in the hole is 114 mW/m^2, and there is some suggestion from the data that the heat flow actually increases with depth, in spite of the decrease in gradient.

INTRODUCTION

Test well OMF-7A was drilled in August-September of 1980 to a total depth of 6,027 feet (1,837 m). The location of the hole is on the west side of Mount Hood at 2S/8E-15DA. The target was production of warm water for district heating to be developed in permeability at the intersection of a steeply dipping normal fault with the Columbia River basalt (see John Hook, this volume). The geology in the general vicinity of the hole is discussed elsewhere in this report (Priest, this volume). In this portion of the report, the data to be discussed are the results of the geophysical and temperature logging, physical property measurements on core samples, an analysis of these two sets of data in order to determine the physical properties of the rock encountered by the drill hole, and an analysis of the thermal regime in and around the drill hole. The regional thermal regime is discussed elsewhere in this report (Steele and others, this volume).

Because this hole was the first deep hole drilled in the High Cascade Range, it was considered important to obtain as much information as possible from the hole. Consequently, an extensive suite of geophysical logs was obtained in the well. The contractor was Schlumberger. These logs are now available as Oregon Department of Geology and Mineral Industries (DOGAMI) Open-File Report O-81-2A/B. The types of logs obtained and many of the technical details of drilling the hole are discussed in a separate report (U.S. Department of Energy [USDOE], 1981). Geophysical logs obtained included borehole compensated sonic travel time (BHC), borehole compensated neutron porosity (CNL), gamma-ray spectroscopy, natural gamma-ray (GR), gamma density (FDC), dual induction (DIL), dip meter, sonic variable density (VDL), fracture identification, and temperature. In addition, temperature logs were run by Southern Methodist University (SMU) and DOGAMI personnel using SMU equipment and by Welex. During the drilling of the hole, six core runs were made. A total of 128 ft (39.0 m) was drilled, with 85 ft (25.9 m) being recovered. Core runs were made at six different depths in the hole, and one core run was made in each of the major lithologic units encountered in the hole. This core plays an important role in the summary of the physical properties of the rocks encountered by the hole.

LOG ANALYSIS

The Schlumberger logs were recorded in digital form, and a digital tape of most of these logs was available for analysis. Figure 1 shows several of the logs. Included are the natural gamma-ray, borehole compensated sonic (plotted as velocity), density, neutron porosity, dual induction and caliper logs. A gamma-ray spectroscopy log was run, as it was felt the log might be very useful in identifying units in this igneous terrain; however, neither run of the log was satisfactory, and therefore this log is not included in Figure 1. Also shown in Figure 1 is a lithologic column based on

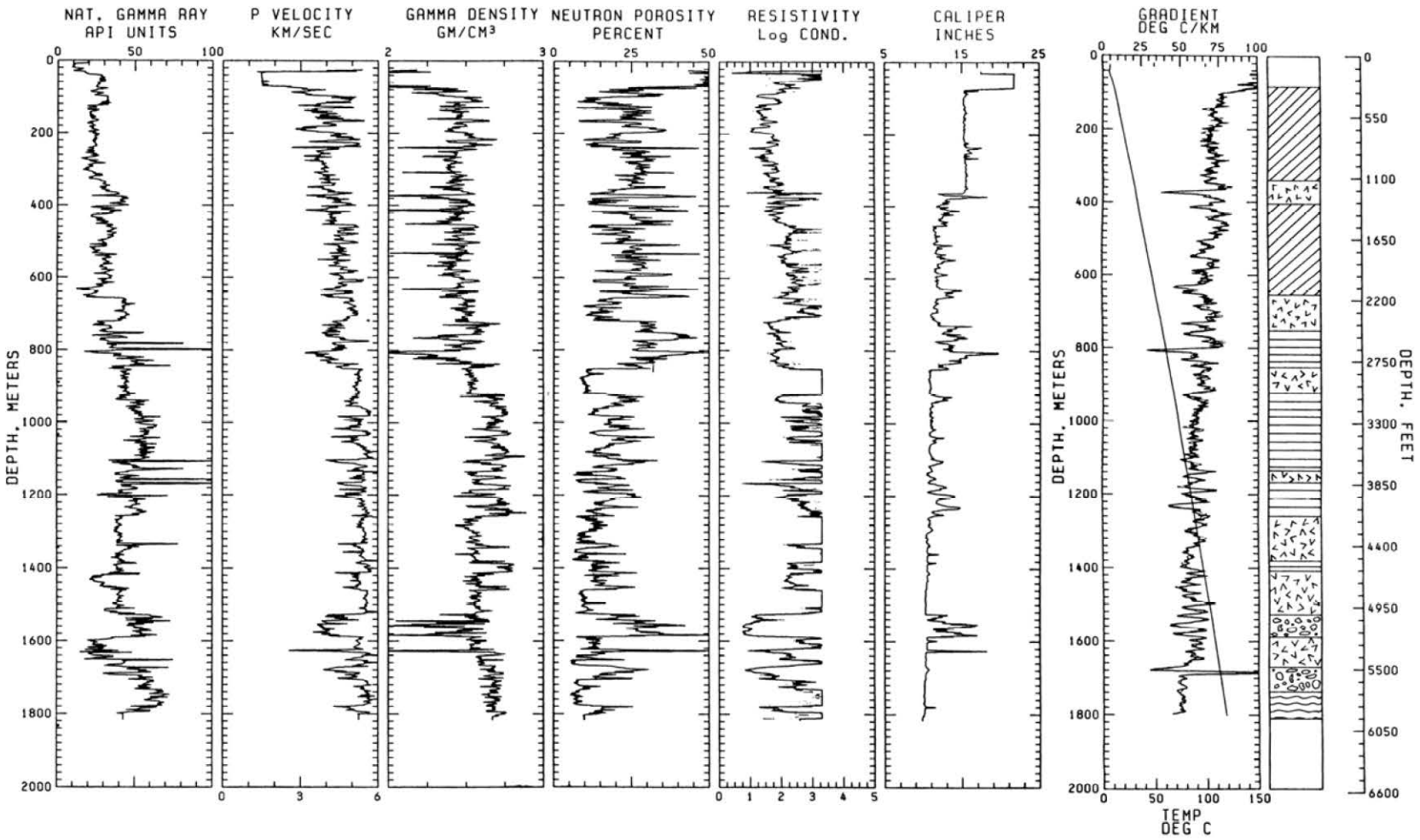

Figure 1. Geophysical well logs for geothermal test well OMF-7A. The logs were plotted from digital tapes supplied by Schlumberger. The points are plotted at 5-ft intervals. The Schlumberger logs include the natural gamma-ray log, travel-time log (plotted as P-wave velocity), gamma-gamma density log, neutron-porosity log, deep-spacing deep-induction lateral log, and caliper (or hole-size) log. Also shown are gradient logs and temperature logs obtained with SMU equipment. Two different gradient logs two weeks apart (July 1 and 15, 1981) are shown. In addition, a summary geologic log for the hole is shown. The key is as follows: diagonal lines = andesitic volcanic rocks, carat pattern = Cenozoic microquartz diorite porphyry intrusives, horizontal lines = Columbia River basalt, pebble pattern = volcaniclastic rocks, wavy pattern = greenstones.

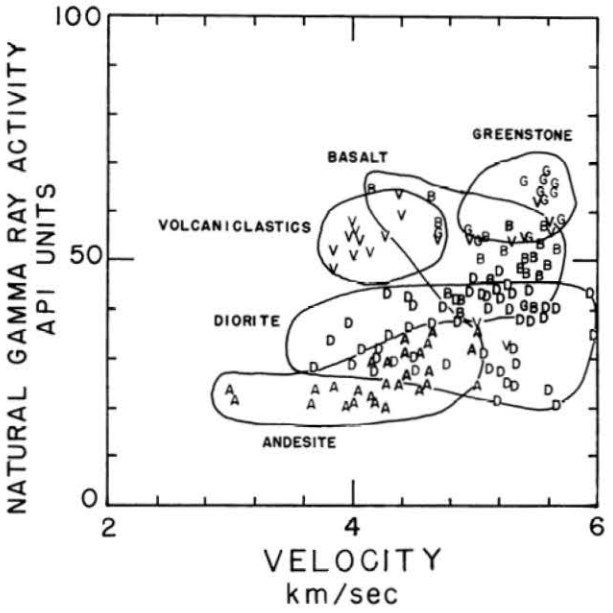

Figure 2. Crossplot of natural gamma-ray activity and velocity. Each letter represents a 5-m (15-ft) interval average for the appropriate property. The general area of the plot occupied by the different lithologies is shown by the line bounding most of the points for each lithology. V = volcaniclastics, B = basalt, G = greenstone, D = diorite, A = andesite.

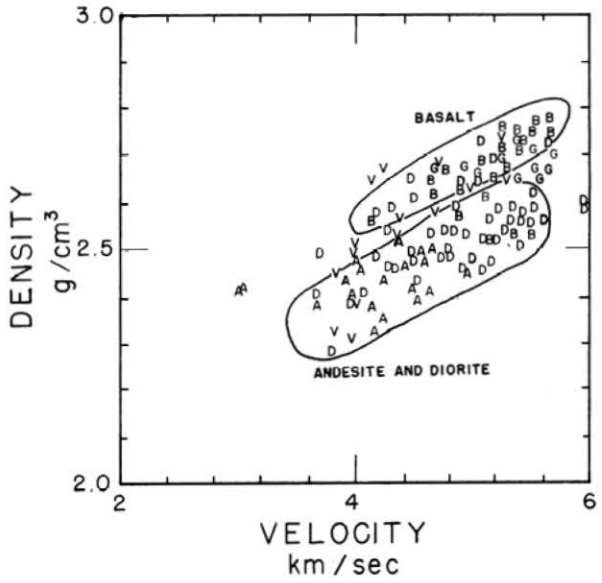

Figure 3. Crossplot of well-log velocity and density. The abbreviations are the same as in Figure 2. Five-m (15-ft) interval averages are plotted.

analyses of cuttings, cores, and logs (Priest and others, this volume). The individual lithologic units are discussed in much more detail in papers by Priest and others and by Holdaway and Bussey in other parts of this report. Basically, the hole consisted of seven different units, as identified in Figure 1. For the purpose of the physical analysis, there are five lithologies of major interest. These lithologies are the various units of andesitic composition (lahars and flows), the Columbia River basalt, a hornblende-microquartz diorite porphyry intrusive, volcaniclastic rocks, and a greenstone unit which appears to be metamorphosed dacite encountered in the bottom of the hole. Each of these particular units has its own characteristic log response, and in general the units can be distinguished by log analysis. The biggest difficulty with log interpretation is that there are relatively large deviations in hole size due to washouts (the caliper log is shown in Figure 1). Virtually the entire hole between the surface casing at 1,190 ft (363 m) and the depth of 2,722 ft (830 m) has been enlarged, and there are numerous zones of the hole where the radius increase is in excess of 2 or 3 in (5-8 cm). The zone from 2,361 to 2,706 ft (720 to 825 m) is particularly enlarged. Similarly, there are enlarged zones around 4,000 ft (1,200 m) and between 5,018 and 5,215 ft (1,530 and 1,590 m). Interpretation of the logs in these enlarged intervals of the hole is uncertain. Three different sets of crossplots were prepared for the hole (see Figures 2, 3, and 4). Each of the points plotted in each of these three figures represents a 15-ft (5-m) average value.

The natural gamma-ray log shows little variation throughout the hole, and values are low; thus most of these rocks are relatively low in uranium, thorium, and potassium content. The highest count rates, about 50 API units, were obtained in the Columbia River basalt section. The dacite has a lower gamma-ray activity than the basalt, and the greenstones in the bottom of the hole have slightly higher gamma-ray activity than the remainder of the units. The response of the greenstones is on the order of 50-70 API units. A crossplot of natural gamma-ray activity and velocity shown in Figure 2 illustrates the general relationships discussed above. Within each group or cluster of data there does not seem to be any systematic relationship between velocity and gamma-ray activity.

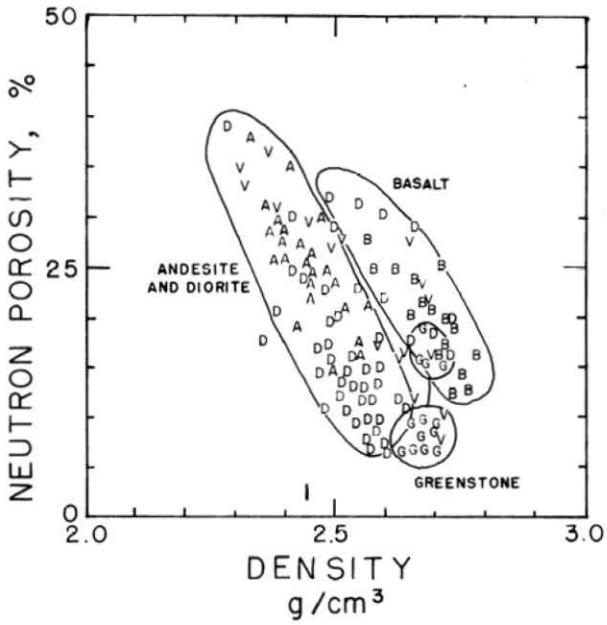

Figure 4. Crossplot of neutron porosity and density. Averages are for 5-m (15-ft) intervals. Abbreviations are the same as those used in Figure 2.

Table 1. *Heat generation (A) from radioactive elements determined from samples from OMF-7A. Samples in first set of columns were measured with a gamma-ray spectrometer system. Samples in the second set of columns were determined by instrumental neutron activation analysis (see Priest, this volume).*

Core depth (m)	Core depth (ft)	Th (ppm)	U (ppm)	K (%)	A ($\mu W/m^3$)	Sample depth (m)	Sample depth (ft)	K (%)	Th (ppm)
486.6	1,596.5	3.0	0.9	1.12	0.6	—	—	—	—
493.2	1,618	4.1	0.9	0.90	0.6	494.4	1,622	0.82	2.3
888.5	2,915	5.3	1.3	1.00	0.8	889.1	2,917	1.43	3.5
1,032.1	3,386.3	7.7	1.5	1.11	1.0	1,034.8	3,395	1.58	6.1
1,341.1	4,400	6.7	2.3	1.38	1.2	—	—	—	—
1,567.6	5,143	9.3	1.9	0.55	1.2	—	—	—	—
1,569.4	5,148.9	8.1	1.8	0.49	1.1	—	—	—	—
1,570.3	5,152	7.8	2.0	0.33	1.1	—	—	—	—
1,834.0	6,017	3.9	3.4	0.94	1.3	1,833.7	6,016	1.18	6.2
1,834.1	6,017.5	3.7	4.1	1.22	1.5	—	—	—	—
1,837.0	6,027	4.2	3.5	1.02	1.3	—	—	—	—

The results of measurements of U, Th, and K contents of certain core samples by pulse height analysis are shown in Table 1. Measurements were made with equipment described by Gosnold (1976). Accuracy of measurements is ± 10 percent of the amount listed. Comparisons with values of K and Th for some samples determined by other techniques (Priest, this volume) are also shown. The results are consistent with the natural gamma-ray log and the rock types encountered. The average heat production for the hole is 1.0 ± 0.1 $\mu W/m^3$.

Figure 3 shows a crossplot of velocity and density. On the basis of their velocity-density relationship, the individual lithologies can be divided into two different groups (see Figure 3). Thus this crossplot is effective in separating the basaltic rocks from the rocks of other compositions. Rocks of andesitic and dacitic composition generally occupy about the same region of the figure. This crossplot, in fact, helped to identify an upper member of the Frenchman Springs basalt section that had been misassigned to andesite on the basis of the preliminary geological studies (2,380-2,460 ft [725-750 m]). On this plot, the greenstones and the volcaniclastic rocks in the bottom part of the hole have the same properties as the Columbia River basalt. The andesite and dacite rocks are about 0.2 g/cm^3 less dense at the same value of velocity than are the basalts. A few intervals in the upper part of the hole have the characteristics of basalt, and there may be thin basalt flows intercalated with the other units there. In the center of individual flows of the Columbia River basalt, relatively high densities (on the order of 2.75-2.8 g/cm^3) are observed. These densities are significantly above those observed in the remainder of the hole. The greenstones average about 2.6 g/cm^3. The dacite averages about 2.55 g/cm^3, while the andesitic rocks, particularly in the upper part of the hole, average less than 2.5 g/cm^3. There is a general tendency for increasing density (and velocity) with depth.

A neutron porosity versus density crossplot is shown in Figure 4. The neutron porosity values are calculated using a limestone matrix and show quite a wide variation, in part due to hole-size variation and in part due to alteration. Based on the log response, hydrogen bound in minerals cannot be distinguished from hydrogen in water in pore spaces. Given the general alteration of the rocks in the hole, it is likely that 5-15 percent of the porosity indicated by the neutron log is related to water bound in minerals. The crossplot of density and neutron porosity shows a relatively clear demarcation between the Columbia River basalt units and the andesites and dacites. As was the case with the velocity-density crossplot, the 2,380-2,460-ft (725-750-m) section of the hole plots in the field of the Columbia River basalt. However, on this plot, the lithologies in the bottom part of the hole are more closely associated with the andesite-dacite field rather than the basalt field. There is some scatter; however, some of the volcaniclastic rocks in the bottom part of the hole have basaltic characteristics.

The induction log shows values of resistivity generally between 10 and 100 ohm-meters to a depth of 2,700 ft (825 m). Below that, the resistivity is generally in excess of 1,000 ohm-meters, except for isolated horizons, such as the volcaniclastic rocks. Resistivity values in a large part of the hole are off scale and thus greater than 2,000 ohm-meters. Because of the fact that so much of the hole is off scale, no attempt was made to calculate crossplots of the induction log and the remainder of the logs.

In view of the existing detailed geologic information, the logs serve primarily to verify the geology; however, in at least one instance, the 2,380-2,460-ft (725-750-m) interval, the logs correctly indicated the geology of a previously misidentified section of the hole. In other holes in the Cascade Range, similar relationships should hold. Thus these results should be useful in evaluating other sections without such complete log, cutting, and core data. The fracturing in the hole was examined using a number of types of logs. However, attempts to produce the hole suggest that the existing fractures are not connected and that the overall permeability of the rocks is very small. A total production rate of less than 4 L/min was calculated for a flow test involving the bottom 3,000 ft (900 m) of the hole. Therefore, although the temperatures are certainly in the range suitable for space heating, it does not appear that any significant amount of fluid can be produced from the hole.

LABORATORY STUDIES OF CORE AND CUTTING SAMPLES

Comparison of log and lab measurements

Six core runs were made during the drilling of the hole. One core was obtained from each of the major units encountered in the drill hole, and these core samples provide

invaluable information that could not have been obtained from the cutting samples alone. We have made measurements of thermal conductivity, density, *P*-wave velocity, and porosity on samples from the recovered core (radioactivity measurements were discussed in the previous section). Ten pieces from the six cores were available, and two samples of each piece studied were analyzed. One of the two samples was a 1-in (2.54-cm)-diameter core prepared with its axis parallel to the main core axis (V); the other was a 1-in (2.54-cm)-diameter core prepared with its axis perpendicular to the main core axis (H). Of all the samples, only the volcaniclastic rocks cored at about 4,400 ft (1,341 m) showed significant anisotropy in velocity and thermal conductivity. The thermal conductivity measurements were made on saturated samples with the conventional divided-bar apparatus described by Roy and others (1968). Thermal conductivity measurements were also made using the divided-bar chip technique (Sass and others, 1971). Bulk density measurements were made on saturated core samples by measurements of volume and weight.

Porosity values were obtained by measuring differences between dry weight and saturated weight on the core samples. These values may be a little low because of incomplete saturation; in particular, samples from the first core (1,596.5 ft and 1,618 ft [486.6 m and 493.2 m]) appear to have much higher porosities, based on assumed bulk density, than were determined from the core samples. Perhaps these samples were not completely saturated. Our saturation procedure is to evacuate the sample and hold it under a vacuum for approximately twelve hours, followed by introduction of water and pressurization to about 300 bars, where the sample is held for about twelve hours. This technique successfully saturates most rocks. However, since the calculated porosity, assuming a bulk density of 2.67 g/cm^3, is 16 percent, whereas the observed porosity is only approximately 7 percent, it appears that the saturation was incomplete in these samples. This sort of discrepancy is not significant for the remainder of the samples.

Laboratory velocity measurements were made on an apparatus similar to that discussed by Birch (1960). This section of the study is part of a continuing investigation into the relationship between velocity and thermal conductivity. Earlier parts of this study were carried out by Phillips (1980) and Williams (1981). The velocity apparatus used does not include a facility for measuring pore pressure independently of confining pressure; therefore, the measurements were made on unsaturated samples. The values listed in Table 2 are the values extrapolated to low pressure from least-squares fits of the data above 500 bars (in the range 500-1,500 bars). This procedure removes the effect of large, open microcracks on the low-pressure sample velocity. The effect of pressure on velocity over the pressure range in the drill hole (about 0-500 bars) is less than 0.1 km/sec and has been ignored in the analysis.

The measurements of bulk density, *P*-wave velocity, and porosity on the laboratory samples and of those derived from the log are compared and shown in Table 2. The log values were obtained by calculating an average over an interval extending 5 ft (1.8 m) in either direction from the depth of the core sample. Differences between the log properties and the laboratory properties are shown as Δ-percent values in the case of bulk density and *P*-wave velocity. In general, for bulk density, the agreement is within 2-3 percent, and the only significant errors are associated with the Columbia River basalt and with volcaniclastic rocks at 4,400 ft (1,341 m). The velocity discrepancy for the Columbia River basalt is probably due to the fact that no large interval of the Columbia River basalt is as unfractured as the small core samples which were studied. The reason for the discrepancy between the log response of the volcaniclastic rocks and the lab measurements is not known. On the velocity-density log crossplot, the volcaniclastic sediments plot in the basalt field. However, it is clear that the actual measured densities, for example, are somewhat less than those derived from the log. Velocity measurements are generally within 10 percent of those observed in the hole, and considering the uncertainties which exist, there is close agreement between log and lab velocities.

Porosity values differ significantly from the laboratory and log determinations. The two sets of determinations really relate to two completely different situations, however, so the discrepancy is not surprising. It has been pointed out (Williams, 1981) that the neutron log counts hydrogen bound in clay minerals and other minerals as porosity, thus generating false values of porosity. In addition, the matrix properties used, in this case limestone, may not be accurate for the rocks in the hole. In any event, the true porosity in the borehole is probably somewhere between that observed in the laboratory and that measured by the neutron porosity log, and probably is most accurately obtained from calculations using bulk density if the matrix density is known.

Thermal conductivity

One of the main objectives of this study is to obtain information on the deep thermal conditions beneath the High Cascade Range. A major geophysical property of interest is thermal conductivity. Thermal conductivity measurements were made on both cuttings and core samples as mentioned above. The results of some of these measurements are shown in Table 2. The measurements of cuttings are corrected for porosity based on the measured core values, using the geometric mean mixing equation. The core samples were not ground up, so the measurements of cuttings are actually on separate samples. Comparison values are shown for the core at 4,400 ft (1,341 m), but the anisotropy of the volcaniclastic rocks renders the measurements of cuttings useless. The average difference of the two sets of data is less than 2 percent, which is well within experimental error and sample-to-sample variations. The agreement is remarkable, considering the overall accuracy of the cuttings measurement technique (see Sass and others, 1971). In general, the thermal conductivity increases with depth in the hole. The unit with highest thermal conductivity in the hole is the greenstone section in the bottom of the hole. The effects of loss of porosity with depth and changing rock type are both important. In the hole itself, the actual thermal conductivity will, of course, be lower because of the temperature effect. No temperature corrections have been applied to the data in Table 2. However, in the calculations of heat flow discussed in the following section, corrections have been made based on the curves presented by Robertson (1979).

Velocity-thermal conductivity relationships

The results of some of the laboratory measurements are shown in Figure 5, a plot of thermal conductivity versus velocity. Shown on this plot are relationships between the velocity and thermal conductivity of (1) rhyolites from the Snake River Plain and (2) basalts from the Snake River Plain and from the Washington portion of the Columbia River basalt (see Phillips, 1980, and Williams, 1981). The equations shown in Figure 5 for the relationship of velocity (V_P) to thermal conductivity (K_L) in units of km/sec and W/mK,

Table 2. *Laboratory and log measurements of physical properties in the Old Maid Flat 7A drill hole, Oregon*

Core depth[1] (m)	Core depth[1] (ft)	Bulk density (g/cm³) lab	Bulk density (g/cm³) log[2]	Bulk density (g/cm³) Δ%[3]	P-wave velocity (km/sec) lab	P-wave velocity (km/sec) log[2]	P-wave velocity (km/sec) Δ%[3]	Porosity (%) lab	Porosity (%) log(N)[2,4]	Thermal conductivity (W/mK) core	Thermal conductivity (W/mK) cuttings[5]	Travel time (μsec/foot) lab	Travel time (μsec/foot) log[2]	Generalized lithology
486.6 V	1,596.5 V	2.40	2.44	−1.8	4.73	4.55	+4.0	7.2	23.4	1.72		64	67	Andesite flow or flow breccia
H	H	2.40			5.00			6.9		1.76	1.64	61		
493.2 V	1,618 V	2.38	2.47	−4.5	4.61	4.61	−0.2	7.6	21.9	1.61		66	66	Andesite flow or flow breccia
H	H	2.37			4.76			6.3		1.54		64		
888.7 V	2,915.7 V	2.56	2.54	+1.1	5.38	5.26	+2.3	3.8	9.6	2.33		57	58	Microquartz diorite
H	H	2.57			5.27			4.1		2.38	2.37	58		
889.8 V	2,919.4 V	2.56	2.55	+0.3	5.26	5.21	+1.0	3.8	9.9	2.41		58	58.5	Microquartz diorite
1,032.1 V	3,386.35 V	2.85	2.76	+3.2	6.05	5.64	+7.3	—	14.1	2.17		50	54	Columbia River basalt
H	H	2.85			5.94					2.15	2.20	51		
1,034.0 V	3,392.5 V	2.84	2.77	+2.4	5.95	5.59	+6.2	5.9	14.1	2.10		51	54.5	Columbia River basalt
H	H	2.84			5.89			0.4		2.09		52		
1,341.1 V	4,400 V	2.64	2.70	−3.3	4.77	5.30	NA	—	17.4	2.11		64	57.5	Volcaniclastic sandstone and mudstone
H	H	2.58			5.59			2.7		2.85		55		
1,832.9 V	6,013.5 V	2.64			5.71			0.7		2.69		53		
1,834.1 V	6,017.5 V	2.72	2.67	+0.0	5.39	5.26	+2.2	0.8	9.9	3.03	3.02	57	58	Greenstone
H	H	2.75			5.37			—		—		57		
1,837.0 V	6,027 V	2.66			5.17			1.7		3.02		59		
H	H	2.63			5.25			1.5		3.08		58		

[1]Sample depth followed by V indicates sample cored parallel to core axis. Sample depth followed by H indicates sample cored perpendicular to core axis.
[2]Sample depths for log values are ± 5 ft (1.8 m).
[3]Δ% = (lab - log values/log values) × 100.
[4]Log(N) = neutron porosity.
[5]Cuttings conductivity calculated using porosity from density log.

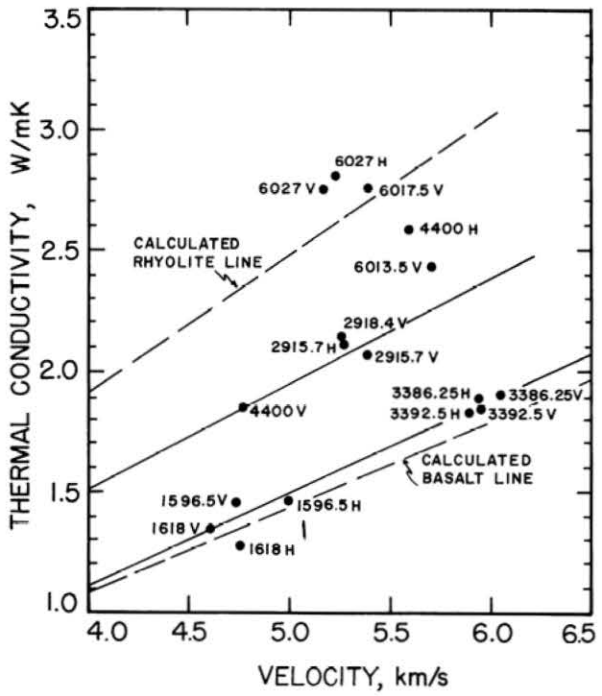

Figure 5. Correlation of laboratory velocity and thermal conductivity measurements on core samples. Dashed lines indicate calculated relationships between velocity and thermal conductivity from Williams (1981). Core samples measured are identified by depth of sample in feet and H or V (which indicates the orientation of the sample with respect to the horizontal and vertical directions). Most of the rocks are isotropic. The only significant anisotropy occurs in the volcaniclastic rocks cored at 4,400 ft (141.1 m).

are:

$$K_L = -0.15 + 0.58\ V_P$$

for the Snake River Plain rhyolites; and

$$K_L = -0.11 + 0.36\ V_P$$

for the basalts.

The measurements of Columbia River basalt from the drill hole fall almost exactly on the calculated basalt line from the results of Williams (1981). In addition, the measurements on the andesite or basaltic andesite core samples at 1,600 ft (488 m) also lie near the Columbia River basalt line, suggesting that the main mineralogic components determining velocity are similar for these two sets of rocks. Two greenstone samples from the bottom of the hole fall near the calculated line for rhyolites in the Snake River Plain, while one of the samples of the greenstone, one of the volcaniclastic samples, and the samples from the microquartz diorite lie intermediate to these two lines.

Since rocks of intermediate chemical composition should generally fall in a range between the two lines, it is not surprising that the values for the microquartz diorites lie between the lines. Unfortunately, there is not a wide enough variation of velocity to allow an accurate determination of the line appropriate for the relationship between velocity and thermal conductivity for the quartz diorite. For the purpose of the log calculation, a line was drawn more or less parallel to the rhyolite-basalt lines through the quartz diorite samples (see Figure 5) and was used in the analysis relating log parameters to thermal conductivity. This analysis is discussed more fully in the following section. A basalt andesitic V_P-K_L relationship slightly different from the one determined by Williams (1981) was used to relate velocity to thermal conductivity in OMF-7A (see Figure 5).

HEAT-FLOW CALCULATIONS

An important result of the study of OMF-7A is that it allows evaluation of the deep thermal situation and the way in which these conditions relate to the shallow drill-hole data. In an area of complicated thermal history and structure, there is always doubt about the applicability of shallow-exploration data to the prediction of true geothermal conditions at depth. Several temperature-depth logs were made in the hole during and immediately after drilling; however, the logs discussed in this section were taken over a period of two weeks, after the hole had been shut in for about nine months. At the completion of the drilling of the hole, it was flushed with water and then flow tested. The flow test showed the hole incapable of producing more than 4 L/min from the bottom of 3,000 ft (900 m) of the hole. After this test, small-diameter tubing was emplaced, and the hole was shut in. Temperature logs were made in July 1981 in order to obtain equilibrium temperature measurements in the hole. The temperatures were recorded in digital form at 1-m intervals. The results of two of the logs (made on 7/1/81 and 7/15/81) are shown in Figure 1. The gradients shown in Figure 1 are 7-point running averages of 1-m temperature differences. These two logs, taken two weeks apart, show such remarkable agreement that they are indistinguishable on the plot. A log taken with another set of equipment to a depth of 1 km also showed similar agreement. The temperature logs illustrated were made with a new type of sensor, an Analog Devices semiconductor temperature sensor attached to a 4-km-long, one-conductor armored cable mounted in a van. The 1-km temperature measurements (made with a conventional thermistor sensor and four-wire cable configuration) showed close agreement as noted. In Figure 1, gradients are plotted at each meter, and each value represents a 7-m average. In this fashion, high-frequency noise (small convection cells) is removed.

The characteristics of the gradient log are that it shows a relatively low-frequency oscillation with an amplitude of about 20° C/km and a frequency of about 60 ft (20 m). There is an overall decrease in gradient with depth in the hole. In general, there are no distinct segments of higher or lower gradient which correspond with the lithologic log shown in Figure 1. There is a significant gradient change due to a lithologic change at 5,510 ft (1,680 m). The greenstones below that depth have a much lower gradient than the rocks in the remainder of the hole. There is evidence of some local water flow at the 5,510-ft (1,680-m) horizon, probably associated with local fracturing.

Instead of a detailed correlation with the lithologic log, the most remarkable correlation of the gradient log is with the caliper log. There is a point-for-point correlation of low gradients and enlarged sections of the drill hole. Variations associated with the hole size obliterate any detailed correlation with rock type. The variations associated with hole size may be related to the inducing of convection in the larger sections of the hole by the relatively high gradients.

The thermal conductivity measurements were made on both core and cutting samples as discussed above, and the heat flow was calculated in a number of different ways. Shown in Figure 6 are 60-ft (20-m) average gradient, thermal

Table 3. *Interval gradient and heat-flow calculations for OMF-7A. Thermal conductivity values are based on core sample measurements corrected for in situ porosity calculated from the density log.*

Depth interval (m)	Uncorrected gradient (°C/km)	Corrected gradient (°C/km)	Thermal conductivity (W/mK)	Heat flow (mW/m²)[1]	Heat flow (mW/m²)[2]	Lithology[3]
90- 335	72.0 0.1	64.4	1.60	103	92	Basalt and andesite
345- 400	66.4 0.6	63.1	2.08	131	118	TDPI
410- 650	68.7 0.2	66.8	1.65	110	103	Andesite
650- 725	67.3 0.2	65.8	2.17	143	141	TDPI
725- 850	60.9 0.3	60.0	1.60	96	97	CRBG and andesite
860- 915	63.7 0.1	63.1	2.27	143	143	TDPI
930-1,250	58.7 0.1	58.3	1.83	116	108	CRBG
1,265-1,375	60.1 0.3	59.8	2.26	135	133	TDPI
1,375-1,415	55.0 0.3	54.8	2.04	112	114	Basalt
1,415-1,520	56.3 0.1	56.1	2.26	127	129	TDPI
1,595-1,665	58.9 0.1	58.8	2.22	131	127	TDPI
1,675-1,730	56.6 0.8	56.5	2.22	125	111	Volcaniclastic
1,745-1,790	50.6 0.1	50.5	2.68	135	132	Greenstone
Heat flow with no TDPI intervals				114± 6	108± 6	
Heat flow in TDPI				135± 3	132± 5	
Weighted average heat flow				119±10	114±11	

[1]Heat flow from measured conductivity.
[2]Heat flow from log-calculated conductivity.
[3]TDPI = microquartz diorite; CRBG = Columbia River Basalt Group.

conductivity, and heat flow as functions of depth in the borehole. The dashed line is uncorrected gradient (or heat flow). The thermal conductivity was calculated from the correlation between velocity, thermal conductivity, and lithology, as discussed in the previous section. A correction has been made for temperature effects on thermal conductivity. The product of the gradient and thermal conductivity averages is plotted in the form of a heat-flow log. The large averaging interval has effectively suppressed t ›scillations shown on the observed temperature data; l..ever, it is clear that there is no good correlation between segments of gradient and lithology except in the case of greenstones in the bottom of the hole.

On the thermal conductivity log in Figure 6, the sections of microquartz diorite stand out with a value about 10 percent higher than the andesites and basalts. However, there is no corresponding decrease in gradient coinciding with these sections of the hole. The lack of correlation may be due to one or more of the following possibilities: (1) the thermal conductivity of the microquartz diorite may be overestimated by the technique used to calculate the value; (2) the microquartz diorite layers may be steeply inclined, and thus the assumptions used to calculate the heat flow are violated; or (3) the disturbance of the gradient associated with the variations in hole size may be so large that the small variations in gradient associated with lithology are lost. Even though the diorite is thought to be an intrusive, correlation with the nearby hole OMF-2 suggests that the diorites are almost flat-lying (Priest, this volume). Thus the second explanation is not likely to be the cause of the lack of gradient-thermal conductivity correlations.

The heat flow was calculated in a more conventional way for comparison. The results are shown in Table 3. Gradients were calculated for the various lithologic intervals shown in Figure 1. Both uncorrected and terrain-corrected gradients are listed in the table. Thermal conductivity values are shown only for the intervals of the hole for which core sample measurements were available or for which values could be estimated using the density log to obtain an estimate of the in situ porosity so that the core measurements could be corrected to in situ conditions. This correction is important in the upper part of the hole. As is the case with the thermal conductivity log, the intervals of diorite have consistently higher heat flow than the rest of the hole. The nondiorite intervals have a mean heat flow of 114±6 mW/m², while the heat flow in the diorite intervals is 135±3 mW/m².

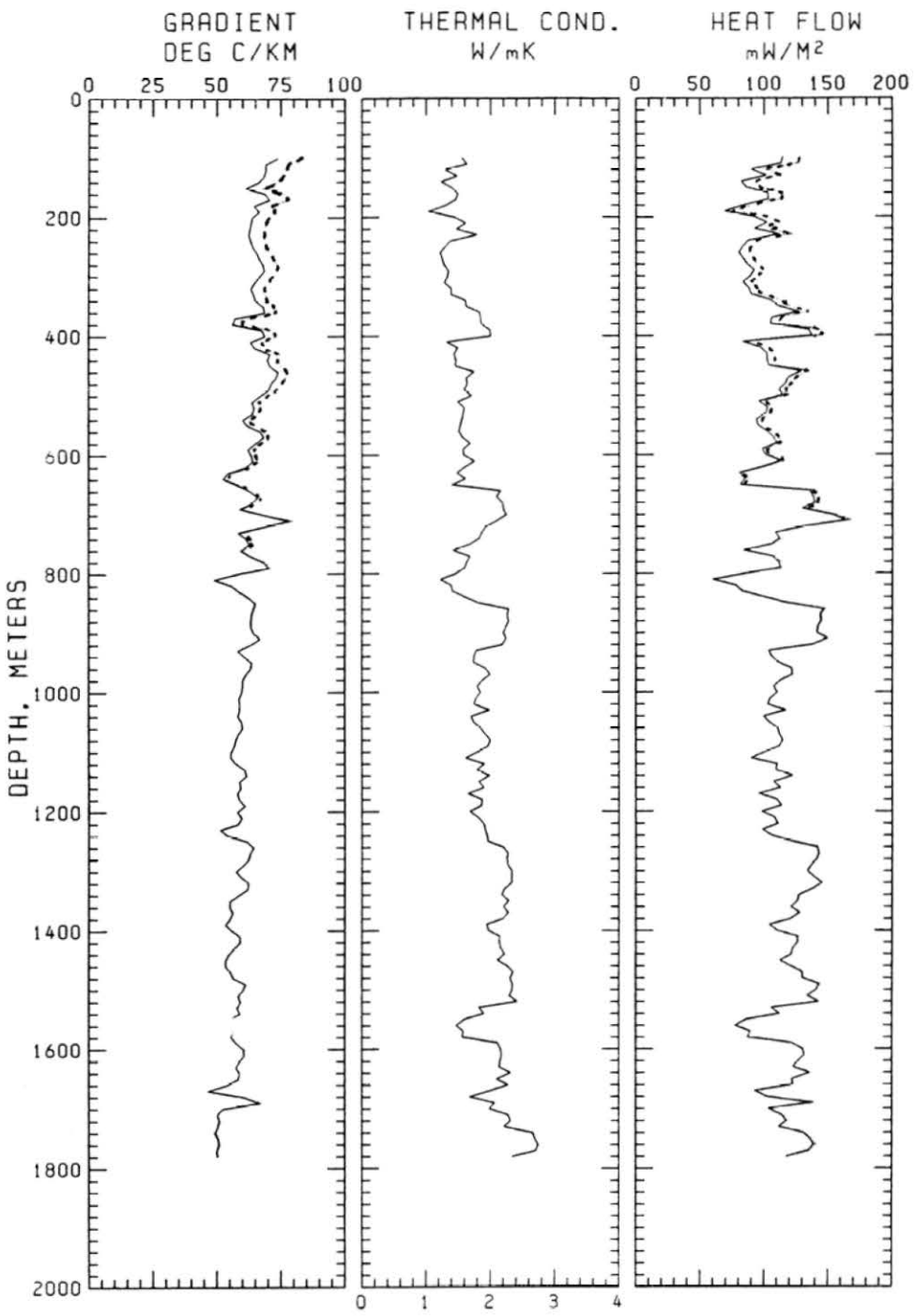

Figure 6. Gradient, thermal conductivity, and heat flow for OMF-7A. Plotted are 60-ft (20-m) interval averages for the various quantities. Dotted curves for gradient and heat-flow logs show the observed values. Solid curves are the terrain-corrected values. The thermal conductivity was calculated from the velocity log using results shown in Figure 5 and the lithologic intervals shown in Figure 1.

The best estimate of heat flow in the hole is taken to be a weighted average (by thickness) of all of the hole. This value is 119±10 mW/m^2. The estimated error of determination is 10 percent.

The equivalent averages for the data shown in Figure 6 over the same intervals are 108±6 mW/m^2 and 135±5 mW/m^2 for the diorite and the remainder of the hole, respectively. The weighted average for the entire hole is 114±10 mW/m^2. This value differs by less than the standard error of the determination from the values determined in the more conventional manner. If only the core samples had been available and the information on porosity had not, it would not have been possible to determine an accurate value of heat flow. The same statement is true if only the cuttings were available for study. The use of the velocity log to calculate a thermal conductivity log and then a heat-flow log directly from the geophysical well logs is a way to obtain detailed heat-flow variations with depth not otherwise possible. Thus, in a hole with only a few measurements of thermal conductivity (or none), it is possible to calculate such a heat-flow log. This procedure may make the calculation of heat-flow values possible for many holes that could not otherwise be studied. The technique seems accurate enough if the lithologies are known to be comparable to heat-flow measurements based on cuttings, thermal conductivity determinations, or isolated core samples.

The results shown in Table 3 and Figure 6 may indicate an increase in heat flow with depth in the hole. The average heat flow below 1,250 m is 127±4 mW/m^2, while the average heat flow above that depth is 113±10 mW/m^2. This apparent increase in heat flow with depth is in contrast with the observed decrease in gradient with depth. There are a number of possible causes for this vertical variation. The difference might be due to (1) systematic errors in determinations of thermal conductivity in either the top or bottom portions of the hole, (2) gradient noise generated by hole size variations so large that changes in gradient associated with the various lithologic units are overridden, (3) a heat-flow variation caused by climatic effects, or (4) a heat-flow variation caused by continuation effects from some heat source. The effect is in the opposite direction to that which might be expected due to the effects of erosion of the deep glacial valley in which the hole is located. Because of the lack of a way to evaluate the actual precision of thermal conductivity information, the most favored explanation is that there are systematic errors in thermal conductivity. This explanation seems most likely, because even the shallow intervals of diorite have much higher apparent thermal conductivity values than are consistent with the lack of observed gradient contrast.

ACKNOWLEDGMENTS

This study was supported by U.S. Department of Energy (DOE) contract No. DE-AS07-79ID12037 and by subcontracts with the Oregon Department of Geology and Mineral Industries from their DOE contracts No. DE-FC07-79ET27220 and No. AC06-77ET-28369. Field data were collected by Steve Worsham, Steve Moelter, and Gerald Black. Laboratory measurements and data reduction were carried out by Cindy Gwinn, Karen Smith, and Shari Kelly. Equipmet was built and maintained by Robert Spafford.

REFERENCES CITED

Birch, A.F., 1960, The velocity of compressional waves in rocks to 10 kilobars, part 1: Journal of Geophysical Research, v. 65, no. 4, p. 1083-1102.

Gosnold, W.D., Jr., 1976, A model for uranium and thorium assimilation by intrusive magmas and crystallizing plutons through interaction with crustal fluids: Dallas, Tex., Southern Methodist doctoral dissertation, 131 p.

Oregon Department of Geology and Mineral Industries, 1981, Geophysical logs, Old Maid Flat No. 7A, Clackamas County, Oregon: Oregon Department of Geology and Mineral Industries Open-File Report O-81-2, 2 parts (A, B).

Phillips, R.L., 1980, Compressional wave velocities to 200 bars of basalts from the Columbia Plateau, Washington: Dallas, Tex., Southern Methodist University master's thesis, 71 p.

Robertson, E.C., 1979, Thermal conductivities of rocks: U.S. Geological Survey Open-File Report 79-356, 52 p.

Roy, R.F., Decker, E.R., Blackwell, D.D., and Birch, F., 1968, Heat flow in the United States: Journal of Geophysical Research, v. 73, p. 5207-5221.

Sass, J.H., Lachenbruch, A.H., and Munroe, R.J., 1971, Thermal conductivity of rocks from measurements on fragments and its application to heat-flow determinations: Journal of Geophysical Research, v. 76, p. 3391-3401.

U.S. Department of Energy (USDOE), 1981, Old Maid Flat geothermal exploratory hole No. 7A drilling and completion report: USDOE Nevada Operations Office, NVO-230, 24 p.

Williams, J.W., 1981, In situ thermal conductivity measurement from geophysical well logs in the eastern Snake River Plain: Dallas, Tex., Southern Methodist University master's thesis, 79 p.

MINERALOGY OF THE OLD MAID FLAT GEOTHERMAL EXPLORATORY HOLE NO. 7A, MOUNT HOOD, OREGON

By M. J. Holdaway and Steven Bussey, Department of Geological Sciences, Southern Methodist University, Dallas, Texas 75275

ABSTRACT

A geothermal exploratory hole at Old Maid Flat 6 miles west of Mt. Hood encounters the following lithologic types in order of first appearance: andesitic mudflow debris, andesite porphyry, andesite tuff, micro-quartz diorite porphyry, Columbia River basalt, volcanic sediments, and greenstone. Cutting and core samples were studied using X-ray diffraction, petrographic microscope, and the electron microprobe. The widespread development of mineral combinations not normally seen in geothermal regions leads to the conclusion that as many as three separate hydrothermal-metamorphic events have affected the rocks encountered. The earliest event, at greenschist-facies conditions, produced greenstones at the bottom of the hole. Following erosion and deposition, a zeolite-grade event produced laumontite, albite, calcite, and chlorite. In the upper part of the hole smectite-chlorite coexisted with chlorite, while below 5000 feet smectite-10 Å formed and was replaced by illite at 5900 feet. Prehnite, epidote, sphene, and pyrite formed locally. The shallowest rocks known to be affected by this event are at 1400 feet. The final, and present, sub-zeolite-grade event affected most of the rocks in the hole. At this stage laumontite was altered to stilbite, smectite formed, and pyrite was oxidized, forming hematite and anhydrite. The three events are widely separated in time; the zeolite-grade event may be broadly synchronous with intrusion of the micro-quartz diorites 8 to 11 m.y. ago.

INTRODUCTION

The Old Maid Flat No. 7A exploratory geothermal hole was drilled under the auspices of the U.S. Department of Energy during August and September, 1980. The drill site is located about 50 miles east of Portland, Oregon, and 6 miles west of the summit of Mt. Hood. The site is on the south side of the Muddy Fork of the Sandy River, 1.6 miles east-northeast of the intersection of the Muddy Fork and the Sandy River (U.S. Department of Energy, 1981). The hole was drilled to a depth of 6027 feet (1837 m). Bottom-hole temperature was measured at 235°F (113°C), and the thermal gradient in the hole is 33°F/1000 feet or 60°C/km.

The purpose of this report is to describe and interpret the mineralogy of cutting samples and core samples provided by the Oregon Department of Geology and Mineral Industries. With the aid of mineralogical data as a function of depth it is possible to make important contributions concerning the history of metamorphic-hydrothermal events in this part of the High Cascades.

Experimental methods

Samples from the Old Maid Flat No. 7A well were studied using three methods: X-ray diffraction, petrographic analysis, and electron microprobe analysis. X-ray diffraction patterns were run on all core samples provided and on chip samples at 100-foot intervals. Standard thin sections were prepared for all core samples and for intervening chip samples at 300-foot intervals (320, 620, 920, 1920, 2220, 2520, 2720, 4220, 4720, 5420 and 5720 feet). Between one and five polished sections were prepared from each cored interval and from a cutting sample at 4720 feet.

For most samples studied by X-ray diffraction, two patterns were run, one of the darker host rock matrix and one of the minor amounts of light-colored cuttings, presumably vein minerals. For a few samples 40- to 100-mesh fractions were separated into light and dark components and X-rayed separately, but the method revealed no additional minerals. Most samples were glycolated, and a few were separated into magnetic and nonmagnetic fractions with the isodynamic separator to resolve problems of chlorite identification.

Textures, rock names, and minerals were determined with the use of standard thin sections. Several minerals, as designated on Figure 1, were mainly identified in thin section or polished section due to their minor amount.

Microprobe work was used to provide chemical analyses of several minerals, and in many cases, to help identify or confirm minerals. Analyses were done using a JEOL Superprobe 733 with Krisel Automation using silicate and oxide standards. Feldspars, pyroxenes, and oxides were analyzed using the Bence-Albee (1968) reduction scheme at 15 kV and 20-nA beam current. Phyllosilicates were similarly analyzed at 10-nA beam current. Zeolites, due to their high volatility, were analyzed using Magic (a ZAF correction scheme) at 10 kV and 5-nA beam current. For feldspars, pyroxenes and oxides three 10-μm spots were analyzed for 30 seconds or 60,000 counts on each of two separate grains or portions of grains. Where the analyses differed significantly, as with zoned plagioclase, both analyses are reported; otherwise they were averaged. For each phyllosilicate five 10-μm spots were analyzed for 20 seconds or 60,000 counts, and the results averaged. For each zeolite analysis six 10-μm spots were analyzed for 20 seconds or 60,000 counts on a given grain or cluster of grains, and the results averaged. Accuracy of analyses is about ±1.5% of the amount present for major elements, up to ±3% of the amount present for minor elements. The quality of some phyllosilicate analyses is somewhat worse due to the fine grain size and poor polish of phyllosilicates.

LITHOLOGIC TYPES

All samples from the Old Maid Flat No. 7A hole cluster in a narrow compositional range which includes andesite, augite basalt, diorite, and closely related volcanic sediments. Almost every specimen studied contains plagioclase, quartz, and chlorite, while many contain smectite, calcite, laumontite, and/or stilbite. Variations in relative amounts of these minerals and presence of other minerals (Fig. 1) are related to specific lithologies and, to a lesser extent, to depth in the hole. The lithology of a thin section or microprobe sample is referred to by a suffix A-G as given in Table 1 and the discussion below.

Mudflow debris, andesitic

The top section of the hole is represented by poorly consolidated andesitic debris. X-ray patterns show that much or all of the glass has gone to cristobalite, tridymite, and locally a 16.7-Å clay, possibly saponite (Fig. 1).

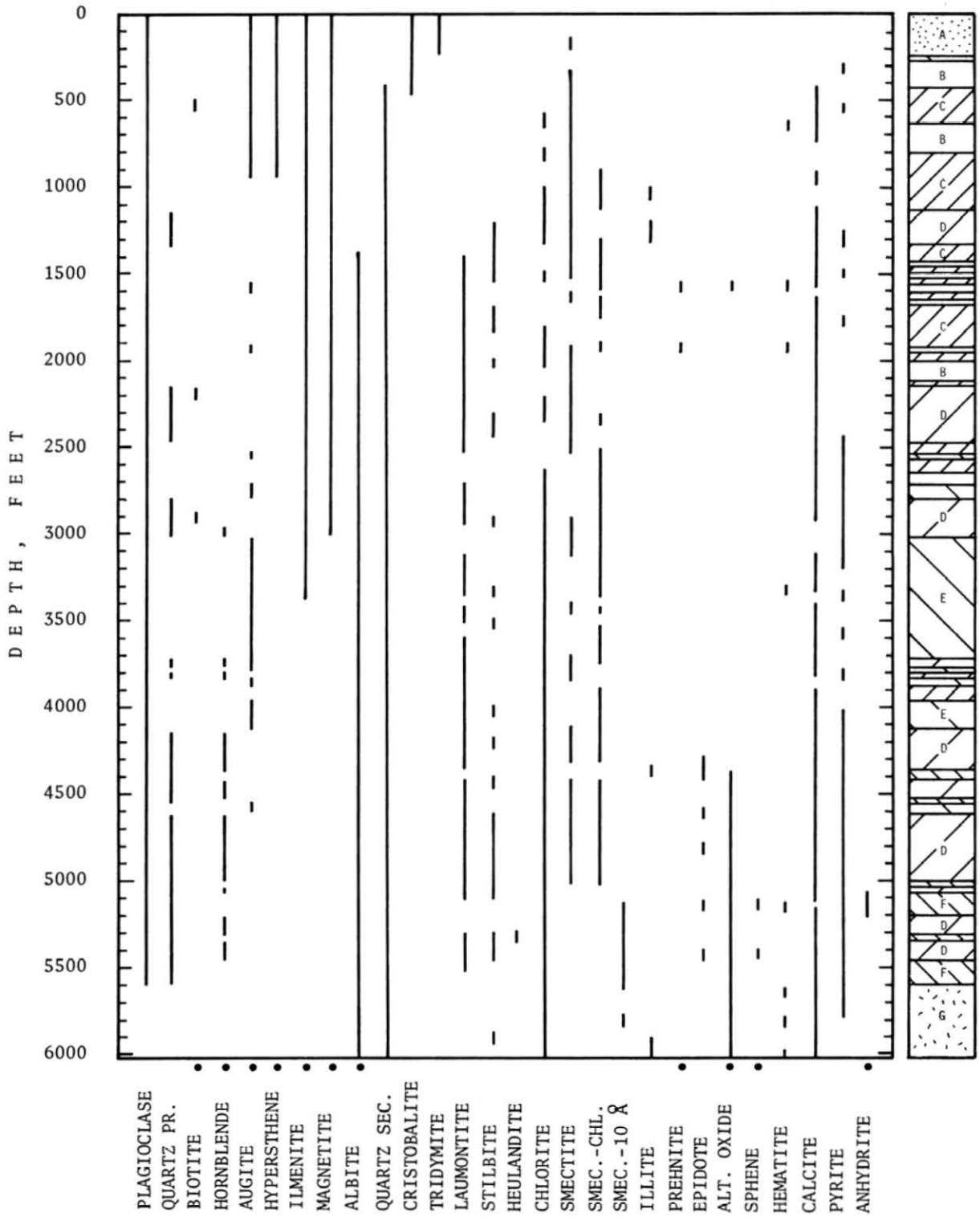

Figure 1. Mineral distribution as a function of depth in the Old Maid Flat No. 7A hole. Plagioclase through magnetite are primary igneous minerals; albite through anhydrite are secondary minerals. A dot indicates that the distribution of the mineral is based on its occurrence in thin sections and generalized from that information (see text). Letters shown on the lithologic log at right refer to lithologic types given in Table 1.

Table 1. Designations for lithologic types

A. Mudflow debris, andesitic

B. Pyroxene andesite porphyry and basaltic andesite porphyry

C. Crystal-vitric andesite tuff and breccia

D. Hornblende micro-quartz diorite porphyry intrusive

E. Augite basalt, mainly Columbia River Basalt Group

F. Volcanic lithic mudstone, wacke, and conglomerate

G. Greenstone: meta-andesite and meta-dacite

Pyroxene andesite porphyry and basaltic andesite porphyry

Flow rocks of andesite and basaltic andesite are included in this category. Andesites are extensively interlayered with andesitic tuffs and breccias throughout the upper 2700 feet of the hole. The primary rock consisted of andesine, augite, and orthopyroxene phenocrysts in a matrix of fine plagioclase, pyroxene, quartz(?), ilmenite, magnetite, and glass. Chlorite and smectite alteration is prevalent in the groundmass of even the shallowest specimens. Alteration to chlorite and zeolites attacks first the groundmass, then the pyroxenes, and finally the plagioclase. In a general way, the degree of hydrothermal alteration increases with depth.

Crystal-vitric andesite tuff and breccia

These rocks, interbedded with andesitic flow rocks (above) are important in the upper 2700 feet of the hole. The primary crystalline material was plagioclase, augite, and orthopyroxene. The largely altered matrix is now brown smectite, green chlorite, opaque minerals, and quartz. The samples in the upper part of the hole show a great variety of somewhat altered ash, lapilli, and reworked tuff and lava fragments. These rocks alter more rapidly than any other lithology, alteration being most complete in the groundmass, somewhat less in the opaque phases and pyroxenes, and least in plagioclase. Veins of zeolite are common. In general, alteration becomes progressively more complete with increasing depth.

Hornblende micro-quartz diorite porphyry intrusive

Intrusive micro-quartz diorites are distributed over parts of an interval between 1220 and 5480 feet. Less altered specimens show a porphyritic texture with euhedral andesine and lesser amounts of hornblende, biotite, and augite in a crystalline aphanitic groundmass of the same minerals with quartz. Even in the least altered specimens, quartz is more abundant than in most other rocks from the hole, perhaps amounting to 20%. Alteration in the quartz diorites is typically less complete than in andesites or andesite tuffs found at a similar depth. Biotite alters first, then the groundmass minerals and hornblende, and finally plagioclase. Alteration products are chlorite, smectite, and zeolites. Alteration is more complete with depth. The deepest rocks contain unaltered portions of plagioclase and unaltered hornblende.

Augite basalt

This category includes basalts, principally, the Columbia River Basalt Group. Most of the basalts are distributed over the interval between 2540 and 4620 feet. The basalts contain crystals of sodic labradorite, augite, and fine opaque phases in a fine intersertal to hyalophitic matrix of altered glass and microlites, now largely smectite, chlorite, and quartz. In some specimens, portions of the matrix are composed entirely of dark-greenish-brown chlorite in radiating crystals. Apart from the matrix alteration and the alteration

of opaque phases (see below), the plagioclase and augite crystals are the least altered of any phases in any of the rocks, being largely preserved in even the deepest specimens. Zeolitic veining and minor zeolitic alteration are present especially in deeper specimens.

Volcanic lithic mudstone, wacke, and conglomerate

All sedimentary rocks encountered fall in this category. Such rocks occur intermittently between 4380 and 5600 feet. They vary from silt- and clay-size mudstones to wackes to matrix-dominated conglomerates. Sorting is generally poor, and clasts are subangular. Clasts are andesine, volcanic rock fragments, and minor opaque material and polycrystalline metamorphic (?) quartz. Matrix materials are clay- and silt-size phyllosilicates and quartz. Some beds are rich in clay, others contain abundant opaque organic material. Alteration of clasts is complete in the opaque phase, partial in andesine which is locally partly altered to sphene or anhydrite. Zeolites are rare in these rocks except in veins.

Greenstone: meta-andesite and meta-dacite

Between 5600 and 6027 feet the rocks are totally metamorphic greenstone. Textures suggest the primary igneous rocks were andesitic and dacitic agglomerates or breccias. No primary minerals prevail, and the rocks are largely composed of well-crystallized chlorite, albite, calcite, and illite. Mixtures of calcite and albite occur as pseudomorphs of plagioclase crystals.

MINERALOGIC VARIATIONS

In this section are described in detail the minerals identified by all three methods, their relationship to lithologic types, and their relationship to depth. The mineral distribution diagram (Fig. 1) lists first the primary minerals, then secondary minerals. All minerals which formed during magmatic igneous processes are termed primary. Secondary minerals originated during cooling, weathering, or hydrothermal or metamorphic alteration. However, the relative simplicity of mineral assemblages suggests that most secondary minerals were at least stable during the hydrothermal phase(s), even though some of them presumably did not originate at that time.

Several of the minerals, including biotite, amphibole, pyroxenes, opaque phases, anhydrite, prehnite, epidote, and sphene cannot generally be identified using X-ray patterns because of their small amount. The distribution of such minerals is based solely on petrographic study of thin sections of cores and cutting samples, the latter at 300-foot intervals. Their occurrence elsewhere is generalized on the basis of depth and lithology. In each case where a given mineral, e.g. hornblende, was found in every section for a given lithology over a given depth interval, its occurrence was generalized to include all horizons containing that lithology over that depth interval. Such minerals are designated on Figure 1 with dots at the lower end of the graph.

Primary minerals

Every cutting sample and core sample from the surface to 5600 feet contains primary igneous minerals.

Plagioclase is present in all samples. The degree of alteration of coarser plagioclase crystals varies widely with lithology and depth. The average degree of alteration is greatest in the tuffs, followed by the andesites, micro-quartz diorites, sediments, and basalts in that order. In the greenstones, primary plagioclase is totally altered

Table 2. Compositions of analyzed plagioclase, mol percent

Sample†	Type*	An	Ab	Or	Weight % Fe_2O_3
1596B		47.1	51.5	1.4	0.48
	Al	4.5	95.3	0.2	0.02
1618B		43.5	55.2	1.4	0.61
2919.4D	Co	45.5	53.3	1.2	0.19
	Ri	36.7	61.9	1.4	0.20
3381E		48.9	48.8	2.3	0.84
3392.5E		51.0	46.8	2.2	0.84
	Gr	45.6	51.7	2.6	1.10
4400F		25.3	74.0	0.7	0.04
	Al	4.9	94.8	0.3	0.01
4720D	Al	1.7	97.7	0.6	n.d.
4140F		34.7	64.4	0.9	0.53
		35.8	60.7	3.6	0.46
5145F		53.1	45.2	1.7	0.89
		57.7	40.8	1.5	0.80
5146F		46.7	52.5	0.8	0.46
		40.0	58.8	1.2	0.52
5148.9F		35.7	61.3	3.0	0.44
		38.6	59.1	2.3	0.49
5152F		39.2	57.6	3.2	0.36
		31.8	66.2	2.0	0.36
6013G	Al	1.4	98.5	0.1	0.01
6027G	Al	0.8	99.1	0.1	0.80

*Co = core, Ri = rim, Gr = groundmass, Al = alteration; others are primary crystals.

†Single letters after numbers designate lithology (Table 1).

both in phenocrysts and groundmass. In composition (Table 2) primary plagioclase varies between An_{25} and An_{58}. In andesites it is An_{43-47}, in the micro-quartz diorites (D) it is An_{37-45}, in the basalts (E) it is An_{49-51}, and in the sediments (F) it is An_{25-58}. Among the igneous rocks, Fe_2O_3 is lowest in the micro-quartz diorites and highest in the basalts. There appears to be no pattern of change in plagioclase composition as alteration progresses. The plagioclase in partly altered crystals remains homogeneous except for the albite which forms as an alteration product. Groundmass plagioclase remains partly unaltered in at least some rocks (3392.5E).

Quartz is most abundant in the micro-quartz diorites and sediments, where it appears to constitute about 20% of the rock, and is at least partly primary in nature. The absence or paucity of quartz in the andesites and tuffs in the top 400 feet of the hole implies that the ubiquitous quartz at deeper levels in these lithologies and in the basalt is largely secondary in nature. In none of the igneous rocks is quartz easily seen in thin section, and where seen it commonly exhibits radiating, fibrous forms indicative of chalcedony.

Biotite is seen rarely as traces remaining from chlorite or smectite alteration of groundmass biotite in diorites. The deepest biotite is at 2900 feet.

Hornblende occurs in the micro-quartz diorite at depths between 3000 and 5460 feet. At shallower depths primary hornblende in the andesites, tuffs, and diorites was replaced by chlorite and calcite. Where it is seen in thin section (3720 to 5420 feet) the hornblende appears unaltered and well crystallized and varies from brownish-green at 3720 feet to light-brown at 5420 feet. Although it reflects original hornblende in the rock, this hornblende certainly appears to have been stable during hydrothermal alteration and may have changed composition at that time.

Table 3. Chemical analyses and end members for primary phenocryst augite*

	1618B	3392.5E
SiO_2	51.84	51.77
TiO_2	0.54	0.93
Al_2O_3	1.84	1.62
FeO	11.22	15.04
MgO	14.46	14.38
MnO	0.35	0.37
CaO	20.20	17.11
Total	100.45	101.22
En	41.0	41.0
Fs	17.8	24.0
Wo	41.2	35.0

*Total Fe reported as FeO.

Augite shows signs of instability in most rocks which contain it. In the tuffs, augite persists to 920 feet before being totally replaced by chlorite; in the andesites it

persists to 1920 feet; in the basalts it is seen in every chip sample down to at least 4620 feet. In the basalts augite commonly shows the least sign of instability, showing minor grain-boundary alteration to chlorite or smectite in deeper specimens. Analyzed augites are given in Table 3. Augite from the basalt (E) is higher in ferrosilite component and lower in wollastonite than that of the andesite (B), consistent with a higher temperature and higher Fe/Mg ratio for the basaltic magmas.

Hypersthene alters rapidly to chlorite, but remnants are seen in the andesites and tuffs down to 920 feet. A low Ca-pyroxene was not detected in the basalts perhaps in part due to compositional controls. One might expect preservation of hypersthene in the shallowest basalts due to their high degree of preservation of primary crystals.

Ilmenite persists as a primary mineral to at least 3400 feet, while magnetite persists to at least 3000 feet. Compositions of some of the opaque phases (Table 4) appear little changed from those of typical calc-alkaline igneous oxides (Carmichael, 1967). However, when corrected for Fe_2O_3, totals are low for some analyses. Ilmenite from 1596B was examined with backscattered electrons. A BSE picture shows it to be an intergrowth of at least two phases, partly replacing the ilmenite. X-ray pictures show presence of Ca and Si, demonstrating that the ilmenite was being sphenitized. The low Ti content of ilmenite in 3392.5E may reflect somewhat oxidizing conditions for part of the Columbia River basalt. Alternatively, its composition may well have been changed by alteration.

Secondary minerals

This category includes mineralogic changes caused by post-magmatic, sedimentary, and hydrothermal (or metamorphic) processes. Wherever possible, the process responsible for formation of each mineral will be suggested.

Albite is present in many of the rocks, but its existence is difficult to prove because its X-ray peaks overlap Ca plagioclase and it occurs as fine replacement material especially in altered groundmass. Its existence was proven by analysis in 1596B, 4400F, and 4720D (Table 2) as well as in the greenstones at the bottom of the hole. Albite is the only alteration mineral which concentrates Na. All the zeolites are highly calcic, and analcite was not detected in thin sections or X-ray patterns. The distribution of albite shown in Figure 1 is hypothetical, based on the assumption that specimens which contain enough Ca zeolite or calcite to be detectable on an X-ray pattern must also contain albite as a product of plagioclase alteration. Albite in all rocks except the greenstones is An_{2-5}, while in the greenstones it is An_1. The more extensive, higher temperature metamorphism in the greenstones produced a feldspar which more nearly approached equilibrium.

Quartz is ubiquitous as a secondary mineral, occuring as fine grains or radiating chalcedony in the groundmass of all but the shallowest volcanic rocks. Quartz was produced by (1) devitrification of oversaturated volcanic glass; (2) chloritization of glass, pyroxene, and hornblende; and (3) alteration of plagioclase or augite to calcite and albite or chlorite. Zeolitization and sphenitization consume silica, but the net effect of alteration of these rocks was to produce quartz.

Cristobalite and tridymite occur instead of quartz at shallow depths. Crystobalite persists to 440 feet, and tridymite persists to 240 feet. These minerals form from deuteric vapor phase alteration and possibly from early stages of devitrification and are not hydrothermal in origin. Quartz becomes abundant at 420 feet.

Laumontite and stilbite are the main zeolite minerals observed. Laumontite occurs almost continuously between 1420 and 5530 feet, while stilbite occurs intermittently over a comparable range. The zeolite minerals are seen both in the host rock and as vein minerals, but are more abundant as vein minerals than in the host rock. Limited microprobe observations show mainly laumontite replacing plagioclase. Commonly plagioclase has patchy replacement with laumontite and, at least locally, albite. Rarely is stilbite present in a rock which does not also contain laumontite. Both minerals are present in all rock types except the greenstone, but the minerals are present only locally as vein minerals in the sediments. The two core samples of micro-quartz diorite (2915.7 and

Table 4. Chemical analyses and structural formulae of ilmenite, magnetite, and altered Fe-Ti oxide*

	1596B		1618B		2919.4D		3392.5E	4400F	5146F
	Mt	Ilm	Mt	Ilm	Mt	Ilm	Ilm	Alt	Alt
TiO_2	13.73	36.60	11.92	41.07	7.59	42.51	25.84	30.23	27.17
Al_2O_3	2.35	0.97	2.12	0.39	0.79	0.19	1.55	1.34	7.51
Fe_2O_3	37.62	21.40	43.16	22.71	52.23	19.09	47.50		
FeO	39.42	30.20	39.37	31.74	36.08	35.39	20.97	0.58	0.45
MgO	2.02	1.44	0.79	2.75	0.03	1.12	0.04	0.12	0.02
MnO	0.27	0.21	1.68	0.40	0.96	0.97	2.15	0.07	0.00
Σ	95.17	90.82	99.04	99.06	97.68	99.47	98.15	36.61	36.15
			Cations on basis of 6 total cations						
Ti	0.798	2.285	0.680	2.338	0.441	2.445	1.523		
Al	0.215	0.095	0.185	0.033	0.070	0.016	0.145		
Fe^{+3}	2.189	1.335	2.455	1.291	3.048	1.094	2.809		
Fe^{+2}	2.548	2.093	2.488	2.004	2.370	2.254	1.375		
Mg	0.232	0.178	0.088	0.314	0.004	0.129	0.004		
Mn	0.017	0.016	0.047	0.022	0.063	0.063	0.145		
Mt	56		62		77				
Usp	44		38		23				
Ilm		76		78		82	49		
Hem		24		22		18	51		

* Oxidation state of Fe based on stoichiometry and charge balance. Altered Fe-Ti oxide presumably contains Ca and Si and is probably sphene (see text).

2919.4) contain only stilbite, while all the cutting samples contain laumontite or laumontite and stilbite. A single heulandite (or epistilbite) X-ray peak was detected at 8.87 Å in a cutting sample at 5320 feet.

Chemical analyses (Table 5, Fig. 2) are characterized by low ratios of (Na+K)/(Ca+Ba), and Si/Al ratios near 2 for laumontite and 3 for stilbite. Stilbite compositions are more variable in Na and H_2O than laumontite. The coupled substitution $NaSi \rightleftharpoons CaAl$ appears to take place in both minerals. This can be seen by noting the parallelism of analyses from the same specimen to the ruled lines which express the above relationship. Water content, estimated by subtracting the oxide sum from 100%, is 13.9 ± 0.6% for laumontite and 14.8 ± 2.0% for stilbite disregarding the high water content for 4720D. The greater variability in stilbite analyses may reflect a lower temperature of origin such that the mineral composition did not approach equilibrium as well as when laumontite crystallized. The laumontite with Si/Al of 2.35 (Fig. 2) is one of two cloudy zeolites analyzed and may have been laumontite altering to stilbite.

Chlorite occurs extensively in samples below 600 feet and continuously below 2600 feet (Fig. 1). In thin section, the chlorite of the andesites, tuffs, and diorites is green to dark-green and variable in birefringence. That of the basalts is dark-brownish-green, while the fine chlorite in the sediments is light-green. The chlorite is distinguished in X-ray patterns by a broad peak at 7.1 to 7.2 Å. In the sediments and greenstones, the peak is considerably narrower. Due to the Fe-rich nature of most of the chlorite, the (001) peak is 5 to 10% as high as the (002) peak (Petruk, 1964) and is only seen in chlorite of the sediments and greenstones where chlorite is abundant. The identification of the mineral as chlorite in the many rocks with no 14-Å peak is confirmed by petrography, microprobe analyses, and enhancement of the (002) peak using the isodynamic separator to concentrate Fe-rich minerals. Chemical analyses (Table 6) show considerable variation in Si/Al and Fe/(Fe+Mg) ratios. The small deficiencies in total cations and the presence of Ca result from saponite-chlorite random interlayering (see below).

Smectite is a dominant mineral between 420 and 720 feet, but occurs in many samples down to 5020 feet. It is present in all lithologies except the sediments and the greenstones. Because of the possibility of drilling-mud contamination with montmorillonite, smectite from eight samples with very small (001) peaks was not shown on Figure 1. Such contamination is considered to be minor because most vein mineral fractions showed no smectite peaks at all. In addition, the hole was drilled with water throughout the lower 3000 feet. In thin section most smectite is tan colored and exists as interstitial material and as small masses of very fine-grained crystals. Analysis of unusually coarse golden-brown radiating crystals with high birefringence (1618B, Table 6) shows it to be saponite. The rock compositions imply that most smectite in the igneous rocks is also saponite. Hoffman and Hower (1979) suggest that smectite (presumably montmorillonite) in shales decomposes at very low temperatures. However, presence of substantial Fe and Mg may stabilize smectite to higher temperature (Velde, 1972). Glycolated samples yield a smectite basal spacing at 16.4 to 17 Å, with the commonest values near 16.7 Å.

Random mixed-layer smectite-chlorite occurs from 820 to 5020 feet in many of the same rocks which contain smectite. In thin section it occurs as very fine fibrous brown crystals grading into chlorite which locally has anomalously high birefringence. It is identified by a broad peak betwen 14.5 and 16.0 Å after glycolation. At 920, 1596, and 5020 feet a small 31 Å peak appears, suggesting a tendency towards ordering in the layers. A chemical analysis (Table 6) suggests the smectite component is saponite. The distribution and textural relations of chlorite and smectite-chlorite suggest that with increasing temperature and depth, smectite-chlorite was converting to chlorite. Comparison to the first three analyses of Table 6 shows that loss of SiO_2 and CaO in the mixed-layer phase would convert it to chlorite.

Regular 1:1 smectite-10 Å mixed clay is common in most samples between 5140 and 5620 feet. The lithologies are mostly interlayered sediments and micro-quartz diorites. X-ray

Table 5. Selected chemical analyses and structural formulae of laumontite and stilbite

	Laumontite				Stilbite		
	1596B	1618B	4720D	2919.4D	4400F	4720D	4720D
SiO_2	54.45	52.63	52.23	59.36	58.96	57.96	52.27
Al_2O_3	21.23	21.40	21.92	17.22	17.57	18.34	14.89
CaO	10.22	10.93	11.36	8.18	8.85	8.96	6.90
BaO	0.11	0.00	0.00	0.05	0.21	0.05	0.00
Na_2O	0.90	0.38	0.16	0.50	0.64	0.70	1.13
K_2O	0.22	0.16	0.10	0.00	0.14	0.04	0.11
Σ	87.13	85.49	85.77	85.32	86.37	86.05	75.29
100 - Σ	12.87	14.51	14.23	14.68	13.63	13.95	24.71
	Cations on anhydrous basis of 36 oxygens						
Si	12.371	12.199	12.085	13.488	13.328	13.148	13.497
Al	5.684	5.848	5.977	4.613	4.680	4.904	4.532
Ca	2.488	2.715	2.816	1.992	2.145	2.180	1.907
Ba	0.012	0.000	0.000	0.004	0.020	0.006	0.000
Na	0.398	0.172	0.074	0.219	0.281	0.305	0.566
K	0.063	0.047	0.029	0.000	0.043	0.012	0.035
Σ	21.016	20.981	20.981	20.316	20.496	20.555	20.537
Si/Al	2.176	2.086	2.022	2.924	2.848	2.681	2.978
(Na+K)/Al	0.081	0.037	0.017	0.047	0.069	0.065	0.133
(Na+K)/(Ca+Ba)	0.184	0.081	0.037	0.110	0.150	0.145	0.315

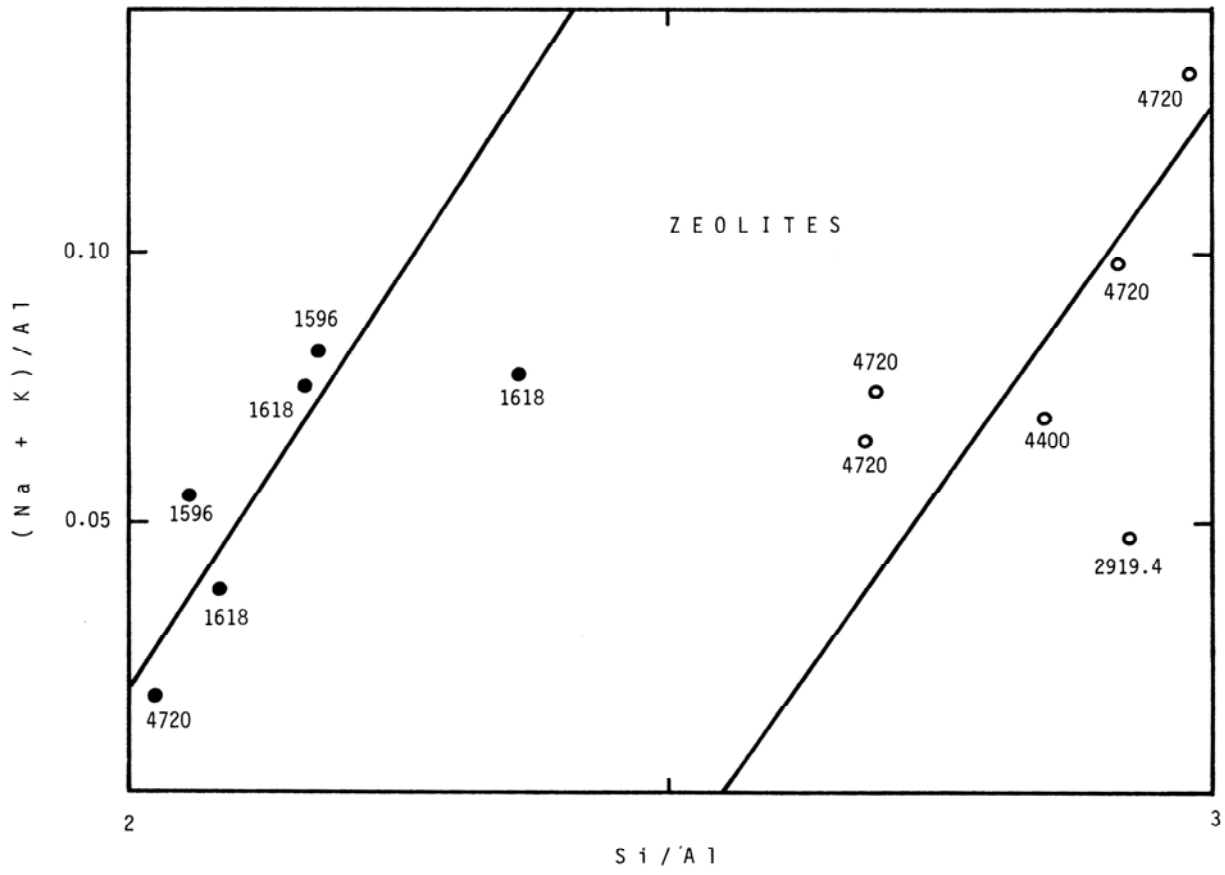

Figure 2. Plot of (Na+K)/Al vs. Si/Al for laumontite (dots) and stilbite (circles). Solid lines give compositional variation which would result from NaSi ⇄ CaAl (plagioclase-type) solid solution. Numbers refer to depths of core samples. The 1618-foot laumontite at Si/Al of 2.35 is cloudy laumontite probably altering to stilbite.

Table 6. Chemical analyses and structural formulae of saponite and chlorite*

	Saponite	Sap.-Chl.	Chlorite				
	1618B	2919.4D	3381E	4400F	4720D	5152F	6027G
SiO_2	39.45	32.29	28.03	25.97	28.87	26.72	24.88
Al_2O_3	10.86	15.39	16.38	21.77	16.82	23.00	20.83
TiO_2	0.04	0.00	0.05	0.05	0.05	0.04	0.05
FeO	17.09	20.79	38.09	33.17	34.23	31.63	37.16
MgO	14.81	16.30	6.63	7.65	8.51	6.70	5.09
MnO	0.18	0.31	0.16	0.31	0.38	0.55	0.40
CaO	3.30	1.05	0.76	0.24	0.89	0.47	0.18
Na_2O	0.41	0.09	0.05	0.02	0.05	0.12	0.03
K_2O	0.18	0.00	0.00	0.02	0.00	0.00	0.00
Σ	86.30	86.21	90.15	89.22	89.81	89.23	88.62
	22 oxygens		Cations on anhydrous basis of 28 oxygens				
Si	6.251	6.698	6.134	5.581	6.208	5.675	5.532
Al	1.749	1.302	1.866	2.419	1.792	2.325	2.468
Al	0.279	2.461	2.354	3.092	2.466	3.431	2.988
Ti	0.004	0.000	0.006	0.006	0.006	0.006	0.006
Fe	2.265	3.605	6.969	5.959	6.151	5.619	6.910
Mg	3.498	5.036	2.158	2.447	2.725	2.120	1.684
Mn	0.023	0.055	0.025	0.057	0.063	0.100	0.074
Ca	0.558	0.231	0.173	0.050	0.202	0.106	0.041
Na	0.125	0.030	0.019	0.006	0.019	0.043	0.013
K	0.032	0.000	0.000	0.000	0.000	0.000	0.000
Σ	14.784	19.418	19.706	19.617	19.632	19.424	19.716
Fe/(Fe+Mg)	0.393	0.417	0.764	0.709	0.693	0.726	0.804

*Total Fe reported as FeO.

patterns show an integral sequence of sharp peaks beginning at 25.2 Å (unglycolated) or 26.8 Å (glycolated). Chemical analysis (Table 7, 5146F) shows that the smectite component is montmorillonite, while the 10-Å component appears to be randomly interlayered illite and pyrophyllite. Formation of regular 1:1 smectite-10 Å in rocks of appropriate composition may be one of the last steps before total disappearance of smectite component. Most smectite-10 Å mixed layer clays are random or ordered with ratios other than 1:1 (Hoffman and Hower, 1979).

A small, broad, 10-Å X-ray peak occurs in a few samples between 1020 and 1340 feet. This peak could result from primary biotite or hydrothermal illite. At 4400 feet in sediments the 10-Å clay is illite-like (Table 7) but is deficient one potassium ion and has 4.9 octahedral ions on a 22 oxygen basis. Possibly it is a hydromica with randomly interstratified di-and trioctahedral components. The greenstones contain both a well-crystallized phengite and light-brown dioctahedral illite clay which fills interstices and fractures. The two phyllosilicates have about the same composition (Table 7).

Prehnite was identified in thin sections at 1596 and 1920 feet. Thompson (1971) has shown that $X(CO_2)$ greater than about 0.01 in hydrothermal fluid eliminates CaAl silicates at low temperatures. Those with the highest Ca/Al ratios such as prehnite react with calcite at lower $X(CO_2)$ than more Al-rich minerals such as laumontite. Rarity of prehnite is thus mainly related to presence of minor CO_2 in the fluids.

Epidote was identified optically in samples at 4400, 5146, 5152, and 5420 feet. A microprobe analysis at 5146 feet shows it to be Ps_{25}. Scarcity of epidote is related to slightly elevated $X(CO_2)$ (Thompson, 1971) and probably to low Fe^{+3} in the rocks. Low Fe-epidote minerals apparently are not stable at low temperatures (Winkler, 1979, p. 175).

Opaque phases from the lower part of the hole are neither ilmenite nor magnetite. Partial analyses of two such opaque phases (Table 4) show them to have very low totals and an amount of Ti consistent with that of sphene. The opaque phases have projections of sphene growing from them, and sphene replaces plagioclase in some of the same rocks. Apparently the opaque sphene results from sphenitization of ilmentite to fine-grained sphene and minor amounts of oxide phases. Transparent sphene partially replaces plagioclase over a more limited range of depth (Fig. 1). Alteration of plagioclase to sphene appears to be related to lower $X(CO)_2$ than that of calcite-rich rocks.

Hematite has replaced the other oxides or pyrite and locally has stained the rock at a number of depths. These have been determined by reference to the lithologic log and thin sections.

Calcite is common in most samples from 420 feet to the bottom of the hole. It is nearly always best developed in the veins where it is associated with laumontite, stilbite, and sometimes quartz as the major vein association. In the host rocks calcite is present in larger amounts in andesites, tuffs, and greenstones than in basalts and sediments. It often appears with chlorite replacing mafic minerals or partly replacing plagioclase. In the greenstones, plagioclase phenocrysts are completely replaced by coarse albite and calcite.

Traces of pyrite have been observed at various depths, expecially below 4000 feet, as determined from the lithologic log and thin sections. Pyrite was confirmed by qualitative microprobe analysis at 4400 and 5146 feet.

Anhydrite was observed partly replacing the plagioclase of sediments in all the core samples between 5140 and 5152 feet. The anhydrite comprises 1 to 3% of the rock. Identification was confirmed by qualitative analysis at 5146 and 5152 feet. Anhydrite presumably has its source from the oxidation of sulfide in pyrite.

Table 7. Chemical analyses and structural formulae of montmorillonite, illite, phengite and prehnite*

	Mont.-10 ^{o}A	Illite	Illite	Phengite	Prehnite
	5146F	4400F	6022.5G	6022.5G	1596B
SiO_2	52.63	43.73	49.53	51.21	43.19
Al_2O_3	25.38	28.20	30.01	29.20	18.84
TiO_2	0.41	0.07	0.13	0.10	0.13
FeO	2.18	11.50	4.62	4.38	6.75*
MgO	1.85	3.32	0.85	1.18	0.12
MnO	0.03	0.08	0.05	0.04	0.05
CaO	3.27	0.50	0.27	0.34	25.45
Na_2O	0.85	0.21	0.25	0.17	0.07
K_2O	1.25	5.14	8.68	8.26	0.00
Σ	87.85	92.75	94.39	94.88	94.60
	Cations on anhydrous basis of 22 oxygens				
Si	7.212	6.165	6.657	6.807	6.128
Al	0.788	1.835	1.343	1.193	1.872
Al	3.311	2.849	3.409	3.380	1.275
Ti	0.040	0.004	0.012	0.008	0.012
Fe	0.249	1.353	0.517	0.484	0.719
Mg	0.378	0.695	0.169	0.232	0.021
Mn	0.000	0.008	0.004	0.003	0.004
Ca	0.479	0.074	0.035	0.045	3.867
Na	0.225	0.054	0.063	0.042	0.017
K	0.217	0.922	1.487	1.398	0.000
Σ	12.898	13.958	13.696	13.592	13.915

* Total Fe reported as FeO in montmorillonite, illite, and phengite, Fe_2O_3 in prehnite.

INTERPRETATION OF RESULTS

The Old Maid Flat No. 7A hole is mineralogicaly unusual in a number of respects: (1) The laumontite-albite assemblage present throughout most of the depth is in other geothermal regions preceded by heulandite-analcite and followed by wairakite or pumpellyite-prehnite (Turner, 1981). (2) The occurrence of laumontite between 1420 and 5530 feet is inconsistent with the measured temperatures for this interval (40 to 105°C). In other geothermal areas involving andesitic or basaltic rocks, laumontite takes the place of heulandite at temperatures varying from 100 to 150°C (Ellis and Mahon, 1977; Browne, 1978). (3) Occurrence of stilbite over the same general depth range as laumontite is not typical of either geothermal or diagenetic systems. Galloway (1974) notes stilbite only at the very beginning of the laumontite zone of sandstones in the Bristol Basin. Kristmannsdottir (1976) finds that stilbite forms between 100 and 120°, while laumontite first forms at 120°C in the low-temperature fields of the Reykjanes area in Iceland. Liou (1971a) shows that stilbite reacts to laumontite with increasing temperature. These inconsistencies and the lack of a clear association between the mineral occurrences and present temperatures must be explained by any model for hydrothermal activity in the Old Maid Flat area.

Metamorphic-hydrothermal events

There is evidence for three metamorphic or hydrothermal events and one or perhaps two unconformities in the Old Maid Flat lithologic sequence. These are as follows:

1. The andesitic greenstones (G, Fig. 1) were affected by a metamorphic event, probably in the greenschist facies. This metamorphism, the oldest in the section, thoroughly reconstituted the andesitic rocks at the base of the hole, forming an assemblage of calcite, chlorite, albite, and quartz typical of the lower greenschist facies. Illite and smectite-10 Å occurrence in this zone is probably caused by the next event. The transition from the greenstones to the overlying sediments, which are not fully reconstituted, is probably an unconformity.

2. The event which affected most of the rocks in the hole was an incomplete zeolite-facies hydrothermal alteration. This event produced most of the hydrothermal effects at depths shallower than 5600 feet as well as retrogressive effects at deeper levels. The typical assemblage produced between 1400 and 5000 feet was laumontite, calcite, chlorite, smectite-chlorite, quartz, and probably albite. Between 5000 and 5600 feet smectite-10 Å occurred instead of smectite-chlorite, partly as a function of increased temperature and partly due to changes in bulk composition. Other phases which crystallized at least locally during this event were prehnite, epidote, hornblende(?), sphene, and pyrite. The upper limit of laumontite at 1400 feet is a possible unconformity separating the laumontite-bearing rocks from those too low in grade to contain any zeolites except stilbite. Alternatively the transition into laumontite-bearing rocks may have been a simple function of temperature at an earlier time.

3. The final hydrothermal event which is presently in progress is a sub-zeolite facies event which produced minor effects throughout the hole. Assignment of minerals to this event is somewhat speculative. Stilbite, heulandite(?), smectite, chlorite, calcite, anhydrite, and hematite are the minerals which probably are stable or nearly stable with the present system. Conditions were locally oxidizing to produce hematite and anhydrite. The high solubility of anhydrite favors its origin as one of the last phases to crystallize. In the absence of an unconformity near 1400 feet, the present hydrothermal event could have followed the zeolite-facies hydrothermal event through a gradual decrease in temperature. However, this possibility does not explain the near or total absence of minerals such as heulandite and analcite.

Temperatures

The temperatures for each of the three hydrothermal-metamorphic events may be estimated by reference to experimental studies and mineral occurrence calibrated against measured temperatures in other geothermal systems. The error of such estimates is in most cases about ±25°C. For these estimates we assume that the average geothermal gradient was 60°C/km or more during all the thermal events.

Considering first the greenschist event, there are no stability data available for an assemblage including chlorite, calcite, albite, and quartz. The assemblage occurs over a wide range of zeolite and lower greenschist conditions. The total reconsitution of the rock but continued lack of schistosity or significant coarsening implies lowest greenschist conditions, or 300 ± 50°C.

The zeolite-facies event has several temperature constraints. At the pressures involved (0.5 to 1 kbar), analcite and quartz react to albite at about 200°C (Liou, 1971b). This must be an upper limit due to the temperature reduction of such stability curves resulting from $P_{fluid} < P_{tot}$. Liou (1971c) considers a number of localities in which the analcite-albite conversion takes place at depths between 2 and 5 km. The shallowest conversions relate to high geothermal gradients, perhaps 60°C/km, while the deepest (Triassic, New Zealand) relate to more normal gradients of about 25°/km. A reasonable temperature value for the disappearance of analcite is thus 120°C.

First appearance of laumontite from heulandite or stilbite approximately coincides with the first appearance of albite as shown by Liou (1971a, b, c). Temperatures near 120°C also appear reasonable for this reaction as measured in Iceland by Kristmannsdottir (1976) and estimated by Juan (1972) and Murata and Whiteley (1973) for diagenetic rocks (cited by Galloway, 1974). A temperature of 120°C is proposed for the first appearance of laumontite at 1400 feet (427 m). Liou (1971c) has shown that laumontite reacts to wairakite in a pure water fluid at 260°C (1.1 kbar), providing an absolute upper limit for the occurrence of laumontite. Prehnite first appears at 1 to 2 km greater depth than the first laumontite.

Hoffman and Hower (1979) propose a temperature of about 200°C for the transition from smectite-illite to illite (5900 feet, 1798 m). According to them the smectite-chlorite to chlorite transition is complete in sandstones at about 180°C. This transition occurs at about 5000 feet (1524 m). A range of conditions from 120 to 205°C for the zeolite-facies event is shown on Figure 3. The occurrence of prehnite and epidote lends further support for temperatures significantly higher than present temperatures for the zeolite-facies hydrothermal event. The possible stable occurrence of hornblende in the micro-quartz diorites presents a problem. (Its Al content has not been established.) While amphiboles have been recorded from other geothermal wells (Browne, 1978), even actinolite is generally thought to be stable only at higher temperatures (Winkler, 1979). The amphibole might be of igneous or contact metamorphic origin prior to or after the time of zeolite-facies metamorphism.

Several of the latest minerals are consistent with the present thermal event. Very little data are available on the diagenetic mineral stilbite. Carpenter (1971) notes its occurrence with low-temperature zeolites heulandite and analcite. Apparently the highest recorded temperature for stilbite is 120°C in the Reykjanes area, Iceland (Kristmannsdottir, 1976). At Old Maid Flat, the deepest stilbite is at the bottom of the hole (113°C), and it is decreasing in abundance. The deepest smectite is at 95°C. According to Hoffman and Hower, smectite becomes unstable in shales at about 60°C. Considering the difference in lithology and composition of the smectite, this agreement is satisfactory. Anhydrite was found at 96°C (0.4 kbar), well above the gypsum--anhydrite transition of 60°C (Blount and Dickson, 1973).

Figure 3 illustrates possible conditions of alteration based on the temperatures derived above and on the assumption of a geothermal gradient of 60°C/km. Pressures were determined using an average rock density of 2.6 g/cm^3. It is important to note that the diagram would be changed considerably if geothermal gradients were significantly different from 60°C/km during one or two of the events. Several kilometers of erosion have occurred

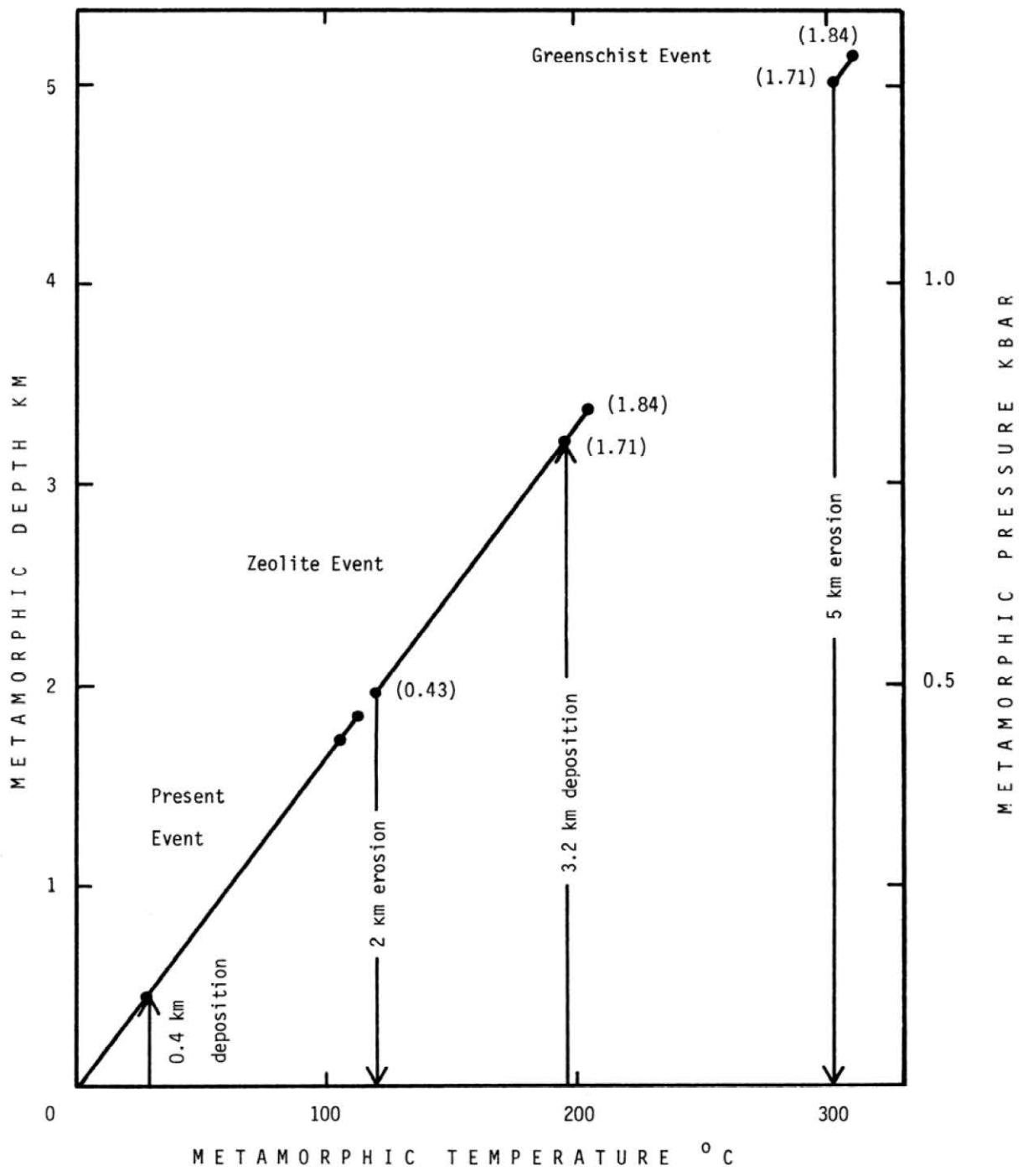

Figure 3. Metamorphic depth vs. metamorphic temperature for the three proposed hydrothermal-metamorphic events based on observational calibrations of mineral occurrences and on the assumption that the geothermal gradient was 60°C/km for each event. Numbers in parentheses are present depths in km for each point.

after the greenschist metamorphism. After the zeolite hydrothermal activity, about 2 km of erosion might have occurred, represented by a possible unconformity at 1400 feet (427 m) or at a shallower depth. If this unconformity does not exist, or if it involved very little erosion, then the first occurrence of laumontite at 1400 feet (427 m) must be explained by either occurrence of hydrothermal laumontite at a temperature well below 120°C or by a geothermal gradient of about 280°C/km or a combination of each during the zeolite-facies event. If there was an unconformity, up to 1400 feet (427 m) of younger material was deposited after the zeolite facies metamorphic event.

Age relations

Absolute ages of units and events are hard to establish for the rocks of the Old Maid Flat No. 7A hole due to a scarcity of data and the difficulty of interpreting dates on hydrothermally altered rocks.

Possible ages of the micro-quartz diorite are 9.4 ± 0.9 m.y. based on a K-Ar date for hornblende at 3750 feet in the hole (George Priest, personal communication, 1981); 11.6 ± 1.2 m.y. based on a whole-rock K-Ar date of the Laurel Hill intrusion 10 km south of the Old Maid Flat No. 7A hole (Wise, 1969); and 8.2 ± 0.2 m.y. based on hornblende K-Ar dates of the Laurel Hill intrusion (Bikerman, 1970). Bikerman has criticized the 11.6-m.y. date on the basis of significant atmospheric argon contamination. On Last Chance Mountain 2 km west and 1000 feet (305 m) vertically higher than the collar of the hole are lavas (compositionally similar to the micro-quartz diorites) which have a K-Ar date of 10.7 ± 0.4 m.y. (George Priest, personal communciation, 1981; date being redetermined).

It is difficult to determine whether these dates indicate an approximate age for the intrusions or an approximate age for the zeolite-grade alteration (or neither). Indeed the two events might be broadly synchronous. If this were the case, geothermal gradients would probably have been in excess of 60°C/km at that time.

A possibility which must be considered is that some or all the micro-quartz diorites postdated the zeolite-grade metamorphic event. Two weak lines of evidence support this possibility: (1) the two micro-quartz diorite cores contain no laumontite; and (2) the micro-quartz diorites at deeper levels contain fresh hornblende.

In summary, the three events which affected the area of the Old Maid Flat No. 7A hole are (1) early greenschist metamorphism of the deepest rocks; (2) zeolite facies metamorphism of at least those rocks below 1400 feet (427 m), an event which may have been caused by or broadly synchronous with intrusion of the micro-quartz diorites 8 to 11 m.y. ago; and (3) the present sub-zeolite-facies event.

ACKNOWLEDGMENTS

This investigation was undertaken with the support of a contract from the Oregon Department of Geology and Mineral Industries and was greatly facilitated by discussions with George Priest of that office. Microprobe analyses were undertaken at Southern Methodist University with the assistance of Dwight Deuring. X-ray diffraction work was also done at S.M.U. Discussions with David Blackwell were helpful. George Priest reviewed the first version of the manuscript. The typing of Nazlee Coburn is gratefully acknowledged.

REFERENCES CITED

Bence, A.E., and Albee, A.L., 1968, Empirical correction factors for the electron microanalysis of silicates and oxides: Journal of Geology, v. 76, p. 382-403.

Bikerman, M., 1970, K-Ar ages of Laurel Hill pluton and dike, Oregon: Ore Bin, v. 32, p. 211-215.

Blount, C.W., and Dickson, F.W., 1973, Gypsum-anhydrite equilibria in systems $CaSO_4$-H_2O and $CaSO_4$-NaCl-H_2O: American Mineralogist, v. 58, p. 323-331.

Browne, P.R.L., 1978, Hydrothermal alteration in active geothermal fields: Annual Reviews of Earth and Planetary Sciences, v. 6, p. 229-250.

Carmichael, I.S.E., 1967, The iron-titanium oxides of salic volcanic rocks and their associated ferromagnesian silicates: Contributions to Mineralogy and Petrology, v. 14, p. 36-64.

Carpenter, A.B., 1971, Graphical analysis of zeolite mineral assemblages from the Bay of Fundy area, Nova Scotia, in Molecular Sieve Zeolites - I: American Chemical Society, Washington, p. 328-333.

Ellis, A. J., and Mahon, W. A. J., 1977, Chemistry and geothermal systems: Academic Press, New York, 392 p.

Galloway, W. E., 1974, Deposition and diagenetic alteration of sandstone in northeast Pacific arc-related basins: implications for greywacke genesis: Geological Society of America Bulletin, v. 85, p. 379-390.

Hoffman, J., and Hower, J., 1979, Clay mineral assemblages as low grade metamorphic geothermometers: application to the thrust faulted disturbed belt of Montana, U.S.A., in Aspects of Diagenesis: Society of Economic Paleontologists and Mineralogists, Special Publication 26, p. 55-79.

Juan, V.C., 1972, Epigenetic diagenesis and low grade metamorphism: Geological Society of China Proceedings 15, p. 7-16.

Kristmannsdottir, H., 1976, Hydrothermal alteration of basaltic rocks in Icelandic geothermal areas, in Second United Nations Symposium on the Development and Use of Geothermal Resources, San Francisco, Calif., 1975, Proceedings: Washington, D.C., U.S. Government Printing Office, v. 1, p. 441-445.

Liou, J.G., 1971a, Stilbite-laumontite equilibrium: Contributions to Mineralogy and Petrology, v. 31, p. 171-177.

Liou, J.G., 1971b, Analcime equilibria: Lithos, v. 4, p. 389-402.

Liou, J.G., 1971c, P-T stabilities of laumontite, wairakite, lawsonite, and related minerals in the system $CaAl_2Si_2O_8$-SiO_2-H_2O: Journal of Petrology, v. 12, p. 379-411.

Murata, K.J. and Whiteley, K.R., 1973, Zeolites in the Miocene Briones Sandstone and related formations of the central Coast Ranges, California: U.S. Geological Survey Journal of Research, v. 1, p. 255-265.

Petruk, W., 1964, Determination of the heavy atom content in chlorite by means of the X-ray diffractometer: American Mineralogist, v. 49, p. 61-71.

Thompson, A.B., 1971, P_{CO_2} in low-grade metamorphism; zeolite, carbonate, clay mineral, prehnite relations in the system CaO-Al_2O_3-SiO_2-CO_2-H_2O: Contributions to Mineralogy and Petrology, v. 33, p. 145-161.

Turner, F.J., 1981, Metamorphic petrology: New York, McGraw-Hill, 524 p.

U.S. Department of Energy, 1981, Old Maid Flat geothermal exploratory hole no.7A drilling and completion report: U.S. Department of Energy, NVO-230, 24 p.

Velde, B., 1972, Celadonite mica: solid solution and stability: Contributions to Mineralogy and Petrology, v. 37, p. 235-247.

Winkler, H.G.F., 1979, Petrogenesis of metamorphic rocks: New York, Springer-Verlag, 348 p.

Wise, W.S., 1969, Geology and petrology of the Mt. Hood area: a study of High Cascade volcanism: Geological Society of America Bulletin, v. 80, p. 969-1006.

APPENDICES

APPENDIX A
DETAILED LITHOLOGIC LOGS OF THE OMF-1 AND OMF-7A DRILL HOLES

Table 1. *Legend for detailed lithologic logs of OMF-1 and OMF-7A (Tables 2 and 3)*


Old Maid mudflow (~200 years B.P., according to Crandell, 1980)


Microquartz diorite


Andesite and basaltic andesite


Debris flow


Basalt


Dacite flow


Priest Rapids Member


Frenchman Springs Member

} Wanapum Basalt


High-MgO chemical type


Low-MgO chemical type


Prineville chemical type

} Grande Ronde Basalt

} Columbia River Basalt Group


Volcaniclastic conglomerate and sandstone


Volcaniclastic mudstone


Volcaniclastic breccia


Andesitic flows and volcaniclastic material


Greenstone


Chlorite* distribution, as determined from thin-section samples and widely spaced samples analyzed by X-ray diffraction


Laumontite* distribution, as determined from widely spaced samples analyzed by X-ray diffraction


Greenschist* facies, as determined from thin-section samples and widely spaced samples analyzed by X-ray diffraction

*Data taken from Holdaway and Bussey (this volume). Only three alteration analyses were available from OMF-1. Some other areas may also have alteration but have not been sampled.

REFERENCE

Crandell, D. R., 1980, Recent eruptive history of Mount Hood, Oregon, and potential hazards from future eruptions: U.S. Geological Survey Bulletin 1492, 81 p.

Table 2. *Detailed log of OMF-1**

(Collar elevation: 2,750 ft. 1 in = 200 vertical ft)
(Legend appears in Table 1, p. 79.)

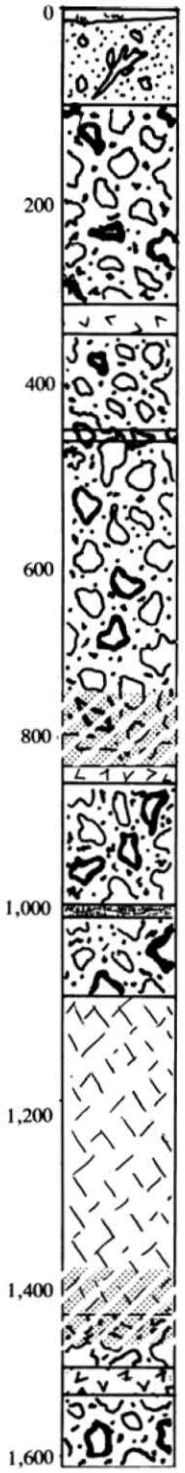

Depth (ft)	Interval (ft)	Description
	0-100	Recent mudflow debris.
	100-320	Reddish-brown to grayish-green lithic-rich epiclastic volcanic breccia. Angular to subrounded andesitic clasts with variable alteration in a matrix of crystal fragments and brown to green clays. Secondary saponite-chlorite (X-ray data at 290 ft), hematite, magnetite, pyrite, quartz, rare calcite.
	320-350	Possible hornblende andesite flow (altered).
	350-830	Light-reddish-gray to brownish-green-gray lithic-rich epiclastic volcanic breccia, similar to above.
	795	Laumontite and saponite-chlorite (X-ray analysis).
	830-850	Purplish-gray plagioclase-porphyritic pyroxene andesite. Plagioclase partly kaolinized; pyroxenes altering to hematite, chlorite, and clay.
	850-990	Epiclastic volcanic breccia, pyrite-rich in places.
	990-1,000	Dark-greenish-brown aphyric aphanitic basalt.
	1,000-1,080	Epiclastic volcanic breccia. Drusy quartz, calcite, pyrite, and chalcopyrite in fractures.
	1,080-1,440	Light to dark, slightly greenish-gray, plagioclase-porphyritic microdiorite. Plagioclase well zoned, up to 2-3 mm in size.
	1,435	Laumontite and saponite-chlorite (X-ray analysis).
	1,440-1,500	Light-greenish-gray epiclastic volcanic breccia.
	1,500-1,530	Medium-gray fine-grained basaltic andesite.
	1,530-1,610	Epiclastic volcanic material, much clay, possibly faulted near base. (Artesian aquifer)

*Lithologic description by Marshall W. Gannett, Portland State University.

Table 2. *Detailed log of OMF-1**—Continued

(Collar elevation: 2,750 ft. 1 in = 200 vertical ft)
(Legend appears in Table 1, p. 79.)

Depth (ft)	Rock type	Interval (ft)	Description
1,600	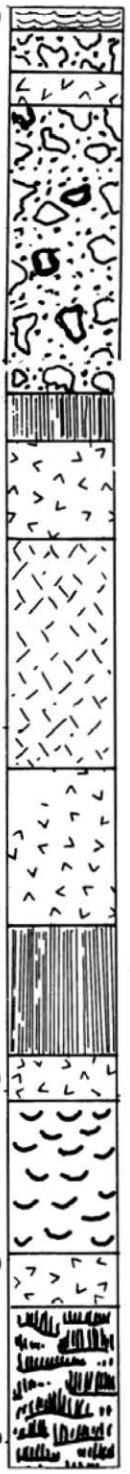	1,610-1,640	PRIEST RAPIDS MEMBER(?), WANAPUM BASALT.
		1,640-1,680	Clay-rich epiclastic debris.
		1,680-1,720	Hydrothermally altered porphyritic basaltic andesite.
1,800		1,720-2,030	Andesite debris flows.
2,000		2,030-2,070	FRENCHMAN SPRINGS MEMBER, WANAPUM BASALT.
		2,070-2,190	Andesite flow (altered).
2,200		2,190-2,440	Altered porphyritic microdiorite.
2,400		2,440-2,810	Hydrothermally altered aphyric lavas; multiple flows; textures and alteration somewhat variable; secondary clay, quartz, zeolites, calcite, and pyrite.
2,600		2,620-2,760	FRENCHMAN SPRINGS MEMBER, WANAPUM BASALT.
2,800		2,760-2,810	Andesite(?).
		2,810-2,980	LOW-MgO GRANDE RONDE BASALT.
3,000		2,980-3,040	Medium-gray, fine-grained andesite(?).
		3,040-3,220	PRINEVILLE CHEMICAL TYPE, GRANDE RONDE BASALT.
3,200			

*Lithologic description by Marshall W. Gannett, Portland State University.

Table 2. *Detailed log of OMF-1**—Continued

(Collar elevation: 2,750 ft. 1 in = 200 vertical ft)
(Legend appears in Table 1, p. 79.)

Depth (ft)	Rock type	Interval (ft)	Description
3,220	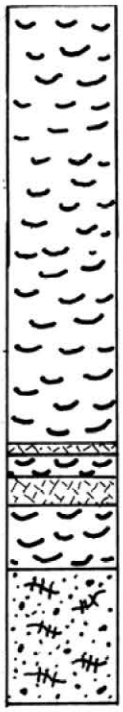	3,220-3,850	LOW-MgO GRANDE RONDE BASALT. Interbeds of andesitic and volcaniclastic material and some possible microquartz diorite sills.
3,400			
3,600			
3,800		3,850-4,002	Andesitic flows and volcaniclastic material.
4,000		T.D. 4,002 ft.	

*Lithologic description by Marshall W. Gannett, Portland State University.

Table 3. *Detailed log of OMF-7A**

(Collar elevation: 2,760 ft. 1 in = 200 vertical ft)
(Legend appears in Table 1, p. 79.)

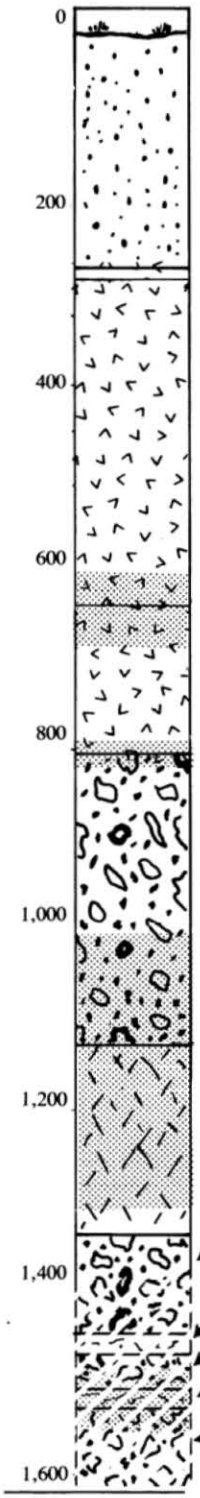

Depth (ft)	Interval (ft)	Description
	0-260	Holocene mudflow.
	260-280	Miocene-Pliocene(?) unit. Dark-grayish-green aphyric pilotaxitic andesite.
	280-640	LAST CHANCE ANDESITE(?). Dark-greenish-gray megacrystic two-pyroxene andesite; subhedral plagioclase; subhedral-anhedral orthopyroxene and clinopyroxene; fresh to slightly altered pyroxene.
	640-800	Gray-green megacrystic two-pyroxene andesite; subhedral plagioclase, orthopyroxene, and clinopyroxene in felty groundmass. Pyroxene fresh to slightly altered.
	800-1,120	Dark-green andesite debris flows; small (1-mm) plagioclase and pyroxene with heavy alteration of pyroxene.
	1,120-1,330	Light-gray to cream biotite-bearing hornblende microquartz diorite. Occasionally large biotite phenocrysts slightly chloritized. Alteration: plagioclase→smectite and calcite; biotite→chlorite and smectite; hornblende→chlorite and smectite.
	1,330-1,440	RHODODENDRON FORMATION. Two-pyroxene andesite debris flow and hornblende(?) dacite. Alteration: mafic silicates→smectite; plagioclase→smectite (slight) and zeolites.
	1,440-1,460	Brownish-green-gray highly altered porphyritic dacite flow. Alteration: plagioclase→calcite (albite→clays); pyroxene→smectite(?) and chlorite(?).
	1,460-1,500	RHODODENDRON FORMATION. Dark-gray-green porphyritic dacite debris flow. Alteration: plagioclase→calcite, albite(?), laumontite(?), and prehnite(?); orthopyroxene→smectite and chlorite.
	1,500-1,520	RHODODENDRON FORMATION. Brownish-green porphyritic two-pyroxene dacite flow. Alteration: plagioclase→laumontite, albite, and prehnite; orthopyroxene→smectite and oxide rims. (Artesian aquifer.)
	1,520-1,650	RHODODENDRON FORMATION. Medium-green pyroxene andesite mudflow. Alteration: plagioclase→zeolite and smectite; clinopyroxene→saponite; hornblende→Fe-Ti oxides + pyroxene(?) and saponite; orthopyroxene→saponite and zeolite.

*Lithologic description by George R. Priest, Oregon Department of Geology and Mineral Industries.

Table 3. *Detailed log of OMF-7A**—Continued

(Collar elevation: 2,760 ft. 1 in = 200 vertical ft)

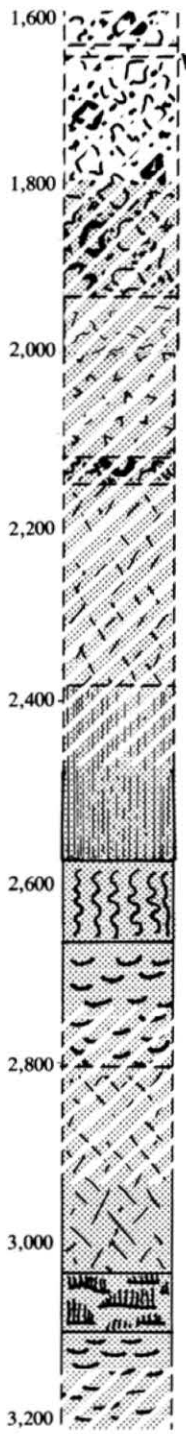

Depth (ft)	Interval (ft)	Description
	1,520-1,650	RHODODENDRON FORMATION. Medium-green pyroxene andesite mudflow. Alteration: plagioclase→zeolite and smectite; clinopyroxene→saponite; hornblende→Fe-Ti oxides + pyroxene(?) and saponite; orthopyroxene→saponite and zeolite.
	1,650-1,660	RHODODENDRON FORMATION. Gray-green pyroxene-bearing andesite. Alteration: plagioclase→laumontite and smectite; orthopyroxene→saponite.
	1,660-1,930	Dark-grayish-green to reddish-gray-green porphyritic two-pyroxene high-K andesite. Alteration: plagioclase→zeolite, calcite, laumontite, and smectite; clinopyroxene→chlorite and saponite; orthopyroxene→chlorite, saponite, and oxides.
	1,930-2,000	Gray-green porphyritic orthopyroxene dacite. Very altered at 1,980-2,000 ft. Alteration: plagioclase→laumontite, calcite, and prehnite; orthopyroxene→saponite and Fe-Ti oxide rims.
	2,000-2,120	RHODODENDRON FORMATION. Gray-green to red-brown porphyritic two-pyroxene andesite. Hematite, calcite, and quartz veins. Alteration (varies through section): plagioclase→smectite, laumontite, calcite and prehnite(?); orthopyroxene 1-100%→chlorite and saponite; clinopyroxene 1-100%→saponite, chlorite, and opaque oxides.
	2,120-2,150	RHODODENDRON FORMATION. Gray-green to red-brown two-pyroxene andesite debris flow. Devitrified glass. Alteration: plagioclase 5-100%→smectite and calcite; orthopyroxene 1%→reddish oxides; orthopyroxene 100%→saponite(?) and chlorite.
	2,150-2,380	Light-gray highly crystalline biotite hornblende microquartz diorite. Large phenocrysts and little alteration. Alteration: plagioclase 1-10%→calcite and laumontite; hornblende 100%→chlorite; biotite 50%→chlorite.
	2,380-2,570	FRENCHMAN SPRINGS MEMBER, WANAPUM BASALT. Medium-green to dark-gray-black clinopyroxene tholeiitic basalt. Aphyric. Alteration: devitrified glass 10%→saponite and chlorite; amygdules with laumontite fillings; olivine(?)→serpentine(?); plagioclase→calcite and quartz.
	2,570-2,660	HIGH-MgO GRANDE RONDE BASALT. Light- to dark-green porphyritic orthopyroxene tholeiitic basaltic andesite flow breccia. Alteration: plagioclase 5-100%→smectite, calcite, and albite. Devitrified glass 100%→smectite(?); minor quartz, calcite, and laumontite(?) veins. Sample highly altered.
	2,660-2,800	LOW-MgO GRANDE RONDE BASALT. Light- to dark-gray aphyric tholeiitic basaltic andesite. Approximate upper 30 ft highly altered. Alteration: plagioclase→chlorite and zeolites with minor pyrite. Some calcareous amygdules present. Clinopyroxene→saponite and chlorite. Devitrified glass→chlorite, quartz, smectite(?), and zeolites(?).
	2,800-3,030	Light-greenish-gray porphyritic hornblende biotite microquartz diorite. Alteration: plagioclase 1-5%→smectite, zeolite, and calcite. Hornblende 100%→calcite, Fe-Ti oxides, and chlorite; biotite 50-100%→chlorite; clinopyroxene 100%→chlorite and smectite.
	3,030-3,098	PRINEVILLE CHEMICAL TYPE, GRANDE RONDE BASALT. Medium-dark-green vesicular clinopyroxene tholeiitic basaltic andesite. Compact. Trace pyrite. Alteration: plagioclase<1%→zeolite and smectite; glass 100%→smectite; chalcedony from opal in vesicles.
	3,098-3,725	LOW-MgO GRANDE RONDE BASALT. Medium-dark-gray clinopyroxene tholeiitic basaltic andesite. Aphyric to sparsely microphyric. Alteration: glass 100%→smectite, chalcedony, and chlorite; plagioclase 1-10%→smectite; orthopyroxene 0-30%→saponite.

*Lithologic description by George R. Priest, Oregon Department of Geology and Mineral Industries.

Table 3. *Detailed log of OMF-7A**—Continued

(Collar elevation: 2,760 ft. 1 in = 200 vertical ft)

(Legend appears in Table 1, p. 79.)

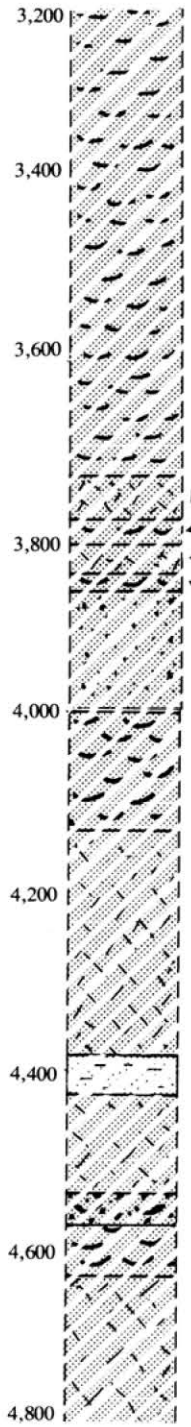

Depth (ft)	Interval (ft)	Description
	3,098-3,725	LOW-MgO GRANDE RONDE BASALT. Medium-dark-gray clinopyroxene tholeiitic basaltic andesite. Aphyric to sparsely microphyric. Alteration: glass 100%→smectite, chalcedony, and chlorite; plagioclase 1-10%→smectite; orthopyroxene 0-30%→saponite.
	3,725-3,770	White to light-green porphyritic phaneritic biotite-bearing hornblende microquartz diorite. Trace disseminated pyrite. Calcite veining. Alteration: plagioclase 15-20%→laumontite and smectite; biotite 100%→chlorite and sphene. Massive calcite fillings.
	3,770-3,800	LOW-MgO GRANDE RONDE BASALT. Medium-dark-gray-green aphanitic clinopyroxene tholeiitic basaltic andesite. Zeolite, calcite, and quartz veins. Trace disseminated pyrite. Alteration: plagioclase 1-5%→laumontite and smectite; glass 100%→chlorite, chlorite-smectite, and quartz.
	3,800-3,830	Hornblende biotite microquartz diorite. Alteration: plagioclase 2-25%→laumontite; biotite 100%→saponite, chlorite, and sphene.
	3,830-3,850	LOW-MgO GRANDE RONDE BASALT. Medium-dark-gray clinopyroxene tholeiitic basaltic andesite. Alteration: plagioclase 1-10%→laumontite and smectite; glass 100%→chlorite.
	3,850-4,000	Poor recovery. Volcaniclastics. Cave-in area.
	4,000-4,130	LOW-MgO GRANDE RONDE BASALT. Light-gray to green-black aphyric clinopyroxene tholeiitic basaltic andesite, "salt and pepper" appearance. Quartz veining. Trace of pyrite. Alteration: plagioclase 1-5%→laumontite(?) and smectite; glass 100%→smectite, laumontite(?), chlorite, and quartz.
	4,130-4,380	Light-gray-green altered biotite hornblende microquartz diorite. Calcite and quartz veining. Trace of pyrite. Alteration: plagioclase 10-90%→zeolite; biotite 100%→smectite and chlorite; Fe-Ti oxides→sphene.
	4,380-4,420	Volcaniclastic mudstone and conglomerate(?).
	4,420-4,530	White to pale-green hornblende biotite microquartz diorite. Sparry calcite veins locally. Alteration: plagioclase 10-90%→zeolite; biotite 100%→smectite and chlorite; Fe-Ti oxides→sphene.
	4,530-4,560	Volcaniclastic conglomerate(?).
	4,560-4,620	LOW-MgO GRANDE RONDE BASALT. Medium-gray aphyric tholeiitic basaltic andesite. Minor quartz veining. Trace of pyrite. Alteration: plagioclase 1% or less→laumontite and smectite; glass 100%→smectite or smectite-chlorite(?).
	4,620-5,010	Light-gray-green altered biotite hornblende microquartz diorite. Calcite and quartz veining. Trace of pyrite. Alteration: plagioclase 10-90%→zeolite; biotite 100%→smectite-chlorite; Fe-Ti oxides→sphene.

*Lithologic description by George R. Priest, Oregon Department of Geology and Mineral Industries.

Table 3. *Detailed log of OMF-7A**—Continued

(Collar elevation: 2,760 ft. 1 in = 200 vertical ft)
(Legend appears in Table 1, p. 79.)

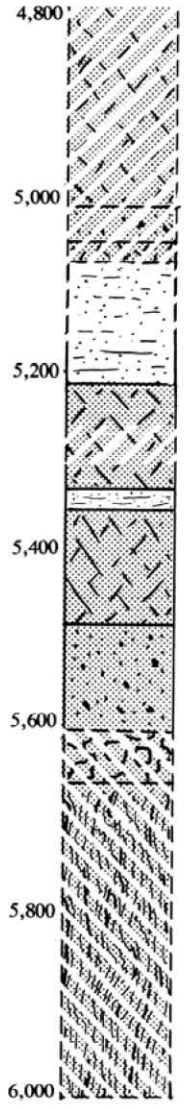

Depth (ft)	Interval (ft)	Description
	4,620-5,010	Light-gray-green altered biotite hornblende microquartz diorite. Calcite and quartz veining. Trace of pyrite. Alteration: plagioclase 10-90%→zeolite; biotite 100%→smectite-chlorite; Fe-Ti oxides→sphene.
	5,010-5,050	Volcaniclastic conglomerate.
	5,050-5,070	Biotite hornblende microquartz diorite. Corresponds to 5,000-5,030 ft in chip samples.
	5,070-5,210	Volcaniclastic mudstone, sandstone, and granule conglomerate with shear zones. Corresponds to 5,030-5,070 ft in chip samples.
	5,210-5,330	Biotite hornblende microquartz diorite. Corresponds to 5,270-5,370 ft in chip samples.
	5,330-5,350	Volcaniclastic mudstone. Corresponds to 5,350-5,370 ft in chip samples.
	5,350-5,480	White to green biotite hornblende microquartz diorite. Trace of magnetite and pyrite. Calcite veining. Alteration: plagioclase→zeolite, calcite, and epidote; hornblende 90%→chlorite. Corresponds to 5,270-5,370 ft in chip samples.
	5,480-5,600	Volcaniclastic sandstone. Corresponds to 5,500-5,630 ft in chip samples.
	5,600-5,660	Volcaniclastic breccia. Corresponds to 5,630-5,700 ft in chip samples.
	5,660-6,027	Gray, brown, green, or black fine-grained dacitic greenstone. Calcareous. Chloritization common. Trace of hematite; trace of calcite and quartz veining. Alteration: plagioclase 100%→calcite, albite, sericite, and hematite. Groundmass pyroxene→chlorite and saponite.
	T.D. 6,027 ft.	

*Lithologic description by George R. Priest, Oregon Department of Geology and Mineral Industries.

APPENDIX B

ROCK CHEMISTRY OF SAMPLES FROM OMF-7A AND OMF-1 DRILL HOLES, OLD MAID FLAT AREA, AND MOUNT HOOD AREA

Table 1. *Major-element compositions of samples from OMF-7A drill hole*
(Location 2S/8E/15Ac)

Stratigraphic unit:	Miocene-Pliocene lavas	Last Chance andesite	Last Chance andesite	Last Chance andesite	Rhododendron Formation	Intrusion	Rhododendron Formation	Rhododendron Formation	Rhododendron Formation	Rhododendron Formation	Rhododendron Formation	Rhododendron Formation	Rhododendron Formation	Rhododendron Formation	Rhododendron Formation	Rhododendron Formation
Depth (ft)[1]:	260	340	520	740	1,040	1,290	1,360	1,440	1,480	1,510	1,622	1,650	1,680	1,850	1,930	1,980
Major oxides[2]																
SiO_2	60.30	62.44	59.72	60.52	61.80	67.36	64.51	66.21	63.73	63.30	61.49	63.35	62.15	62.14	64.09	63.21
TiO_2	0.95	1.09	1.02	1.08	0.79	0.58	0.75	0.71	0.74	0.75	0.78	0.75	0.91	0.76	0.74	0.75
Al_2O_3	18.78	17.31	18.17	18.13	18.90	17.17	17.33	16.80	17.91	18.20	19.05	18.69	18.04	18.83	17.81	18.15
FeO	6.56	5.97	6.15	6.40	5.68	4.00	5.33	5.47	5.08	5.00	5.79	5.21	5.73	5.61	5.02	5.36
MnO	0.12	0.07	0.12	0.08	0.09	0.08	0.11	0.08	0.11	0.10	0.09	0.08	0.11	0.09	0.09	0.09
MgO	2.44	2.68	3.56	2.83	2.56	1.69	2.34	2.80	2.47	2.52	2.40	2.64	4.94	2.73	2.25	2.54
CaO	5.70	5.37	6.73	6.15	5.83	4.15	5.10	3.55	5.25	5.35	5.87	5.84	3.18	5.56	5.12	4.63
Na_2O	3.90	3.17	3.25	3.34	3.41	3.16	2.78	3.01	3.24	3.35	3.42	3.21	1.32	1.14	1.30	3.74
K_2O	0.92	1.68	1.07	1.27	0.81	1.67	1.58	1.24	1.30	1.25	0.98	1.07	3.43	2.98	3.41	1.39
P_2O_5	0.32	0.22	0.20	0.19	0.13	0.14	0.16	0.14	0.17	0.17	0.14	0.16	0.18	0.16	0.16	0.14
Recalculated total[3]	99.99	100.00	99.99	99.99	100.00	100.00	99.99	100.01	100.00	99.99	100.01	100.00	99.99	100.00	99.99	100.00
Original total	99.98	100.02	100.00	99.99	100.00	100.02	99.99	99.99	100.02	100.00	99.99	100.01	99.99	99.98	99.99	99.98
CIPW norms[4]																
AP	0.76	0.52	0.90	0.45	0.31	0.33	0.38	0.33	0.40	0.40	0.33	0.38	0.43	0.38	0.38	0.33
IL	1.81	2.07	3.94	2.06	1.50	1.10	1.43	1.35	1.41	1.43	1.48	1.41	1.73	1.45	1.41	1.43
MT	2.31	2.10	3.93	2.25	2.00	1.41	1.88	1.93	1.79	1.76	2.04	1.82	2.02	1.97	1.77	1.89
OR	5.45	9.94	9.90	7.52	4.79	9.88	9.35	7.34	7.69	7.40	5.80	6.33	20.24	17.58	20.12	8.23
AB	32.98	26.77	21.52	28.23	28.81	26.68	23.47	25.42	27.36	28.30	28.90	28.64	11.19	9.66	11.02	31.61
AN	26.14	25.19	23.50	29.22	28.01	19.64	24.24	16.67	24.91	25.41	28.15	27.61	14.57	26.48	24.34	22.04
COR	1.77	1.03	0.00	0.53	2.13	2.96	2.15	4.38	2.03	2.01	2.02	1.97	6.79	4.01	3.05	2.40
QTZ	16.02	20.06	15.47	16.49	20.23	29.69	25.77	29.92	23.04	21.94	19.32	21.83	24.99	25.89	27.22	20.26
EN	6.06	6.66	8.17	7.04	6.36	4.21	5.81	6.96	6.13	6.26	5.96	6.51	12.30	6.79	5.59	6.31
FS	6.74	5.68	12.69	6.24	5.86	4.11	5.54	5.71	5.25	5.10	6.01	5.29	5.76	5.81	5.13	0.00
FO	0.00	0.00	0.00	0.00	0.00	0.00	0.00	0.00	0.00	0.00	0.00	0.00	0.00	0.00	0.00	0.00
FA	0.00	0.00	0.00	0.00	0.00	0.00	0.00	0.00	0.00	0.00	0.00	0.00	0.00	0.00	0.00	0.00
DI	0.00	0.00	4.05	0.00	0.00	0.00	0.00	0.00	0.00	0.00	0.00	0.00	0.00	0.00	0.00	0.00
HY	12.80	12.34	16.81	13.28	12.22	8.32	11.35	12.67	11.38	11.36	11.97	11.80	18.05	12.60	10.71	11.83
OL	0.00	0.00	0.00	0.00	0.00	0.00	0.00	0.00	0.00	0.00	0.00	0.00	0.00	0.00	0.00	0.00
D.I.[5]	54.442	56.772	46.891	52.228	53.837	66.246	58.593	62.681	58.090	57.632	54.019	55.015	56.417	53.126	58.358	60.094
Rock name[6]	and	and	and	and	and db fl	qtz di	and db fl	dac	dac db fl	dac	and	dac	and db fl	and db fl	dac	dac
Modal analyses[7]																
Plagioclase	1	10	25	•[8]		•[8]	•[8]	•[8]	25	25		25	25	20	27	27
Clinopyroxene		2	3				•[8]	•[8]		3		3	2	2	1	1
Orthopyroxene		3	4	•[8]			•[8]		5	5		1	2	2	5	3
Olivine																
Hornblende						•[8]	•[8]									
Biotite						•[8]										
Quartz						•[8]										
Fe-Ti oxide																

[1]Old Maid Flat drill hole 7-A, 2S/8E/15Ac; depth in feet.
[2]Percent by weight; Peter R. Hooper, analyst.
[3]Volatile-free, total Fe as FeO.
[4]Calculated with $Fe_2O_3/FeO = 0.31$.
[5]Thornton-Tuttle Differentiation Index.
[6]Rock name: bas = basalt; bas and = basaltic andesite; and = andesite; hi-K and = high potassium andesite; db fl = debris flow; dac = dacite; qtz di = microquartz diorite; volc ms = volcanic mudstone.
[7]Volume percent of phenocrysts; George R. Priest, petrographer.
[8]Present, but mode not determined.

Table 1. *Major-element compositions of samples from OMF-7A drill hole* — Continued
(Location 2S/8E/15Ac)

Stratigraphic unit:	Rhododendron Formation	Rhododendron Formation	Rhododendron Formation	Rhododendron Formation	Intrusion	Frenchman Springs, Wanapum Basalt	Frenchman Springs, Wanapum Basalt	Interbed	Interbed	Low-MgO Grande Ronde Basalt	Low-MgO Grande Ronde Basalt	Intrusion	Intrusion	Low-MgO Grande Ronde Basalt	Low-MgO Grande Ronde Basalt	Low-MgO Grande Ronde Basalt
Depth (ft)[1]:	2,000	2,030	2,100	2,120	2,210	2,520	2,550	2,610	2,680	2,720	2,770	2,900	2,917	3,070	3,220	3,370
Major oxides[2]																
SiO_2	62.82	61.78	61.13	60.16	67.49	51.30	51.42	54.82	59.53	57.13	55.88	66.10	69.71	51.13	56.13	55.58
TiO_2	0.75	0.88	0.95	0.96	0.55	3.18	3.18	2.16	2.37	2.27	2.29	0.52	0.65	2.76	1.95	2.42
Al_2O_3	18.19	18.10	18.57	18.80	17.36	14.33	14.65	16.22	15.39	14.98	15.02	17.68	14.64	14.99	14.71	14.03
FeO	5.23	5.77	5.68	6.15	3.86	14.63	14.29	9.93	9.36	12.06	11.71	3.69	5.33	12.31	11.29	12.87
MnO	0.09	0.09	0.10	0.10	0.20	0.27	0.27	0.17	0.15	0.19	0.20	0.07	0.18	0.26	0.19	0.20
MgO	2.31	3.01	2.95	3.07	1.35	3.90	4.02	3.98	2.81	3.33	3.54	1.72	0.77	3.86	3.57	3.20
CaO	5.84	5.07	6.21	6.47	4.28	8.59	8.38	5.83	4.00	4.34	6.17	5.37	3.82	9.16	7.55	7.00
Na_2O	3.47	3.53	3.29	3.10	2.96	2.36	2.17	1.93	2.96	3.13	3.32	3.31	3.00	2.86	2.71	2.50
K_2O	1.13	1.57	0.92	0.99	1.83	0.72	0.86	4.59	3.02	2.16	1.45	1.42	1.71	1.22	1.54	1.78
P_2O_5	0.16	0.19	0.20	0.20	0.12	0.73	0.77	0.36	0.40	0.41	0.43	0.12	0.18	1.46	0.35	0.42
Recalculated total[3]	99.99	99.99	100.00	100.01	100.00	100.01	100.01	99.99	99.99	100.00	100.01	100.00	99.99	100.01	99.99	100.00
Original total	100.01	100.00	100.02	100.00	100.00	100.01	100.01	99.98	100.01	100.01	100.00	100.00	100.00	99.99	99.98	100.01
CIPW norms[4]																
AP	0.38	0.45	0.47		0.28	1.71	1.81	0.86	0.95	0.97	1.02	0.28	0.43	3.45	0.83	1.00
IL	1.43	1.67	1.81		1.05	6.02	6.02	4.09	4.49	4.31	4.34	0.99	1.24	5.22	3.70	4.59
MT	1.84	2.03	2.00		1.36	5.14	5.02	3.49	3.29	4.24	4.12	1.30	1.88	4.33	3.97	4.52
OR	6.69	9.29	5.44		10.82	4.21	5.04	27.08	17.83	12.74	8.53	8.40	10.12	7.17	9.07	10.49
AB	29.31	29.83	27.79	norm	25.00	19.87	18.34	16.29	25.02	26.39	28.00	27.95	25.33	24.11	22.83	21.05
AN	27.91	23.90	29.44	not	20.42	26.32	27.59	21.98	17.17	18.81	21.73	25.83	17.75	24.41	23.40	21.74
COR	1.02	1.82	1.36	calculated	3.02	0.00	0.00	0.00	0.93	0.58	0.00	1.23	1.34	0.00	0.00	0.00
QTZ	20.33	17.73	18.75		30.48	9.07	9.74	5.49	15.45	12.29	10.00	25.93	34.18	5.97	11.45	12.25
EN	5.74	7.48	7.33		3.37	9.67	9.97	1.88	6.99	8.27	8.79	4.29	1.92	9.59	8.87	7.94
FS	5.36	5.82	5.61		4.22	12.01	12.83	9.89	7.90	11.44	11.00	3.82	5.83	11.08	11.04	12.20
FO	0.00	0.00	0.00		0.00	0.00	0.00	8.97	0.00	0.00	0.00	0.00	0.00	0.00	0.00	0.00
FA	0.00	0.00	0.00		0.00	0.00	0.00	0.00	0.00	0.00	0.00	0.00	0.00	0.00	0.00	0.00
DI	0.00	0.00	0.00		0.00	9.56	7.38	3.72	0.00	0.00	4.96	0.00	0.00	9.46	9.74	8.51
HY	11.10	13.30	12.94		7.59	18.14	19.11	17.03	14.89	19.71	17.32	8.10	7.75	15.97	15.05	15.87
OL	0.00	0.00	0.00		0.00	0.00	0.00	0.00	0.00	0.00	0.00	0.00	0.00	0.00	0.00	0.00
D.I.[5]	56.330	56.848	51.990		66.293	33.151	33.116	48.853	58.295	51.422	46.537	62.276	69.634	37.253	43.346	43.793
Rock name[6]	and	and	and	and	qtz di	bas	bas	db fl	hi-K and	bas and	bas and	qtz di	qtz di	bas	bas and	bas and
Modal analyses[7]																
Plagioclase	27	25	20	15	30	•[8]	•[8]	2	1	1	1	30	10			1
Clinopyroxene	2	3	3	2		•[8]	•[8]	1								1
Orthopyroxene	3	2	2	2												
Olivine																
Hornblende					6							5	2			
Biotite					2							1	1			
Quartz																
Fe-Ti oxide																

[1]Old Maid Flat drill hole 7-A, 2S/8E/15Ac; depth in feet.
[2]Percent by weight; Peter R. Hooper, analyst.
[3]Volatile-free, total Fe as FeO.
[4]Calculated with $Fe_2O_3/FeO = 0.31$.
[5]Thornton-Tuttle Differentiation Index.
[6]Rock name: bas = basalt; bas and = basaltic andesite; and = andesite; hi-K and = high potassium andesite; db fl = debris flow; dac = dacite; qtz di = microquartz diorite; volc ms = volcanic mudstone.
[7]Volume percent of phenocrysts; George R. Priest, petrographer.
[8]Present, but mode not determined.

Table 1. *Major-element compositions of samples from OMF-7A drill hole* — Continued
(Location 2S/8E/15Ac)

Stratigraphic unit:	Low-MgO Grande Ronde Basalt	Low-MgO Grande Ronde Basalt	Intrusion	Low-MgO Grande Ronde Basalt	Low-MgO Grande Ronde Basalt	Low-MgO Grande Ronde Basalt	Low-MgO Grande Ronde Basalt	Intrusion	Intrusion	Low-MgO Grande Ronde Basalt	Intrusion	Intrusion	Interbed	Intrusion	Ducitic greenstone	Ducitic greenstone	Ducitic greenstone
Depth (ft)[1]:	3,395	3,670	3,760	3,780	3,840	4,020	4,110	4,280	4,510	4,580	4,760	5,000	5,330	5,470	5,820	5,940	6,016
Major oxides[2]																	
SiO_2	55.90	57.77	66.52	57.75	60.70	56.29	57.87	66.73	66.76	57.97	60.86	65.83	63.33	66.30	63.96	60.51	65.35
TiO_2	2.31	2.08	0.53	2.08	1.82	2.18	1.88	0.52	0.50	1.82	1.07	0.64	0.86	0.64	1.28	1.90	0.67
Al_2O_3	14.22	14.65	17.62	15.57	14.59	15.01	15.20	17.88	17.66	15.44	17.75	17.57	18.94	18.29	17.65	17.97	17.30
FeO	12.24	11.19	3.31	9.98	10.14	11.29	10.64	3.32	3.20	10.19	6.58	4.22	5.57	3.98	7.91	8.10	4.60
MnO	0.18	0.17	0.06	0.18	0.17	0.19	0.18	0.06	0.06	0.16	0.11	0.08	0.11	0.08	0.15	0.16	0.09
MgO	3.23	3.29	1.48	3.29	2.96	3.37	3.20	1.51	1.52	3.57	2.67	1.85	1.97	1.63	1.04	1.34	1.96
CaO	7.13	6.23	4.64	6.49	5.28	6.83	6.50	5.30	5.40	6.68	5.94	4.74	4.92	4.16	3.09	4.75	5.04
Na_2O	2.48	2.55	3.73	2.96	2.28	3.00	2.68	3.15	3.45	2.42	3.51	3.53	3.62	3.99	3.17	3.22	3.42
K_2O	1.90	1.68	2.00	1.29	1.64	1.41	1.50	1.41	1.33	1.48	1.26	1.39	0.51	0.80	1.36	1.27	1.41
P_2O_5	0.40	0.38	0.12	0.41	0.42	0.43	0.35	0.12	0.13	0.27	0.24	0.15	0.17	0.13	0.38	0.78	0.16
Recalculated total[3]	99.99	99.99	100.01	100.00	100.00	100.00	100.00	100.00	100.01	100.00	99.99	100.00	100.00	100.00	99.99	100.00	100.00
Original total	99.99	99.99	100.00	100.00	100.00	100.00	100.00	100.01	100.00	100.01	99.99	100.01	100.00	99.99	100.00	99.99	100.01
CIPW norms[4]																	
AP	0.95	0.91	0.28	0.97	1.00	1.02	0.83	0.28	0.31	0.64	0.57	0.36	0.40	0.31		1.85	0.38
IL	4.38	4.02	1.01	3.94	3.45	4.13	3.56	0.99	0.95	3.45	2.04	1.22	1.64	1.22		3.60	1.27
MT	4.30	0.00	1.16	3.51	3.56	3.97	3.74	1.17	1.13	3.58	2.32	1.49	1.96	1.40		2.85	1.62
OR	11.20	10.05	11.83	7.58	9.66	8.30	8.83	8.34	7.87	8.71	7.46	8.22	3.02	4.73		7.46	8.34
AB	20.97	21.93	31.50	25.02	19.26	25.29	22.65	26.67	29.13	20.44	29.67	29.81	30.59	33.71	norm	27.22	28.88
AN	21.95	23.93	22.20	25.31	23.36	23.29	24.94	25.48	25.91	26.82	27.85	22.51	23.28	19.76	not	18.41	23.93
COR	0.00	0.00	1.18	0.00	0.48	0.00	0.00	1.81	1.04	0.00	0.38	2.00	3.88	3.61	calculated	4.53	1.36
QTZ	12.20	14.57	23.84	14.60	22.10	11.81	15.14	28.17	26.65	15.80	16.56	25.51	24.72	27.22		23.66	24.61
EN	8.02	5.80	3.69	8.16	7.37	8.37	7.94	3.76	3.79	8.86	6.64	4.61	4.89	4.06		3.32	4.89
FS	11.58	16.74	3.31	9.19	9.80	10.66	10.33	3.34	3.23	9.85	6.54	4.30	5.64	3.99		7.14	4.72
FO	0.00	0.00	0.00	0.00	0.00	0.00	0.00	0.00	0.00	0.00	0.00	0.00	0.00	0.00		0.00	0.00
FA	0.00	0.00	0.00	0.00	0.00	0.00	0.00	0.00	0.00	0.00	0.00	0.00	0.00	0.00		0.00	0.00
DI	8.97	4.24	0.00	3.44	0.00	6.40	4.14	0.00	0.00	3.73	0.00	0.00	0.00	0.00		0.00	0.00
HY	15.10	20.36	7.00	15.65	17.16	15.83	16.20	7.10	7.02	16.86	13.18	8.91	10.53	8.05		10.46	9.61
OL	0.00	0.00	0.00	0.00	0.00	0.00	0.00	0.00	0.00	0.00	0.00	0.00	0.00	0.00		0.00	0.00
D.I.[5]	44.366	46.557	67.174	47.208	51.013	45.386	46.615	63.177	63.651	44.947	53.687	63.541	58.323	65.664		58.343	61.832
Rock name[6]	bas and	bas and	qtz di	bas and	and	bas and	bas and	qtz di	qtz di	bas and	qtz di	qtz di	volc ms	qtz di	and	and	and
Modal analyses[7]																	
Plagioclase	1	1	28	1		1		•[8]	•[8]		5	•[8]	•[8]	•[8]	•[8]	•[8]	•[8]
Clinopyroxene														•[8]			
Orthopyroxene											1						
Olivine																	
Hornblende			3					•[8]	•[8]		5	•[8]		•[8]			
Biotite			1					•[8]	•[8]			•[8]					
Quartz													•[8]				
Fe-Ti oxide																	

[1]Old Maid Flat drill hole 7-A, 2S/8E/15Ac; depth in feet.
[2]Percent by weight; Peter R. Hooper, analyst.
[3]Volatile-free, total Fe as FeO.
[4]Calculated with $Fe_2O_3/FeO = 0.31$.
[5]Thornton-Tuttle Differentiation Index.
[6]Rock name: bas = basalt; bas and = basaltic andesite; and = andesite; hi-K and = high potassium andesite; db fl = debris flow; dac = dacite; qtz di = microquartz diorite; volc ms = volcanic mudstone.
[7]Volume percent of phenocrysts; George R. Priest, petrographer.
[8]Present, but mode not determined.

Table 2. *Major-element compositions of samples from OMF-1 drill hole and the Old Maid Flat area*

Stratigraphic unit:	Frenchman Springs, Wanapum Basalt	Rhododendron Formation	Rhododendron Formation	Rhododendron Formation	Rhododendron Formation	Rhododendron Formation	Rhododendron Formation	Rhododendron Formation	Rhododendron Formation	Rhododendron Formation	Rhododendron Formation	Rhododendron Formation	Rhododendron Formation	Rhododendron Formation	Laurel Hill Intrusion
Area:	OMF-1	Last Chance Mtn.	Last Chance Mtn.	Last Chance Mtn.	Last Chance Mtn.	Last Chance Mtn.	Last Chance Mtn.	Last Chance Mtn.	Last Chance Mtn.	Last Chance Mtn.	Last Chance Mtn.	Last Chance Mtn.	Last Chance Mtn.	Last Chance Mtn.	Laurel Hill
Sample no.:	Depth 1,620 ft.	MH-8	MH-8B1	MH-8B2	MH-9	MH-10	MH-15	MH-16	MH-17	MH-20	MH-21	MH-22	MH-23	MH-25	STILL
Location:	2S/8E/15Cd	2S/8E/15Bcd	2S/8E/15Bcd	2S/8E/15Bcd	2S/8E/15Bcd	2S/8E/15Bd	2S/8E/16Cac	2S/8E/16Cac	2S/8E/16Caa	2S/8E/16Dbb	2S/8E/16Dbb	2S/8E/16Dbd	2S/8E/16Dbd	2S/8E/16Dca	3S/8E/16Dcb
Major oxides[1]															
SiO_2	53.03	58.81	60.56	63.94	59.99	56.20	59.35	64.09	63.90	63.40	64.74	62.74	65.33	59.37	60.73
TiO_2	3.57	0.84	0.85	0.76	0.86	0.99	0.86	0.62	0.61	0.91	0.67	0.78	0.69	0.85	1.06
Al_2O_3	16.06	19.75	19.97	17.94	17.73	19.17	17.97	17.58	17.56	17.83	18.08	17.94	18.61	19.71	16.87
FeO	12.70	6.58	5.08	5.24	6.61	7.69	6.89	4.56	5.01	4.80	4.63	5.97	3.76	6.44	7.17
MnO	0.83	0.12	0.17	0.07	0.15	0.09	0.13	0.08	0.08	0.12	0.07	0.10	0.09	0.13	0.10
MgO	3.83	2.86	2.53	2.06	3.29	3.62	3.33	2.61	2.59	2.05	2.38	2.87	1.20	3.61	3.37
CaO	6.75	7.35	6.99	5.00	7.09	7.91	7.27	5.95	5.75	6.01	5.03	5.55	5.05	6.23	5.88
Na_2O	0.05	3.25	3.31	3.51	3.22	3.28	3.19	3.35	3.30	2.24	3.03	3.35	3.84	3.34	3.33
K_2O	2.45	0.29	0.39	1.26	0.88	0.87	0.82	1.03	1.07	2.52	1.24	0.52	1.26	0.18	1.26
P_2O_5	0.73	0.14	0.15	0.21	0.16	0.17	0.16	0.13	0.12	0.11	0.12	0.19	0.16	0.13	0.23
Recalculated total[2]	100.01	99.99	100.00	99.99	99.98	99.99	99.97	100.00	99.99	99.99	99.99	100.01	99.99	99.99	100.00
Original total	100.00	100.00	100.00	100.01	99.99	100.00	99.99	100.00	100.00	99.99	99.99	100.01	99.99	100.00	100.01
CIPW norms[3]															
AP	Norm	0.33	0.36	0.50	0.38	0.40	0.38	0.31	0.29	0.26	0.29	0.45	0.38	0.31	0.55
IL		1.60	1.62	1.45	1.64	1.88	1.64	1.18	1.16	1.73	1.27	1.48	1.31	1.62	2.02
MT	not	2.32	1.79	1.85	2.33	2.70	2.43	1.61	1.76	1.69	1.63	2.10	1.32	2.27	2.52
OR		1.72	2.31	7.46	5.21	5.15	4.85	6.09	6.33	14.85	7.34	3.08	7.45	1.07	7.46
AB	calc.	27.46	27.96	29.65	27.21	27.72	26.96	28.29	27.87	18.89	25.59	28.30	32.44	28.22	28.14
AN		35.51	33.64	23.41	31.26	34.93	32.23	28.65	27.73	29.09	24.15	26.23	23.98	30.01	27.29
COR		1.06	1.76	2.21	0.00	0.00	0.00	0.44	0.80	0.76	2.89	2.24	2.14	3.00	0.00
QTZ		15.98	19.12	23.04	15.63	8.91	14.78	22.21	22.32	22.99	26.21	22.76	24.34	17.78	16.27
EN		7.11	6.28	5.11	8.18	9.01	8.28	6.48	6.43	5.11	5.91	7.13	2.99	8.98	8.38
FS		6.94	5.18	5.34	7.00	7.99	7.32	4.74	5.31	4.63	4.73	6.25	3.65	6.76	7.26
FO		0.00	0.00	0.00	0.00	0.00	0.00	0.00	0.00	0.00	0.00	0.00	0.00	0.00	0.00
FA		0.00	0.00	0.00	0.00	0.00	0.00	0.00	0.00	0.00	0.00	0.00	0.00	0.00	0.00
DI		0.00	0.00	0.00	2.33	2.57	2.27	0.00	0.00	0.00	0.00	0.00	0.00	0.00	0.27
HY		14.05	11.46	10.45	14.03	15.73	14.48	11.22	11.75	9.74	10.64	13.38	6.65	15.74	15.51
OL		0.00	0.00	0.00	0.00	0.00	0.00	0.00	0.00	0.00	0.00	0.00	0.00	0.00	0.00
D.I.[4]		45.152	49.390	60.149	48.047	41.782	46.588	56.599	56.527	56.739	59.129	54.134	64.230	47.066	51.866
Rock name[5]		and	and	dac	and	bas and	and	dac	dac	dac	dac	and	dac	and	and
Modal analyses[6]															
Plagioclase		20	20	20	20	20	17	28	25	7	15	30	20	28	4
Clinopyroxene					2	2	2	2	2	2	1	4		1	
Orthopyroxene		5	5	5	3	3	2	5	3	5	2	2	1	7	
Olivine															
Hornblende					1	1	2				5		3		3
Biotite															
Quartz															
Fe-Ti oxide					1	1	1			1			1		

[1]Percent by weight; Peter R. Hooper, analyst.
[2]Volatile-free, total Fe as FeO.
[3]Calculated with $Fe_2O_3/FeO = 0.31$; in percent.
[4]Thornton-Tuttle Differentiation Index.
[5]Rock name: bas and = basaltic andesite; and = andesite; dac = dacite.
[6]Volume percent of phenocrysts; George R. Priest, petrographer.

Table 2. *Major-element compositions of samples from OMF-1 drill hole and the Old Maid Flat area*—Continued

Stratigraphic unit:	Last Chance andesite	Last Chance andesite	Last Chance andesite	Miocene-Pliocene lavas	Miocene-Pliocene lavas	Miocene-Pliocene lavas	Miocene-Pliocene lavas	Miocene-Pliocene lavas	Miocene-Pliocene lavas	Miocene-Pliocene lavas
Area:	Last Chance Mtn.	Last Chance Mtn.	Last Chance Mtn.	Last Chance Mtn.	Last Chance Mtn.	Last Chance Mtn.	Last Chance Mtn.	Last Chance Mtn.	Last Chance Mtn.	Last Chance Mtn.
Sample no.:	MH-18	MH-19	LCM	MH-11	MH-12	MH-13	MH-14	MH-5	MH-6	MH-7
Location:	2S/8E/16Caa	2S/8E/16Dbb	2S/8E/16Bdb	2S/8E/15Bdc	2S/8E/15Bdc	2S/8E/15Bdd	2S/8E/15Acc	2S/8E/15Acb	2S/8E/15Acb	2S/8E/15Bdb
Major oxides[1]										
SiO_2	60.18	57.31	59.03	59.93	61.30	58.78	58.67	58.91	59.91	61.29
TiO_2	1.03	1.00	1.00	1.00	0.84	0.92	1.06	0.87	0.86	0.83
Al_2O_3	17.02	19.14	17.76	17.60	18.33	20.37	18.62	18.26	17.76	18.22
FeO	6.84	6.95	7.16	6.47	6.15	5.87	7.64	6.83	6.89	5.99
MnO	0.10	0.09	0.10	0.12	0.08	0.10	0.15	0.13	0.12	0.09
MgO	3.84	3.88	3.55	3.62	2.81	2.34	2.71	3.51	3.26	2.83
CaO	6.51	7.34	7.02	6.53	5.99	6.69	6.32	6.91	6.86	5.95
Na_2O	3.11	3.16	3.12	3.36	3.02	3.55	3.64	3.43	3.19	3.47
K_2O	1.17	0.92	1.05	1.18	1.32	1.18	0.88	0.97	0.98	1.15
P_2O_5	0.18	0.18	0.21	0.18	0.14	0.19	0.31	0.17	0.16	0.18
Recalculated total[2]	99.98	99.97	100.00	99.99	99.98	99.99	100.00	99.99	99.99	100.00
Original total	100.01	100.00	100.01	100.00	99.99	99.99	100.01	100.01	100.02	100.00
CIPW norms[3]										
AP	0.43	0.43	0.50	0.43	0.33	0.45	0.74	0.40	0.38	0.43
IL	1.96	1.90	1.90	1.90	1.60	1.75	2.02	1.66	1.64	1.58
MT	2.41	2.45	2.52	2.28	2.16	2.07	2.69	2.40	2.43	2.11
OR	6.93	5.45	6.22	6.98	7.81	6.98	5.21	5.74	5.80	6.81
AB	26.27	26.70	26.39	28.39	25.51	30.00	30.77	28.99	26.95	29.32
AN	28.98	35.20	31.32	29.38	28.75	31.90	29.28	31.49	31.17	28.28
COR	0.00	0.02	0.00	0.00	1.38	1.54	0.92	0.00	0.00	0.88
QTZ	15.71	11.13	14.33	14.35	19.14	13.61	13.74	12.71	15.51	17.40
EN	9.55	9.66	8.59	9.01	6.99	5.81	6.74	8.73	8.11	7.03
FS	6.91	7.08	7.35	6.54	6.33	5.90	7.93	7.21	7.29	6.17
FO	0.00	0.00	0.00	0.00	0.00	0.00	0.00	0.00	0.00	0.00
FA	0.00	0.00	0.00	0.00	0.00	0.00	0.00	0.00	0.00	0.00
DI	1.71	0.00	1.75	1.46	0.00	0.00	0.00	1.34	1.45	0.00
HY	15.62	16.73	15.08	14.83	13.32	11.71	14.67	15.29	14.68	13.20
OL	0.00	0.00	0.00	0.00	0.00	0.00	0.00	0.00	0.00	0.00
D.I.[4]	48.906	43.277	46.942	49.724	52.464	50.597	49.718	47.431	48.258	53.528
Rock name[5]	and	and	and	and	and	and	and	and	and	and
Modal analyses[6]										
Plagioclase	20	30	30	25	25	25	1	15	15	30
Clinopyroxene	3	3	3	3	4	2		1	1	2
Orthopyroxene	2	6	6	5	3	3		4	4	4
Olivine								1	1	
Hornblende								1	1	
Biotite										
Quartz										
Fe-Ti oxide	1			1		1				1

[1]Percent by weight; Peter R. Hooper, analyst.
[2]Volatile-free, total Fe as FeO.
[3]Calculated with $Fe_2O_3/FeO = 0.31$; in percent.
[4]Thornton-Tuttle Differentiation Index.
[5]Rock name: bas and = basaltic andesite; and = andesite; dac = dacite.
[6]Volume percent of phenocrysts; George R. Priest, petrographer.

Table 3. *Trace-element analyses, OMF-7A drill hole*[1]
(Location 2S/8E/15Ac. Values in ppm except as noted. Analytical error at 1σ in parentheses.)

Stratigraphic unit:	Miocene-Pliocene lavas	Last Chance andesite	Last Chance andesite	Last Chance andesite	Rhododendron Formation	Intrusion	Rhododendron Formation	Rhododendron Formation	Rhododendron Formation	Rhododendron Formation	Rhododendron Formation	Rhododendron Formation	Rhododendron Formation	Rhododendron Formation	Rhododendron Formation	Rhododendron Formation
Depth (ft):	260	340	520	740	1,040	1,290	1,360	1,440	1,480	1,510	1,622	1,650	1,680	1,850	1,930	1,980
$\%Na_2O$	4.42(0.02)	3.85(0.02)	3.63(0.02)	3.67(0.02)	3.62(0.02)	3.51(0.02)	3.12(0.02)	3.54(0.02)	3.45(0.02)	3.81(0.02)	3.75(0.02)	3.75(0.02)	3.94(0.02)	3.54(0.02)	4.37(0.06)	4.40(0.02)
Cs	0.65(0.13)	0.99(0.19)	0.86(0.19)	—	0.88(0.16)	1.9 (0.3)	3.4 (0.5)	1.9 (0.3)	1.1 (0.2)	0.86(0.16)	2.4 (0.4)	—	1.05(0.19)	2.9 (0.5)	0.51(0.14)	1.7 (0.3)
Rb	—	38 (5)	19 (5)	25 (5)	17 (5)	36 (4)	35 (5)	21 (5)	24 (5)	21 (5)	—	19 (5)	23 (5)	22 (5)	30 (6)	19 (5)
Ba	370 (50)	390 (70)	320 (70)	370 (70)	340 (60)	400 (50)	310 (60)	270 (60)	320 (60)	300 (60)	250 (60)	390 (60)	360 (70)	410 (70)	400 (80)	400 (70)
Eu	1.44(0.04)	1.31(0.04)	1.22(0.04)	1.22(0.04)	0.93(0.03)	1.00(0.03)	1.06(0.03)	0.99(0.03)	1.11(0.03)	1.16(0.03)	1.06(0.03)	1.13(0.03)	1.13(0.03)	1.15(0.03)	1.33(0.04)	1.09(0.03)
Sr	690 (60)	320 (60)	420 (60)	340 (60)	310 (50)	320 (50)	280 (50)	240 (50)	250 (50)	400 (70)	380 (50)	340 (50)	330 (60)	400 (60)	420 (70)	400 (60)
La	15.1 (0.3)	17.7 (0.4)	14.5 (0.3)	13.6 (0.3)	11.4 (0.3)	17.1 (0.4)	15.2 (0.3)	12.6 (0.3)	14.0 (0.3)	14.8 (0.4)	14.9 (0.3)	13.5 (0.3)	12.4 (0.3)	14.6 (0.4)	17.1 (0.6)	14.0 (0.4)
Ce	34.0 (1.2)	44.3 (1.5)	34.6 (1.2)	33.2 (1.2)	24.0 (0.9)	36.7 (1.2)	34.1 (1.2)	28.8 (1)	32.7 (1.1)	34.6 (1.2)	31.9 (1.1)	33.5 (1.2)	27.8 (1)	33.4 (1.2)	41.9 (1.5)	33.2 (1.2)
Nd	19 (3)	16 (4)	17 (3)	14 (3)	11 (3)	16 (3)	18 (3)	16 (3)	11 (3)	15 (3)	15 (3)	14 (3)	—	—	—	15 (3)
Sm	4.64(0.04)	5.94(0.06)	4.70(0.05)	4.85(0.05)	3.02(0.04)	3.23(0.04)	3.89(0.05)	3.64(0.04)	3.82(0.04)	4.09(0.04)	3.61(0.04)	3.83(0.04)	3.81(0.04)	4.15(0.05)	4.82(0.08)	3.70(0.04)
Tb	0.59(0.07)	0.95(0.11)	0.67(0.08)	0.81(0.10)	0.43(0.06)	0.51(0.07)	0.64(0.07)	0.54(0.07)	0.54(0.07)	0.63(0.08)	0.58(0.07)	0.61(0.08)	0.67(0.08)	0.60(0.08)	0.77(0.09)	0.54(0.07)
Yb	1.6 (0.2)	2.4 (0.3)	1.9 (0.2)	2.3 (0.3)	1.2 (0.3)	1.6 (0.2)	1.8 (0.2)	1.6 (0.2)	1.5 (0.2)	1.8 (0.2)	1.4 (0.2)	1.6 (0.3)	1.5 (0.2)	1.5 (0.2)	1.8 (0.2)	1.4 (0.2)
Lu	0.31(0.05)	0.30(0.05)	0.29(0.05)	0.36(0.05)	0.17(0.05)	0.15(0.04)	0.23(0.04)	0.28(0.05)	0.19(0.04)	0.25(0.05)	0.22(0.04)	0.18(0.04)	0.24(0.05)	0.27(0.05)	0.28(0.05)	0.22(0.05)
Th	1.26(0.08)	4.05(0.12)	2.72(0.11)	2.91(0.11)	2.00(0.10)	3.96(0.10)	2.81(0.10)	2.25(0.10)	2.62(0.10)	2.70(0.10)	2.33(0.08)	2.17(0.10)	1.84(0.11)	2.59(0.13)	3.30(0.11)	2.41(0.11)
Hf	3.6 (0.2)	7.7 (0.4)	4.9 (0.3)	5.7 (0.3)	3.2 (0.2)	4.1 (0.2)	4.6 (0.3)	4.2 (0.2)	4.7 (0.3)	4.8 (0.3)	4.4 (0.3)	4.7 (0.3)	4.1 (0.3)	4.7 (0.3)	6.0 (0.3)	4.1 (0.2)
$\%Fe_2O_3$	6.95(0.04)	6.92(0.05)	6.56(0.05)	7.02(0.05)	5.62(0.05)	4.46(0.04)	5.46(0.04)	5.56(0.04)	5.52(0.04)	5.69(0.05)	5.59(0.04)	5.93(0.04)	6.49(0.05)	6.00(0.05)	6.49(0.05)	5.58(0.04)
Ta	0.56(0.03)	0.77(0.04)	0.49(0.03)	0.57(0.03)	0.44(0.03)	0.75(0.03)	0.61(0.03)	0.57(0.03)	0.62(0.03)	0.63(0.03)	0.56(0.03)	0.57(0.03)	0.61(0.03)	0.63(0.03)	0.72(0.04)	0.61(0.03)
Co	14.3 (0.2)	21.2 (0.3)	23.4 (0.3)	21.2 (0.3)	19.6 (0.3)	11.5 (0.2)	15.8 (0.2)	17.4 (0.3)	16.3 (0.2)	17.1 (0.3)	16.7 (0.2)	17.6 (0.3)	19.9 (0.3)	17.9 (0.3)	18.6 (0.3)	16.4 (0.3)
Sc	8.64(0.04)	17.02(0.06)	17.81(0.06)	18.15(0.07)	13.37(0.05)	6.63(0.04)	10.96(0.05)	11.75(0.05)	11.29(0.04)	11.92(0.05)	11.40(0.04)	12.66(0.05)	14.82(0.05)	12.90(0.06)	13.29(0.06)	12.06(0.05)
Cr	3.4 (0.9)	136 (3)	112 (2)	79.7 (1.9)	41.0 (1.4)	17.1 (1)	36.0 (1.3)	46.2 (1.4)	37.7 (1.2)	43.3 (1.4)	25.9 (1.2)	39.3 (1.4)	49.4 (1.6)	48 (2)	48.3 (1.7)	29.1 (1.3)
Zn	76 (5)	70 (6)	64 (6)	64 (6)	61 (6)	85 (5)	92 (6)	59 (5)	66 (5)	195 (10)	64 (5)	70 (6)	65 (6)	63 (6)	82 (7)	60 (6)

[1]Marvin H. Beeson, analyst.

Table 3. *Trace-element analyses, OMF-7A drill hole*[1] — Continued
(Location 2S/8E/15Ac. Values in ppm except as noted. Analytical error at 1σ in parentheses.)

Stratigraphic unit:	Rhododendron Formation	Rhododendron Formation	Rhododendron Formation	Rhododendron Formation	Intrusion	Frenchman Springs, Wanapum Basalt	Frenchman Springs, Wanapum Basalt	Interbed	Interbed	Low-MgO Grande Ronde Basalt	Low-MgO Grande Ronde Basalt	Intrusion	Intrusion	Intrusion	Low-MgO Grande Ronde Basalt	Low-MgO Grande Ronde Basalt
Depth (ft):	2,000	2,030	2,100	2,120	2,210	2,520	2,550	2,610	2,680	2,720	2,770	2,900	2,917	3,070	3,220	3,370
$\%Na_2O$	3.79(0.02)	3.16(0.02)	3.56(0.02)	3.48(0.05)	3.32(0.02)	2.18(0.01)	2.16(0.01)	2.03(0.01)	3.15(0.01)	3.45(0.01)	3.64(0.02)	3.82(0.02)	3.73(0.02)	2.69(0.01)	2.62(0.01)	2.65(0.01)
Cs	—	0.97(0.18)	—	1.6 (0.3)	1.7 (0.3)	1.1 (0.2)	0.85(0.18)	0.8 (0.2)	—	—	—	1.34(0.18)	0.47(0.10)	0.74(0.17)	0.46(0.14)	0.71(0.16)
Rb	20 (5)	19 (4)	18 (5)	21 (6)	34 (4)	27 (7)	—	75 (7)	80 (7)	63 (7)	32 (7)	29 (4)	29 (5)	—	42 (7)	47 (7)
Ba	400 (70)	360 (60)	350 (70)	—	350 (50)	710 (90)	700 (90)	950 (90)	1,240 (90)	820 (90)	790 (90)	420 (50)	360 (50)	1,730 (100)	850 (80)	840 (90)
Eu	1.10(0.03)	1.01(0.03)	1.21(0.04)	1.16(0.03)	0.94(0.03)	2.66(0.05)	2.59(0.05)	2.05(0.04)	2.00(0.04)	2.03(0.04)	1.99(0.04)	1.08(0.03)	1.03(0.02)	3.65(0.06)	1.88(0.04)	2.25(0.04)
Sr	360 (60)	290 (50)	390 (60)	260 (60)	370 (50)	—	—	—	—	—	—	500 (60)	520 (60)	310 (80)	270 (70)	300 (80)
La	14.3 (0.4)	9.6 (0.3)	12.4 (0.3)	12.6 (0.4)	16.0 (0.4)	25.2 (0.5)	24.2 (0.4)	22.2 (0.4)	24.1 (0.5)	23.2 (0.5)	21.8 (0.5)	16.2 (0.4)	16.0 (0.4)	25.0 (0.5)	21.1 (0.4)	24.6 (0.5)
Ce	32.9 (1.2)	26.0 (1)	29.9 (1.1)	31.1 (1.2)	35.4 (1.2)	58.5 (1.9)	58.2 (1.9)	52.0 (1.7)	56.1 (1.8)	54.0 (1.8)	53.1 (1.8)	35.8 (1.2)	34.2 (1.1)	57.8 (1.8)	46.2 (1.5)	55.6 (1.8)
Nd	—	10 (3)	—	12 (4)	14 (3)	32 (5)	24 (4)	31 (4)	33 (4)	30 (5)	30 (4)	10 (3)	16 (2)	34 (4)	29 (4)	33 (4)
Sm	3.88(0.05)	2.82(0.03)	4.13(0.04)	4.01(0.07)	3.13(0.05)	8.92(0.07)	8.65(0.07)	7.56(0.06)	7.66(0.07)	7.72(0.07)	7.46(0.06)	3.49(0.05)	3.41(0.05)	10.40(0.07)	6.64(0.06)	7.73(0.06)
Tb	0.52(0.08)	0.51(0.07)	0.56(0.08)	0.62(0.08)	0.42(0.06)	1.49(0.15)	1.46(0.15)	1.29(0.13)	1.34(0.13)	1.39(0.14)	1.32(0.13)	0.49(0.06)	0.48(0.06)	1.68(0.17)	1.12(0.11)	1.38(0.14)
Yb	1.3 (0.2)	1.3 (0.2)	1.5 (0.2)	1.5 (0.2)	1.2 (0.2)	4.0 (0.4)	3.5 (0.4)	3.5 (0.3)	3.2 (0.3)	3.5 (0.4)	3.4 (0.3)	1.2 (0.2)	1.1 (0.2)	4.4 (0.4)	3.2 (0.3)	3.3 (0.3)
Lu	0.24(0.05)	0.20(0.04)	0.24(0.05)	0.26(0.04)	0.18(0.04)	0.54(0.07)	0.57(0.07)	0.50(0.07)	0.44(0.07)	0.54(0.08)	0.56(0.09)	—	0.19(0.05)	0.69(0.07)	0.48(0.07)	0.47(0.07)
Th	2.06(0.09)	1.71(0.11)	2.03(0.12)	2.08(0.12)	3.48(0.08)	4.49(0.17)	4.29(0.16)	4.03(0.16)	6.18(0.15)	5.79(0.17)	5.06(0.16)	3.86(0.11)	3.53(0.09)	4.15(0.15)	4.83(0.15)	6.13(0.16)
Hf	4.5 (0.3)	3.6 (0.2)	4.1 (0.2)	4.2 (0.3)	4.0 (0.2)	5.3 (0.3)	5.2 (0.3)	4.6 (0.3)	5.6 (0.3)	5.5 (0.3)	5.2 (0.3)	3.9 (0.2)	3.54(0.19)	4.5 (0.3)	4.6 (0.3)	5.4 (0.3)
$\%Fe_2O_3$	5.78(0.05)	5.60(0.04)	6.55(0.05)	6.63(0.05)	4.02(0.04)	16.76(0.09)	16.13(0.09)	10.92(0.07)	9.81(0.06)	13.01(0.07)	13.39(0.08)	4.52(0.04)	4.41(0.04)	12.64(0.07)	12.81(0.07)	14.34(0.08)
Ta	0.62(0.10)	0.54(0.03)	0.61(0.03)	0.63(0.03)	0.67(0.03)	1.03(0.07)	1.02(0.07)	0.84(0.06)	0.95(0.07)	1.00(0.07)	0.87(0.06)	0.86(0.05)	0.86(0.05)	0.56(0.05)	0.78(0.06)	0.95(0.06)
Co	17.2 (0.3)	17.6 (0.3)	20.3 (0.3)	20.6 (0.3)	9.6 (0.2)	43.1 (0.5)	40.7 (0.4)	44.0 (0.5)	34.3 (0.4)	37.3 (0.4)	38.6 (0.4)	11.4 (0.2)	11.3 (0.2)	27.6 (0.3)	36.9 (0.4)	38.5 (0.4)
Sc	12.65(0.06)	12.86(0.05)	16.01(0.06)	15.79(0.06)	6.26(0.03)	38.49(0.09)	37.01(0.08)	35.29(0.08)	30.21(0.07)	32.71(0.07)	32.83(0.07)	7.31(0.04)	7.72(0.03)	36.01(0.08)	30.24(0.07)	31.99(0.07)
Cr	37.7 (1.5)	44.2 (1.4)	57.4 (1.7)	55.2 (1.7)	13.0 (0.9)	18.3 (1.8)	16.2 (1.7)	35.3 (1.9)	11.6 (1.5)	11.6 (1.7)	17.1 (1.7)	17.3 (1.1)	17.8 (0.9)	10.8 (1.6)	14.8 (1.5)	7.5 (1.5)
Zn	60 (6)	80 (6)	74 (6)	79 (6)	158 (8)	156 (15)	142 (14)	186 (17)	127 (12)	113 (12)	120 (12)	79 (8)	66 (7)	132 (13)	113 (11)	139 (13)

[1]Marvin H. Beeson, analyst.

Table 3. *Trace-element analyses, OMF-7A drill hole*[1] — Continued
(Location 2S/8E/15Ac. Values in ppm except as noted. Analytical error at 1σ in parentheses.)

Stratigraphic unit:	Low-MgO Grande Ronde Basalt	Low-MgO Grande Ronde Basalt	Intrusion	Low-MgO Grande Ronde Basalt	Low-MgO Grande Ronde Basalt	Low-MgO Grande Ronde Basalt	Low-MgO Grande Ronde Basalt	Intrusion	Intrusion	Low-MgO Grande Ronde Basalt	Intrusion	Intrusion	Interbed	Intrusion	Greenstone	Greenstone	Greenstone
Depth (ft):	3,395	3,670	3,760	3,780	3,840	4,020	4,110	4,280	4,510	4,580	4,760	5,000	5,330	5,470	5,820	5,940	6,016
%Na_2O	2.43(0.04)	2.87(0.01)	3.91(0.01)	3.43(0.01)	2.53(0.01)	3.03(0.01)	3.14(0.01)	4.02(0.02)	3.71(0.02)	2.75(0.01)	3.85(0.06)	4.19(0.02)	4.22(0.02)	4.62(0.02)	3.55(0.02)	3.66(0.02)	2.85(0.01)
Cs	0.93(0.19)	2.0 (0.3)	1.7 (0.2)	1.8 (0.3)	2.7 (0.4)	0.85 (0.17)	1.7 (0.3)	2.3 (0.3)	1.8 (0.2)	0.86(0.18)	0.95(0.16)	1.13(0.16)	1.3 (0.2)	0.95(0.14)	1.9 (0.3)	2.0 (0.3)	1.27(0.19)
Rb	47 (7)	53 (7)	41 (4)	34 (7)	44 (7)	37 (7)	42 (8)	37 (5)	30 (4)	40 (7)	30 (6)	30 (5)	—	18 (4)	30 (6)	27 (6)	48 (5)
Ba	950 (100)	790 (100)	480 (40)	750 (100)	780 (90)	770 (90)	830 (100)	290 (50)	340 (50)	710 (90)	480 (70)	440 (60)	460 (70)	390 (80)	650 (80)	570 (80)	700 (70)
Eu	2.22(0.04)	2.04(0.04)	0.95(0.02)	2.09(0.04)	1.82(0.04)	2.02(0.04)	1.91(0.04)	1.07(0.03)	1.00(0.03)	1.82(0.04)	1.47(0.03)	1.04(0.03)	1.42(0.03)	1.18(0.03)	2.53(0.05)	2.64(0.05)	2.14(0.04)
Sr	300 (80)	280 (80)	580 (50)	370 (90)	—	290 (80)	320 (90)	580 (60)	500 (60)	500 (100)	560 (70)	370 (60)	540 (70)	550 (60)	280 (70)	390 (70)	190 (60)
La	25.4 (0.6)	22.7 (0.5)	14.2 (0.3)	21.9 (0.5)	21.00(0.4)	21.1 (0.4)	20.5 (0.4)	14.3 (0.4)	13.4 (0.4)	18.1 (0.4)	14.5 (0.5)	15.4 (0.4)	16.0 (0.5)	16.1 (0.4)	31.0 (0.6)	25.8 (0.5)	29.6 (0.6)
Ce	56.6 (1.9)	52.6 (1.8)	30.7 (1)	52.1 (1.8)	47.7 (2)	49.6 (1.7)	49.1 (1.7)	32.6 (1.1)	29.7 (1)	43.8 (1.5)	35.0 (1.2)	32.1 (1.1)	39.8 (1.4)	34.8 (1.2)	72 (2)	58.0 (1.8)	68 (2)
Nd	32 (5)	31 (5)	15 (2)	27 (6)	24 (4)	24 (4)	28 (5)	14 (3)	15 (3)	26 (4)	21 (3)	17 (3)	21 (4)	12 (3)	41 (5)	33 (4)	36 (4)
Sm	7.88(0.09)	7.50(0.07)	2.85(0.04)	7.35(0.07)	6.83(0.06)	7.17(0.06)	6.81(0.06)	3.17(0.05)	3.02(0.04)	6.38(0.06)	4.94(0.07)	3.41(0.05)	4.72(0.06)	3.56(0.05)	10.43(0.08)	9.72(0.08)	9.66(0.08)
Tb	1.33(0.13)	1.30(0.14)	0.44(0.05)	1.17(0.13)	1.08(0.12)	1.19(0.12)	1.17(0.13)	0.45(0.06)	0.41(0.05)	1.08(0.12)	0.74(0.09)	0.52(0.06)	0.66(0.08)	0.50(0.06)	1.67(0.16)	1.49(0.14)	1.55(0.14)
Yb	3.5 (0.4)	3.6 (0.4)	0.9 (0.2)	3.2 (0.4)	3.1 (0.3)	3.3 (0.3)	2.9 (0.3)	1.0 (0.4)	0.8 (0.2)	2.9 (0.3)	1.7 (0.3)	1.2 (0.2)	1.7 (0.2)	1.3 (0.2)	4.8 (0.4)	4.1 (0.4)	4.9 (0.4)
Lu	0.55(0.07)	0.60(0.08)	—	0.55(0.07)	0.45(0.07)	0.52(0.07)	0.44(0.07)	—	—	0.47(0.07)	0.26(0.04)	0.23(0.07)	0.26(0.06)	0.20(0.06)	0.82(0.09)	0.57(0.07)	0.86(0.09)
Th	6.11(0.17)	4.84(0.17)	3.15(0.08)	4.82(0.17)	4.63(0.16)	4.70(0.16)	4.70(0.2)	3.18(0.09)	3.19(0.10)	3.94(0.16)	2.17(0.12)	3.53(0.09)	3.22(0.13)	3.86(0.11)	6.25(0.15)	4.31(0.14)	6.18(0.13)
Hf	5.5 (0.3)	5.6 (0.3)	3.5 (0.2)	5.4 (0.3)	5.1 (0.3)	5.0 (0.3)	5.4 (0.3)	3.9 (0.2)	3.5 (0.2)	5.0 (0.3)	4.3 (0.2)	3.7 (0.2)	4.6 (0.3)	3.9 (0.2)	8.7 (0.4)	6.0 (0.3)	8.6 (0.4)
%Fe_2O_3	14.37(0.08)	12.81(0.08)	3.69(0.03)	12.04(0.08)	11.17(0.07)	12.97(0.07)	12.93(0.08)	3.99(0.04)	3.76(0.04)	11.67(0.07)	7.45(0.05)	4.64(0.04)	6.23(0.06)	4.43(0.04)	8.62(0.06)	8.21(0.05)	4.97(0.04)
Ta	0.90(0.06)	0.94(0.07)	0.72(0.05)	0.85(0.06)	0.87(0.06)	0.79(0.06)	0.89(0.06)	0.79(0.05)	0.72(0.05)	0.78(0.06)	0.72(0.05)	0.79(0.05)	0.77(0.05)	0.80(0.05)	1.47(0.09)	1.09(0.07)	1.39(0.08)
Co	39.1 (0.4)	35.6 (0.4)	9.6 (0.2)	32.3 (0.4)	28.1 (0.4)	34.8 (0.4)	35.3 (0.4)	10.5 (0.2)	10.2 (0.2)	34.8 (0.4)	21.0 (0.3)	13.0 (0.2)	15.9 (0.3)	11.8 (0.2)	13.3 (0.2)	16.7 (0.3)	2.03(0.11)
Sc	31.88(0.07)	30.23(0.07)	5.67(0.03)	30.30(0.07)	25.43(0.06)	31.22(0.07)	29.75(0.07)	6.90(0.03)	6.59(0.03)	28.86(0.06)	15.78(0.05)	8.57(0.04)	12.80(0.05)	8.95(0.04)	21.26(0.07)	23.51(0.05)	13.19(0.04)
Cr	—	21.4 (1.7)	20.8 (0.9)	26.8 (1.9)	28.2 (1.7)	18.3 (1.6)	25 (3)	20.9 (1.1)	22.6 (1.1)	19.8 (1.6)	20.7 (1.3)	20.6 (1.1)	26.4 (1.4)	24.2 (1.1)	13.9 (1.4)	7.6 (1.3)	3.8 (1.1)
Zn	121 (14)	127 (13)	49 (5)	121 (12)	121 (12)	132 (13)	112 (12)	58 (6)	57 (6)	107 (11)	86 (9)	56 (6)	80 (10)	86 (8)	106 (10)	121 (12)	98 (9)

[1]Marvin H. Beeson, analyst.

Table 4. *Trace-element analyses, Old Maid Flat area*[1]
(Values in ppm except as noted. Analytical error at 1σ in parentheses.)

Stratigraphic unit:	Miocene-Pliocene lavas	Rhododendron Formation	Rhododendron Formation	Rhododendron Formation	Rhododendron Formation	Rhododendron Formation	Rhododendron Formation	Rhododendron Formation	Rhododendron Formation	Lavas of Last Chance Mtn.	Laurel Hill Intrusion
Area:	Last Chance Mtn.	Last Chance Mtn.	Last Chance Mtn.	Last Chance Mtn.	Last Chance Mtn.	Last Chance Mtn.	Last Chance Mtn.	Last Chance Mtn.	Last Chance Mtn.	Last Chance Mtn.	Laurel Hill
Sample no.:	MH-5	MH-10	MH-13	MH-14	MH-16	MH-20	MH-21	MH-22	MH-23	LCM	STILL
Location:	2S/8E/15Acb	2S/8E/15Bdc	2S/8E/15Bdd	2S/8E/15Acc	2S/8E/16Cac	2S/8E/16Dbb	2S/8E/16Dbb	2S/8E/16Dbd	2S/8E/16Dbd	2S/8E/16Bdb	3S/8E/16Dcb
$\%Na_2O$	3.59(0.02)	3.66(0.02)	4.05(0.02)	4.18(0.02)	3.54(0.02)	2.24(0.01)	3.30(0.02)	3.72(0.02)	4.10(0.02)	3.71(0.02)	4.00(0.02)
Cs	1.24(0.19)	—	—	—	0.57(0.11)	1.8 (0.3)	2.3 (0.3)	0.47(0.10)	3.9 (0.5)	1.8 (0.3)	0.78(0.14)
Rb	31 (6)	—	21 (5)	17 (5)	20 (5)	59 (6)	22 (4)	—	20 (5)	—	33 (5)
Ba	350 (70)	380 (80)	370 (70)	410 (60)	240 (50)	540 (70)	360 (80)	280 (60)	320 (60)	390 (90)	420 (70)
Eu	1.29(0.03)	1.22(0.04)	1.21(0.03)	1.56(0.03)	0.87(0.02)	1.06(0.03)	0.88(0.02)	1.01(0.02)	0.90(0.02)	1.39(0.04)	1.33(0.04)
Sr	290 (60)	350 (70)	540 (70)	700 (70)	530 (60)	270 (60)	390 (50)	380 (60)	380 (50)	560 (80)	350 (60)
La	14.4 (0.4)	12.6 (0.3)	10.4 (0.3)	15.2 (0.4)	9.7 (0.3)	13.8 (0.3)	14.2 (0.3)	13.8 (0.3)	13.1 (0.3)	15.8 (0.4)	15.3 (0.4)
Ce	31.4 (1.1)	25.8 (1)	24.6 (0.9)	36.7 (1.2)	21.3 (0.8)	19.9 (0.9)	28.2 (1)	27.9 (1)	27.9 (1)	35.2 (1.3)	37.4 (1.3)
Nd	—	—	—	23 (3)	9 (3)	—	14 (3)	16 (3)	11 (3)	21 (4)	16 (3)
Sm	4.26(0.05)	4.08(0.04)	3.81(0.04)	4.66(0.05)	2.59(0.04)	3.07(0.05)	2.98(0.04)	3.84(0.04)	3.07(0.04)	5.41(0.05)	4.95(0.06)
Tb	0.67(0.08)	0.63(0.08)	0.55(0.07)	0.63(0.07)	0.41(0.05)	0.46(0.07)	0.48(0.06)	0.57(0.07)	0.45(0.05)	0.99(0.12)	0.76(0.09)
Yb	2.0 (0.2)	2.4 (0.2)	1.5 (0.2)	1.4 (0.2)	0.9 (0.2)	1.1 (0.2)	1.1 (0.2)	1.2 (0.2)	1.0 (0.2)	2.2 (0.3)	2.0 (0.3)
Lu	0.35(0.06)	0.37(0.06)	0.24(0.05)	0.24(0.05)	0.19(0.04)	0.16(0.04)	0.19(0.04)	0.23(0.04)	0.18(0.04)	0.36(0.07)	0.30(0.06)
Th	2.70(0.13)	1.96(0.15)	1.46(0.11)	1.41(0.10)	1.85(0.11)	1.68(0.10)	3.17(0.10)	1.98(0.10)	2.96(0.11)	2.33(0.14)	3.07(0.11)
Hf	4.0 (0.2)	3.2 (0.2)	3.5 (0.2)	3.6 (0.2)	2.96(0.17)	2.89(0.18)	3.32(0.19)	3.48(0.19)	3.15(0.18)	4.8 (0.3)	5.2 (0.3)
$\%Fe_2O_3$	7.60(0.06)	8.01(0.06)	6.05(0.04)	8.40(0.05)	4.73(0.03)	5.29(0.04)	4.26(0.04)	5.99(0.04)	3.68(0.03)	7.66(0.06)	7.66(0.06)
Ta	0.65(0.05)	0.58(0.06)	0.54(0.04)	0.61(0.04)	0.38(0.03)	0.53(0.04)	0.61(0.04)	0.54(0.04)	0.71(0.05)	0.44(0.03)	0.71(0.03)
Co	24.6 (0.3)	25.2 (0.3)	17.0 (0.3)	19.3 (0.3)	17.1 (0.2)	19.1 (0.3)	14.5 (0.2)	20.5 (0.3)	8.63(0.17)	27.7 (0.4)	20.6 (0.3)
Sc	18.42(0.06)	21.86(0.07)	14.58(0.05)	10.62(0.04)	10.87(0.03)	17.47(0.05)	10.05(0.04)	12.62(0.04)	10.64(0.03)	20.31(0.07)	16.63(0.06)
Cr	111 (3)	151 (3)	20.1 (1.3)	—	81 (2)	99 (2)	32.8 (1.2)	62.0 (1.6)	34.2 (1.8)	163 (3)	86 (2)
Zn	66 (8)	61 (7)	61 (7)	81 (8)	46 (5)	43 (6)	46 (6)	54 (6)	50 (6)	74 (7)	61 (6)

[1]Marvin H. Beeson, analyst.

Table 5. *Trace-element analyses from Mount Hood region*[1]
(Values in ppm except as noted. Analytical error at 1σ in parentheses.)

Stratigraphic unit:	Rhododendron Formation	Rhododendron Formation	Rhododendron Formation	Rhododendron Formation	Rhododendron Formation	Rhododendron Formation	Rhododendron Formation	Rhododendron Formation	Rhododendron Formation	Rhododendron Formation	Rhododendron Formation
Area:	Zigzag Mtn.	Zigzag Mtn.	Zigzag Mtn.	Zigzag Mtn.	Zigzag Mtn.	Lolo Pass area	Lolo Pass area	Lolo Pass area	Hunchback Mtn.	Hunchback Mtn.	Zigzag Mtn.
Sample no.:	1	2	3	4	5	6	7	8	9	10	11
Location:	3S/7E/3Ab	2S/7E/34Dc	2S/7E/34Dc	2S/7E/34Dc	2S/7E/34Dc	2S/8E/19Bd	2S/8E/19Ab	2S/8E/17Bc	3S/7E/10Bb	3S/7E/3Cc	2S/8E/34Db
$\%Na_2O$	3.65(0.01)	3.77(0.01)	3.49(0.01)	3.86(0.02)	4.23(0.02)	4.05(0.02)	3.93(0.01)	3.88(0.02)	4.07(0.02)	4.05(0.02)	4.23(0.02)
$\%P_2O_5$	0.17	0.12	——	——	0.12	0.19	0.16	——	0.12	0.13	——
Eu	1.03(0.03)	0.95(0.02)	1.02(0.03)	0.97(0.02)	1.00(0.02)	1.13(0.03)	1.00(0.02)	1.06(0.03)	0.95(0.02)	0.96(0.02)	1.18(0.03)
La	14.1 (0.4)	9.2 (0.3)	11.9 (0.4)	11.3 (0.3)	16.3 (0.4)	9.9 (0.3)	12.2 (0.4)	15.5 (0.4)	11.4 (0.4)	11.00(0.4)	16.7 (0.5)
Ce	31.7 (1.3)	17.4 (0.9)	23.8 (1.1)	23.6 (1.1)	33.9 (1.4)	24.3 (1.1)	27.0 (1.2)	35.7 (1.5)	25.6 (1.2)	23.5 (1.1)	34.5 (1.4)
Nd	——	12.67(4.31)	——	——	15.12(4.05)	14.58(4.03)	12.96(3.78)	14.55(4.8)	14.19(4.84)	——	20.09(5)
Sm	3.56(0.05)	3.09(0.04)	3.19(0.05)	3.08(0.04)	3.94(0.05)	3.62(0.05)	3.11(0.04)	3.84(0.05)	3.28(0.05)	3.02(0.05)	4.13(0.05)
Tb	0.58(0.07)	0.38(0.06)	0.48(0.06)	0.40(0.06)	0.59(0.07)	0.56(0.07)	0.45(0.06)	0.55(0.07)	0.41(0.06)	0.44(0.06)	0.54(0.07)
Yb	1.40(0.20)	0.98(0.18)	1.30(0.20)	1.10(0.19)	1.7 (0.2)	1.6 (0.3)	1.28(0.20)	1.60(0.20)	1.1 (0.2)	1.4 (0.2)	1.6 (0.3)
Th	3.7 (0.4)	1.8 (0.2)	2.9 (0.3)	2.7 (0.3)	4.4 (0.4)	1.7 (0.2)	3.0 (0.3)	4.4 (0.4)	2.6 (0.3)	2.3 (0.3)	4.2 (0.4)
Hf	4.0 (0.3)	3.2 (0.2)	3.6 (0.3)	3.3 (0.3)	4.0 (0.3)	3.3 (0.3)	3.6 (0.3)	4.4 (0.3)	3.3 (0.2)	3.3 (0.2)	4.3 (0.3)
$\%TiO_2$	0.74	0.78	——	——	0.64	0.92	0.73	——	0.63	0.69	——
%FeO	5.66(0.04)	4.58(0.03)	4.95(0.03)	4.88(0.03)	4.83(0.03)	5.60(0.04)	4.54(0.03)	4.87(0.03)	4.32(0.03)	4.69(0.03)	4.95(0.03)
Co	19.5 (0.3)	18.7 (0.3)	20.0 (0.3)	18.0 (0.3)	16.0 (0.3)	18.0 (0.3)	16.0 (0.3)	17.4 (0.3)	19.3 (0.3)	19.4 (0.3)	17.1 (0.3)
Sc	12.92(0.06)	13.94(0.06)	12.64(0.06)	12.07(0.05)	11.7 (0.05)	13.13(0.06)	12.42(0.06)	13.25(0.06)	11.94(0.05)	11.73(0.05)	11.78(0.05)
Cr	24.3 (1.5)	68.2 (2)	53.2 (1.8)	49.0 (1.7)	17.1 (1.3)	15.1 (1.4)	58.0 (1.9)	42.8 (1.7)	86.0 (2)	45.0 (1.7)	25.2 (1.5)

[1]Marshall W. Gannett, analyst.

Table 5. *Trace-element analyses from Mount Hood region*[1] — Continued
(Values in ppm except as noted. Analytical error at 1σ in parentheses.)

Stratigraphic unit:	Post-Rhododendron Formation	Post-Rhododendron Formation	Post-Rhododendron Formation	Post-Rhododendron Formation	Post-Rhododendron Formation	Post-Rhododendron Formation	Post-Rhododendron Formation	Post-Rhododendron Formation	Rhododendron Formation	Rhododendron Formation	Rhododendron Formation
Area:	Zigzag Mtn.	Lolo Pass area	Lolo Pass area	Hunchback Mtn.	Zigzag Mtn.	Last Chance Mtn.	Zigzag Mtn.	Alder Creek	Lolo Pass area	Last Chance Mtn.	Last Chance Mtn.
Sample no.:	12	13	14	15	16	17	18	19	20	21	22
Location:	2S/7E/35Cb	2S/8E/9Bb	2S/8E/4Da	3S/7E/10Bb	2S/7E/34Da	2S/8E/9Db	2S/8E/33Ba	2S/6E/34Bd	2S/8E/18Dd	2S/7E/17Da	2S/8E/9Ca
$\%Na_2O$	4.03(0.01)	3.84(0.01)	4.08(0.02)	3.90(0.02)	3.73(0.01)	3.76(0.01)	3.58(0.02)	3.47(0.01)	4.52(0.02)	4.34(0.02)	3.72(0.01)
$\%P_2O_5$	0.14	0.18	0.22	——	——	0.20	——	——	——	0.16	——
Eu	1.19(0.03)	1.12(0.03)	1.58(0.03)	1.18(0.03)	1.13(0.03)	1.21(0.03)	1.12(0.03)	0.96(0.02)	0.97(0.02)	1.45(0.03)	1.24(0.03)
La	13.1 (0.4)	12.5 (0.4)	20.4 (0.5)	11.1 (0.4)	15.2 (0.4)	15.9 (0.4)	12.7 (0.4)	8.5 (0.3)	16.9 (0.5)	25.7 (0.6)	16.5 (0.4)
Ce	29.7 (1.3)	32.1 (1.4)	39.3 (1.6)	25.1 (1.2)	28.8 (1.3)	40.9 (1.7)	32.0 (1.4)	17.7 (0.8)	35.5 (1.5)	40.1 (1.6)	39.9 (1.6)
Nd	15.62(4.46)	16.95(4.71)	24.57(5.94)	15.13(5.30)	13.56(4.32)	16.98(5.89)	——	15.0 (5)	15.4 (4.8)	27.04(5.99)	15.68(4.23)
Sm	4.07(0.05)	4.41(0.06)	6.03(0.07)	4.25(0.05)	4.33(0.06)	5.57(0.07)	4.49(0.06)	3.07(0.04)	3.67(0.05)	6.31(0.07)	4.18(0.05)
Tb	0.56(0.08)	0.67(0.08)	0.79(0.09)	0.60(0.08)	0.65(0.08)	0.80(0.09)	0.58(0.08)	0.41(0.06)	0.49(0.06)	0.85(0.09)	0.50(0.06)
Yb	1.7 (0.3)	1.9 (0.3)	2.3 (0.3)	2.2 (0.3)	2.3 (0.3)	2.8 (0.4)	2.2 (0.3)	1.23(0.17)	1.5 (0.2)	2.0 (0.3)	1.4 (0.2)
Th	3.1 (0.3)	3.3 (0.3)	4.1 (0.4)	1.9 (0.3)	4.5 (0.4)	5.0 (0.5)	3.8 (0.4)	1.15(0.14)	4.3 (0.4)	3.3 (0.3)	4.4 (0.4)
Hf	4.0 (0.3)	5.2 (0.4)	3.0 (0.3)	3.3 (0.3)	4.1 (0.3)	6.9 (0.5)	5.0 (0.3)	2.37(0.18)	4.1 (0.3)	4.0 (0.3)	4.2 (0.3)
$\%TiO_2$	0.79	0.99	1.02	——	——	1.03	——	——	——	0.58	——
%FeO	6.44(0.04)	6.12(0.04)	6.61(0.04)	5.77(0.04)	5.62(0.04)	6.04(0.04)	6.48(0.04)	6.12(0.04)	4.85(0.03)	4.16(0.03)	4.42(0.03)
Co	23.2 (0.4)	24.6 (0.4)	26.8 (0.4)	27.1 (0.4)	21.4 (0.3)	23.2 (0.4)	26.7 (0.4)	23.2 (0.3)	12.6 (0.3)	11.9 (0.3)	14.3 (0.3)
Sc	18.73(0.07)	17.51(0.06)	19.45(0.07)	17.09(0.06)	16.69(0.06)	17.37(0.06)	18.41(0.07)	16.33(0.05)	11.04(0.05)	7.98(0.04)	10.11(0.05)
Cr	96.0 (3)	128 (3)	72.31(2.8)	83.0 (2)	135.0 (3)	125.0 (3)	155.0 (3)	82.2 (1.7)	44.8 (1.6)	24.7 (1.3)	31.93(1.49)

[1]Marshall W. Gannett, analyst.

Table 6. *Trace-element analyses from OMF-1 drill hole*
(All trace elements in ppm with error at 1σ in parentheses)

A. *Analyses by Beeson and Moran*[1]

Stratigraphic unit:	Frenchman Springs, Wanapum Basalt	Low-MgO Grande Ronde Basalt	Prineville Grande Ronde Basalt	Low-MgO Grande Ronde Basalt	Gabbro dike	Low-MgO Grande Ronde Basalt	Low-MgO Grande Ronde Basalt	Low-MgO Grande Ronde Basalt
Depth (ft.):	2,072	2,900	3,140	3,290	3,518	3,530	3,680	3,850
$\%Na_2O$	2.76(0.04)	2.61(0.04)	3.28(0.04)	2.97(0.04)	2.72(0.04)	3.14(0.04)	2.70(0.04)	3.03(0.04)
Ba	490 (150)	550 (140)	2,400 (300)	1,030 (170)	170 (100)	1,290 (180)	590 (140)	630 (140)
Eu	2.18(0.09)	1.90(0.08)	3.57(0.13)	2.32(0.09)	1.10(0.06)	2.69(0.11)	1.81(0.08)	2.17(0.09)
La	25.7 (1.8)	22.8 (1.6)	23.4 (1.8)	23.5 (1.6)	11.1 (1.2)	23.6 (1.8)	26.7 (1.8)	26.5 (2.0)
Ce	57 (3)	49 (3)	53 (3)	50 (3)	30 (2)	51 (3)	58 (3)	60 (3)
Lu	0.60(0.09)	0.54(0.08)	0.62(0.09)	0.62(0.09)	0.35(0.06)	0.51(0.09)	0.44(0.08)	0.58(0.09)
Th	4.1 (0.4)	5.2 (0.4)	3.9 (0.4)	4.4 (0.4)	1.5 (0.4)	4.4 (0.4)	6.2 (0.4)	6.6 (0.5)
Hf	3.8 (0.6)	3.6 (0.6)	3.1 (0.6)	3.4 (0.6)	2.4 (0.4)	3.6 (0.6)	4.3 (0.6)	6.0 (0.7)
%FeO	13.18(0.15)	11.25(0.14)	11.18(0.14)	10.86(0.14)	8.89(0.12)	11.05(0.14)	11.16(0.14)	12.02(0.15)
Co	38.4 (1.1)	38.3 (1.1)	27.4 (0.9)	33.0 (1.0)	42.7 (1.0)	30.9 (1.0)	35.9 (1.0)	35.3 (1.1)
Sc	36.6 (0.2)	34.0 (0.2)	36.4 (0.2)	33.3 (0.2)	26.0 (0.2)	35.3 (0.2)	32.0 (0.2)	33.5 (0.2)
Cr	31 (10)	17 (8)	8 (7)	20 (8)	340 (80)	31 (10)	17 (8)	21 (9)

[1]Taken from Figure III-3 of Beeson, M. H., and Moran, M. R., 1979, Stratigraphy and structure of the Columbia River Basalt Group in the Cascade Range, Oregon, *in* Riccio, J. F., ed., Geothermal resource assessment of Mount Hood: Oregon Department of Geology and Mineral Industries Open-File Report 0-79-8, p. 5-77.

Table 6. *Trace-element analyses from OMF-1 drill hole*—Continued
(All trace elements in ppm with error at 1σ in parentheses)

B. *Analyses by Marshall W. Gannett*

Stratigraphic unit:	Rhododendron Formation	Rhododendron Formation	Rhododendron Formation	Intrusion	Intrusion	Intrusion	Priest Rapids Member	Intrusion	Frenchman Springs Member	Low-MgO Grande Ronde Basalt	Low-MgO Grande Ronde Basalt
Sample no.:	OMF-835	OMF-990	OMF-1060	OMF-1190	OMF-1290	OMF-1320	OMF-1620	OMF-2380	OMF-2640	OMF-2680	OMF-2820
Depth (ft):	835	990	1,060	1,190	1,290	1,320	1,620	2,380	2,640	2,680	2,820
$\%Na_2O$	5.20(0.02)	2.57(0.01)	3.98(0.01)	4.03(0.01)	3.73(0.01)	3.85(0.01)	3.25(0.01)	4.19(0.02)	3.64(0.02)	3.68(0.02)	3.99(0.02)
Cs	1.1 (0.2)	—	—	—	—	—	—	0.50(0.16)	—	1.0 (0.3)	—
Rb	36 (8)	—	19 (5)	25 (6)	23 (6)	22 (6)	—	33 (9)	—	63 (14)	36 (10)
Ba	540 (70)	—	470 (60)	480 (60)	430 (60)	390 (60)	540 (110)	530 (90)	1,490 (160)	1,240 (150)	920 (120)
Eu	0.93(0.02)	1.01(0.03)	1.03(0.02)	1.05(0.02)	0.98(0.02)	1.04(0.02)	2.94(0.06)	1.16(0.04)	2.48(0.07)	2.09(0.05)	2.09(0.04)
Sr	250 (70)	240 (90)	310 (90)	330 (100)	330 (100)	290 (90)	—	450 (130)	—	—	270 (100)
La	13.3 (0.4)	7.3 (0.3)	16.7 (0.5)	16.3 (0.4)	15.3 (0.4)	16.7 (0.5)	23.9 (0.6)	18.1 (0.6)	27.6 (0.7)	24 (0.07)	24.0 (0.6)
Ce	28.9 (1.0)	16.9 (0.9)	37.0 (1.2)	36.3 (1.2)	33.9 (1.1)	37.4 (1.2)	60 (2)	42.2 (1.5)	71 (2)	60 (2)	59 (2)
Nd	16 (5)	—	22 (6)	22 (6)	24 (8)	23 (6)	36 (11)	27 (8)	49 (14)	47 (11)	35 (10)
Sm	3.11(0.04)	3.09(0.04)	3.65(0.05)	3.59(0.05)	3.48(0.05)	3.89(0.06)	9.84(0.08)	4.18(0.07)	9.14(0.10)	8.05(0.10)	7.72(0.09)
Tb	—	0.50(0.07)	0.50(0.05)	0.47(0.05)	0.36(0.04)	0.45(0.05)	—	0.54(0.07)	1.48(0.15)	1.45(0.14)	1.34(0.14)
Yb	1.31(0.18)	1.75(0.16)	1.00(0.13)	1.07(0.13)	1.02(0.15)	1.02(0.13)	4.1 (0.4)	1.23(0.19)	3.7 (0.4)	4.0 (0.5)	3.6 (0.4)
Lu	—	0.35(0.07)	—	—	—	—	0.82(0.12)	0.30(0.09)	0.54(0.08)	0.74(0.13)	0.60(0.08)
Th	3.6 (0.2)	1.30(0.15)	4.5 (0.3)	4.2 (0.3)	4.0 (0.2)	4.4 (0.3)	4.1 (0.3)	5.2 (0.3)	8.5 (0.6)	7.5 (0.5)	7.2 (0.5)
Hf	3.6 (0.2)	2.5 (0.2)	3.8 (0.3)	3.7 (0.3)	3.6 (0.2)	3.8 (0.3)	5.0 (0.4)	4.5 (0.3)	5.4 (0.5)	5.8 (0.4)	5.3 (0.4)
$\%Fe_2O_3$	4.89(0.03)	7.56(0.05)	4.27(0.03)	4.30(0.03)	3.93(0.03)	4.28(0.03)	12.84(0.07)	4.69(0.05)	14.73(0.08)	13.89(0.07)	13.63(0.08)
Co	14.7 (0.2)	30.3 (0.4)	11.05(0.19)	11.40(0.2)	10.3 (0.2)	11.2 (0.2)	47.3 (0.5)	11.8 (0.3)	42.0 (0.6)	39.9 (0.5)	39.5 (0.5)
Sc	10.24(0.04)	26.09(0.06)	7.55(0.03)	7.53(0.03)	7.29(0.03)	7.60(0.03)	38.39(0.11)	8.32(0.05)	36.76(0.10)	39.5 (0.5)	33.37(0.09)

APPENDIX C

CHEMICAL ANALYSES AND GEOTHERMOMETRY OF WATER SAMPLES FROM OMF-7A DRILL HOLE

Table 1. *Chemical analyses of water samples from OMF-7A drill hole.* (All values in ppm)

Depth (ft):	Artesian[1]	Artesian[1]	1,470[2] (2nd sample)	2,050[2] (2nd sample)	3,115[2]	4,876[3]
Na	39	31	170	169	141	265
K	< 2.50	< 2.50	< 2.50	< 2.50	4	9
Ca	8	7	19	19	28	168
Mg	1	1	< 0.500	< 0.500	< 0.500	< 0.500
Fe	1.31	0.59	0.14	0.36	1.13	< 0.025
Al	0.7	< 0.625	< 0.625	< 0.625	< 0.625	< 0.625
SiO_2	14	8	21	23	35	25
Ti	< 0.125	< 0.125	< 0.125	< 0.125	< 0.125	< 0.125
P	< 0.625	< 0.625	< 0.625	< 0.625	< 0.625	< 0.625
Sr	0.06	0.06	0.27	0.26	0.25	2.15
Ba	< 0.625	< 0.625	< 0.625	< 0.625	< 0.625	< 0.625
V	< 1.25	< 1.25	< 1.25	< 1.25	< 1.25	< 1.25
Cr	< 0.050	< 0.050	< 0.050	< 0.050	< 0.050	< 0.050
Mn	< 0.250	< 0.250	< 0.250	< 0.250	< 0.250	0.4
Co	< 0.025	< 0.025	< 0.025	< 0.025	< 0.025	< 0.025
Ni	< 0.125	< 0.125	< 0.125	< 0.125	< 0.125	< 0.125
Cu	< 0.063	< 0.063	< 0.063	< 0.063	< 0.063	< 0.063
Mo	< 1.25	< 1.25	< 1.25	< 1.25	< 1.25	< 1.25
Pb	< 0.250	< 0.250	< 0.250	< 0.250	< 0.250	< 0.250
Zn	1.3	0.2	< 0.125	0.4	3.8	3.9
Cd	< 0.063	< 0.063	< 0.063	< 0.063	< 0.063	< 0.063
Ag	< 0.050	0.06	< 0.050	< 0.050	< 0.050	< 0.050
Au	< 0.100	< 0.100	< 0.100	< 0.100	< 0.100	< 0.100
As	< 0.625	1.8[4]	< 0.625	< 0.625	< 0.625	< 0.625
Sb	< 0.750	< 0.750	< 0.750	< 0.750	< 0.750	< 0.750
Bi	< 2.50	< 2.50	< 2.50	< 2.50	< 2.50	< 2.50
U	< 6.25	213[4]	< 6.25	< 6.25	< 6.25	< 6.25
Te	< 1.25	< 1.25	< 1.25	< 1.25	< 1.25	< 1.25
Sn	< 0.125	1.3[4]	< 0.125	< 0.125	< 0.125	< 0.125
W	< 0.125	< 0.125	< 0.125	< 0.125	< 0.125	< 0.125
Li	< 0.050	< 0.050	< 0.050	< 0.050	< 0.050	0.10
Be	< 0.005	< 0.005	< 0.005	< 0.005	< 0.005	< 0.005
B	< 0.125	< 0.125	0.5	0.6	0.3	0.6
Zr	< 0.125	< 0.125	< 0.125	< 0.125	< 0.125	< 0.125
La	< 0.125	< 0.125	< 0.125	< 0.125	< 0.125	< 0.125
Ce	< 0.250	1.1[4]	< 0.250	< 0.250	< 0.250	< 0.250
Th	< 2.50	7[4]	< 2.50	< 2.50	< 2.50	< 2.50
TDS	ND[5]	ND[5]	584	582	656	1241
Cl	ND[5]	ND[5]	181	158	151	573
F	0.3	ND[5]	2	1.7	1.2	1.3
SO_4	ND[5]	ND[5]	140	126	100	136

[1]Sample taken at surface.
[2]Sampled with downhole water sampler; sample exsolved gas phase at surface pressure.
[3]Swab sample.
[4]Spurious value from spectral interference during analysis.
[5]ND = not determined.

Table 2. *Estimated reservoir temperatures* (°C)

Depth (ft):	Artesian[1]	Artesian[1]	1,470[2] (2nd sample)	2,050[2] (2nd sample)	3,115[2]	4,876[3]
Na-K-Ca[4]	•[5]	•[5]	•[5]	•[5]	4/3 Ca = 65.4 1/3 Ca = 116.3	4/3 Ca = 60.3 1/3 Ca = 120.0
Na-K[6]	•[5]	•[5]	•[5]	•[5]	100.1	109.2
Si_{COND}[7]	50.5	32.2	65.3	68.8	85.9	72.0
Si_{ADIA}[8]	57.4	40.9	70.6	73.7	88.7	76.6
Si_{CHAL}[9]	18.0	−0.6	33.3	37.0	55.0	40.3
Si_{CRIS}[10]	2.03	−15.2	16.0	19.4	36.0	22.6
Si_{AMOR}[11]	−56.5	−71.1	−44.6	−41.8	−27.5	−39.0
Mg_{CORR}[12]	•[5]	•[5]	•[5]	•[5]	•[5]	•[5]
Na/Li[13]	•[5]	•[5]	•[5]	•[5]	•[5]	262.9

[1] Sample taken at surface.
[2] Sampled with downhole sampler.
[3] Swab sample.
[4] For temperature calculation, see Fournier and Truesdell (1973).
[5] One or more parameters not within detectable limits.
[6] For temperature calculation, see Fournier (1979).
[7] SiO_2 conductive heat loss. For temperature calculation, see Fournier and Rowe (1966).
[8] SiO_2 adiabatic heat loss. For temperature calculation, see Fournier and Rowe (1966).
[9] SiO_2 chalcedony saturation. For temperature calculation, see Fournier and Rowe (1966).
[10] SiO_2 cristobalite saturation. For temperature calculation, see Fournier and Rowe (1966).
[11] Amorphous silica saturation. For temperature calculation, see Fournier and Rowe (1966).
[12] Magnesium correction applied to Na-K-Ca geothermometer. See Fournier and Rowe (1966).
[13] For temperature correction, see Fouillac and Michard (1981).

References

Fouillac, C., and Michard, G., 1981, Sodium/lithium ratio in water applied to geothermometry of geothermal reservoirs: Geothermics, v. 10, no. 1, p. 55-70.

Fournier, R. O., 1979, A revised equation for the Na/K geothermometer, *in* Geothermal Resources Council Annual Meeting, Reno, Nev., 1979, Transactions: Davis, Calif., Geothermal Resources Council, v. 3, p. 221-224.

Fournier, R. O., and Rowe, J. J., 1966, Estimation of underground temperatures from the silica content of water from hot springs and wet-steam wells: American Journal of Science, v. 264, p. 685-697.

Fournier, R. O., and Truesdell, A. H., 1973, An empirical Na:K:Ca geothermometer for natural waters: Geochimica et Cosmochimica Acta, v. 37, p. 1255-1275.